EXPLORING ANTI-TUBERCULOSIS DRUGS THROUGH GREEN SOLVENTS FOR EFFECTIVE TREATMENT OF TUBERCULOSIS

MÁRCIA FILIPA CARVALHO DOS SANTOS

Master in Biochemistry applied to Biomedicine

DOCTORATE IN SUSTAINABLE CHEMISTRY

NOVA University Lisbon

March, 2022

EXPLORING ANTI-TUBERCULOSIS DRUGS THROUGH GREEN SOLVENTS FOR EFFECTIVE TREATMENT OF TUBERCULOSIS

MÁRCIA FILIPA CARVALHO DOS SANTOS

Master in Biochemistry applied to Biomedicine

DOCTORATE IN SUSTAINABLE CHEMISTRY

NOVA University Lisbon

March, 2022

EXPLORING ANTI-TUBERCULOSIS DRUGS THROUGH GREEN SOLVENTS FOR EFFECTIVE TREATMENT OF TUBERCULOSIS

MÁRCIA FILIPA CARVALHO DOS SANTOS

Master in Biochemistry applied to Biomedicine

Adviser: **Ana Rita Cruz Duarte**
Associate Professor with habilitation, NOVA School of Science and Technology

Co-advisers: **Luís Alexandre Almeida Fernandes Cobra Branco**
Assistant Professor, NOVA School of Science and Technology

Examination Committee:

Chair: Susana Filipe Barreiros,
Full Professor, NOVA School of Science and Technology

Rapporteurs: Sophie Fourmentin-Lamotte,
Full Professor, Université du Littoral-Côte d'Opale, Dunkerque, France
Filomena Elisabete Lopes Martins Elvas Leitão,
Assistant Professor, Faculdade de Ciências da Universidade de Lisboa

Adviser: Ana Rita Cruz Duarte,
Associate Professor with habilitation, NOVA School of Science and Technology

Members: Joana Fernandes da Silva Magalhães,
Researcher, Faculdade de Farmácia da Universidade do Porto
Miguel Maurício Machado dos Santos,
Researcher, NOVA School of Science and Technology

DOCTORATE IN SUSTAINABLE CHEMISTRY

NOVA University Lisbon
March, 2022

Exploring anti-tuberculosis drugs through green solvents for effective treatment of tuberculosis

PREFACE

The thesis presented here involves the work developed between 2018 and 2022 in Des.solve group with Prof. Ana Rita Cruz Duarte from LAQV-REQUIMTE of the Chemistry Department of NOVA School of Science and Technology, and also with Prof. Luís Branco from LAQV-REQUIMTE of the Chemistry Department of NOVA School of Science and Technology, within the scope of the doctoral program in Sustainable Chemistry.

This work also includes different collaborations such as in Des.solve group, mainly with Ana Roda and Hugo Monteiro; also, with Dra. Ana Matias from iBET; Inês Leitão and Dra. Ana Petronilho from ITQB NOVA; Dr. Christoph Held from Laboratory of Thermodynamics, Department of Biochemical and Chemical Engineering, TU Dortmund in Germany; Dr. Ricardo Ferreira from Red Glead Discovery AB in Sweeden; Prof. Elsa Anes and Dr. David Pires from the Host-Pathogen Interactions group from iMed – Research Institute for Medicines from Faculty of Pharmacy of Lisbon University; Prof. Iolanda de Marco from Department of Industrial Engineering of Salerno University, and Prof. Mário Diniz from UCIBIO - Applied Molecular Biosciences Unit, Chemistry Department of NOVA School of Science and Technology.

The thesis is organized into different chapters, being chapter 1 an introduction to tuberculosis infection, including its history, epidemiology, several problematics, and current treatment, which leads to the presentation of different approaches for its treatment, that includes sustainable strategies for the delivery of anti-tuberculosis drugs. Chapter 2 is focused on the experimental part comprising all the methodologies used during the work and different approaches. Chapter 3 is about the synthesis and characterization of organic salts based on isoniazid. Chapter 4 comprises on the development of therapeutic liquid mixtures for tuberculosis treatment, including the study, characterization, and application in tuberculosis therapy. Chapter 5 compares the main achievements regarding the synthesis of organic salts and preparation of therapeutic liquid mixtures, giving an overview on these two approaches. Chapter 6 comprises the application of prepared systems with encapsulation techniques for drug delivery. Finally, chapter 7 includes a brief conclusion of all the developed work as well as the relevant studies that could be pursued from now on.

The studies herein presented resulted in different original scientific research manuscripts already published or prepared for submission.

ACKNOWLEDGEMENTS

At the end of this journey, I realize that, during my PhD, I shared different moments and ideas with so many people that helped me in different ways to move on and pursue my research and I am grateful for that.

Firstly, I would like to thank my supervisor Prof. Ana Rita Duarte for her guidance, patience, support (scientific and personal), interesting discussions about the huge world of eutectic systems, enthusiasm, and encouragement to embrace this project, helping me in every stage of this work. Also, I acknowledge Prof. Luís Branco for his advice, support, and co-supervision.

I would like to acknowledge my thesis committee members, Prof. Filomena Martins and Dr. Alexandre Paiva for their suggestions and fruitful discussions that were important guidance, during this work.

I honestly acknowledge all people involved in the collaborations established, for all the support and opportunity to learn from them, also all the co-authors of the works performed in this thesis for their scientific expertise and contribution either in the laboratory or in the review of the works herein presented.

A special thanks to Prof. Iolanda de Marco from Salerno University in Italy, for accepting me on a short-term scientific mission and receiving me so well, also, the girls Irma and Stefania for the assistance in the world of supercritical atomization processes and for teaching me a little bit of Italian.

I would like to specially thank my colleagues from Des.solve group: Luísa, Sílvia, Inês, Cláudio, Hugo, Filipe, Joana, Reza, Jelena, Marta, Liane, Rita Gameiro, Rita Craveiro, Ângelo and also, from 427 to Mónica and Bruno, for all the support over these years, productive discussions, team buildings, happy hours and for relaxing moments. A special thanks to Ana Roda that besides being there as a colleague and a friend, helped me in different phases of this thesis and also reviewing some parts of the thesis.

I would also like to thank the girls from the 5th floor: Inês Paninho, Maria, Catarina, Sofia Messias, Clarinda, Gosia, Raquel and Ana for friendship, animated lunchtimes and also for the support at the beginning of my journey at NOVA School of Science and Technology.

Also, thanks to my family, parents, sisters (Rita and Joana), and some of my closest friends: Sabrina, Ana, Maria João, Joana Pinto, Maria Miguel, Mafalda, Paulo, Hugo, Pedro, Miguel, Ana Carolina, Adriana, Vânia, Joana Silva, Luísa, Inês, Rita, Sofia, Beatriz and Alexandra for always being there!

Finally, I acknowledge the financial support from European Union's Horizon 2020 (ERC) under grant agreement no. ERC-2016-CoG 725034 and was also supported by Associate Laboratory for Green Chemistry-LAQV which is financed by national funds from FCT/MCTES (UIDB/5006/2020).

"Inspira, Respira, Não pira!"

ABSTRACT

Tuberculosis is an airborne infectious disease caused by *Mycobacterium tuberculosis* that remains to be one of the deadliest infectious diseases worldwide. Despite being considered treatable, the treatment of this disease involves a combination of different antibacterial drugs administrated for several months. This may cause serious adverse effects and lead to low treatment compliance by the patient, contributing to the ineffectiveness of the therapy and the emergence of drug resistance. The approaches used for treating tuberculosis are the same since their development, around 50 years ago. Therefore, and given the emergence and persistence of drug resistance to the various antibiotics used, it is of the utmost importance to conduct a breakthrough investigation to find alternatives able to rapidly reduce the incidence of tuberculosis, mainly in low-income countries. Considering the drawbacks of tuberculosis therapy, it is proposed in this work to explore alternative strategies to address long term therapies and poor patient compliance, which include the use of alternative solvents, such as ionic systems, therapeutic liquid mixtures, and supercritical fluid technology. In a first step, the preparation of ionic systems (organic salts) and eutectic mixtures incorporating anti-tuberculosis drugs in their structure were explored. Then, all prepared compounds were fully characterized both in terms of their physicochemical properties and their *in vitro* biological performance through a myriad of different procedures and techniques, such as polarized optical microscopy, differential scanning calorimetry, nuclear magnetic resonance, infrared spectroscopy, solubility, permeability (using Franz cells and transwell inserts), cytotoxicity in different cell lines, antibacterial activity, among others. Additionally, eutectic mixtures were prepared by dissolving first-line treatment anti-tuberculosis drugs and an organic salt (isoniazid di-chloride, $[INH][Cl]_2$) in the system composed by citric acid, ethambutol, and water in a ratio of 1:1:5. In order to obtain inhalable particles for targeted site-infection delivery of these formulations, supercritical fluid technology was used to encapsulate the eutectic mixtures and formulate biocompatible particles with a suitable size for pulmonary administration. In general, the main objectives of

the work were achieved, being the alternative strategies explored (ionic systems, eutectic mixtures, and supercritical fluid technology) capable to improve some essential characteristics of anti-tuberculosis drugs, in particularly, its solubility and stability. Hereupon, their potential should be further explored with different and more complex biological models.

Keywords: tuberculosis; ionic liquids; organic salts; eutectic mixtures; therapeutic deep eutectic systems; supercritical CO_2 technology.

RESUMO

A tuberculose é uma doença infeciosa transmitida por via aérea, causada pela bactéria *Mycobacterium tuberculosis*, continuando a ser uma das doenças infeciosas que causa maior mortalidade mundialmente. Apesar de existir um tratamento eficaz para a tuberculose, este engloba uma combinação de diferentes antibióticos administrados durante vários meses, o que pode causar efeitos adversos graves e, consequentemente, levar à reduzida adesão ao tratamento pelo paciente, o que contribui para a ineficácia do tratamento e aparecimento de resistência aos diferentes antibióticos. O tratamento e a combinação de fármacos utilizada na tuberculose é o mesmo desenvolvido há mais de 50 anos. Posto isto, e considerando também o aparecimento e persistência da resistência aos vários antibióticos utilizados, torna-se urgente o avanço da investigação de forma a encontrar alternativas capazes de reduzir a incidência da tuberculose, principalmente em países subdesenvolvidos. Considerando os problemas existentes na terapia da tuberculose, o objetivo desta tese é explorar estratégias alternativas que visem melhorar as abordagens terapêuticas utilizadas no seu tratamento, as quais incluem o uso de solventes sustentáveis alternativos, como sistemas iónicos, misturas eutécticas e tecnologia supercrítica. Inicialmente, foram preparados diferentes sistemas iónicos (sais orgânicos) e misturas eutécticas que incluem na sua estrutura fármacos utilizados na terapêutica da tuberculose. De seguida, os sistemas foram caracterizados, relativamente às suas propriedades físico-químicas e biológicas através de diferentes técnicas e abordagens, tais como microscopia ótica de luz polarizada, calorimetria diferencial de varrimento, ressonância magnética nuclear, espectroscopia de infravermelho, solubilidade, permeabilidade (usando células de Franz e *inserts* transwell), citotoxicidade em diferentes linhas celulares, entre outras. Além de misturas eutécticas, também foram preparadas diferentes formulações baseadas na mistura composta por ácido cítrico, etambutol e água no rácio 1:1:5, em que foram dissolvidos diferentes fármacos utilizados na primeira linha de tratamento da tuberculose e um sal orgânico (di-cloreto de isoniazida, $[INH][Cl]_2$). De modo a obter partículas inaláveis que possam ter uma ação específica no local da infeção, foi

utilizada tecnologia supercrítica para encapsular as misturas líquidas e formular partículas biocompatíveis e com um tamanho adequado à administração pulmonar. Em geral, os principais objetivos deste trabalho foram alcançados, tendo sido exploradas diferentes estratégias alternativas (sistemas iónicos, misturas eutécticas e tecnologia supercrítica), capazes de melhorar algumas características essenciais dos fármacos administrados na tuberculose, como a sua solubilidade e estabilidade. Considerando os resultados obtidos neste trabalho e o potencial apresentado por este tipo de compostos, é importante continuar a estudar as suas propriedades e explorar as suas potencialidades em modelos biológicos mais complexos.

Palavras-chave: tuberculose; líquidos iónicos; sais orgânicos; misturas eutécticas; misturas eutécticas terapêuticas; tecnologia supercrítica com CO_2.

LIST OF PUBLICATIONS

Research Articles:

Monteiro H., **Santos F**., Paiva A., Duarte A.R.C. and Ferreira R.J. Molecular Dynamics studies of therapeutic liquid mixtures and their binding to mycobacteria. Frontiers In Pharmacology (2021). 12 (626735). DOI: 10.3389/fphar.2021.626735.

Roda A., **Santos F.**, Chua Y.Z., Kumar A., Do H.T., Paiva A., Duarte A.R.C. and Held C. Unravelling the nature of citric acid:L-arginine:water mixtures: the bifunctional role of water. Physical Chemistry Chemical Physics (2021). 23: 1706-1717. DOI: 10.1039/D0CP04992A.

Santos F., Branco L.C., Duarte A.R.C. Organic salts based in isoniazid drug: synthesis, bioavailability and cytotoxicity studies. Pharmaceutics (2020). 12 (10): 952. DOI: 10.3390/pharmaceutics12100952.

Roda A., **Santos F.**, Matias A.A., Paiva A. and Duarte A.R.C. Design and processing of drug delivery formulations of therapeutic deep eutectic systems for tuberculosis. Journal of Supercritical Fluids (2020). 161 (104826). DOI: 10.1016/j.supflu.2020.104826.

Santos F., Leitão M.I.P.S., Duarte A.R.C. Properties of therapeutic deep eutectic solvents of L-arginine and ethambutol for tuberculosis treatment. Molecules (2019). 24 (1): 55. DOI: 10.3390/molecules24010055.

Book Chapters:

Santos F. and Duarte A.R.C. Combination drug delivery approaches for tuberculosis - Chapter 10 of Section 1 of Combination drug delivery approach as an effective therapy for

various diseases. Kesharwani P. (editor). 2022, Academic Press, Elsevier. ISBN: 9780323858731.

Santos F. and Duarte A.R.C. Therapeutic deep eutectic systems for the enhancement of drug bioavailability - Chapter 3 of Deep Eutectic Solvents for Medicine, Gas solubilization and Extraction of Natural Substances, Environmental Chemistry for a Sustainable World. Fourmentin S., Costa Gomes M., Lichtfouse E. (editors). 56 (2020), Springer. ISBN: 978-3-030-53069-3. DOI: 10.1007/978-3-030-53069-3_3.

Communications in Conferences:

Filipa Santos and Ana Rita C. Duarte. Using therapeutic liquid mixtures for improve anti-tuberculosis therapy outcome. 15th to 20th August 2021, XXIX International Materials Research Congress, Online Meeting (oral communication).

Filipa Santos and Ana Rita C. Duarte. Solubility, stability and cytotoxic evaluation of different anti-tuberculosis drugs combined in therapeutic liquid mixtures. 15th to 17th June 2021. 2nd International Meeting on Deep Eutectic Systems, Online Meeting (poster communication).

Filipa Santos and Ana Rita C. Duarte. Improving the bioavailability of anti-tuberculosis drugs through deep eutectic systems. 11th to 14th May 2021, 12th World Meeting on Pharmaceutics, Biopharmaceutics and Pharmaceutical Technology, Online Meeting (poster communication).

Filipa Santos and Ana Rita C. Duarte. The potential of therapeutic liquid mixtures on tuberculosis therapy. 15th and 16th February 2021, 1st GREENERING International Conference, Online Meeting (poster communication).

Filipa Santos, Luís C. Branco and Ana Rita C. Duarte. Preparing therapeutic deep eutectic systems for tuberculosis treatment using natural compounds. 28th to 31st July 2019, PSE Meeting – Natural Products in Drug Discovery and Human Health, Lisbon, Portugal (oral communication).

Filipa Santos, Luís C. Branco and Ana Rita C. Duarte. Exploring the properties of therapeutic deep eutectic solvents with isoniazid for tuberculosis treatment. 24th to 27th June 2019, 1st International Meeting on Deep Eutectic Systems, Lisbon, Portugal (poster communication).

Filipa Santos, Luís C. Branco and Ana Rita C. Duarte. Strategies for improving the bioavailability of the anti-tuberculosis drug isoniazid through ionic liquids and deep eutectic solvents. 10th to 13th June 2019, 3rd International Caparica Conference in Antibiotic Resistance, Caparica, Portugal (shotgun presentation).

Filipa Santos, Luís C. Branco and Ana Rita C. Duarte. Tailoring the properties and bioavailability of the anti-tuberculosis drug isoniazid through green approaches. 13th to 17th May 2019, ISGC Symposium, La Rochelle, France (poster communication).

Ana Roda, Filipa Santos, Alexandre Paiva, Ana M. Matias and Ana Rita C. Duarte. Green technologies for design of drug delivery systems for tuberculosis treatment. 13th to 17th May 2019, ISGC Symposium, La Rochelle, France (oral communication).

Ana Roda, Filipa Santos, Alexandre Paiva, Ana M. Matias and Ana Rita C. Duarte. Phase equilibria of pseudo-binary mixtures (THEDES+CO_2) to optimize processing for the design of drug delivery systems aiming tuberculosis treatment. 12th to 16th May 2019, International Conference on Properties and Phase Equilibria for Product and Process Design, Vancouver, Canada (oral communication).

Ana Roda, Filipa Santos, Alexandre Paiva, Ana M. Matias and Ana Rita C. Duarte. Phase equilibria of pseudo-binary mixtures of therapeutic deep eutectic solvents and CO_2 (THEDES+CO_2). 8th to 11th April 2019, 17th European Meeting on Supercritical Fluids, Ciudad Real, Spain (oral communication).

Filipa Santos and Ana Rita C. Duarte. Engineering ethambutol delivery for the treatment of tuberculosis through therapeutic deep eutectic solvents. 26th to 30th August 2018, 7th EuCheMS Chemistry Congress, Liverpool, United Kingdom (oral communication).

Filipa Santos and Ana Rita C. Duarte. Properties of therapeutic deep eutectic solvents with L-arginine and ethambutol for effective treatment of tuberculosis. 13th to 16th May 2018, 3rd Green and Sustainable Chemistry Conference, Berlin, German (oral communication).

TABLE OF CONTENTS

LIST OF FIGURES

LIST OF TABLES

ABBREVIATIONS/ACRONYMS

A

A549	Human alveolar epithelial cell line
ACP	Enoyl-acyl-carrier protein
AMM	Ag85B-MPT64$_{190\text{-}198\text{-}Mtb8.4}$
API	Active pharmaceutical ingredient

B

BCG	Bacillus-Calmette Guérin
BCS	Biopharmaceutics classification system
BSA	Bovine serum albumin

C

CA	Citric acid
Caco-2	Epithelial cell line from human colon cancer
CAT	Catalase
CD	Cyclodextrins
cDNB	1-chloro-2,4-dinitrobenzene
CFU	Colony forming units
CFZ	Clofazimine
COVID-19	Coronavirus disease 2019

D

DES	Deep eutectic solvents/systems

DLS Dynamic light scattering

DMSO Dimethyl sulfoxide

DOTS Directly Observed Treatment Short-Course

DPPC Dipalmitoylphosphatidylcholine

DSC Differential scanning calorimetry

E

EDS Energy dispersive X-ray spectroscopy

EDTA Ethylenedinitrilotetraacetic acid

EE Encapsulation efficiency

EGCG Epigallocatechin

ELISA Enzyme-linked immunosorbent assay

EMB Ethambutol

F

FBS Fetal bovine serum

FDA Food and Drug Administration

FDC Fixed-dose combination

FTIR-ATR Fourier transform infrared spectroscopy with attenuated total reflection

G

GMS Glycerol monostearate

GRAS Generally recognized as safe

GSH Reduced glutathione

GST Glutathione S-transferase

H

H37Rv Susceptible and virulent strain from *Mycobacterium tuberculosis*

HBs Hydrogen-bonds

HBA	Hydrogen bond acceptor
HBD	Hydrogen bond donor
HDT	Host-directed therapies
HEPES	4(2-hydroxyethyl)-1-piperazineethanesulfonic acid
HIV	Human immunodeficiency virus
HPLC	High-performance liquid chromatography

I

ICP-AES	Inductively coupled plasma-atomic emission spectrometer
IFN-γ	Interferon-gamma
IGEPAL®	Octylphenoxy poly(ethyleneoxy)ethanol
IL	Ionic liquid
IL-12	Interleukin-12
INH	Isoniazid; isonicotinic acid hydrazide
[INH][Cl]	Isoniazid chloride
[INH][S-CsO]; [INH][R-CsO]	Isoniazid camphorsulfonate
[INH][GcO]	Isoniazid glycolate
[INH][MsO]	Isoniazid mesylate
[INH][Sac]	Isoniazid saccharinate
[INH][VanO]	Isoniazid vanillate
IR	Infrared spectroscopy

L

L929	Mouse fibroblasts of connective tissue cell line
L-arg	L-arginine
LCA	Life cycle assessment
LPPs	Large porous particles

LTBI	Latent tuberculosis infection
LTTMs	Low transition temperature mixtures
M	
mAGP	Mycolic acid-arabinogalactan-peptidoglycan
MBC	Minimal bactericidal concentration
MD	Molecular dynamics
MDA	Malondialdehyde bis(dimethyl acetal)
MDR-TB	Multidrug-resistant tuberculosis
MEM	Eagle's minimum essential medium
MIC	Minimal inhibitory concentration
MLSD	Multiple ligand simultaneous docking
MMPS	Matrix metalloproteinases
MOI	Multiplicity of infection
MOX	Moxifloxacin
Mtb	*Mycobacterium tuberculosis*
MTS	3-(4,5-dimethylthiazol-2-yl)-5-(3-carboxymethoxyphenyl)-2-(4-sulfophenyl)-2H-tetrazolium
N	
NADES	Natural deep eutectic solvents/systems
NBT	Nitroblue tetrazolium
NMR	Nuclear magnetic resonance
NOESY	Nuclear overhauser effect spectroscopy
O	
OSILs	Organic salts and ionic liquids

P

PAS	*para*-aminosalicylic acid
PBS	Phosphate saline buffer
PC-SAFT	Perturbed-chain statistical associating fluid theory
PDI	Polydispersity index
PES-U	Polyethersulfone
PGA	Polyglycolic acid
PGSS	Particle from gas saturated solution
PLA	Polylactic acid
PLG	Poly(DL-lactide-co-glycolide)
PMA	Phorbol-12-myristate-13-acetate
POM	Polarized optical microscopy
PS	Penicillin and streptomycin
Purpald	4-amino-3-hydrazino-5-mercapto-1,2,4-triazole
PVP	Polyvinylpyrrolidone
PZA	Pyrazinamide

R

RESS	Rapid expansion of supercritical solution
RDF	Radial distribution functions
RFB	Rifabutin
RIF	Rifampicin
ROS	Reactive oxygen species
RPMI 1640	Rosewell Park Memorial Institute 1640 medium
RR-TB	Rifampicin-resistant tuberculosis

S

SAA	Supercritical assisted atomization

SAS	Supercritical anti-solvent
scCO$_2$	Supercritical carbon dioxide
SCF	Supercritical fluid
SD	Standard deviation
SDF	Spatial distribution functions
SDS	Sodium dodecyl sulfate
SEDS	Supercritical enhanced dispersion solution
SEM	Scanning electron microscopy
SLE	Solid-liquid equilibrium
SLNs	Solid lipid nanoparticles
SOD	Superoxide dismutase

T

TB	Tuberculosis
TBA	Thiobarbituric acid
TBARS	Thiobarbituric acid reactive substance
T_c	Crystallization temperature
TCA	Trichloroacetic acid
TDR-TB	Totally drug-resistant tuberculosis
TEER	Transepithelial electrical resistance
T_g	Glass transition temperature
THEDES	Therapeutic deep eutectic solvents/systems
THP-1	Human acute monocytic leukemia cell line
T_m	Melting temperature/ melting point
TMB	3,3',5,5'-tetramethylbenzidine
TNF	Tumor necrosis factor

V

VOCs	Volatile organic compounds

W

WHO	World Health Organization

X

XDR-TB	Extensively drug-resistant tuberculosis
XOD	Xanthine-oxidase

The following chapter was adapted from the publications:

Santos F. and Duarte A.R.C. Combination drug delivery approaches for tuberculosis - Chapter 10 of Section 1 of Combination drug delivery approach as an effective therapy for various diseases. Kesharwani P. (editor). 2022, Academic Press, Elsevier. ISBN: 9780323858731.

Santos F. and Duarte A.R.C. Therapeutic deep eutectic systems for the enhancement of drug bioavailability - Chapter 3 of Deep Eutectic Solvents for Medicine, Gas solubilization and Extraction of Natural Substances, Environmental Chemistry for a Sustainable World. Fourmentin S., Costa Gomes M., Lichtfouse E. (editors). 56 (2020), Springer. ISBN: 978-3-030-53069-3. DOI: 10.1007/978-3-030-53069-3_3.

1

INTRODUCTION

Tuberculosis infection is caused by *Mycobacterium tuberculosis* (*Mtb*) which had its outbreak in the 1800s. Although it is considered a curable and preventive disease, it is still reported by the World Health Organization (WHO) as one of the deadliest infections worldwide, that killed an average of 1.3 million people in 2020. Tuberculosis (TB) presents a higher incidence in regions under development, with a poor health care system and characterized by poverty, economic distress, marginalization and vulnerability.[1]

The WHO established policies to promote a decrease of the number of cases of tuberculosis and prevent deaths triggered by this infection. In this sense, they encouraged the investigation of new drugs for TB treatment as well as more effective therapies.[2] The increase of drug resistance to anti-TB drugs, mainly the ones that are used as first-line treatment, makes it crucial to find sustainable strategies for the delivery of these drugs, decreasing the time of the treatment and side effects and increasing the compliance to the treatment by the patients, thus reducing drug resistance.

One possible approach that could be envisaged to improve existing drugs and its formulations as well as to create new alternatives for drug delivery of anti-TB drugs, is the investigation of green and sustainable chemistry strategies. In the last decades, green chemistry has been studied for pharmaceutical applications and could add innovative and sustainable paths for the research of effective forms of drug delivery and/or improve the properties of active pharmaceutical ingredients (APIs). Sustainability in the pharmaceutical industry is, nowadays, an essential point to take into consideration, due to the possibility of reducing manufacturing costs and the risk of environmental contamination while producing safer products that contribute to the decrease of their toxicity to human health.[3–7] The research on green solvents has been one of the most active areas in green chemistry research,

representing alternatives to organic solvents that usually produce large amounts of mass waste in synthetic processes, present high toxicity, flammability and can also be corrosive.[8] The implementation of processes that avoid the use of these solvents and encourage the use of alternative solvents such as water, supercritical fluids, ionic liquids and, more recently, deep eutectic systems are now taken into consideration by industry and research for improvements in industrial processes, research methods, and formulations.[8,9] Concerning TB infections and drug delivery of anti-TB drugs, green chemistry is an important field that is being explored and has recently seen more developments for targeting *Mtb*.

1.1 Tuberculosis

Tuberculosis is described as an ancient plague that exists since known human history and it is characterized by its epidemic cycles with emergent outbreaks that then recede (Figure 1.1).[10–16] Molecular genetic techniques estimated that *Mtb* appeared in East Africa about 3 million years ago, and according to the rate of mutation analysis, the current diversity of strains was originated about 250 to 1000 years ago.[10,14,15] Before Johann Lucas Schönlein named tuberculosis in 1839, TB was known by different names, for example, in ancient Hebrew it was called *schachepheth*[10] and in Greece it was named *phthisis*.[10,15,17] Later on, between 1600-1800, TB was also called *the white plague*, *consumption*, *captain of all these men* and *scrofula*.[10,15]

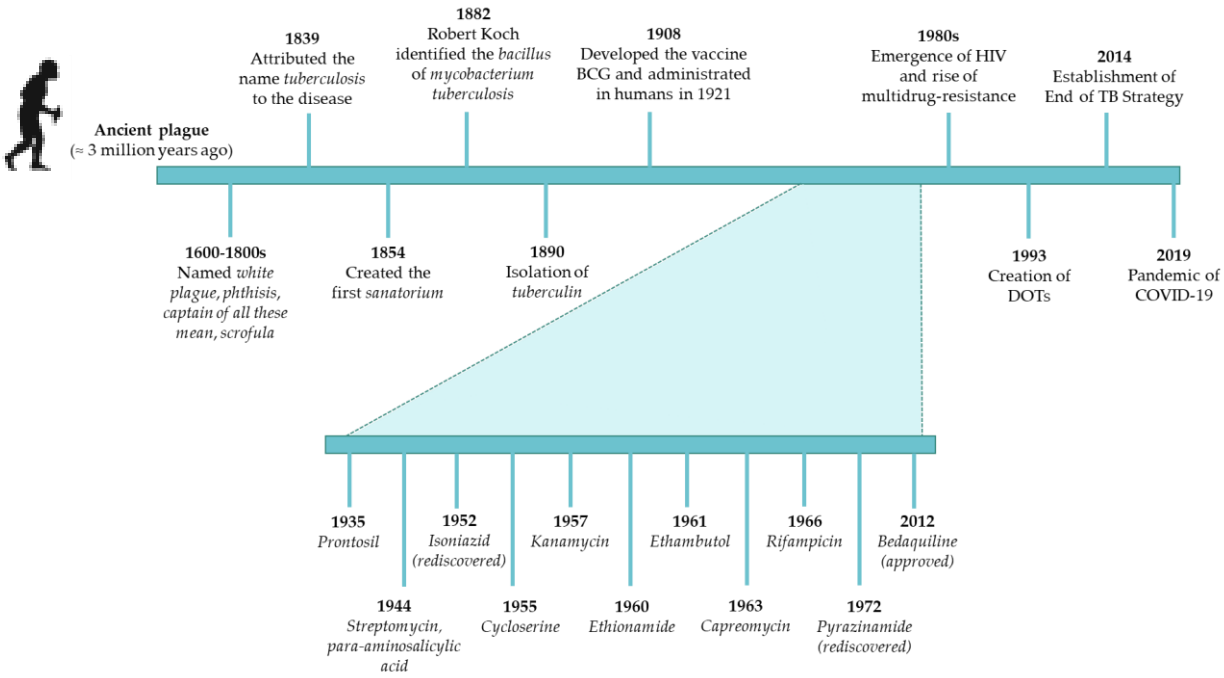

Figure 1.1 - Throwback from some of the relevant points along with the history of tuberculosis. (Created with BioRender.com)[10–16]

In 1882, the doctor and microbiologist Robert Koch identified and described the bacillus of *Mtb*, which became known as *Koch bacillus*. Its discovery changed the history of the disease since it directed the research towards the development of a treatment.[10,11,18–21] Then, in 1890, Koch isolated a substance from TB bacillus that he described as "render harmless the pathogenic bacteria that are found in a living body and do this without disadvantage to the body", and named it tuberculin (purified protein derivative used for the diagnosis of TB).[18,21]

In 1854, the first *sanatorium* was created by Hermann Brehmer, medical facilities that were constructed throughout the world to control and treat the different forms of tuberculosis disease.[15,19] Later, in 1908, a vaccine, Bacillus-Calmette Guérin (BCG) factor was developed. This was the first immunizing agent for tuberculosis infection, yet only used on humans in 1921.[13,15,20] Around the 1940s, effective drugs to treat TB started to appear,[11] and the existence of *sanatoriums* became unessential, which lead to their closure in the middle of the 1960s.[15,18]

After the discovery of antibiotics, in 1929, scientists started to explore these chemotherapeutic substances for the treatment of TB and the first candidate, presented in

1935, was Prontosil (sulfonamide). However, it was considered too toxic to administrate in humans.[15] Then, in 1944, Albert Schatz, Elizabeth Bugia and Selaman Waksman discovered streptomycin, and the co-workers Hinshaw and Feldman tested this new antibiotic in guinea pigs infected with virulent *Mtb*, obtaining promising results and achieving approval for its use in the treatment of TB.[15,19,22] In the meantime, the researcher Jörgen Lehmann reported a new chemical agent that would be capable to feed the *tubercle bacillus* and lead to its death. This compound became known as *para*-aminosalicylic acid (PAS), which was also approved for TB treatment.[15,19,22] Although streptomycin and PAS were effective in TB treatment, they presented several side effects, and when administered alone, caused the development of drug resistance. This lead medical research centers to conclude that to treat active TB, a combination of drugs should be used instead of a single drug.[19]

Later, one of the most effective agents against *Mtb* was discovered, isoniazid (INH), which is still used nowadays as one of the first-line drugs to treat TB. INH was firstly synthesized in 1912, but it was not used until 1952, when its potential use in TB disease was discovered. Further, this drug represented a huge advance in the treatment of TB, since it was considered the most potent, well-tolerated and safe drug introduced in TB therapy. However, just like the previously described agents for TB therapy, the single administration of INH does not avoid drug resistance and has also to be used in combination therapy.[15,19,22] Later, a multidrug therapy was introduced for the treatment of all TB forms, combining the oral administration of INH and PAS, from 18 to 24 months with the intramuscular administration of streptomycin during the first 6 months. Although this "triple therapy" had been a success for almost 15 years, the severity of the side effects and the increase of drug resistance to these drugs led to the research and development of other antibiotics that could be effective in TB, such as ethambutol (EMB), reported in 1961.[15] EMB is considered an effective therapeutic agent in organisms that were resistant to INH and streptomycin. Furthermore, in 1966, rifampicin (RIF) was introduced in TB therapy and by combination with INH and EMB, allowed to decrease the time of treatment to 9 months.[15,19] Pyrazinamide (PZA) was also introduced in TB therapy, when it was discovered that it could shorten TB therapy to 6 months, by combination with INH and RIF. More antibiotics with anti-TB activity were reported along this time, such as cycloserine (1955), kanamycin (1957), ethionamide (1960) and capreomycin (1963) that were considered important to treat cases of drug-resistant TB.[19,22] Nevertheless, after rifamycins, the discovery and introduction of new anti-TB drugs stopped for more than 40 years, and it was only in 2012 that a new drug,

bedaquiline, was reported for the treatment of TB in cases of multidrug resistance,[23,24] followed by other drugs, such as delamanid, pretonamid and linezolid. Meanwhile, these entered in clinical trials for TB therapy.[25]

In the 19th century, the progress in research and knowledge on TB led to the decline of morbidity and mortality rates,[10,15] and the study of new drugs slowed down. Yet, the appearance of tuberculosis resistant strains and human immunodeficiency virus (HIV), in the 1980s, caused once again an increase in the rates of morbidity and mortality. Therefore, a new interest from health authorities to finance and encourage research for new drugs has arisen, not only focused on the design of more effective drug delivery combinations, but also investing in the discovery of alternatives to control and prevent TB.[10,11,18] In 1993, the WHO created the Directly Observed Treatment Short-Course (DOTS), a program to control the TB epidemic disease.[15,26] Later, in 2014, the WHO established a strategy to control and end TB by 2035, the so-called "End TB Strategy".[1,27,28]

Even though TB can affect everyone and all age groups, people from low-middle income-countries[1,15] accounts for approximately 90% of all TB cases worldwide.[1,18] These are more susceptible to TB, particularly in South-East Asia (43%), Africa (25%) and Western Pacific (18%), which represent the majority of cases, against 8.3% in Eastern Mediterranean, 3% in America and 2.3% in Europe.[1]

TB has changed along with history, being dormant or active for different periods. It seems to be more active in areas with high population density, during periods of industrialization, migration, economic distress and in places where starvation, poverty, vulnerability and lack of access to healthcare and social protection still prevail.[1,12,15] Globally, in 2020, 9.9 million cases of TB were estimated, a number that has been decreasing very slowly in the last years. From this, around 1.3 million of deaths by TB were reported and more than 214 000 deaths were HIV-positive. In 2020, male adults accounted for 56% of the cases of TB infection, women for 33% and children for 11%.[1] Some of the risk factors that can contribute to an increase in the people's vulnerability to TB are drug addiction, alcoholism, smoking, undernourishment, chronic diseases, lung parenchyma abnormalities, polymorphism in vitamin D receptors or *IL-12* and *IFN-γ* genes, a compromised immune system (e.g., HIV, cancer, leukemia) and therapeutics with drugs that could weak/suppress the immune system (e.g., long-term use of corticosteroids, TNF-α blockers).[18,29]

Drug resistance continues to present a high prevalence, mainly for drugs used as first-line treatment. Besides drug resistance to anti-TB drugs, the arising of a pandemic

disease (e.g., coronavirus disease 2019 (COVID-19)), led to a reversal of the progress in the falling rates of global TB incidence, contributing to an increase in the number of TB cases and deaths.[1]

1.2 Mechanism of tuberculosis disease

Tuberculosis infection is spread by inhalation of infectious aerosol particles (e.g., by coughing, sneezing, or speaking). The bacteria are transmitted from person-to-person contact as represented in Figure 1.2,[18,20,30] and through the use of contaminated material, consumption of contaminated food and transfusion of infected blood.[30] The *Mtb* is an aerobic, filamentous, nonmotile, rod-shaped, weakly gram-positive and acid-fast bacillus.[30–32]

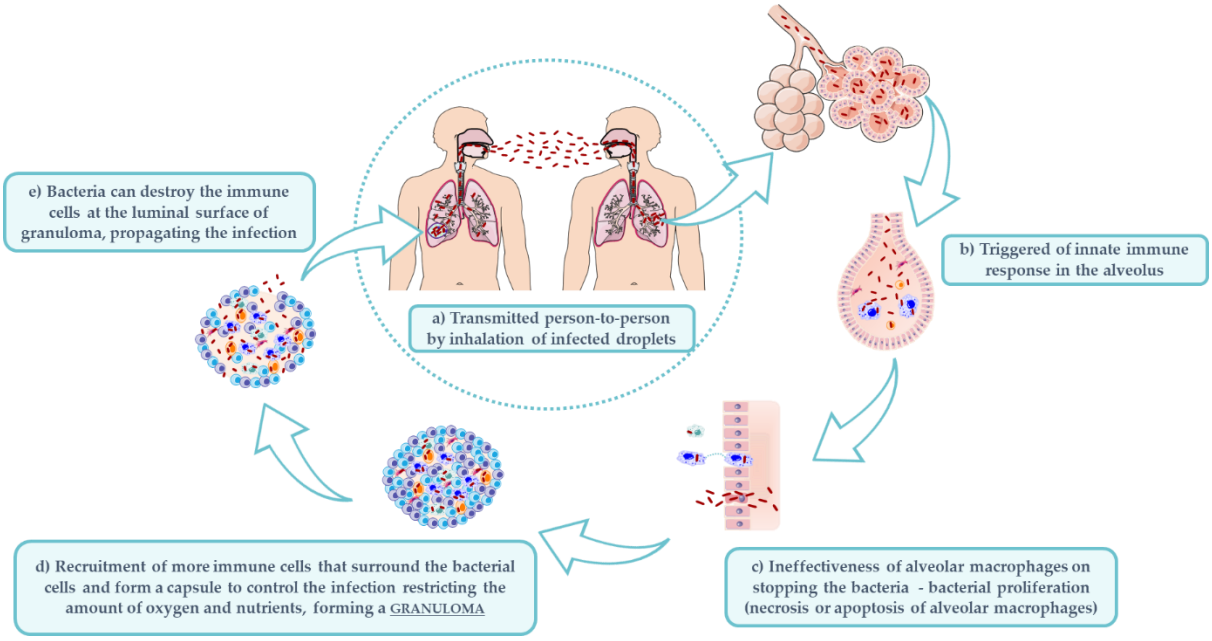

Figure 1.2 - Pathogenesis mechanisms of tuberculosis infection. **a)** TB is transmitted from person-to-person. **b)** An innate immune response is triggered (alveolar macrophages recruited to phagocyte the bacilli). **c)** Ineffectiveness of macrophages to block the bacteria can occur, which leads to bacterial proliferation (necrosis or apoptosis of alveolar macrophages). **d)** Bacteria spread to alveolar tissues and replicate, which leads to an increase of immune response that surrounds those bacterial cells and forms a capsule to control the infection and restrict the amount of oxygen and nutrients – **Granuloma**. **e)** A suppression of the immunological system can occur and bacteria destroy the immune cells and replicate to further tissues, propagating the infection. (Created with smart.servier.com)[18,20,30]

When a person inhales an infected droplet with *Mtb*, the bacteria faces the mucus secreting goblet cells localized in the upper airways that will trap the bacteria.[30] The ones that can escape from the mucociliary system silt on the alveolus and trigger an innate immune response. The alveolar macrophages are recruited to internalize and phagocyte the bacilli in the site of infection, where replication of bacteria occurs, which will inhibit the growth and propagation of the infection to the whole body. However, the alveolar macrophages can be ineffective in destroying the bacilli and survive to the first interaction with immune cells, blocking the fusion of the phagosome with lysosome and allow intracellular bacterial proliferation that could lead to necrosis and/or apoptosis of the alveolar macrophages, which allows the bacteria to escape and spread to alveolar tissues.[16,18,20,33] Hence, the bacteria continue to replicate in extracellular airspace, and immune cells such as dendritic cells, macrophages, and monocytes are recruited and release pro-inflammatory cytokines and tumor necrosis factor (TNF), which permeabilize the vascular endothelium inducing the recruitment of additional immune cells to the infection site.[18,20] These cells will form an early granuloma that is characterized by a group of immune cells (epithelioid macrophages, dendritic cells and polymorphonuclear leukocytes), that surround the bacterial cells and form a capsule that to control the infection and prevent it from progressing by restricting the amount of oxygen and nutrients.[18,20,31,34] The high lipid content presented by the wall of bacteria[30] allows its survival, inside the granuloma, in a dormant stage which limits the bacterial cell wall synthesis, cell division and dependence of aerobic respiration.[34] This stage that remain controlled for many years or a lifetime, is being called latent tuberculosis infection (LTBI). Yet, if a suppression of the immune system of the individual occurs, the granuloma can be destroyed by the bacterial population at the luminal surface and replicate toward further tissues, propagating the infection and causing active TB disease.[18,20,31]

The LTBI stage of infection is characterized by an asymptomatic and non-transmissible infection. However, when it progresses to an active stage of infection, it becomes contagious and it can present different symptoms such as fever, fatigue, lack of appetite, weight loss, persistent cough and pulmonary disease.[18,21,31] The risk that people infected with *Mtb* in the latent stage progress to active disease is between 5-15%, and depends on changes in the immune system, presence of comorbidities and genetic mutations.[20,30,35,36] When a dysregulation through immune cells occurs and bacterial cells proliferate, this leads to the formation of caseous necrosis lesions that accumulate, enlarge

and merge inducing secretion of host matrix metalloproteinases (MMPs), which modulate the immune chemokines. These lesions could proliferate to larger respiratory airways discharging the liquefied necrotic *caseum* into the bronchia and proliferate into the lungs (pulmonary TB) and/or other organs, spreading through lymph nodes and bloodstream (extrapulmonary TB), and presenting different symptoms depending on the organ affected.[18,35] Once the bacteria break the granuloma and it becomes able to multiply to other parts of the lung the transmission to other individuals through aerosolization becomes active.[18,20]

1.3 Current treatment, limitations, and drug-resistance

As mentioned before, the first way of immunizing people and prevent tuberculosis disease is to administrate the BCG vaccine. This vaccine was developed more than 100 years ago and is effective for the prevention of severe forms of TB in children. However, until now, no vaccine is effective in preventing TB in adults, either before or after exposure to TB infection.[1] Anti-TB drugs started to be investigated in the 1940s and 1960s, and it was established, a treatment that combines four anti-TB drugs (INH, EMB, PZA and RIF), requiring their administration for several months (minimum 6 months). This drug regimen used for treating tuberculosis is still the combination of drugs that is used as first-line treatment of TB and it is considered the most effective treatment available.[1,30]

As a measure to end TB, the WHO has established regimens of drugs that should be prescribed to people with TB infection, who present a higher risk of developing tuberculosis disease and becoming infectious, after initial infection.[1,37] The risk of progression for active TB disease after infection depends on numerous factors, yet the most significant is the weakness of the immunological system.[37,38] Therefore, HIV-positive individuals, people in contact with TB patients, people who receive treatment with drugs that could affect the immune system (anti-TNF treatment, dialysis), patients preparing for organ transplantation, recent immigrants from countries with a high TB burden and people with other comorbidities that could cause immunodeficiency, present a higher risk of developing TB disease, which make them a priority for receiving TB preventive treatments, as presented in Table 1.1.[21,37]

Table 1.1 - Current approaches approved for preventive care and treatment of tuberculosis.[21,35,37]

PREVENTIVE REGIMENS			TREATMENT DRUGS	
Drugs	**Time of treatment**	**Applications**		**Drugs**
INH	6 months (daily)	-HIV infected children doing protease inhibitor-based regimen, nevirapine or integrase inhibitors -Confirmed isoniazid-susceptible people and rifampicin-resistant	First-line anti-TB drugs	Isoniazid Rifapentine Rifampicin Rifabutin Pyrazinamide Ethambutol
INH + Rifapentine	3 months (weekly) or 1 month (daily)	-Shorter regimens duration preferred: prisoners for short-term, patients that started anti-TNF therapy and preparing for transplantation	Second-line anti-TB drugs	Streptomycin Ofloxacin Kanamycin Gatifloxacin Amikacin *p*-aminosalicylic acid Capreomycin Cycloserine Viomycin Terizidone Ciprofloxacin Ethionamide Levofloxacin Prothionamide Moxifloxacin Thioacetazone
INH + RIF	3 months (daily)	-Children	Third-line anti-TB drugs	Clofazimine Bedaquiline Linezolid Clarithromycin Amoxicillin + Clavulanate Imipenem + Cilastin
RIF	4 months (daily)	-Confirmed rifampicin-susceptible people and isoniazid-resistant	New/Clinical trials anti-TB drugs	Delamanid Sutezolid Pretonamid
INH + Pyridoxine + Cotrimazole	6 months (daily)	-HIV-positive when shorter regimens are not available and drug-drug interactions occur	Clinical trial vaccines	VPM1002 MIP/Immuvac

Along the years, the control of TB has faced challenges in the implementation of several measures and the use of numerous drugs and their combinations for the treatment and control of this disease. To achieve faster reductions in TB incidence and deaths, advances in the access to diagnosis and care are necessary at universal scale. There is also the need to develop new treatments and/or a vaccine that could reduce significantly the risk of developing TB.[1] At the same time, it is essential to implement active policies for the notification and report of detected TB cases by health care workers, and invest in health care systems that could respond to the necessities of patients with TB infection.[1]

One of the major concerns in TB treatment and prevention is related to drug resistance, which can emerge by spontaneous mutations of bacteria, and trigger resistance to one or more effective anti-TB drugs, like the ones that are administered as first-line treatment such as INH and RIF (multidrug-resistant tuberculosis, MDR-TB or rifampicin-resistant tuberculosis, RR-TB).[21,26,32] This problem can be even more serious when drug resistance to second-line anti-TB drugs occurs. These drugs are used in cases where MDR-TB persists, and this type of resistance is called extensively drug-resistant tuberculosis (XDR-TB).[1,21,32,39,40] The worst-case scenario is when the bacteria do not respond to either first or second-line anti-TB drugs, and in this case, it is named totally drug-resistant tuberculosis (TDR-TB),[40,41] although this term is still not recognized by WHO. These situations leave patients without many additional treatment options that are safe and effective.[1,2] Moreover, drugs used in the second and third-lines of treatment are, in general, less effective, more toxic and comprise higher costs as the time of treatment will increase with these drugs, for approximately 18- 20 months.[21,35]

Another limitation related to TB treatment includes the incidence of serious adverse effects of anti-TB drugs (e.g., hepatotoxicity, gastrointestinal disorders, allergic reactions, peripheral neuropathy, central nervous system toxicity, gout, ocular toxicity).[2,31] This adds to what was previously described, further contributes to the poor treatment compliance and therefore to drug resistance. The existing therapy presents a limited capability to enter in the granuloma,[30] allowing the bacteria to stay dormant at a low metabolic rate; also the dormancy of the bacteria in a deep location in pulmonary cavities difficults drugs to reach them and penetrate these cavities, limiting the action of the antibiotics and also contributing to their inefficacy and drug resistance.[21,34,35]

Additionally, the *Mtb* cell wall presents an unusual structure with low permeability, which prevents the entrance of therapeutic agents, and contributes to create resistance to its action.[16,42,43] The cell envelope that mediates the boundary between the host and bacteria, and regulates which immune factors will be produced and released, is essential for defining the stage of infection.[16,42,44] The *Mtb* cell envelope is composed by the cytoplasmatic membrane, cell wall and surface lipids. The cell wall presents two parts, with peptidoglycan covalently attached to arabinogalactan that is, on its turn, attached to mycolic acids and forms a cell wall core with the mycolic acid-arabinogalactan-peptidoglycan (mAGP) complex.[16,34,36,44,45] Dispersed inside the cell wall are proteins, phosphatidylinositol mannosides, phthiocerol-containing lipids, lipomannan and lipoarabinomannan that are dissolved when the cell wall

is disrupted. Contrarily, the mAGP complex stays as an insoluble residue for lipids, proteins and lipoglycans, signalling the effector molecules during the disease. Yet, the insoluble part contributes to the viability of the bacteria and is very important to consider for drug development.[34,36,42]

Regarding the anti-TB drugs used as first-line treatment as well as their mechanisms of action and drug resistance, it is observed that INH and EMB, for example, have an important role in the inhibition of cell envelope synthesis. INH prevents the synthesis of mycolic acids of the cell wall when activated by katG enzyme, that inhibits the *inhA* gene, consequently, mutations that occur in *katG* and *inhA* genes will contribute to turning bacteria resistant to INH. EMB also inhibit the cell wall synthesis through inhibition of arabinosyl transferase (arabinose acceptor), and it can suffer from mutations in the *embCAB* operon that facilitates the production of the arabinose acceptor. In turn, rifamycins are a group of anti-TB drugs that limit the synthesis of nucleic acids by inhibiting the RNA polymerase and mutations that could cause drug resistance occurs in *rpoB* gene. PZA, the other anti-TB drug used in the first-line treatment of TB, disrupts plasma membranes by binding to mRNA in bacteria, and the mutation that can turn the bacteria resistant to PZA occurs in the genes *rpsA* and *pncA*.[21,31,46] The low levels of drugs reaching the target, due to insufficient bioavailability or malabsorption, can also contribute to drug resistance. Moreover, the continued use of the same combination of drugs may not reach different bacteria populations that already accumulate some mutations and do not respond to these drug combinations. The anti-TB drugs used as the second and third-line treatment present similar mechanisms of action to the first-line anti-TB drugs, however they are used in cases of multidrug resistance to first-line drugs due to their higher toxicity.[21]

The concomitant infection of TB and HIV requires the use of both anti-TB and anti-retroviral therapies, which increases the survival of HIV-infected individuals, but it also increases the risk of drug interactions, for example, between rifamycins, protease inhibitors and non-nucleoside reverse transcriptase inhibitors. Since rifamycins induce liver enzymes and decrease the serum concentrations of protease inhibitors (indinavir, nelfinavir, saquinavir, ritonavir, amprenavir, atazanavir, fosamprenavir), rifabutin (RFB) is presented as an alternative in patients that are taking anti-retroviral drugs, since it is also an inducer of liver enzymes but less potent.[21]

Treatment failures and the emergence of multidrug resistance are some of the challenges that are presented when treating TB. Along the years, researchers have been

investigating and developing new forms to combat drug resistance, decrease the treatment duration and frequency of dosing, reducing the adverse effects, toxicity and drug interactions.[32] Another regimen of drug administration that has been adopted, in the last years, attempting to increase patient compliance to TB therapy, is based on the use of fixed-dose combination (FDC) therapies that combine a list of two or more anti-TB drugs. The FDC was suggested to simplify the dose scheme of therapeutics and minimize resistance associated to RIF monotherapy.[32]

Continuous search for a treatment that could be easily administrated and still be effective on TB, with rapid reduction of TB incidence worldwide, achieving the levels observed in developed countries, where TB is considered a disease of the past, is the main goal of the targeted research.[1,12,31] It is also under investigation the use of new approaches for "old" anti-TB drugs or other drug classes that could present positive effects in TB therapy (Table 1.2). These could be, for example, more effective, and present different routes of administration, new schemes of treatment or different combinations that could reduce the time of treatment or even overcome drug resistance problems. Overall, the current research lines emphasize the effectiveness in the prevention and treatment of TB infection, avoidance of disease progression, and development of an effective vaccine for all age groups.

Table 1.2 - Studies that report different drugs and adjuvants that could be used in TB therapy.

Drugs	Effect on *Mycobacterium tuberculosis*	Reference
Imatinib	A tyrosine kinase inhibitor that reduces the bacteria accumulation in the lung and granulomatous lesions. Demonstrated to be effective against RR-TB strains when co-administered with current first-line anti-TB drugs.	38, 47
Gefitinib	An inhibitor of the epidermal growth factor receptor that demonstrates the ability to inhibit the *Mtb* growth in macrophages, reducing mycobacterial replication in the lungs.	34
Non-steroidal anti-inflammatory and analgesic drugs	Reduce the bacteria accumulation in the lungs and reduce existing lesions.	38, 48–52
Verapamil **Reserpine**	Efflux pumps inhibitory properties and decreases macrophage-induced drug tolerance.	54, 55
Ivermectin	Demonstrated bactericidal activity against *Mtb*.	53
Cilostazol **Sildenafil**	Accelerates bacteria clearance and reduce the time of treatment.	54
Lansoprazole	Effective against intracellular *Mtb*.	55
Metformin	Inhibits bacteria growth, promoting phagolysosome fusion and increasing mitochondrial ROS production.	38, 56
Vitamin D	High single dose supplementation promotes faster recovery and improves the health-related quality of life of TB patients. Triggers anti-inflammatory response in macrophages, restricting bacteria growth and acts as a regulator of the innate immune response.	37, 38, 57–59
L-Arginine	Beneficial when used in the treatment of active TB, by mediating the production of nitric oxide.	60, 61

1.4 Formulations and drug delivery routes for tuberculosis treatment

TB infection is spread through aerosol particles with an aerodynamic diameter smaller than 5 μm, that holds 1-3 bacterial cells.[20] The current formulations used in TB treatment are mainly for oral, intravenous or intramuscular administration, and some formulations include more than one anti-TB drug in the same formula. The small size of the infected droplets enables the deposition of the bacterial cells in the alveolus of the lungs instead of other tissues that are localized in higher airways.[20] One of the problems associated

with current therapy used for TB is the limited ability of the drugs to reach and enter the granulomas, which make them less effective in dormant bacilli.[34,62]

Several approaches have been studied in a quest for constant improvement of TB therapy and the carrier for delivering these drugs is one of them, as they may enhance the bioavailability of the drugs and allow possible target-specificity. The carriers are, in general, polymeric matrices, classified as natural (e.g., alginic acid, chitosan, gelatin, dextrin, guar-gum) or synthetic (e.g., polylactic acid (PLA), polyglycolic acid (PGA), poly(DL-lactide-co-glycolide)(PLG), carbomer, polyanhydride, polymethyl acrylate).[30,38] The existence of this wide variety of carriers opens many possibilities for the design of different delivery systems with adequate requirements for drug and target-specificity. Several studies in recent years have been done envisaging the encapsulation of anti-TB drugs aiming to present an efficient and controlled release of the drugs through different routes of administration.[30,32,63] The use of colloidal drug carriers for TB therapy represents an alternative to conventional therapy that demonstrates numerous advantages, such as better systemic bioavailability, fast therapeutic action, avoidance of first-pass metabolism, sustained and controlled release and a decreased dosing frequency.[30] Some of the colloidal drug delivery systems developed over the years include liposomes, nanoparticles, microparticles, niosomes, polymeric micelles, solid lipid nanoparticles (SLNs), dendrimers, cyclodextrin inclusion complexes, nanosuspensions and nanoemulsions.[30]

Another key factor for the formulation of drugs is the excipient used, that facilitates the preparation and administration of the drugs, allowing a consistent drug release and protecting it from degradation. These substances are not always inert, and they can influence the rate or extent of drug absorption and then determine the bioavailability of the drug.[39] In this context, when designing a formulation, the rule of four "D's" (drug, destination, disease and delivery) is considered to reach the maximum therapeutic effect.[39]

Over the years, with the evolution of knowledge about TB infection mechanisms and the constant improvement of new technologies applied to biomedicine, a crescent investment in research of new formulations and administration routes of anti-TB drugs is observed, in an attempt to reach a more effective therapy, which includes the use of micro and nanotechnology for encapsulation of drugs, for example.

1.4.1 Oral administration

The oral administration route is the most common route for drug delivery, due to the fact that is less expensive, simple and easily self-administrated by the patient.[35,64] Nevertheless, the oral administration of anti-TB drugs requires prolonged administration with high drug doses to reach the site of infection, given the fact that they have to surpass the hepatic first-pass metabolism and the gastrointestinal environment, that difficult the absorption.[30,35,62,65]

The drugs administered orally must pass through the gastrointestinal tract, to be absorbed in its lumen and cross gastrointestinal mucosa, capillaries of the small and large intestine, via the liver portal venous system, and then throughout the body, although some drugs could be absorbed by the lymphatic system or distal rectum.[35,66] Despite the oral route presenting advantages in terms of easiness of administration, as well as it supplying a large surface area of absorption, it may also present problems related to stability, permeability and solubility of drugs.[35,67] When a drug is orally administered it faces several barriers present in the oral cavity (saliva and digestive enzymes), esophagus (gastroesophageal reflux), stomach (digestive enzymes and acidic environment), pancreas (digestive enzymes in alkaline fluid), small intestine (bacteria, bile salts and enzyme degradation), large intestine (low absorption and dissolution, luminal pressure and microbial flora) and anus (luminal pressure).[35] Consequently, pharmaceutical research focus on finding alternatives that could alter oral dosage forms (e.g., FDC of different drugs), use alternative systems for drug delivery (e.g., micro- and nanocarriers; prodrugs; add absorption enhancers and/or enzyme inhibitors; hydrogels; mucoadhesive systems; cyclodextrins; low transition temperature mixtures) or even investigate alternative administration routes of the same drugs to overcome the physiological barriers imposed by the gastrointestinal tract.[35,67,68]

Other factors that have to be taken into account when developing drugs for oral delivery are the inherent physicochemical barriers of the drugs, such as molecular weight, pH stability, hydrophobicity, molecular size, ionization constant and the biological barriers, for instance, the presence of different digestive enzymes, proteolysis in the stomach, low permeability and membrane efflux.[68]

In oral TB therapy (Table 1.3), it is common that drugs are formulated alone and then co-administered or otherwise, formulated in FDC formulations to increase the patient compliance. However, combining different antibiotics in the same formulation, may present problems related to the stability of the formulation before and after the administration. RIF,

for example, besides being a hydrophobic drug, when administered with INH has proven efficacy in TB therapy. However, when administered in the same formulation through the oral route, due to the acidic pH of the tract, INH promotes the hydrolysis of RIF.[63,69] Avachat and co-workers studied the stability of RIF in the presence of INH and observed an acidic degradation of RIF that was enhanced by concentrations of INH higher than 25% (w/v).[69,70] To minimize these effects, it is important to have formulations that allow a controlled and targeted release of the drugs in the gastrointestinal tract, since RIF is better absorbed in the stomach and INH in the intestine.[69,71] Some approaches have been used for the oral administration of these two drugs, at the same time, are formulations of compressed bilayer tablets[71,72] and/or gastroretentive tablets of RIF combined with entero-coated INH capsules, allowing the formation of a compartmentalized delivery system with physical isolation of anti-TB drugs.[71] Another reported interaction between anti-TB drugs administered by oral route occurs with EMB and RIF in patients with HIV, who present a lower intestinal absorption.[32] Additionally, when administered in FDC, EMB proves to be unstable in the presence of other anti-TB drugs.[32]

Table 1.3 - Examples of studies presenting formulations for oral delivery of anti-TB drugs.

Drugs	Formulation/System	Study/Therapeutic improvement	Reference
RIF	Polymeric nanoparticles	Entrap a combination of RIF-curcumin into polymeric nanoparticles for high uptake of drugs at the site of infection.	[73]
INH	3D-printed tablets	Different formulations containing INH that allows personalized and adjustment of dosage forms.	[74]
INH	Lipid-drug conjugate nanoparticles	Treatment of extrapulmonary infections.	[75]
INH	SLNs	Improve oral bioavailability of INH.	[76]
INH + PZA + RIF	Polymeric nanoparticles	Development of polymeric nanoparticles for the administration of anti-TB drugs and reduce the dose frequency and better management of TB.	[77]
INH	Hydrogels	Development of blend hydrogel microspheres for controlled release of INH.	[78]
INH + RIF	Nanogels	Nanogels with INH and RIF reduce the cytotoxicity of these drugs in the digestive tract.	[79]

1.4.2 Parenteral administration

The parenteral administration route avoids the major problems associated with the gastrointestinal tract and usually includes injectable forms for intravenous, intramuscular, subcutaneous, intradermal, intrapleural, intra-arterial, intraperitoneal and intrathecal administration. Apart from injectable formulations, the parenteral forms also include biodegradable implants, transdermal patches and ocular systems.[80] The injectable formulations present useful advantages when it is necessary to have a rapid onset of action, administrate mixtures of APIs and when patients cannot take the oral form or are unconscious.[80] In turn, the parenteral administration is considered to have higher bioavailability than the oral route, presents the advantage of not suffering from first-pass metabolism, avoids the acidic environment in the stomach, enables the delivery of molecules with low gastrointestinal absorption and reaches faster the target-site.[80] Nonetheless, the injectable formulations are, usually, not self-administrated and their administration can be painful, requiring the presence of healthcare workers. Furthermore, due to fast clearance in the body, it can cause a higher frequency of dosing too, depending on the parenteral delivery applied.[35,62,81] For instance, intravenous delivery presents a faster delivery than subcutaneous or intramuscular. The parenteral administration of drugs has been explored for targeted delivery, yet it is, in general, a route of administration more invasive and the systemic exposure could more easily lead to toxic doses.[63]

The formulations usually prepared for injectable administration are presented as solutions, suspensions or emulsions,[80] however, to improve the efficiency and circumvent some of the problems of parenteral formulations, the use of other forms have been investigated. In this context, the use of nanoparticles (e.g., liposomes, nanoemulsions, solid lipid nanoparticles[82]) has been reported to enhance the solubility of poorly water-soluble drugs, thus improving the bioavailability and absorption, and achieving a controlled, prolonged and target release, drug protection, and lower toxicity, by manipulating the surface of the particles and the carriers used, for example.[80,83,84]

Regarding TB therapy, there are injectable formulations for the delivery of anti-TB drugs (Table 1.4), however, normally, these formulations are not considered the first option in drug regimens for the treatment of TB. The investigation of formulations with better efficiency and which are less invasive continues. An example is the use of nanotechnology to improve drug efficacy and search for alternative forms of administration (e.g., transdermal or buccal delivery), that can also be used in children. Since they usually have difficulty

swallowing tablets, frequently the formulations have to be crushed and/or mixed with food to facilitate the administration. These practices could lead to errors in dosage, consequently reducing the therapeutic effect or causing toxicity.[85] The buccal delivery of anti-TB drugs is presented as an easy way to administrate drugs as well as to prevent gastric environment, and increase patients compliance to the treatment. Also, it does not require potable water for administration or reconstitution, being instantly disintegrated in the mouth.[85]

Table 1.4 - Examples of studies presenting formulations for parenteral delivery of anti-TB drugs.

Drugs	Formulation/System	Study/Therapeutic improvement	Reference
EMB	Niosomes	Encapsulation of ethambutol hydrochloride in niosomal formulations to improve the efficacy and safety compared with free drug.	[86]
PZA	Liposomes	Encapsulate PZA in liposomes to enhance targeting properties and monitor intracellular degradation of PZA.	[87]
Ag85B-MPT64$_{190\text{-}198\text{-}Mtb8.4}$ (AMM)	Microspheres	Chitosan microspheres with a fusion polypeptide to induce an immune response against *Mtb* antigens.	[88]
RIF	Nanoparticles	Preparation of RIF-loaded nanoparticles with MPEO$_{5k}$-b-PCL$_{4k}$ for evaluation of their pharmacokinetic and biorelevance in clinic.	[89]
INH	Orodispersible strips	Orodispersible strips loaded with INH for buccal absorption.	[90]
INH	Orodispersible films	Orodispersible films for the administration of INH in children.	[85]
RIF + INH + PZA + EMB	Hydrogel-forming microneedles	Development of hydrogel-forming microneedles reservoirs for delivering high doses of first-line treatment anti-TB drugs.	[91]

1.4.3 Pulmonary administration

The administration of drugs through the pulmonary route avoids first-pass metabolism and the gastrointestinal tract (acidic environments)[62] however, the pulmonary route of administration involves some challenges too, due to the barriers that the pulmonary system presents (e.g., biological, anatomical), which might compromise the effectiveness of the drugs.[35]

In the last decades, the pulmonary delivery of anti-TB drugs has been explored by researchers, because the infection occurs mainly in the lungs and a local administration could present better efficacy. These factors arouse the interest of scientists and the pharmaceutical industry to pursue alternatives that potentiate the effect of antibiotics and

reduce drug resistance. Meanwhile, being the pulmonary delivery a route that aims to be specific and reach higher drug concentrations around granuloma, it is expected that the dose of anti-TB drugs necessary to be effective could be reduced and, consequently, lower the incidence of side effects and reduce the potential development of drug resistance.[62,63,65,92] This type of formulation accomplishes another advantage related to the easier administration of the drugs that could be managed by the patient and also contributes to an increase in compliance with the treatment.[62,92]

The lung is where the infection by TB occurs, mainly in alveolar macrophages that presents a large surface area, a thin alveolar epithelium and good vascularization. These features provide an adequate environment for an increase of bioavailability and absorption of drugs in the infection site and, consequently, allow to lower doses while maintaining the efficacy. Because of the intense vascularization in the lungs, pulmonary delivery is also a suitable administration route to treat extrapulmonary TB, as anti-TB drugs could be easily absorbed.[62,93]

The advances in encapsulation technology for drug delivery purposes accompany huge advantages for stabilizing drugs during delivery, promoting a sustained release and enhancing the bioavailability of poorly soluble drugs.[93] In order to reach the alveolus where the infection is concentrated, the particles have to overcome some barriers and pass through the trachea, mucociliary system, bronchi, and bronchioles. This means that the particle size is one of the essential key points to achieve target-specificity, since it is important that particles can reach the deep lung (≈ 1-5 μm) to be phagocyted by alveolar macrophages (≈ 0.5-1 μm).[62,93,94] The path that the drugs have to cross until the alveolus, can affect the particle dissolution, diffusion, interactions between drugs and the cell surface. For that reason, the approaches to pulmonary drug delivery, studied more recently focus on formulations based on nanomedicines (Table 1.5), that contain anti-TB drugs and present a size that could reach the alveolus, escape from protective barriers, and be phagocyted by alveolar macrophages, making possible the internalization in granuloma, and acting directly in the bacilli.[62,93]

Table 1.5 - Examples of studies presenting formulations for pulmonary drug delivery of anti-TB drugs.

Drugs	Formulation/System	Study/Therapeutic improvement	Reference
PZA	Large porous particles (LPPs)	Development of PZA-LPPs for lung delivery and deposition in deep lungs, improving bioavailability and absorption of PZA.	65
Clofazimine (CFZ)	Cyclodextrins (CD)	Formulations with CFZ-CD and L-Leucine-CFZ-CD complexes to improve dissolution in lung mucus.	95
RFB	SLNs	Preparation of RFB-containing SLN formulations as potential vehicles for pulmonary delivery of anti-TB drugs.	96
PZA + Moxifloxacin (MOX)	Dry powder	Combination of dry powder containing two anti-TB drugs (PZA and MOX) with excipients L-Leucine and 10% DPPC for improved delivery into deep lung.	97
RFB	Nanostructures lipid carriers	Develop lipid carrier systems for selective delivery of RFB.	98
RIF	SLNs	Develop mannose-SLNs to encapsulate rifampicin and promote selective activity.	99
RIF	SLNs	Develop chitosan-coated lipid nanoparticles loaded with RIF for efficient drug delivery.	100
INH + RIF	Microparticles	Test therapeutic efficacy of locust beam gum with INH and RIF microparticles for inhaled formulations.	101
all-*trans*-retinoic acid	Microparticles	Test inhalable poly(lactic-*co*-glycolic acid) microparticles encapsulating all-*trans*-retinoic-acid as adjunctive treatment of *Mtb* infection.	102
EMB	Nanoparticles	Formulate nanoparticles with EMB-hydrochloride to minimize the duration of treatment and risk of multidrug resistance, compared to non-formulated drug.	103
Epigallocatechin (EGCG)	Microspheres	Formulation of microspheres of EGCG of trehalose to improve bioavailability and efficacy of EGCG against *Mtb*.	104
RIF	SLNs	Biodistribution profile of mannosylated SLNs loaded with RIF for treating pulmonary TB.	105
INH + RFB	Microparticles	Preparation of starch/carrageenan microparticles with INH and RFB for inhaled administration.	106

1.4.4 Alternative approaches for drug delivery in tuberculosis disease

Tuberculosis therapy has been the same along the years and, although research presents some alternatives to the delivery of anti-TB drugs, providing an increase of their bioavailability and efficacy, through other routes of administration or different regimens. It

is challenging, which limits the implementation and approval of these new formulations. These strategies have been investigated to be an alternative to commercially available therapies that present some gaps in which concerns the metabolic stability of drugs, lack of solubility and permeability, many adverse effects, and high doses required due to poor distribution and bioavailability which facilitate the occurrence of drug resistance.[107,108] The reformulation of TB therapy should envisage solving problems related to the patient compliance, number of doses required and facilitate drug administration. In addition, it is also a goal of alternative therapies and/or drug delivery systems to be non-toxic, non-immunogenic, biodegradable, maintain stability upon storage[108] and reduce the costs of production and implementation to reach low-income countries, where TB is more incident.

The global emergence of finding ways to solve drug resistance leads to the promotion of the development of alternative therapeutic approaches, that should allow shorten treatment times, reduce the quantity of medicines and the frequency of doses, treat multidrug resistance and allow the concomitant administration of other important drugs.[109] The development of novel anti-TB drugs or the reformulation of the "old ones" to be more effective in treating the infection is essential for the control of TB infection worldwide. Apart from nanotechnology approaches, other alternatives have been studied for TB therapy such as ionic liquids, antimicrobial peptides, bacteriophages, iron chelators, therapeutic liquid mixtures and host-directed therapies (HDT).[40,109]

Recently, and together with the investigation of the use of nanoparticles, the use of green chemistry approaches has been explored envisaging the use of green solvents to circumvent some characteristics of the APIs, particularly the ones that affect their therapeutic effect and may lead to sub-therapeutic doses or overdoses, and an increase of the incidence of side effects.

1.4.4.1 Green chemistry approaches

The investigation of new compounds or materials and processes for different applications by chemists, pharmaceutics, biochemists, and engineers contributes to the production of several substances that have potential hazards to the environment and human life.[110] In an attempt to raise awareness of the scientific community about the life cycle and toxic effects of some substances produced in the laboratory, the concept of green and sustainable chemistry emerged.[110] In the 90s, green and sustainable chemistry was

designated by the Environmental Protection Agency as a "design of chemical products and processes to reduce or eliminate the use and generation of hazardous substances".[8,111,112] The establishment of this concept led to the development of guidelines that help to understand and adopt the principles of green chemistry, as well as to choose processes and compounds that have a lower environmental impact, determined by their life cycle assessment (LCA).[110,113] Among these principles are, for instance, the implementation of processes that prevent waste formation, innovate through atom economy and carbon efficiency, circumvent harmful synthesis processes, use non-toxic chemicals, work with alternative solvents, apply catalysts for energy efficient processes, use renewable feedstocks, design products considering their final life stage and degradation, and promote prevention of accidents.[110]

The green chemistry principles were since then applied in different fields of research, including pharmaceutical research and the development of novel compounds, materials, and biomedical devices. Currently, it represents a crucial point for the pharmaceutical industry to find solutions that might be less expensive, with minimal toxicity for humans and the environment.[3,4,110] The implementation of green chemistry in pharma starts with the application of the principles of green and sustainable chemistry in medicinal drug discovery and biomedical devices, for example producing drug candidates using a lower amount of materials and generating less residues in a short period of time.[114] The process of synthesis of an API comprises four main steps: reaction, separation, purification and drying. In turn, each of these steps requires one or more organic solvents that present problems of toxicity, flammability, and volatility, for example. Thus, one of the strategies adopted for reducing or eliminating the waste generated, its hazardous effects and the use of organic solvents was the development of green or alternative solvents.[114,115]

In the last decade, the study of alternative solvents has been intensified, and their implementation for the development of new drugs and processes has been pursued.[114] These green solvents present several advantages, such as low toxicity, in general, non-flammability and non-explosiveness, natural abundant and availability, low cost and biodegradability.[116] Some examples of compounds that have been described as alternative solvents are super- and sub-critical fluids, low transition temperature mixtures (e.g., ionic liquids (ILs), eutectic mixtures), solvents derived from biomass (e.g., 2-methyltetrahydrofuran), liquid polymers and switchable solvents.[3,9,113,116–118] Even when using green solvents, each one of them presents inherent advantages and disadvantages, and their choice depends on the final

application and how to maximize their best characteristics, accomplishing a huge part or all of green chemistry principles.[116]

1.4.4.1.1 Ionic liquids and organic salts

ILs are described as organic salts formed after a reaction that combines a cation and an anion, and commonly present a melting point below 100°C,[119–122] being the ones with melting temperatures above 100°C designated molten salts.[113,121] Depending on the definition adopted and what is considered an IL, these compounds are reported in different periods in the history of science. Nonetheless, since 1914 ILs have been studied by different researchers for different applications, and Paul Walden reported the synthesis of one of the first ILs, ethylammonium nitrate salt.[121,123] Since then, some synonyms to designate ILs were presented, such as room temperature molten salts, low temperature molten salts, ambient temperature molten salts, ionic fluids and liquid organic salts.[121,124]

ILs have drawn the attention as alternative solvents due to their characteristics of low vapor pressure, which allow to substitute the volatile organic compounds (VOCs). Moreover, they present chemical and thermal stability, non-flammability, high conductivity and a vast liquid range that can have useful properties to apply, for example, in synthesis processes, catalysis, analytical chemistry, extraction, biotechnology, electrochemistry, biomedical applications, among others.[117,120,125,126]

Over time, ILs were appearing in sequent generations. The first generation, describes ILs developed according to the physical properties needed, like hydrophobicity, viscosity, density, thermal stability, conductivity, refractive index and melting point, but they were sensitive to the presence of water and air.[127–130] The second generation of ILs, was reported as being stable under contact with air and water and considered advanced materials that combine physical and chemical properties (e.g., chemical reactivity, energy density, oxygen balance, electrochemical window, coordination, solvation, and chiral induction).[127,129–131] Later, the third generation of ILs emerged considering the design of ILs that combines both physicochemical and biological properties (e.g., antibacterial, anaesthetic, antifungal, anticholinergic, emollient, and anti-inflammatory).[127,129,130,132]

For the pharmaceutical industry, the prevention of polymorphic conversion of drugs is extremely important and it has been reported that ILs presenting minimal symmetry in the cation tends to lower their melting temperature and contribute to the inhibition of crystallization.[113,120,129] Furthermore, the existence of many possible choices for the

combination of cations and anions[120] to form an IL allows to have a plentiful of different combinations and thus design adequate ILs for a desired effect or application, for example, increasing the length of an alkyl chain in a cation leads to the decrease of the IL solubility in water.[120] The alkyl side chains can also behave as a shield for the IL charge core , which will decrease the Coulomb interactions and consequently the viscosity of the IL.[133] Ions present in ILs interact predominantly through Coulomb forces, but also through hydrogen bonds, π-π interactions, and dispersion forces.[134–136] Different forms have been explored to apply ILs in therapeutics, such as combining salts with two APIs, one working as a cation and the other as an anion. The attempt to combine ions with double functionality is another option that allows adding functional groups with specific properties and activity, for example, adding two acidic groups or double chiral ILs,[130] or even adding benzyl substituents in the cation that promote π-π interactions with aromatic groups, contribute to boost extraction efficiencies.[137] One of the downsides of ILs is, however, their toxicity. Still, this can, be overcome by choosing counterions that are considered safe, like docusate, quaternary ammonium counterions (e.g., choline, *p*-toluenesulfonate, saccharinate, acesulfamate, cyclamate) and naturally occurring molecules (e.g., amino acids, fatty acids).[123,125,138,139]

In TB therapy diverse studies have been reported using ILs as alternative solvents for chemical reactions in the synthesis of new compounds with possible anti-TB activity. For example, Bhat et al. synthesized a series of diarylpyrazole clubbed with polyhydroquinoline derivatives with a potential anti-TB activity using an IL ((Bbpy)$(HSO_4)_2$) as solvent and catalyst in microwave-assisted synthesis[140] and recently, they used $[Et_3NH][HSO_4]$ IL as a catalyst for the synthesis of 2-chloro quinoline with xanthene derivatives with anti-TB activity.[141]

In another study, Faria et al. reported the study of solubilities of anti-TB drugs (INH and PZA) in a hydrophobic ionic liquid (trihexyl(tetradecyl)phosphonium bis[(trifluoromethyl)sulfonyl]amide) that showed a limited solubility compared to trihexyl(tetradecyl)phosphonium chloride.[142] Cherukuvada and Nangia reported the formation of the salt ethambutol dibenzoate characterized as being a polymorphic IL. However, the authors alerted that, despite being unusual, in some cases, ILs can present polymorphic forms.[139,143] Later, the same authors investigated the formation of other salts (sulfate, dimesylate, ditosylate, dibesylate and fumarate) and ILs (adipate) to avoid the polymorphism and high hygroscopicity presented by dihydrochloride ethambutol salt. When present in FDC combinations it promoted the degradation of RIF and INH, during

time. Different salts and ILs prepared have shown that for instance, ethambutol dihydrochloride is hygroscopic, hence being a drawback of the system.[144] The search for salts formed with EMB that may prevent its high hygroscopicity continued and, Diniz and coworkers prepared four salts, namely, oxalate, maleate, terephthalate and trichloroacetate, from which oxalate proved to reduce the hygroscopicity of EMB.[145] Furthermore, Divya et al. explored the effect that water miscible aprotic ILs could have in α/β-serine hydrolase domain in PE1 and PE2 proteins of *Mtb*, observing that these ILs promote the enzyme activity of esterase, prevent their unfolding and aggregation at higher temperatures.[146] The various approaches that can be studied using ILs and the different compounds that can be synthesized turn this strategy attractive to improve the drugs used in TB therapy.

1.4.4.1.2 Therapeutic liquid mixtures

The designation of eutectic, derived from the Greek word "*eutectos*", was introduced by Frederik Guthrie in 1884. It was used to describe "bodies made up of two or more constituents, which constituents are in such proportion to one another as to give to the result compound body a minimum temperature of liquefaction, that is, a lower temperature of liquefaction than that given by any other proportion".[147] Eutectic mixtures have been used for pharmaceutical applications since the beginning of the century. However, just recently these mixtures have been explored as alternative solvents used for different applications and appearing as an alternative to ionic liquids.[122,131,148–151]

In 2003, Abbott et al. identified a new group of green solvents, the deep eutectic solvents (DES), to refer to mixtures with two or more starting materials with high melting points that are able to form a stable liquid at room temperature, with a melting point significantly lower than those of the initial components.[148,152–154] They suggested that these mixtures are formed due to hydrogen bonding, between hydrogen bond acceptors (HBA) and hydrogen bond donors (HBD), which decrease their entropic differences and allow a decrease of the melting temperature.[148,155] Another type of interactions that could mediate and modulate the physicochemical properties of DES are van der Waals and/or electrostatic forces.[148,156] DES mixtures could be formed by a variety of combinations (up to 10^6),[157] and include different types of compounds tailoring their properties (e.g., pH, viscosity, density, water content, thermodynamic transitions, human and environmental toxicity, affinity to extract compounds, solubility, and membrane permeability) to the desired application (e.g., extraction, biotechnology, electrochemistry, analytical chemistry, biomass processing,

catalysis, polymerization, carbon dioxide adsorption, organic chemistry, nanotechnology, biomedicine, and pharmacy).[158] Choi and co-workers reported a series of different eutectic mixtures formed by natural compounds like carboxylic acids, sugars, amino acids and water and named them natural deep eutectic solvents (NADES).[159–161] Stott et al. have incorporated an API as a component of a DES and observed an increase on the solubility, permeability and absorption of the API,[162] which led Aroso and co-workers to name these type of DES as therapeutic deep eutectic solvents (THEDES). They described them as DES that are formed from at least one API, including an API as a component of the eutectic mixture or referring to a DES that can dissolve an API, potentiating its properties.[159,163]

Therapeutic liquid mixtures, eutectic mixtures or THEDES are considered alternative solvents and low transition temperature mixtures (LTTMs) and lately, they have also been used in research for pursuing improvements in TB therapy. For instance, Zakrewsky et al. reported the use of a eutectic mixture (choline bicarbonate and geranic acid 1:2) as presenting antimicrobial activity against *Mtb* drug-resistant strains.[164,165] Another study reported the use of anti-TB drugs (PZA and INH) to obtain binary and ternary solid eutectic compositions from co-crystallization of these drugs with succinic acid and fumaric acid, showing that during co-crystallization synthesis, the formation of eutectic mixtures can occur when cohesive interactions are predominant and the size/shape of the components is mismatched.[166] If adhesive interactions dominate, the resulting compound is characterized as a cocrystal, yet, if the adhesive and cohesive interactions are balanced and a match of size/shape between the components occurs, a solid solution is formed.[166] Furthermore, Rajbongshi et al. also studied the formation of eutectics through crystallization processes with PZA and different aromatic carboxylic acids that were characterized by a "V" shape phase diagram.[167]

The studies of eutectic mixtures and DES for pharmaceutical applications have increased along the years. In particular, for application in TB therapy, they have shown promising results, where the properties of anti-TB drugs could be improved, facilitating TB treatment.

1.4.4.1.3 Low transition temperature mixtures (LTTMs)

The concept of LTTMs was introduced in 2012, to refer to mixtures that present a large liquid range, high thermal stability, negligible vapor pressure, non-flammability and, usually, are biocompatible and biodegradable.[148,168,169] LTTMs also refer to liquid mixtures

with a low freezing point[168] and appeared after the definition of ionic liquids and deep eutectic solvents, representing the mixtures that do not fit completely in the category of an IL or a DES.[154] It is not straightforward to differentiate these solvents due to the similar characteristics that they present. However, in the case of ILs, the depression of the melting point occurs due to the interactions between cations and anions, while in the case of DES, the depression of the melting point is, mainly, due to the hydrogen bonding between the components, which may be non-ionic.[123,159,170] Since many of the mixtures developed and studied do not present melting points but present glass transitions, the LTTMs term appeared to designate these liquid mixtures, representing a family of liquid mixtures that comprise both ILs and DES.[148,169,170]

For the pharmaceutical industry, the physical form of the drug is very important for its formulation because it will affect the characteristics and properties of the drug (e.g. solubility, permeability, dissolution rate), and ultimately the patient.[119] The pharmaceutical formulations presented by the market are mainly in solid form owing to purity, thermal stability, and production processes that are optimized and consequently become easy to handle.[119] Hence, LTTMs as stable liquid mixtures could represent potential alternatives for the development of formulations with new and "old" drugs to achieve an improved bioavailability and a possible controlled and targeted drug release, which may be useful to solve some of the challenges that anti-TB therapy still present.

1.4.4.1.4 Supercritical fluid technology

A supercritical fluid (SCF) is designated as "a fluid that is heated above its critical temperature and compressed above its critical pressure, but below the pressure required to condense it into a solid".[113,117,171,172] Supercritical fluid technology has been applied in biomedicine and drug discovery, as an alternative technology mostly for formulation purposes. This technology allows the production of different size particles, eliminating or reducing significantly the use of organic solvents, which are commonly used for particle preparation.[173] SCF allows the formulation of micro- or nanoparticles of highly pure compounds in a single-step process, controlling the polymorphism of solid compounds and allowing the processing of thermolabile molecules with environmentally friendly technology.[174,175] Several compounds can be used as a supercritical solvent, however, the most reported is supercritical carbon dioxide ($scCO_2$), due to its low critical temperature and easily achievable pressure. Furthermore, carbon dioxide (CO_2) is gaseous under ambient

pressure and temperature, which allows the separation of the product from the solvent just by depressurizing the apparatus.[117,173] The use of $scCO_2$ presents other advantages being considered a GRAS solvent, environmentally benign, with high purity, low cost, non-toxic, non-corrosive, and non-flammable.[113,117,173,176–178]

This technology enables the formulation of different particles, modulating the characteristics of the particles simply by varying the conditions of pressure and temperature.[113,177] SCF could be used in different processes for the formulation of controlled release drug delivery systems or the impregnation of drugs into polymeric devices. Using particle generating processes, $scCO_2$ could work as a solvent (rapid expansion of supercritical solution (RESS)), anti-solvent (supercritical anti-solvent (SAS), supercritical enhanced dispersion solution (SEDS)), or solute (particles from gas saturated solution (PGSS), supercritical assisted atomization (SAA)). Additionally, $scCO_2$ can be used as a solvent for impregnation processes.[171,173,177]

In TB therapy, this technology has been used to produce controlled release formulations, target-specific and with high stability in body fluids. For instance, Lovskaya et al. prepared silica and starch aerogels with SCF technology to be used as carriers of RFB for oral drug delivery, demonstrating a higher bioavailability of these drug-loaded aerogels compared to the pure drug.[179] Patomchaiviwat and co-workers used SAS to formulate inhalable microparticles of RIF and poly(L-lactide) and concluded that it was possible to produce homogeneous microparticles in regards shape, size and size distribution, suitable for inhalation and presenting a sustained release with RIF, with no burst release effect.[180] Another study aimed to produce RIF loaded micro- and nanoparticles using semi-continuous SAS precipitation, using different solvents to control particle size and particle size distribution. Reverchon et al. designed a promising micronization process using dimethyl sulfoxide (DMSO) and RIF particles, which became amorphous and did not degrade during supercritical processing.[181] Following this, Reverchon et al. used different solvents (water and methanol) for the optimization of a micronization process of RIF through SAA for aerosol delivery and verified that by varying the operating conditions it was possible to control the particle size and reach different targets inside the lung.[182] The production of new formulations for TB therapy that could be target specific is essential and the use of green technologies for the development of these formulations, like SCF, represent an important advance for the pharmaceutical industry.

1.4.5 Exploring combinatorial approaches for effective tuberculosis therapies: perspectives and challenges

Given the history of tuberculosis disease and all the research that has been carried out to discover an effective treatment, exploring combinatorial approaches focused on the treatment of TB might be the path to follow. It becomes essential to use combinatorial therapies to achieve target-specificity, an increased bioavailability, lower toxicity and controlled release of anti-TB drugs, while incorporating technologies that could be more efficient to formulate systems that may be modulated and designed for a specific route of administration.

One example of combinatorial technologies, herein presented, associates the use of LTTMs, as THEDES, design for TB therapy and SCF technology. This work, describes the preparation of THEDES with L-arg (described as an adjuvant in TB therapy) and the design of inhalable particles through SCF technology (PGSS), revealing promising results for the encapsulation of THEDES.[183] The combination of different strategies like nanotechnology with green solvents and/or SCF technology for the formulation of nanoparticles to be applied in TB therapy, appears to represent a promising line of research.

1.5 Aims of the thesis

As stated before, tuberculosis persists to be on the top list of fatal infections worldwide. Thus, continuous research and investigation on areas as different as prevention, development of novel vaccines, antibiotics, formulations, and the combination of therapies for effective treatment of TB infection is necessary. However, when developing new formulations or combination therapies, it is still essential to commit everyone involved (doctors, patients, and care givers), to simplify the treatment regimens and to develop formulations that could be easily self-administrated. It is also important to develop new anti-TB drugs and/or new effective drug combinations that reduce their adverse side effects and toxicity. These could contribute to improve treatment rates, decrease the risk of drug resistance, and contribute to the patient compliance, by providing a patient-friendly therapy. At the same time, it will be highly significant if research lines privilege the use of green and sustainable approaches that could be less toxic to humans and to the environment.

Hereupon, the strategy adopted in this work was focused on finding alternative approaches for TB therapy, in particular, using green solvents (ionic systems, THEDES and supercritical fluids) to modify the pharmacokinetics and pharmacodynamics of anti-TB drugs that could be therefore used to develop formulations that could result in a better efficacy, bioavailability, as well as an easy administration. Also, one of this thesis goals is to study different green solvents and understand their advantages and disadvantages, in which concerns drug delivery in TB therapy. To achieve these goals, different tasks were established such as the preparation and characterization of ionic systems (organic salts) based on anti-TB drugs as well as the preparation and characterization of therapeutic liquid mixtures (THEDES), also based on anti-TB drugs, focusing on drugs used in first-line treatments. Another objective was to evaluate their antimicrobial activity against *Mtb*, and finally develop matrices and formulations suitable to the delivery the different systems prepared, exploring combinatorial approaches.

The following chapter was adapted from the publications:

Santos F., Branco L.C., Duarte A.R.C. Organic salts based in isoniazid drug: synthesis, bioavailability and cytotoxicity studies. Pharmaceutics (2020). 12 (10): 952. DOI: 10.3390/pharmaceutics12100952.

Santos F., Leitão M.I.P.S., Duarte A.R.C. Properties of therapeutic deep eutectic solvents of L-arginine and ethambutol for tuberculosis treatment. Molecules (2019). 24 (1): 55. DOI: 10.3390/molecules24010055.

Roda A., **Santos F.**, Matias A.A., Paiva A. and Duarte A.R.C. Design and processing of drug delivery formulations of therapeutic deep eutectic systems for tuberculosis. Journal of Supercritical Fluids (2020). 161 (104826). DOI: 10.1016/j.supflu.2020.104826.

Santos F., Pires D., Anes E., Duarte A.R.C. Insights into therapeutic liquid mixtures and formulations towards tuberculosis therapy (2022) - **In preparation for submission**.

2

MATERIALS AND METHODS

2.1 Materials

Specific chemicals and materials were used in different parts of the work and are herein reported:

- **Chapter 3**

Isonicotinic acid hydrazide (INH, CAS no. 54-85-3, 98% purity) from Alfa Aesar was used as a cation for combination with organic anions (reagents commercially available and purchased from Alfa Aesar and Sigma Aldrich). The organic salts prepared in this work were isoniazid chloride [INH][Cl] in the molar ratio of 1:1 and 1:2, isoniazid mesylate [INH][MsO], isoniazid glycolate [INH][GcO], isoniazid camphorsulfonate S and R [INH][S-CsO] and [INH][R-CsO] in the ratio 1:1 and 1:2, isoniazid vanillate [INH][VanO], and isoniazid saccharinate [INH][Sac].

For the evaluation of aquatic toxicity different reagents were used, namely L-glutathione reduced (GSH, CAS no. 70-18-8), 1-chloro-2,4-dinitrobenzene (cDNB, CAS no. 97-00-7, ≥ 99% purity), 4-amino-3-hydrazino-5-mercapto-1,2,4-triazole (Purpald, CAS no. 1750-12-5, ≥ 99% purity), hydrogen peroxide 30% (H_2O_2 30%, CAS no. 7722-84-1), formaldehyde, xanthine (CAS no. 69-89-6, ≥ 99% purity), nitroblue tetrazolium (NBT, CAS no. 298-83-9, ≥ 90% purity), xanthine-oxidase (XOD, CAS no. 9002-17-9), sodium dodecyl sulfate (SDS, CAS no. 151-21-3, ≥ 98.5% purity), thiobarbituric acid (TBA, CAS no. 504-17-6, ≥ 98% purity), tween-20 solution (CAS no. 9005-64-5) from Sigma Aldrich. Methanol (CAS no. 67-56-1, ≥ 99.8% purity) from Scharlau; potassium hydroxide (KOH, CAS no. 1310-58-3, ≥ 85% purity), potassium periodate (KIO_4, CAS no. 7790-21-8, 99.8% purity) from Chem-Lab.

Ethylenedinitrilotetraacetic acid (EDTA, CAS no. 60-00-4, ≥ 99% purity) from Honeywell; trichloroacetic acid (TCA, CAS no. 76-03-9, ≥ 99% purity) from PanReac AppliChem; malondialdehyde bis(dimethyl acetal) (MDA, CAS no. 102-52-3, 99% purity), 3,3',5,5'-tetramethylbenzidine (TMB, CAS no. 54827-17-7, ≥ 98% purity) from Merck; albumine bovine fraction (BSA, CAS no. 9048-46-8) from Nzytech; primary antibody for total ubiquitin (Ub P4D1 (sc-8017)) from Santa Cruz.

- **Chapters 4, 5 and 6**

Citric acid monohydrate (CA, CAS no. 5949-29-1, ≥ 99,5% purity) from PanReac AppliChem and Sigma Aldrich; L-arginine (L-arg, CAS no. 74-79-3, ≥ 98% purity) from Sigma Aldrich; ethambutol (EMB, CAS no. 74-55-5, ≥ 98% purity) from Alfa Aesar and Santa Cruz Biotechnology; isonicotinic acid hydrazide (INH, CAS no. 54-85-3, 98% purity), pyrazinamide (PZA, CAS no. 98-96-4, 98% purity) from Alfa Aesar; rifampicin (RIF, CAS no. 13292-46-1, ≥ 95% purity) from Sigma Aldrich. Deionized water was used to prepare the mixtures. Sodium hydroxide pellets (NaOH, CAS no. 1310-73-2, > 99% purity) and hydrochloric acid 37% (HCl, CAS no. 7647-01-0) from Normax-Chem.[184] Glycerol monostearate (GMS, CAS no. 31566-31-1, > 95% purity) from Gatefossé and carbon dioxide (CO_2, CAS no. 124-38-9, 99.95% purity) from Air Liquide. 4-(2-hydroxyethyl)-1-piperazineethanesulfonic acid) (HEPES, CAS no. 7365-45-9) and sodium pyruvate from Gibco. Phorbol-12-myristate-13-acetate (PMA, CAS no. 16561-29-8), IGEPAL® CA-630 (CAS no. 9002-93-1) and polyvinylpyrrolidone (PVP, CAS no. 9003-39-8) from Sigma Aldrich. Middlebrook 7H10 agar, Middlebrook 7H9 and OADC from Becton.

General reagents used throughout the work carried out under the scope of the thesis were: phosphate buffered saline (PBS) solution, prepared from PBS tablets (Fisher BioReagents) as indicated: one tablet dissolved in 200 mL of deionized water, yielding 0.01M phosphate buffer, 0.0027 M potassium chloride, 0.137 M sodium chloride, pH 7.4 solution at 25 °C; dimethyl sulfoxide-d_6 (DMSO-d_6, 99,96% D, CAS no. 2206-27-1) from Eurisotop. Eagle's minimum essential medium (MEM, Corning), Roswell Park Memorial Institute 1640 medium (RPMI 1640, Gibco), fetal bovine serum (FBS, Corning and Gibco), antibiotic-antimycotic solution (penicillin and streptomycin (PS), Corning, Gibco) and CellTiter96® AQueous One Solution Cell Proliferation Assay from Promega.

2.2 Methods

Different techniques were used to prepare, characterize, and study the compounds obtained, in order to understand how they work in different environments, their activity and potential applications, being the techniques used described in the next sections.

2.2.1 Preparation of organic salts based on isoniazid

2.2.1.1 Isoniazid monochloride [INH][Cl]

INH (1.068 g; 7.79 mmol; 1 eq.) was dissolved in 20 mL of deionized H_2O, then a solution of HCl 1M (7.80 mL; 7.79 mmol; 1 eq.) was slowly added to the INH solution. The reaction mixture was stirred at room temperature for 3h. Then, the solvent was evaporated, and the final product was dried under vacuum. The product was obtained as a pale pink solid (1.235 g; η = 91.3 %). ^{1}H NMR (400.13 MHz, DMSO-d_6): δ = 8.83 (d, 2H, J=4.0 Hz), 7.90 (dd, 2H, J=4.0 Hz) ppm (Figure A.1.2, Appendix A). ^{13}C NMR (100.62 MHz, DMSO-d_6): δ = 164.39, 150.32, 140.67, 138.88, 122.32, 122.26 ppm (Figure A.1.3, Appendix A). IR: 3099, 2951, 1981, 1658, 1533, 1493, 1316, 1246, 1141, 1063, 1012, 967, 863, 758, 690, 660, 607, 489, 409 cm^{-1} (Figure A.1.4, Appendix A). Anal. calcd. for $C_6H_8ClN_3O$, C 41.51, H 4.65, N 24.21, found: C 41.48, H 4.60, N 24.66. M.p. 93 °C.

2.2.1.2 Isoniazid dichloride [INH][Cl]$_2$

INH (1.148 g; 8.37 mmol; 1 eq.) was dissolved in 20 mL of deionized H_2O, then a solution of HCl 1M (16.70 mL; 16.74 mmol; 2 eq.) was slowly added to the INH solution. The reaction mixture was stirred at room temperature for 3h. Then, the solvent was evaporated, and the final product was dried under vacuum. The product was obtained as pale white solid (1.144 g; η = 64.8 %). ^{1}H NMR (400.13 MHz, DMSO-d_6): δ = 8.92 (d, 2H, J=4.0 Hz), 8.06 (d, 2H, J=4.0 Hz) ppm (Figure A.1.5, Appendix A). ^{13}C NMR (100.62 MHz, DMSO-d_6): δ = 164.34, 150.67, 140.61, 140.56, 121.79, 121.48 ppm (Figure A.1.6, Appendix A). IR: 3094, 3050, 2950, 2500, 2074, 1991, 1684, 1637, 1609, 1565, 1515, 1496, 1360, 1311, 1243, 1211, 1184, 1156, 1100, 1059, 1039, 1009, 869, 835, 750, 682, 561, 505, 419 cm^{-1} (Figure A.1.7, Appendix A). Anal. calcd for $C_6H_9Cl_2N_3O$, C 34.31, H 4.32, N 20.00, found: C 34.36, H 4.32, N 20.00. M.p. 160 °C.

2.2.1.3 Isoniazid mesylate [INH][MsO]

INH (1.034 g; 7.54 mmol; 1 eq.) was dissolved in 20 mL of deionized H_2O, then a solution of mesylic acid 1M (7.50 mL; 7.54 mmol; 1 eq.) was slowly added to the INH solution. The reaction mixture was stirred at room temperature for 3h. Then, the solvent was evaporated, and the final product was dried under vacuum. The product was obtained as pale white solid (1.748 g; η = 99.5 %). ^{1}H NMR (400.13 MHz, DMSO-d_6): δ = 11.24 (s, 1H), 8.96 (d, 2H, J=8.0 Hz), 8.09-8.06 (m, 2H), 2.44-2.42 (m, 3H) ppm (Figures A.1.8, Appendix A). ^{13}C NMR (100.62 MHz, DMSO-d_6): δ = 163.83, 148.42, 142.61, 124.73, 123.27, 53.34 ppm (Figure A.1.9, Appendix A). IR: 3424, 3191, 2985, 1676, 1654, 1540, 1497, 1419, 1298, 1223, 1152, 1061, 1030, 1001, 934, 846, 777, 744, 686, 664, 551, 535, 522, 459, 426, 403 cm^{-1} (Figure A.1.10, Appendix A). Anal. calcd for $C_7H_{11}N_3O_4S$, C 36.05, H 4.75, N 18.02 found: C 36.83, H 4.90, N 18.05. M.p. 133 °C.

2.2.1.4 Isoniazid glycolate [INH][GcO]

INH (1.272 g; 9.28 mmol; 1 eq.) was dissolved in 20 mL of deionized H_2O, then the glycolic acid was weighed (0.705 g; 9.28 mmol; 1 eq.) slowly added to the INH solution. The reaction mixture was stirred at room temperature for 3h. Then, the solvent was evaporated, and the final product was dried under vacuum. The product was obtained as white solid (1.867 g; η = 94%). ^{1}H NMR (400.13 MHz, DMSO-d_6): δ = 10.10 (s, 1H), 8.71 (d, 2H, J=4.0 Hz), 7.74 (d, 2H, J=8.0 Hz), 3.90 (s, 2H) ppm (Figure A.1.11, Appendix A). ^{13}C NMR (100.62 MHz, DMSO-d_6): δ = 171.49, 164.30, 150.86, 139.99, 139.75, 121.78, 121.45, 61.22 ppm (Figure A.1.12, Appendix A). IR: 3370, 3249, 1652, 1605, 1539, 1511, 1495, 1417, 1343, 1304, 1226, 1080, 1061, 1001, 983, 952, 847, 744, 685, 663, 577, 513, 436 cm^{-1} (Figure A.1.13, Appendix A). Anal. calcd for $C_8H_{11}N_3O_4$, C 45.07, H 5.20, N 19.71 found: C 46.68, H 4.81, N 20.16.

2.2.1.5 Isoniazid mono(S-Camphorsulfonate) [INH][S-CsO]

INH (1.110 g; 8.09 mmol; 1 eq.) was dissolved in 20 mL of deionized H_2O, then the S-camphor sulfonic acid was weighed (1.880 g; 8.09 mmol; 1 eq.) and slowly added to the INH solution. The reaction mixture was stirred at room temperature for 3h. Then, the solvent was evaporated, and the final product was dried under vacuum. The product was obtained as yellow solid (2.882 g; η = 96.3 %). ^{1}H NMR (400.13 MHz, DMSO-d_6): δ = 11.10 (s, 1H), 8.96-8.86 (m, 2H), 8.41-8.15 (m, 2H), 3.47-3.22 (m, 1H), 2.78-2.65 (m, 2H), 2.45-2.39 (m, 1H), 2.33 (d,

1H, J=16.0 Hz), 2.04-1.79 (m, 2H), 1.64-1.57 (m, 1H), 1.30-1.23 (m, 1H), 0.98 (t, 3H, J=20.0, 32.0 Hz), 0.75 (t, 3H, J=20.0, 32.0 Hz) ppm (Figure A.1.14, Appendix A). ^{13}C NMR (100.62 MHz, DMSO-d_6): δ = 178.51, 162.13, 146.06, 143.63, 127.36, 124.35, 55.05, 50.61, 49.41, 43.80, 43.23, 28.53, 26.91, 19.90, 19.67 ppm (Figure A.1.15, Appendix A). IR: 3429, 2584, 1674, 1651, 1559, 1501, 1304, 1259, 1240, 1193, 1150, 1101, 1022, 995, 930, 842, 792, 764, 664, 647, 609, 590, 539, 519, 451 cm^{-1} (Figure A.1.16, Appendix A). Anal. calcd for $C_{16}H_{23}N_3O_5S.H_2O$, C 49.60, H 6.50, N 10.85 found: C 50.83, H 6.32, N 11.09.

2.2.1.6 Isoniazid di(S-Camphorsulfonate) [INH][S-CsO]$_2$

INH (0.775 g; 5.65 mmol; 1 eq.) was dissolved in 20 mL of deionized H_2O, then the S-camphor sulfonic acid was weighed (2.830 g; 11.30 mmol; 2 eq.) and slowly added to the INH solution. The reaction mixture was stirred at room temperature for 3h. Then, the solvent was evaporated, and the final product was dried under vacuum. The product was obtained as yellow solid (3.010 g; η = 88.5 %). ^{1}H NMR (400.13 MHz, DMSO-d_6): δ = 11.17 (s, 1H), 9.04-9.00 (m, 2H), 8.32-8.30 (m, 2H), 3.26-2.87 (m, 2H), 2.79-2.72 (m, 2H), 2.49-2.48 (m, 4H), 2.41-2.23 (m, 2H), 2.05-1.95 (m, 2H), 1.90-1.67 (m, 2H), 1.35-1.29 (m, 2H), 1.04-0.97 (m, 6H), 0.83-0.67 (m, 6H) ppm, (Figure A.1.17, Appendix A). ^{13}C NMR (100.62 MHz, DMSO-d_6): δ = 216.41, 216.38, 191.45, 149.19, 144.27, 142.61, 125.35, 56.33, 55.23, 51.40, 50.96, 49.57, 49.06, 47.61, 47.38, 43.16, 43.11, 42.69, 42.60, 26.84, 24.65, 20.43, 19.97, 19.48, 19.40 ppm (Figure A.1.18, Appendix A). IR: 3110, 1635, 1590, 1531, 1412, 1293, 1248, 1149, 1030, 970, 831, 742, 668, 598, 524 cm^{-1} (Figure A.1.19, Appendix A). Anal. calcd for $C_{26}H_{39}N_3O_9S_2$, C 51.90, H 6.53, N 6.98 found: C 51.57, H 6.26, N 7.48.

2.2.1.7 Isoniazid mono(R-Camphorsulfonate) [INH][R-CsO]

INH (1.252 g; 9.13 mmol; 1 eq.) was dissolved in 20 mL of deionized H_2O, then the R-camphor sulfonic acid was weighed (2.120 g; 9.13 mmol; 1 eq.) slowly added to the INH solution. The reaction mixture was stirred at room temperature for 3h. Then, the solvent was evaporated, and the final product was dried under vacuum. The product was obtained as pale white solid (3.232 g; η = 96.2 %). ^{1}H NMR (400.13 MHz, DMSO-d_6): δ = 11.16 (d, 1H, J=20.0 Hz), 8.98-8.87 (m, 2H), 8.41-8.00 (td, 2H, J=4.0 Hz), 3.34-3.23 (dd, 1H, J=12.0 Hz), 2.94-2.64 (m, 2H), 2.46-2.39 (m, 1H), 2.34-2.22 (m, 1H), 2.04-1,79 (m, 2H), 1.65-1.47 (m, 1H), 1.30-1.17 (m, 1H), 0.98 (t, 3H, J=20.0, 32.0 Hz), 0.75 (t, 3H, J=20.0, 32.0 Hz) ppm (Figure A.1.20,

Appendix A). ^{13}C NMR (100.62 MHz, DMSO-d_6): δ = 178.45, 162.05, 145.60, 143.41, 127.43, 124.52, 55.02, 50.61, 49.40, 43.79, 43.22, 28.49, 26.90, 19.89, 19.64 ppm (Figure A.1.21, Appendix A). IR: 3433, 1666, 1626, 1555, 1499, 1242, 1200, 1151, 1022, 1000, 838, 748, 677, 591, 537, 509, 405 cm^{-1} (Figure A.1.22, Appendix A). Anal. calcd for $C_{16}H_{23}N_3O_5S.0.5H_2O$, C 50.79, H 6.35, N 11.11 found: C 50.35, H 6.39, N 11.09.

2.2.1.8 Isoniazid di(R-Camphorsulfonate) [INH][R-CsO]$_2$

INH (1.073 g; 7.82 mmol; 1 eq.) was dissolved in 20 mL of deionized H_2O, then the R-camphor sulfonic acid was weighed (3.637 g; 15.60 mmol; 2 eq.) and slowly added to the INH solution. The reaction mixture was stirred at room temperature for 3h. Then, the solvent was evaporated, and the final product was dried under vacuum. The product was obtained as yellow solid (4.164 g; η = 88.7 %). ^{1}H NMR (400.13 MHz, DMSO-d_6): δ = 11.17 (s, 1H), 9.04-8.92 (m, 2H), 8.47-8.15 (td, 2H, J=4.0, 8.0 Hz), 3.26-3.21 (dd, 2H, J=4.0 Hz), 2.96 (d, 2H, J=16.0 Hz), 2.87-2.64 (m, 4H), 2.48-2.46 (m, 4H), 2.42-2.22 (m, 2H), 2.09-1.99 (m, 2H), 1.91-1.62 (m, 2H), 1.36-1.26 (m, 2H), 1.05-0.97 (m, 6H), 0.83-0.67 (m, 6H) ppm (Figure A.1.23, Appendix A). ^{13}C NMR (100.62 MHz, DMSO-d_6): δ = 216.51, 191.52, 147.16, 144.71, 142.75, 125.29, 124.97, 56.35, 55.25, 51.38, 51.02, 49.55, 49.01, 47.59, 47.30, 43.14, 43.12, 42.69, 42.59, 26.85, 24.62, 20.51, 19.99, 19.55, 19.44 ppm (Figure A.1.24, Appendix A). IR: 3207, 3112, 2974, 1635, 1536, 1412, 1293, 1248, 1134, 1035, 841, 747, 668, 603, 524 cm^{-1} (Figure A.1.25, Appendix A). Anal. calcd for $C_{26}H_{39}N_3O_9S_2$, C 51.90, H 6.53, N 6.98 found: C 52.56, H 6.48, N 7.54. M.p. 129 °C.

2.2.1.9 Isoniazid vanillate [INH][VanO]

INH (1.602 g; 11.70 mmol; 1 eq.) was dissolved in 20 mL of deionized H_2O, then the vanillic acid was weighed (1.964 g; 11.70 mmol; 1 eq.) and slowly added to the INH solution. The reaction mixture was stirred at room temperature for 3h. Then, the solvent was evaporated, and the final product was dried under vacuum. The product was obtained as pale brown solid (3.456 g; η = 96.8 %). ^{1}H NMR (400.13 MHz, DMSO-d_6): δ = 9.84 (s, 1H), 8.72 (d, 2H, J=4.0 Hz), 7.74-7.73 (dd, 2H, J=4.0 Hz), 7.46-7.44 (dd, 2H, J=8.0 Hz), 6.86 (d, 1H, J=8.0 Hz), 3.81 (s, 3H) ppm (Figure A.1.26, Appendix A). ^{13}C NMR (100.62 MHz, DMSO-d_6): δ = 167.66, 164.33, 151.54, 150.66, 147.66, 140.72, 123.92, 122.05, 121.45, 115.47, 113.16, 55.99 ppm (Figure A.1.27, Appendix A). IR: 3244, 1674, 1591, 1512, 1484, 1451, 1408, 1330, 1288, 1268, 1235, 1202, 1170, 1122, 1064, 1022, 997, 888, 844, 780, 763, 750, 680, 581, 535, 471, 414, 404 cm^{-1}

(Figure A.1.28, Appendix A). Anal. calcd for $C_{14}H_{15}N_3O_5$, C 55.08, H 4.95, N 13.76 found: C 55.38, H 4.91, N 13.74.

2.2.1.10 Isoniazid saccharinate [INH][Sac]

[INH][Cl] (1.026 g; 5.90 mmol; 1 eq.) was dissolved in 20 mL of methanol, then the saccharin sodium salt was weighed (1.212 g; 5.90 mmol; 1 eq.) and was slowly added to the [INH][Cl] solution. The reaction mixture was stirred at room temperature for 3h. Then, the solvent was evaporated and precipitate the NaCl with acetone, the final product was dried under vacuum. The product was obtained as pale orange solid (1.782 g; η = 94.3 %). ^{1}H NMR (400.13 MHz, DMSO-d_6): δ = 11.19-10.80 (dd, 2H, J=4.0 Hz), 8.83-8.78 (m, 2H), 8.01 (d, 1H, J=8.0 Hz), 7.90-7.76 (m, 3H), 7.25 (s, 2H) ppm (Figure A.1.29, Appendix A). ^{13}C NMR (100.62 MHz, DMSO-d_6): δ = 167.89, 164.79, 150.77, 141.90, 139.74, 133.01, 132.65, 131.37, 130.17, 127.82, 121.99, 121.97 ppm (Figure A.1.30, Appendix A). IR: 3192, 3112, 3008, 1625, 1536, 1412, 1327, 1288, 1248, 1134, 1124, 970, 841, 742, 663, 608, 534 cm^{-1} (Figure A.1.31, Appendix A). Anal. calcd for $C_{13}H_{12}N_4O_4S.0.5H_2O$, C 47.42, H 3.95, N 17.02 found: C 47.26, H 3.79, N 16.69. ICP for Na^+ < 200 ppm. M.p. 179 °C.

2.2.2 Preparation of therapeutic deep eutectic systems

During this work various mixtures were prepared, being only the ones that form a stable mixture object of study on this thesis (Table 2.1). All systems prepared are listed in Table A.2.1, Appendix A. Different components of the eutectic mixtures were weighed and mixed, in different molar ratios. Then the liquid mixtures were obtained by heating the combination until 50/60 °C, under constant stirring, until a clear viscous liquid was formed.[153,185]

Table 2.1 - Different THEDES prepared and used along the different studies.

Component A	Component B	Component C	Component D	Molar Ratio	Abbreviation	Visual Aspect
Citric Acid	Ethambutol	H_2O	-	1:1:5 ; 2:1:10	CA:EMB:H_2O	Transparent viscous liquid at room temperature
Citric Acid	Ethambutol	L-arginine	H_2O	2:1:1:7	CA:EMB:L-argH_2O	
Citric Acid	L-arginine	H_2O	-	1:1:4 ; 1:1:5 ; 1:1:6 ; 1:1:7 ; 2:1:7 ; 2:1:8 ; 2:1:9	CA:L-argH_2O	

The molar mass (g mol^{-1}) of a liquid mixture was calculated according to the equation:

$$M_{DES} = X_A \times M_A + X_B \times M_B + X_C \times M_C \quad (1)$$

where X and M are the mole fraction and molar mass, respectively.

Considering TB therapy, we also tried the solubilization of small amounts of first-line anti-TB drugs into system CA:EMB:H_2O (1:1:5), as presented in Table 2.2.

Table 2.2 - Different formulations prepared by solubilizing different amounts of anti-TB drugs in the mixture CA:EMB:H_2O (1:1:5).

	Anti-TB drugs added	Mass ratio	Abbreviation
CA:EMB:H_2O (1:1:5)	RIF + PZA + INH	1:1:1	CA:EMB:H_2O + RPI (1:1:1)
	RIF + PZA + INH	2:3:1	CA:EMB:H_2O + RPI (2:3:1)
	RIF + PZA + INH	2:5:1	CA:EMB:H_2O + RPI (2:5:1)
	RIF + PZA + $[INH][Cl]_2$	1:1:1	CA:EMB:H_2O + RP$[INH][Cl]_2$
	PZA	-	CA:EMB:H_2O + PZA

2.2.3 Formulation of particles by supercritical fluid technology

2.2.3.1 Phase Equilibria of therapeutic liquid mixtures and CO_2

The solubility of CO_2 and therapeutic liquid mixtures was studied through visual observation of the phase equilibrium of the pseudo-binary mixture. A variable-volume view cell apparatus (hand-made) was used for this purpose. The equipment is composed by a cylindric equilibrium cell of stainless-steel with an internal volume between 35 to 70 cm^3,

regulated by a piston coupled to a hydraulic pump (HP145, HI-force). It can operate up to a pressure of 60 MPa. Two sapphire windows were oppositely positioned, for observation of the cell interior. The cell was heated through two electrical band heaters coupled to an LMS temperature controller (EroElectronics) and the internal temperature was measured by a sensor (type K) in contact with the fluid mixture. The pressure was controlled by a Digibar PE300 transducer (HMB, European Community) with an accuracy of 0.05 MPa. Stirring of the mixture inside the cell was performed by a mechanical stirrer coupled device electronically controlled by a power supply (VLP-1303 PRO, Voltcraft) at 6 V, 16 mA.

Known amounts of THEDES and CO_2 were injected into the cell. The mixture was stirred continuously, and the temperature stabilized at 40 °C. At different CO_2:THEDES molar ratios and constant temperature, the mixture was compressed to higher pressures and the phase behaviour of the mixture (one or two phases) was observed.

2.2.3.2 Encapsulation of therapeutic deep eutectic systems through Particle from Gas-Saturated Solutions (PGSS)

The PGSS apparatus (Recipient of pulverization A30, Sepharex, France) represented in Figure 2.1, was described by Lack and coworkers.[186] Briefly, THEDES and GMS were loaded into the stirring vessel at a ratio of 9:1 GMS:THEDES (w/w) and mixed with CO_2 at 8.5 MPa and 65 °C. The mixture was stirred for 15 minutes and further depressurized through a 250μm nozzle to a cyclone flushed with compressed air. The particles accumulated in the collector vessel were collected and stored.

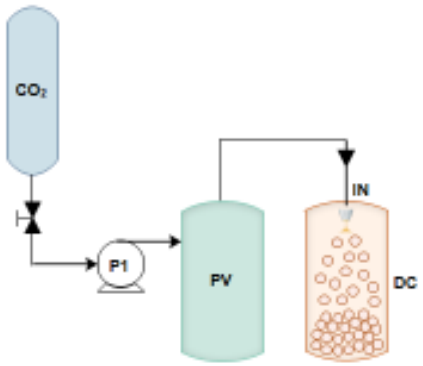

Figure 2.1 - Representation of the apparatus of PGSS processing. **P1**: pump; **PV**: high-pressure vessel; **IN**: injector nozzle; **DC**: depressurization chamber.[186]

2.2.3.3 Encapsulation of therapeutic deep eutectic systems through Supercritical Anti-solvent (SAS)

The SAS apparatus, represented in Figure 2.2, and described by Reverchon et al,[181] presented two HPLC pumps (Gilson, mod. 305), being one for the liquid solution and another for $scCO_2$. Firstly, CO_2 was pumped to the precipitator vessel (cylindrical vessel, I.V. of 0.5 L) until reaching the desired pressure (12 MPa). Then, when the anti-solvent steady flow was established the pure solvent was injected through the nozzle to the chamber in order to obtain steady-state conditions for solute precipitation.[181] The liquid solution (THEDES + carrier + solvent) flows through the nozzle (stainless-steel nozzle of 100 μm) to the precipitator chamber (cylindric vessel with an internal volume of 500 cm^3) and the flow was controlled by HPLC pumps. The precipitator vessel was heated with thin band heaters (40 °C; Watlow, mod. STB3J2J1) and the pressure in the chamber was measured with a standard pressure gauge (Salmoiraghi, mod. SC- 3200) and regulated with a micrometering valve (Hoke, mod. 1315G4Y), present at the exit of the chamber, that was heated by a cable heater (Watlow, mod. 62H24ASX), connected to a controller (Watlow, model 920). In the bottom of the chamber was a stainless-steel frit (pore diameter of 0.1μm) to collect the particles. A second exit vessel was located at downstream of the micrometering valve, to collect the liquid solvent. A backpressure valve (Tescom, mod. 26-1723-44) regulated the pressure in the vessel and a dry test meter was used to measure the CO_2 flow rate and the total amount of anti-solvent.[181,187] The experiment ended when the delivery of the liquid solution to the chamber was stopped, however, the supercritical CO_2 continued to flow to wash the chamber from any residual liquid solution. If the final purge with pure CO_2 did not take place, the solvent condensates during depressurization, disrupting the particles.[181]

In all experiments, polyvinylpyrrolidone (PVP), as a biocompatible polymer was used. This polymer allowed an homogeneous dispersion of the THEDES, at a ratio of 4:1 of PVP:THEDES (w/w). In the case of the SAS technology different solvents were tested, namely, DMSO, and a mixture of ethanol and acetone (50:50), with a concentration of 10 mg mL^{-1} in the liquid solution. The operating conditions used were 12 MPa and 40 °C in the precipitator vessel.

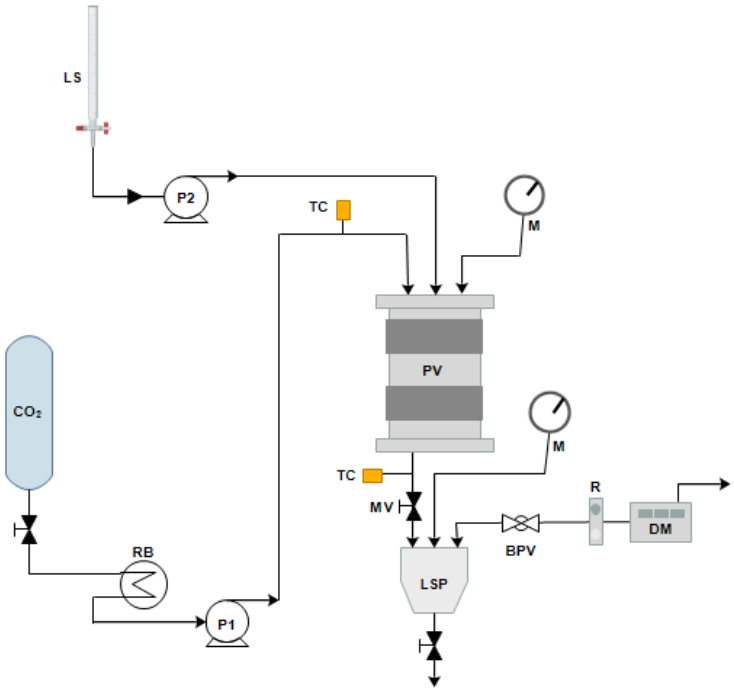

Figure 2.2 - Representation of the SAS processing apparatus. **LS**: liquid solution; **P1**, **P2**: pumps**; RB**: refrigerating bath; **TC**: thermocouple; **M**: manometer; **PV**: precipitator vessel; **MV**: micrometering valve; **LSP:** liquid separator; **BPV**: back pressure valve; **R**: rotameter; **DM**: dry test meter.[181,188]

2.2.3.4 Encapsulation of therapeutic deep eutectic systems through Supercritical Assisted Atomization (SAA)

The apparatus of SAA, represented in Figure 2.3, and described by Reverchon et al,[189] presented a cylinder with CO_2 that flowed through a high-pressure pump (Gilson model 305), and then to a heated bath (Forlab, Carlo Erba, TR12) before entering in the contactor, where CO_2 was solubilized in the liquid solution (THEDES + carrier + solvent). The liquid solution was pressurized with a high-pressure pump (Gilson model 305), heated, and sent to the saturator. The N_2 gas was taken from a cylinder to a calibrated rotameter (ASA model N5 2600) and was heated in a heat exchanger (Watlow model CBEN 24G6). The temperature control was assured through controllers connected with electrically thin bands. The saturator was a high-pressure vessel with an internal volume of 50 cm^3 that was loaded with a stainless-steel perforated saddle. The high surface area favours the contact between CO_2 and liquid solution in order to obtain a dissolution of the gaseous phase in the liquid. The liquid-gas solution moves through a thin wall injector (100 μm internal diameter). The injector consisted in a stainless-steel cylinder with a conical hole in the first part and a cylindrical one

in the second part, that produced a spray and formed droplets in the precipitator. In the precipitator, the N_2 was used to favour the evaporation of the liquid solvent in the vessel that operates near atmospheric conditions in a stainless-steel vessel, with an internal volume of 3dm^3. The particles were obtained from the evaporation of the liquid droplets and, the mixture of gas formed by CO_2, N_2 and liquid solvent vapours were pushed to an ordinate motion inside the precipitator by a flux conveyor. Finally, the particles were collected at the bottom of the precipitator on a stainless-steel filter (pore diameter of 0.1 μm). The gases were discharged in a cooled condenser for liquid solvent and the gas mixture went to a dry test meter (Schlumberger model 2000AP LPG G2.5) to measure the flow rate.[189]

In the experiments conducted by SAA technology, similarly to what was performed with SAS, PVP was used in a ratio of 4:1 of PVP:THEDES (w/w), using ethanol as solvent and a concentration of 10 mg mL^{-1} in the liquid solution. The operating conditions employed were 7 MPa and 40 °C, 70 °C, 70 °C in the saturator, precipitator, and condensator, respectively.

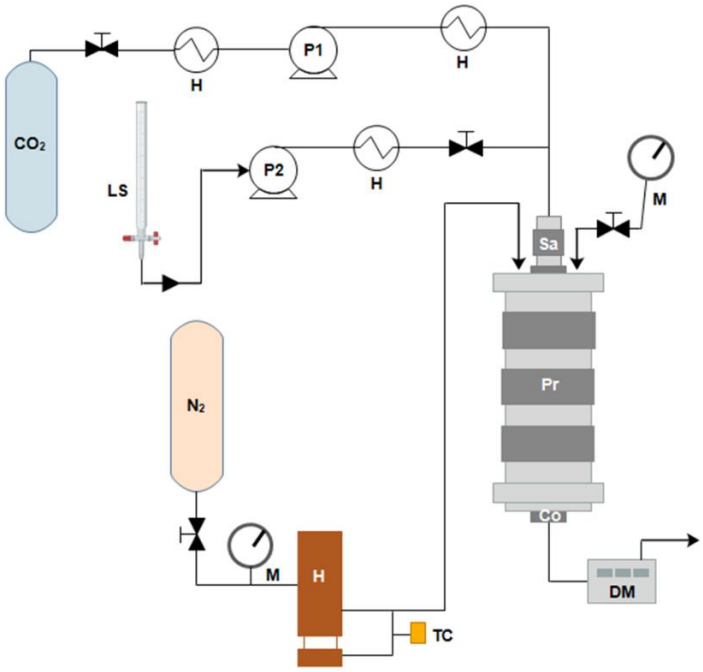

Figure 2.3 - Representation of SAA processing apparatus. **LS**: liquid solution; **H**: nitrogen heater and heat exchangers; **P1, P2**: pumps; **M**: manometer; **TC**: thermocouple; **Sa**: saturator; **Pr**: Precipitator; **Co**: condensator; **DM**: dry test meter.[189,190]

2.2.4 Physicochemical characterization

2.2.4.1 Polarized Optical Microscopy (POM)

Optical characterization of THEDES was carried out at room temperature using a transmission mode of an Olympus BX-51 and BX-53 polarized optical microscope connected to an Olympus KL2500 LCD cold light source. A droplet of THEDES was placed on a microscope glass slide and placed then observed. The images were obtained with an equipped camera (Olympus DP73 and SC50) and Olympus Stream Basic 1.9 software and Olympus Stream Start 2.4.2 (Olympus).

2.2.4.2 Nuclear Magnetic Resonance (NMR)

All NMR spectra ^{1}H, ^{13}C and ^{1}H-^{1}H NOESY were recorded at room temperature on Bruker Avance III spectrometer 400 (400.13 MHz for ^{1}H and 100.62 MHz for ^{13}C, Bruker) and chemical shifts were referenced to Me_4Si (δ in ppm). The samples were placed in a 5 mm NMR tube with deuterium dimethyl sulfoxide (DMSO-d_6) and data analysis was performed with MestReNova software (11.0.4-18998).

2.2.4.3 Fourier-transform Infrared Spectroscopy with Attenuated Total Reflection (FTIR-ATR)

FTIR spectra were recorded on a PerkinElmer Spectrum Two (Waltham) with attenuated total reflection (ATR) in the transmittance mode and with a wavenumber range between 400-4000 cm^{-1}. Spectra were acquired from 16 scans with 4 cm^{-1} resolution, at room temperature.

2.2.4.4 Inductively Coupled Plasma-Atomic Emission Spectrometer (ICP-AES)

The quantity of sodium in the samples of [INH][Sac] was measured by an inductively coupled plasma-atomic emission spectrometer from Horiba Jobin-Yvon, a model equipped with a 40.68 MHz RF.

2.2.4.5 Elemental Analysis

Organic salts were also characterized by elemental analysis with 2-3 mg of a sample in an Elemental analyzer Thermo Finnigan-CE Instruments Flash EA 1112 CHNS series.

2.2.4.6 pH measurements

The pH of liquid mixtures and aqueous solutions was measured using an analogic pH meter (914 pH/Conductometer, model 2.914.0220, Metrohm), with a glass electrode coupled to a temperature sensor (NTC) (6.0228.010, Metrohm). All measurements were performed at room temperature.

2.2.4.7 Energy dispersive x-ray spectroscopy

Energy dispersive x-ray spectroscopy (EDS) from particles made with PGSS was used to perform a chemical analysis of the particles surface and evaluate the presence or absence of nitrogen, an arginine component. The analysis was performed in five sample regions, using a Link eXL-II spectroscope (Oxford Instruments), at low vacuum mode (50 Pa) with an acceleration voltage of 15 kV, coupled to SEM.

2.2.5 Thermal characterization

2.2.5.1 Differential Scanning Calorimetry (DSC)

The DSC experiments were performed using a DSC Q200 from TA Instruments and a Setaram DSC 131 equipment.

- Organic salts were placed in aluminium hermetic pans with a pinhole and the measurements were made under a dry nitrogen atmosphere (flow rate of 50 mL min^{-1}) with samples between 3-10 mg. The samples were equilibrated at 25 °C for 5 minutes and then 2 cycles for INH and 3 cycles for organic salts in a range of temperatures between -90 °C and 180 °C were performed. Each cycle was performed with a ramp up to 180 °C with a heating rate of 10 °C min^{-1}, followed by an isothermal period of 1 minute, and a cooling ramp to -90 °C with a cooling rate of 10 °C min^{-1}.
- THEDES were analysed in a Setaram DSC 131 equipment. The measurements were, also under performed a dry nitrogen atmosphere, with samples of 5-10 mg packed in

aluminium hermetic pans. The samples of the initial compounds were equilibrated at 20 °C for 5 minutes, then a cycle in a range of temperatures between 5 °C - 230 °C for EMB; 5 °C - 260 °C for L-arg, and 5 °C - 170 °C for CA was performed. Each cycle was performed with an isothermal period of 2 minutes, and cooling/heating rate of 10 °C min^{-1}. The samples with THEDES were equilibrated at 20 °C for 5 minutes, then a cycle in a range of temperatures between 5 °C - 230 °C for EMB systems and 5 °C - 260 °C for systems with L-arg was performed, followed by an isothermal period of 2 minutes, and cooling/heating rate of 10 °C min^{-1}.

THEDES of CA:L-arg:H_2O were also analysed with the DSC Q200 to determine the melting temperature of CA and the ternary mixtures of CA:L-arg:H_2O. In this case, the samples were sealed in an aluminium hermetic pan and were submitted to two cooling/heating cycles between -90 °C and 200 °C, with a rate of 10 °C min^{-1}, at a nitrogen flow rate of 50 mL min^{-1}. The thermic events were acquired through the TA Universal Analysis 2000 (4.7.0.2) software.

2.2.6 Morphological characterization

2.2.6.1 Scanning Electron Microscopy (SEM)

- PGSS particles: particle size, size distribution and morphology of the produced particles were analysed through SEM (JEOL, model JSM6010-LV). The samples were prepared for observation by covering them with gold (Au), in a sputter coater (Cressington, model 108 auto). Micrographs of the prepared aliquots were taken at an acceleration voltage of 10 kV. The median size of the particles and their size distribution were obtained from ImageJ (version 1.52a) by measuring the particles diameter (500 particles per sample). The polydispersity index (PDI) was calculated by dividing the standard deviation (SD) of 500 diameter measurements by the respective mean particle size.
- SAA particles: size distribution and morphology of the produced particles were analysed through SEM (Carl Zeiss AURIGA CrossBeam (FIB-SEM)) workstation. The samples were prepared for observation by covering them with gold (Au) in a sputter coater of Quorum.

2.2.6.2 Dynamic light scattering (DLS)

Particle size and size distribution from particles made with SAA were measured with a DLS Zetasizer Nano ZS (Malvern). The particles were dispersed in 1 mL of acetone and the measurements were made using quartz cuvettes at 25 °C and with a scattering angle of 173°. The measurements were taken assuming the refractive index of PVP (1.53).

2.2.7 Encapsulation efficiency

The particles were dispersed in deionized H_2O at 15 mg mL^{-1} and destroyed in an ultrasound bath (XUB5, Grant) at 25 °C. THEDES contained in the particles remained solubilized in the H_2O whereas the lipid component was separated through centrifugation at 14 000 rpm for 10 minutes and further filtration of the supernatant (0.22 μm filter), being the assay made in triplicates.

- PGSS particles: The filtrated collected was analysed by UV-VIS spectrophotometry (VICTOR Nivo™, PerkinElmer). The amount of therapeutic liquid mixtures was determined at a wavelength of 220 nm, using a calibration curve of THEDES linear within the range of 0.05-1.5 mg mL^{-1}.

The encapsulation efficiency was determined as the amount of encapsulated THEDES relatively to the initial THEDES added, as follows:

$$EE\ (\%) = \frac{Encapsulated\ therapeutic\ liquid\ mixture}{Total\ therapeutic\ liquid\ mixture\ added} \times 100 \quad (2)$$

2.2.8 Drug release profile

Particles were dispersed in PBS (PGSS particles - 10 mg mL^{-1}) and agitated at 60 rpm and 37 °C. Aliquots of 0.5 mL were collected at different time points, filtered (0.22 μm) and analysed by UV-VIS spectrophotometry with a similar method of quantification as that described for encapsulation efficiency. The volume was replaced by fresh PBS and the assay was made in triplicates.

2.2.9 *In vitro* bioavailability assessment

2.2.9.1 Solubility Studies

- Solubility of organic salts with INH was performed in water and PBS at 37 °C. Briefly, an excess of organic salt was added to water and PBS solution and stirred (60 rpm) for 24 h. The determination of the solubility of organic salts was made by UV spectroscopy in a microplate reader (VICTOR Nivo ™, PerkinElmer). The absorbance of the solutions was measured at the maximum absorption wavelength of INH (263 nm). The calibration curve was made using INH as standard in each of the solvent for quantification (R^2 = 0.9974 for water and R^2 = 0.9993 for PBS). All samples were measured in triplicates.
- Solubility of THEDES was made with a similar method to the one described to organic salts, also in PBS solution at 37 °C, to simulate physiological conditions. The determination of the API solubility was made by UV spectroscopy in 1 mL quartz cuvettes, using the UV/VIS Spectrometer Lambda 35 (PerkinElmer) and the software PerkinElmer UV WinLab. The absorbance of the solutions was measured at the wavelength of 203 nm for EMB and 211 nm for L-arg. The calibration curve was made using the respective API as standard for quantification (R^2 = 0.9873 for EMB and R^2 = 0.9982 for L-arg).
- Solubility of anti-TB THEDES as carriers was made by dissolving an excess of an anti-TB drug (INH, PZA or RIF) in, approximately 1 g of different liquid mixtures and then of was added 1 mL of PBS solution and kept stirring (60 rpm) for 24 h. The determination of the solubility of anti-TB drugs using THEDES as a carrier was made by UV spectroscopy using a microplate reader (VICTOR Nivo ™, PerkinElmer). The absorbance of solutions was measured at 263 nm for INH, 270 nm for PZA and 335 nm for RIF. The calibration curve was made using the respective drugs as standard in PBS for quantification (R^2 = 0.9957 (INH), R^2 = 0.9919 (PZA), R^2 = 0.9977 (RIF). All samples were measured in triplicates.

2.2.9.2 Permeability using a Synthetic Membrane

The permeability studies were made with glass Franz diffusion cells (PermeGear) with 8 mL in the receptor compartment, 2 mL in the donor compartment and an effective mass transfer area of 1 cm^2.

The membrane used was a polyethersulfone (PES-U) membrane, with 150 μm thickness and 0.45 μm pore size (Sartorius Stedim Biotech). The membrane was placed between the receptor and donor compartment and held with a stainless-steel clamp. The

receptor compartment was filled with PBS solution and the air bubbles were removed by carefully tilting the Franz cells for the air bubbles to escape through the sampling arm. Then the donor compartment was filled with the API, THEDES or organic salts and 2 mL of PBS solution. Samples were taken at different time points and the amount of diffused API was measured by UV spectroscopy, similarly to what was described above for solubility studies. The experiments were performed at 37 °C in a water bath with stirring at 60 rpm.

The permeability (P) was calculated by the following equation:

$$-\ln\left(1-\frac{2C_t}{C_0}\right) = \frac{2A}{V} \times P \times t \quad (3)$$

where C_t is the concentration in the receptor compartment at time t, C_0 is the initial concentration in the donor compartment, V is the total volume in the two compartments, and A is the effective area of permeation. The permeability can be calculated from the slope of the curve $-(V/2A) \times \ln(1-2C_t/C_0)$ versus t (cm s^{-1}).[185,191,192]

The diffusion coefficient (D) across the membrane was calculated according to Fick's Law of diffusion, following the equation:

$$D = \frac{V_1 V_2}{V_1+V_2} \times \frac{h}{A} \times \frac{1}{t} \ln\left(\frac{C_f - C_i}{C_f - C_t}\right) \quad (4)$$

where D is the diffusion coefficient ($cm^2\ s^{-1}$), C_i and C_f are the initial and final concentrations, and C_t is the concentration at time t in the receptor compartment (mol L^{-1}), V_1 and V_2 are the volume of liquid in donor and acceptor compartment, respectively (cm^3), h is the thickness of the membrane (cm) and A is the effective diffusion area of the membrane (cm^2).[185,191,192]

2.2.10 *In vitro* biological performance

2.2.10.1 Cell Culture

Different cell lines were used, during this work, to evaluate the biological performance of different systems prepared, such as L929, Caco-2, A549 and THP-1 cells. L929 cells are mouse fibroblasts of connective tissue (DSMZ, ACC 2), reported as a model for cytotoxicity studies according to ISO/EN 10993 guidelines.[193] Caco-2 cells are epithelial cells from human colon cancer (DSMZ, ACC 169) used as a model of human intestinal absorption of drugs and other substances. A549 are human alveolar epithelial cells from human lung carcinoma (DSMZ, ACC 107), and THP-1 are human acute monocytic leukemia cells (ATCC TIB202).

Cell lines L929 and A549 were cultured in MEM media (Corning) supplemented with 10% heat-inactivated fetal bovine serum (FBS, Corning) and 1% antibiotic-antimycotic solution (Corning). Caco-2 cells were cultured in RPMI 1640 media (Gibco) supplemented with 10% FBS (Gibco) and 1% antibiotic (PS, Gibco). THP-1 were grown in RPMI 1640 media also and supplemented with 10% FBS, 10 mM HEPES and 1 mM sodium pyruvate. All cultured cell lines were maintained at 37 °C in a humidified incubator with 5% CO_2. Before use in different assays, THP-1 monocytes were differentiated into macrophages by induction with 20 nM phorbol-12-myristate-12-acetate (PMA), overnight.

2.2.10.2 Cell Viability Assays

Cell viability was evaluated with L929, Caco-2 and A549 confluent and non-differentiated cells and confluent macrophages seeded on a 96-well plate ($1x10^4$ cells/well for L929; $2x10^4$ cells/well for Caco-2; $2x10^4$ cells/well for A549; $5x10^4$ macrophages/well) and after 24h of seeding the medium was removed and the cells were incubated with different concentrations of pure components (RIF diluted in culture media with 5% DMSO), organic salts and THEDES diluted in culture media, during 20-24h. After the incubation time, the cells were washed with PBS and cell viability was evaluated using CellTiter96® AQueous One Solution Cell Proliferation Assay based on MTS reagent (3-(4,5-dimethylthiazol-2-yl)-5-(3-carboxymethoxyphenyl)-2-(4-sulfophenyl)-2H-tetrazolium)). The amount of formazan produced was measured at 490 nm in a microplate reader (Epoch Microplate Spectrophotometer, Bio-Tek Instruments or VICTOR Nivo™, PerkinElmer) and cell viability was expressed in percentage of living cells compared to the control (untreated cells). The assay was performed with at least three independent experiments, in triplicate, and the data were analysed by GraphPad Prism 8.0.1.

2.2.10.3 Permeability using a Biological Membrane

The permeability of different combinations of THEDES and APIs was evaluated using the A549 cell line adapting the method described by Vieira and co-workers.[100] The cells were seeded on 12-well transwell inserts (Falcon cell culture PET inserts, pore size 0.4 μm, area 0.9 cm^2) at a cell density of $1.26x10^4$ cells/well.[100] The cells were grown in supplemented and culture media that was added to both apical and basolateral sides. The media was changed every 2 days, for 8 days, until a homogenous monolayer was achieved. The

transepithelial electrical resistance (TEER) was measured in all wells and in a well of medium without cells to be considered as blank. The TEER was checked before the assay using an EVOM 3 (epithelial voltohmmeter, World Precision Instruments), equipped with a pair of electrodes placed on the apical and basolateral sides. The TEER value obtained in this study was 294 ± 14 ohm cm^2 (mean ± SD). The samples were incubated at 37 °C with 5% CO_2 for 6 hours and was collected 0.5 mL of sample from the basolateral side at different time points, then replaced with the same quantity of fresh PBS. The samples were analysed and quantified by HPLC (Dionex ICS3000; MERCK Purosphere STAR RP18 250x4 mm column; UV detection at 210, 238, 280, 320 and 510 nm; eluents: 20 mM NAH_2PO_4 + 0.2% triethylamine at pH 7.0 and acetonitrile). The analyses were performed at 40 °C. The apparent permeability (P_{app}) for pure compounds and THEDES was calculated following the equation:

$$P_{app\ (cm/s)} = \frac{\Sigma m_a}{A \times m_d \times t} \quad (5)$$

where m_a is the mass of compound permeated at each time point (g), A is the effective area of permeation where the monolayer is seeded (cm^2), m_d is the initial mass of compound added to the apical side (g) and t is the time of permeation (s). The cellular uptake by A549 cells was estimated by the following equation:

$$Cellular\ uptake = C_0 - C_{Bf} - C_{Af} \quad (6)$$

where C_0 is the initial concentration added on the apical side, C_{Bf} is the final concentration on the basolateral side and C_{Af} is the final concentration on the apical side.

2.2.11 Toxicity assessment

2.2.11.1 Exposure of zebrafish to compounds

Zebrafish (*Danio rerio*) obtained from Aquaplante (Portugal) were acclimated under laboratory conditions at least for 48 h (housed in a glass aquarium with a closed-circuit system with filtered de-chlorinated tap water). Zebrafish of both sexes were randomly distributed by 10 aquariums of 15 L, in groups of four fishes per aquarium (n = 40; weight 0.52 ± 0.4 g; length 1.8 ± 90.3 cm). Then, zebrafish were exposed for 4 days to different concentrations of organic salts based on INH and INH itself (2 μM, 5 μM and 15 μM), being monitored the pH (Hanna Instrumentation, USA), temperature (manual thermometer), total dissolved solids (TDS, test kit API, CHarfont) and dissolved oxygen (Hanna

Instrumentation, USA) during the assay (pH of 7.32 ± 0.07, temperature of 21.8 ± 0.3 °C, TDS of 263 ± 1 ppm and dissolved oxygen higher than 6 mg L^{-1}). During the assays, fishes were fed every day with commercial flakes of dry food (Tetra) and the mortality rate was verified daily. At the end of the assay, fishes were sampled, euthanized by freezing method at -80 °C and stored at the same temperature.

2.2.11.2 Samples homogenization and quantification of total protein content

Fishes were defrosted and homogenized in 2 mL of PBS using a Tissue Homogenizer (Tissue Master 125, Omni, Kennesaw). Homogenates were centrifuged at 15,000xg for 10 minutes, at 4 °C (VWR, model CT 15RE from Hitachi Koki Co.). Total protein content in samples was quantified by Bradford used to normalize biomarkers results.[194]

2.2.11.3 Glutathione S-transferase (GST) activity

The GST activity was measured by adapting the method described by Habig et al.[195] The assay is based on the quantification of a conjugate that was formed by a reaction between GSH and cDNB leading to an increase of absorbance at 340 nm. To perform the assay, a reaction mixture solution with PBS, 200 mM GSH and 100 mM cDNB was prepared. Then, a dilution of 1:10 was made with the reaction media and a sample of 200 μL per well was added to a 96-well plate. The GST activity was measured at 340 nm each minute for 6 minutes, using a microplate reader (Synergy HTX, BioTek). Differences in absorbance per minute was then estimated and the reaction rate was calculated using cDNB extinction coefficient of 0.0053 μM cm^{-1}. Therefore, the results were normalized with the total protein concentration in each sample.

2.2.11.4 Catalase (CAT) activity

The catalase activity was determined accordingly to Johansson and Borg.[196] The method was based on a reaction of the enzyme with methanol in the presence of an optimal concentration of H_2O_2. The formaldehyde produced was measured using Purpald as a chromogen. Briefly, 20 μL of each sample and standard was added to a 96-well plate, then 100 μL of assay buffer (100 mM PBS) and 30 μL of methanol was also added. The reaction was initiated by adding 20 μL of 0.035 M of H_2O_2 (30%) and incubating for 20 minutes on a

shaker. After incubation, 30 μL of 10 M KOH and 30 μL of Purpald (34.2 M in 0.5 M HCl) were added to each well and incubated for 10 minutes on a shaker. Afterwards, 10 μL of potassium periodate (KIO_4 65.2 mM in 0.5 M KOH) was added to each well and allowed to incubate for 5 minutes. Then, the absorbance was measured at 540 nm in a microplate reader (Synergy HTX, BioTek). Formaldehyde concentration of the samples was determined based on a calibration curve using formaldehyde standards in a range of concentrations from 0 to 75 μM. Results were normalized with total protein concentration in each sample.

2.2.11.5 Superoxide dismutase (SOD) activity

The superoxide dismutase assay was made by adapting the method described by Sun et al.[197] In this method, superoxide radicals ($^{\bullet}O_2^-$) were generated by a reaction of xanthine with XOD, which reduce NBT to formazan. SOD competes with NBT for the dismutation of $^{\bullet}O_2^-$, inhibiting its reduction. Briefly, 200 μL of 50 mM PBS (pH 8.0) was added to a 96-well plate, followed by 10 μL of 3 mM EDTA, 10 μL of 3 mM xanthine, 10 μL of 0.75 mM NBT and 10 μL of sample or standard. Then, the reaction was started by adding 10 μL of XOD and the absorbance was measured at 560 nm, every 2 minutes, until reaching 26 minutes, using the microplate reader (Synergy HTX, BioTek). The SOD results were expressed as percentage (%) of inhibition of NBT-diformazan, regarding the total protein concentration in each sample.

2.2.11.6 Lipid peroxide assay

The lipid peroxides assay was based on the protocol described by Uchiyama and Mihara.[198] Concisely, 5 μL of each sample was added to 45 μL of PBS. Next, 12.5 μL of SDS (8.1%), 93.5 μL of TCA (20%, pH 3.5) and 93.5 μL of TBA (1%) were added to each microtube. Then, 50.5 μL of MiliQ-grade ultrapure water was added to each microtube and stirred for 30 seconds in a vortex. After, microtube lids were punctured with the aid of a needle and incubated in water (10 minutes at 100 °C). Then, they were placed on ice for a few minutes to cool down and 62.5 μL of MiliQ-grade ultrapure water was added. Then, microtubes were centrifuged at 5000xg for 5 minutes. Duplicates of 150 μL of the supernatant of each reaction were added to a 96-well plate and the absorbance was read at 530 nm (Synergy HTX, BioTek). The lipid peroxides were quantified by building a calibration curve (based on

thiobarbituric acid reactive substance (TBARS) 0-0.1 μM) using MDA as standard and normalising data dividing by the total amount of protein for each sample.

2.2.11.7 Total Ubiquitin quantification

The total ubiquitin was quantified through an Enzyme-linked immunosorbent assay (ELISA) as described elsewhere by Madeira et al.[199] In this assay, 50 μL of each sample and respective standards were added to a 96-well plate and incubated overnight at 4 °C. Then, the microplate was washed 3x with PBS solution containing 0.05% Tween-20 and 200 μL of blocking solution (PBS with 1% BSA) was added to each well and incubated at 37 °C for 90 minutes (Labnet, Edison). Next, the microplates were washed one more time with PBS solution containing 0.05% Tween-20, and the primary antibody (Ub P4D1) was added to the microplate after a proper dilution (0.5 μg mL^{-1}) and incubated for 90 minutes at 37 °C. Then, the microplate was washed again 3x with PBS solution containing 0.05% Tween-20, and 100μL of the substrate (TMB) was added to each well and incubated for 30 minutes at room temperature. Subsequently, 100 μL of stop solution (1 M HCl) was added to each well and the absorbance was measured at 415 nm. The calibration curve was made with serial dilutions of purified ubiquitin (0-0.8 μg mL^{-1}) and the results were normalized with the total amount of protein for each sample.

2.2.12 Microbiological evaluation

2.2.12.1 Antimicrobial activity in *Mtb* (H37Rv)

Microbiological assays were performed in a Biosafety Level 3 laboratory at the Faculty of Pharmacy of the University of Lisbon, according to the national and European academic containment level 3, laboratory management and biosecurity standards, based on applicable EU Directives. *Mycobacterium tuberculosis* H37Rv (ATCC 27294), a drug-susceptible strain, was used for the determination of minimal inhibitory concentration (MIC) and minimal bactericidal concentration (MBC) of THEDES, by the broth dilution method with concentrations varying between 0.125-16 μg mL^{-1}. Briefly, *Mtb* cultures on the exponential growth phase were centrifuged and washed with PBS, then re-suspended in a fresh culture medium. Bacterial clusters were dismantled and removed by ultrasonic treatment for 5 minutes followed by low-speed centrifugation (500xg) for 2 minutes. Single

cell suspension was verified by fluorescence microscopy. The selected concentrations of THEDES were incubated with bacterial suspensions containing approximately 10^5 colony-forming units (CFUs) per mL. The MIC was determined at day 10 of incubation, by visual examination of the plates. For MBC determination, the bacterial samples were recovered from MIC test plates, diluted 1:10 in water and platted in 7H10 + 10% OADC solid medium. The MBC corresponded to the concentration that produced no visible colonies on the solid medium.

2.2.12.2 Macrophages infection with *Mtb* (H37Rv)

Mtb cultures were prepared as described above and resuspended in a macrophage culture medium. Macrophages in 96-well plates were infected with *Mtb* at a MOI of 0.1 for 3h, at 37 °C with 5 % CO_2. Following internalization, cells were washed three times with PBS and re-suspended in an appropriate culture medium with the respective treatments. On day 3 post-infection, half the culture medium was replenished with or without treatment reinforcement.

2.2.12.3 Intracellular survival of bacteria

When required, infected cells were lysed within 10 minutes of treatment with 0.05% IGEPAL® solution in water, a non-ionic, non-denaturing detergent that disrupted eukaryotic cells but did not affect mycobacterial viability, with the goal being to assess the CFU of viable intracellular bacteria. Serial dilutions of the resulting bacterial suspension were plated in Middlebrook 7H10 agar with 10 % OADC and incubated for 2-3 weeks at 37 °C.

2.2.13 Statistical analysis

The statistical analysis was performed using GraphPad Prism 8.0.1 software. All measurements were made in triplicate and the data were presented as mean ± SD. Normality was evaluated by Shapiro-Wilk test. Data that obey to a normal distribution were tested with one-way and two-way ANOVA analysis with Bonferroni post-hoc test for multiple comparisons or t-test for pairs of samples. Data that do not follow a normal distribution were tested with non-parametric tests: the Kruskal-Wallis test and Dunn's test were used for

multiple comparisons. The differences were considered significant when the p value was ≤ 0.05.

The following chapter was adapted from the publication:

Santos F., Branco L.C., Duarte A.R.C. Organic salts based in isoniazid drug: synthesis, bioavailability and cytotoxicity studies. Pharmaceutics (2020). 12 (10): 952. DOI: 10.3390/pharmaceutics12100952.

3

ORGANIC SALTS BASED ON ISONIAZID

The pharmaceutical industry and research community are continuously trying to improve their approaches and redesign drugs to enhance their therapeutic efficiency, while at the same time reducing the waste produced in the research and manufacture of drugs. The use of alternative solvents is one of the approaches that has been explored over the years for pharmaceutical and medicinal applications, namely in the improvement and modulation of the pharmacokinetics of drugs. Ionic systems such as ionic liquids and organic salts as well as eutectic mixtures are examples of alternative solvents that have been commonly investigated in pharmaceutical research.[148] Several studies reported that these solvents can avoid polymorphic forms of the drugs, and improve the solubility, permeability, and therapeutic activity of different APIs.[119,138,152,200–203] Lately, the use of organic salts and ionic liquids (OSILs) for therapeutic applications has been explored, using an API in its ionic form (e.g., ampicillin,[204–206] zoledronic acid,[207] and ibuprofen[208]) and combining it with biocompatible counterions, producing API-OSILs. The use of API-OSILs allows the design of improved drugs that may modify the functionality and can provide important characteristics to the original API.[130,138,209]

TB infection as mentioned in chapter I presents different problems associated with its therapy and the main challenges are related to the decrease in treatment time, improvement of the stability of the drugs, and finding alternatives that can reduce cumulative adverse effects and prevent multidrug resistance.[63,210] The development of drug resistance is mostly due to genetic modifications in genes that encode drug targets, non-permeability of their cell wall, and the activity of efflux pumps.[211,212] INH has been used for the prevention and treatment of TB infection since the 1950s.[213] This drug presents high resistance associated with mutations in its activator enzyme (KatG, a multifunctional catalase–peroxidase that

activates INH and leads to the inhibition of inhA (enoyl-acyl-carrier protein (ACP) reductase) and consequently, to the inhibition of the biosynthesis of mycolic acids).[213,214] Machado and co-workers mentioned that besides the mutations that occur in the *inhA* gene and cause resistance to the INH drug, other genes could suffer from mutations and contribute to INH resistance, like *ndh*, *kasA* and *oxyR-ahpC* from the intergenic region.[212,215] Despite the low stability and fast degradation when administered with other anti-TB drugs,[216–218] INH continues to be an essential drug recommended by WHO to integrate different drug regimens to treat tuberculosis infections.[213] Some studies reported with this drug showed an improvement of the INH solubility by the simple dissolution of the API in different imidazolium-based ILs, observing that the solubility of the INH decreases with the increase of the alkyl chain in the IL cation.[219] Another approach reported in the literature, to improve the physicochemical properties and stability of INH is the use of cocrystals with INH, combining with numerous conformers like *p*-hydroxybenzoic acid,[220] nicotinamide,[220] fumaric acid,[220] succinic acid,[220] vanillic acid,[217] ferulic acid,[217] caffeic acid,[217] and resorcinol.[217] However, to our knowledge, it was not reported any study that included INH in the IL structure by protonation approach or combination with a biocompatible counterion forming API-OSILs.

Considering the importance of contributing to the enhancement of TB therapy for better adherence of the patients to the treatment, finding well-tolerated drugs as well as more stable formulations is mandatory. The main goal of the following work was the synthesis and characterization of different API-OSILs based on INH cation and the subsequent study of their bioavailability (solubility and permeability studies), cytotoxic profiles and toxicity in zebrafish.

3.1 Synthesis and characterization of INH-based salts

In the synthesis of OSILs based on INH, the INH drug was used as an organic cation and different counterions were selected. The counterions selected to be combined with INH were chosen as they are generally considered biocompatible and are commercially available.[221,222] Two possible synthetic approaches involving direct protonation by suitable acid addition or anion-exchange reactions in optimized conditions were performed. No additional purification steps were required in the case of the direct protonation approach,

while in the case of the anion-exchange approach, the inorganic salt was removed by precipitation using an appropriate organic solvent. All obtained organic salts were characterized by ^{1}H and ^{13}C NMR, FTIR-ATR and elemental analysis in order to prove the desired organic chemical structure as well as final purities. Additionally, the ICP-AES technique was used in the case of anion-exchange reaction in order to quantify the Na content in the final compounds. Figure 3.1 illustrates the synthetic approaches and type of anions used for synthesizing the organic salts.

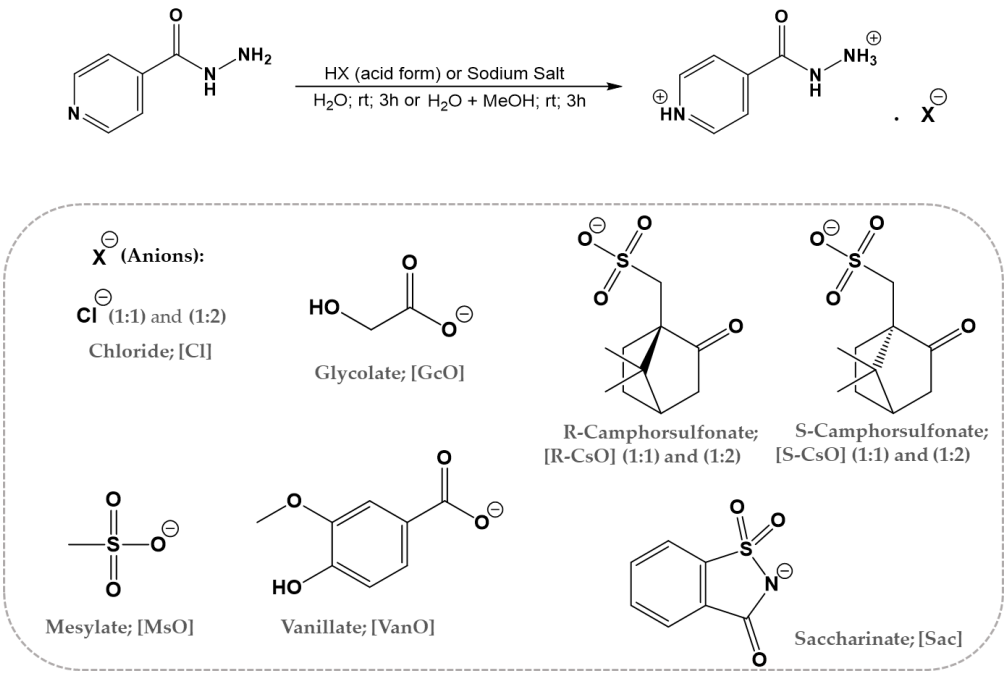

Figure 3.1 - Scheme with methods used for preparation of organic salts with INH as cation.

In some cases, it was possible to prepare INH based organic salts in the mono- and dicationic form and then characterized them by ^{1}H-NMR. A clear chemical shift from aromatic protons of neutral INH (7.73 and 8.70 ppm) compared to mono-protonated (7.89 and 8.82 ppm, for [INH](Cl]) and di-protonated structures (8.05 and 8.91 ppm for $[INH][Cl]_2$), was detected (Figure 3.2). In FTIR-ATR spectra, a characteristic peak at 3300 cm^{-1} was detected which corresponded to the stretching of N-H in the hydrazide group. This group in protonated forms was not observed due to the vibrational changes that take place when protonation occurs. For all FTIR spectra, the peaks in the region of 3100–2900 cm^{-1} observed were attributed to stretching vibrations of heteroatoms groups, and in protonated

compounds the region that appears between 2100–1900 cm^{-1} gets more intense in dicationic form, appearing a new band at 2500 cm^{-1}.

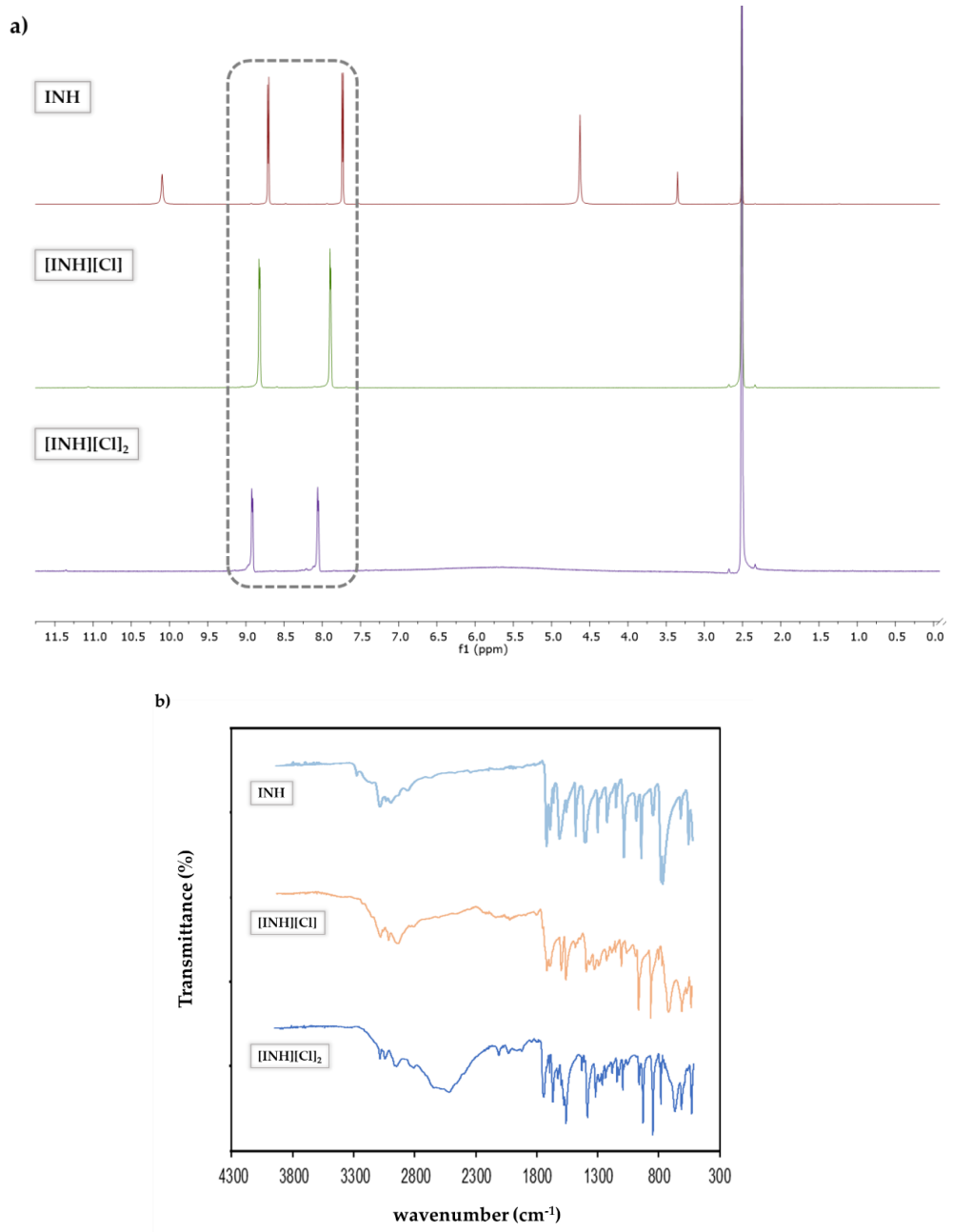

Figure 3.2 - Characterization of mono and diprotonation of INH with counterion chloride. (**a**) ^{1}H-NMR spectra of INH (top), [INH][Cl] (middle) and [INH][Cl]$_2$ (down). (**b**) FTIR-ATR spectra of INH (top), [INH][Cl] (middle) and [INH][Cl]$_2$ (down).

3.2 Thermal characterization

The melting point (T_m), crystallization (T_c), and glass transition (T_g) temperatures were measured using DSC and are summarized in Table 3.1. From thermogram data of [INH][Cl], the lowest melting temperature and a higher reduction in its melting point compared to starting INH was observed for this salt. In general, the other organic salts showed melting points lower than INH, except for [INH][Sac], which presented a melting point slightly above the 173 °C of INH. The organic salts containing [GcO], [S-CsO], [S-CsO]$_2$, [R-CsO], [R-CsO]$_2$ and [VanO] anions seem to become amorphous after the first cycle, which indicated that crystallization of INH was suppressed by these different organic anions, reducing or eliminating its polymorphic behaviour.

Table 3.1 - Thermodynamic parameters determined for organic salts prepared (Data obtained from Figures A.1.32 to A.1.42, Appendix A).

Compounds	Physical state at room temperature	T_g (ºC)	T_m (ºC)	T_c (ºC)
INH	White crystalline powder	-	173	86
[INH][Cl]	Pale pink solid	-	93	-10
[INH][Cl]$_2$	Pale white solid	7	160	65
[INH][MsO]	Pale white solid	-	133	54
[INH][GcO]	White solid	39	-	-
[INH][S-CsO]	Yellow solid	-	-	-
[INH][S-CsO]$_2$	Yellow solid	14	-	-
[INH][R-CsO]	Pale white solid	-	-	-
[INH][R-CsO]$_2$	Yellow solid	17	129	-
[INH][VanO]	Pale brown solid	37	-	-
[INH][Sac]	Pale orange solid	-64	179	-88

3.3 Solubility and permeability studies

The solubility studies were carried out in water and PBS at 37 °C to simulate the physiological conditions and the results are represented in Table 3.2 and Figure 3.3.

Table 3.2 - Solubility of INH and respective organic salts, at 37 ºC, in water and PBS.

Compounds	Solubility in H_2O (mg mL^{-1})	pH (H_2O)	Solubility in PBS (mg mL^{-1})
INH	152.02 ± 2.93	6.56	182.58 ± 2.04
[INH][Cl]	141.57 ± 3.52	2.63	130.69 ± 0.89
$[INH][Cl]_2$	174.90 ± 0.92	1.56	204.48 ± 10.49
[INH][MsO]	73.04 ± 2.92	2.46	38.97 ± 7.24
[INH][GcO]	89.79 ± 1.73	4.27	84.21 ± 2.81
[INH][S-CsO]	119.07 ± 0.76	3.12	174.99 ± 0.26
$[INH][S\text{-}CsO]_2$	133.11 ± 11.57	2.02	189.99 ± 29.23
[INH][R-CsO]	67.07 ± 1.04	3.03	115.62 ± 2.81
$[INH][R\text{-}CsO]_2$	177.38 ± 5.62	1.60	198.41 ± 8.14
[INH][VanO]	47.98 ± 1.28	4.55	45.23 ± 1.02
[INH][Sac]	42.72 ± 2.57	5.79	54.74 ± 4.26

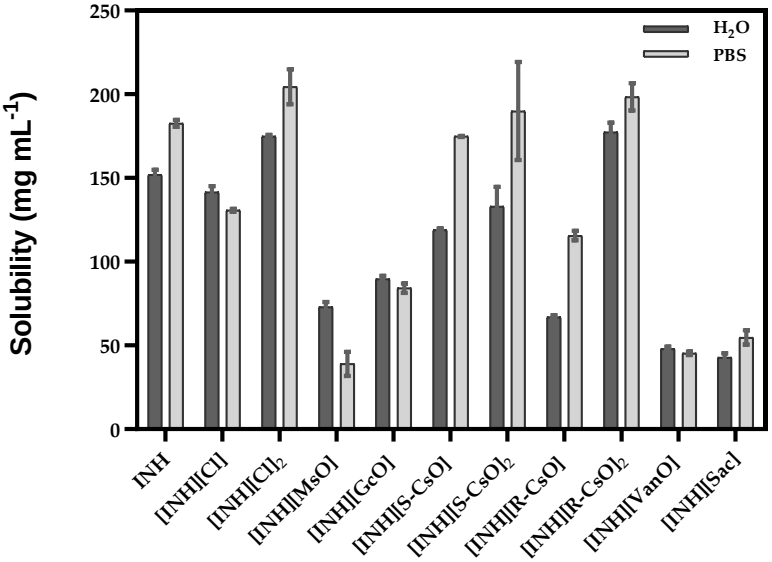

Figure 3.3 - Solubility of INH and organic salts prepared with INH in water and PBS. The results are represented as mean ± SD.

The anions that presented higher values of solubility were double protonated and the corresponding anions monoprotonated presented a solubility profile similar to INH, except for [INH][R-CsO]. The other organic salts did not present an improvement on the solubility

of INH in the selected media, and in most cases presented values that were lower than the API itself. Regarding the measurement of the pH of all organic salts dissolved in water, a decrease in pH was observed, presenting an acidic pH, that was, lower than the pH of INH.

The permeability studies were only carried out with the organic salts that seemed more promising in terms of solubility characteristics, such as [INH][Cl] in both ratios and [INH][CsO] in the R and S form and both ratios, and the results are presented in Table 3.3.

Table 3.3 - Permeability of INH and organic salts through synthetic membranes, at 37 ºC in PBS.

Compounds	Permeability (10^{-5} cm s^{-1})	Diffusion Coefficient (10^{-6} cm^2 s^{-1})
INH	3.63 ±0.03	6.77 ± 0.6
[INH][Cl]	2.14 ± 0.01	4.09 ± 0.1
$[INH][Cl]_2$	3.35 ± 0.04	9.53 ± 1.2
[INH][S-CsO]	2.40 ± 0.01	6.53 ± 0.8
$[INH][S\text{-}CsO]_2$	-	-
[INH][R-CsO]	1.38 ± 0.01	7.49 ± 0.7
$[INH][R\text{-}CsO]_2$	-	-

The permeability assays with synthetic membranes as the first screening of diffusion coefficients and cumulative mass release were performed. A lower permeability of organic salts tested comparing to the one presented by pure INH was observed, with the exception of the organic salt in dicationic form, chloride, which presented a value near to the one presented by INH. In terms of the diffusion coefficient in the media, the dicationic form chloride presented higher diffusion coefficient and the other organic salts presented a diffusion coefficient value near to the isoniazid itself, with exception of chloride monoprotonated that presented the lower value of diffusion coefficient. The organic salts composed by INH diprotonated and camphorsulfonates presented values of permeability and diffusion coefficients too low to allow an accurate measure, possibly due to the larger size of the molecules that cannot permeate the membrane.

3.4 *In vitro* biological performance

Cell viability of INH and organic salts was evaluated in two different cell lines, L929 and A549, and at different concentrations, ranging between 100 mM - 1 mM (Figure 3.4). At a concentration of 100 mM, all organic salts prepared compromised cell viability in both cell lines. At a concentration of 25 mM, the salts with camphorsulfonic acids and diprotonated salt with chloride presented high toxicity in both cell lines. With a concentration of 1 mM, all compounds tested do not compromised cell viability and were considered non-toxic.

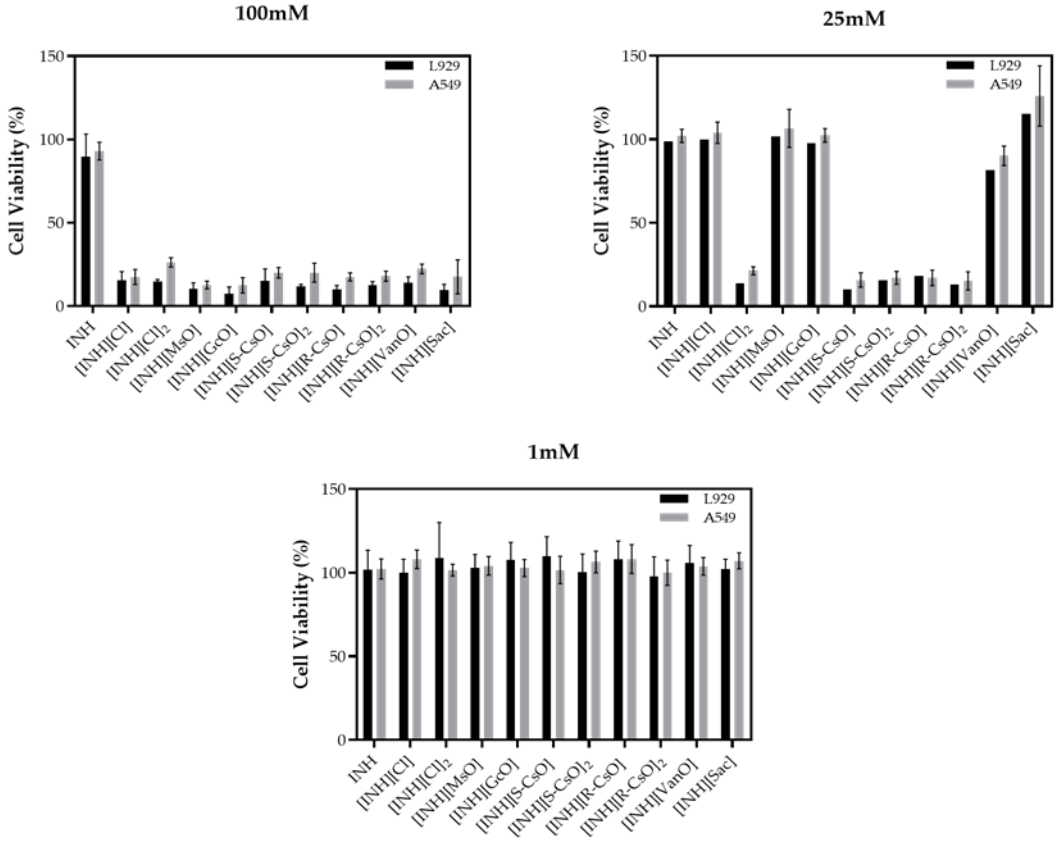

Figure 3.4 - Cell viability of INH and organic salts with INH in L929 and A549 cell lines, at different concentrations.

3.5 Toxicity assessment

The effect of the prepared organic salts in a mycobacteria strain can be assessed, although the model selected for screening assays was zebrafish model infected with *Mycobacterium marinum*. Even though, it was not possible to perform these assays, because *Mycobacterium marinum* was not delivered on time, an initial screening of the toxicity of the compounds in zebrafish was performed. Toxicity was, hence, evaluated through different biomarkers measured in zebrafish (*Danio rerio*) for different organic salts, that appeared to be more promising, regarding solubility studies. From all the organic salts based on INH prepared two of them were selected, namely, $[INH][Cl]_2$ and $[INH][R\text{-}CsO]_2$, that showed better solubility and, in the case of $[INH][Cl]_2$ also a similar permeability to INH, despite higher diffusion coefficient. These compounds together with INH were evaluated, in concentrations considered non-toxic for cell lines (< 1 mM). Different biomarkers regarding oxidative stress (SOD, CAT, GST), membrane integrity and protein homeostasis were evaluated, as indicative of the possible damage that the compounds could cause in aquatic organisms, for instance, when disturbing their ecosystems after being discharged as wastewater effluents.

3.5.1 Mortality rate

The mortality rate was evaluated after exposure of the fish to different concentrations of the compounds dissolved in water (2, 5 and 15 μM). After 24 h of exposure, death was observed for fish exposed to 5 and 15 μM. At 5 μM and 15 μM a mortality of 25% for $[INH][Cl]_2$ and $[INH][R\text{-}CsO]_2$ was observed. When pure INH was tested mortality was only observed at 15 μM, which corresponded to a mortality rate of 50%, in the first 24 h.

3.5.2 Antioxidant enzymes

The activity of antioxidant enzymes such as CAT, GST and SOD was evaluated in zebrafish (Figure 3.5). Regarding catalase activity, INH at concentrations of 2 and 15 μM presented higher activity, which was statistically significant ($p \leq 0.05$) when compared to the respective control. However, when we observe the activity of catalase in fish exposed to the organic salts, it was possible to detect that only in fish exposed to 2 μM of $[INH][Cl]_2$

significant statistical differences when compared to the control were observed, presenting an increased activity in relation with other concentrations tested. Concerning the GST activity, no significant statistical differences ($p \leq 0.05$) were observed between the control and the different concentrations tested for all the compounds evaluated. Regarding the measurement of SOD inhibition percentage, for INH an increased inhibition at 15 μM was detected when compared to the control.

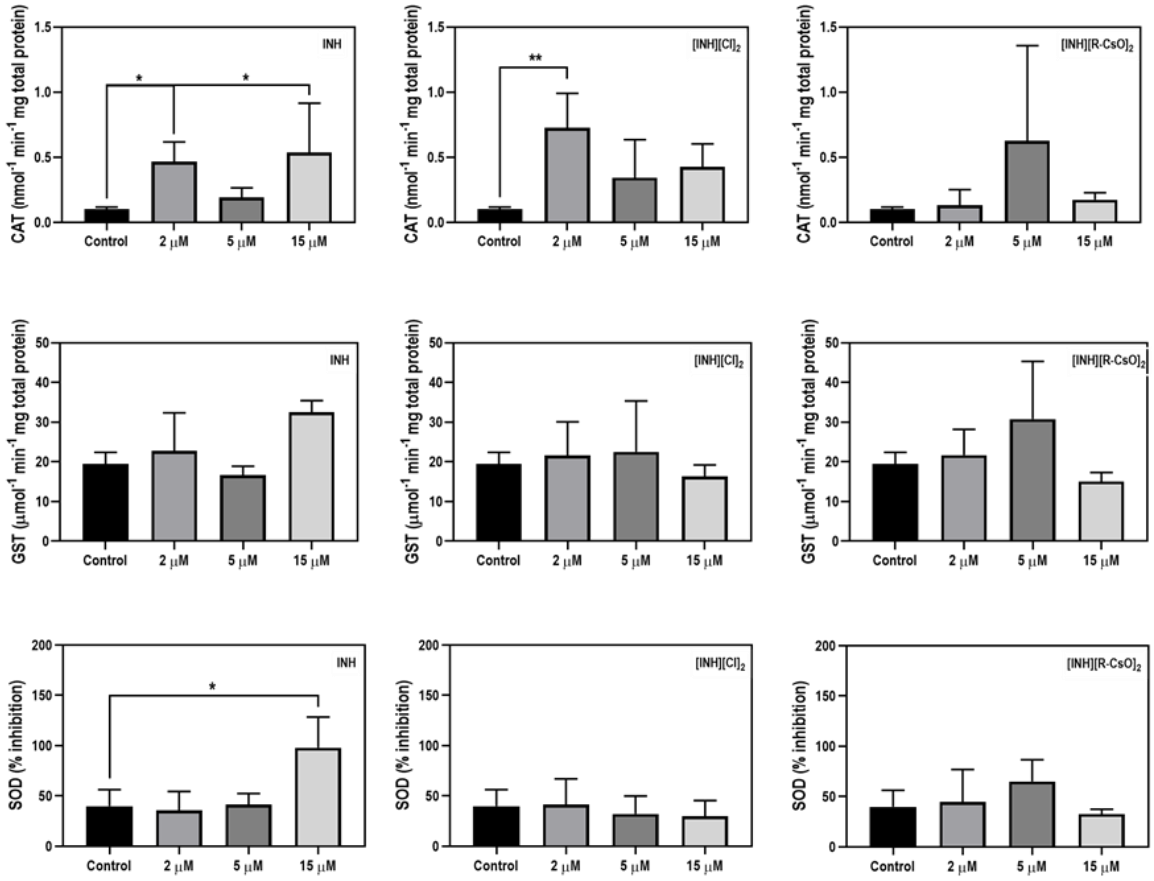

Figure 3.5 - Activity of antioxidant enzymes CAT, GST and SOD inhibition for concentrations 2, 5 and 15 μM of compounds INH, $[INH][Cl]_2$ and $[INH][R\text{-}CsO]_2$. The results are expressed as mean ± SD, $*p \leq 0.05$; $**p \leq 0.005$.

3.5.3 Lipid peroxidation and total ubiquitins assessment

The cellular injury was evaluated through lipid peroxidation assay (TBARS) and protein homeostasis was evaluated by quantification of total ubiquitins. From Figure 3.6, the MDA content was observed and, in general, was higher compared with the control, except

for [INH][R-CsO]$_2$ at 2 μM, which presented a similar MDA content compared to the control and at 15 μM the MDA content showed a decrease in comparison with the control. At the same concentration of 15 μM for INH, a statistically significant ($p \leq 0.05$) increase in the MDA content was observed, that indicated cell membrane damage. Regarding the quantification of the total ubiquitins, an increase of the total ubiquitins for all compounds and concentrations, when compared to the control was noticed. However, statistically differences ($p \leq 0.05$) were only observed at 15 μM for INH and 5 μM for [INH][R-CsO]$_2$, when compared to the control.

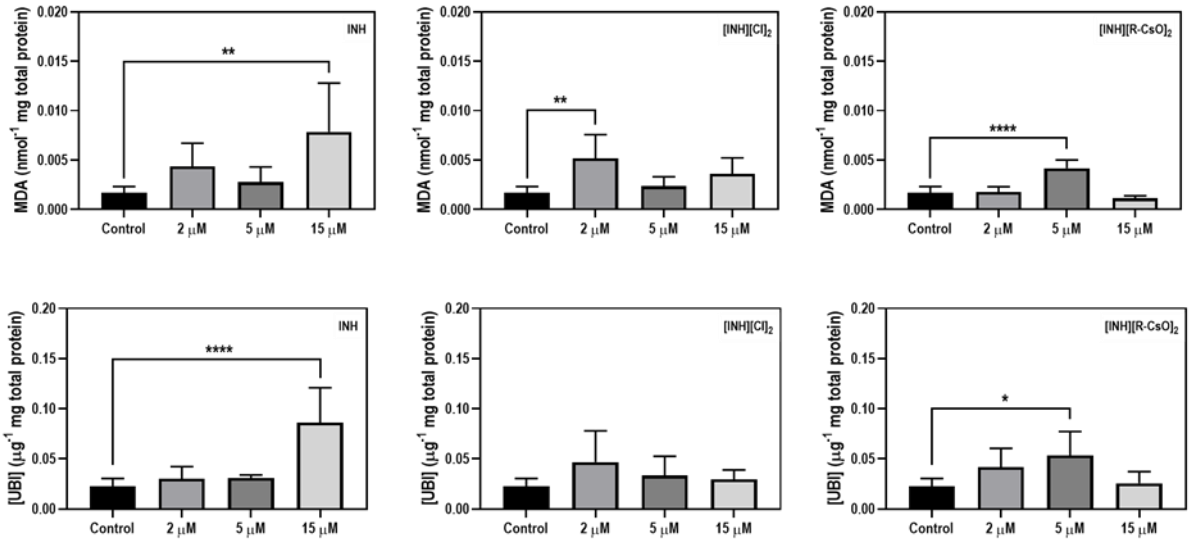

Figure 3.6 - Measurement of MDA content during lipid peroxidation assay and total ubiquitins for concentrations 2, 5 and 15 μM of compounds INH, [INH][Cl]$_2$ and [INH][R-CsO]$_2$. The results are expressed as mean ± SD, *$p \leq 0.05$; **$p \leq 0.005$; ****$p \leq 0.0001$, when compared to the control.

3.6 Discussion

Isoniazid is a first-line anti-TB drug that presents proven efficacy in TB treatment but presents some serious adverse effects, like hepatotoxicity and a high level of multidrug resistance. Despite INH, in the pure state, is stable for a long period of time, when administrated with other anti-TB drugs, INH interacts and becomes unstable, suffering degradation. INH may be sensitive to light, when exposed for long periods of time, and is an active substance that, usually, is vulnerable to hydrolysis, oxidation, and interaction with

other compounds (e.g., excipients used in formulation) to form hydrazones.[217,223] Recently, two polymorphs formed by hydrogen bonding, one in the pyridine group (N-H . . . N) and another one in hydrazide groups (N-H . . . O), were reported to overcome some of these drawbacks.[224] With the knowledge of the problems that INH presents in terms of stability and interaction with other drugs, it was important to explore new approaches that could overcome this.

During this work, a new strategy for the synthesis of organic salts using INH drug as cation and combined with sulfonate and carboxylate counterions was explored. This new approach for the synthesis of organic salts with the INH drug had the main goal of stabilizing the drug, avoiding polymorphic forms,[224] understanding if its properties could be tuned by the protonation of INH with biocompatible counterions. The synthesis of the organic salts was performed either by protonation with acids or by metathesis reaction when salts were used for the preparation of organic salts. ^{1}H-NMR, FTIR-ATR, and elemental analysis allowed us to differentiate the compounds from monoprotonated or diprotonated form and observe some deviations, in ^{1}H-NMR, of the chemical shift that occurred more visibly in the diprotonated form of [INH][Cl]$_2$. The thermal events were observed by DSC and the thermograms showed that the organic salts prepared had melting points below the melting point of INH, except for [INH][Sac], that presented a melting point of 179°C, which was slightly superior to INH itself. However, in the case of salts prepared with [GcO], [R-CsO], [S-CsO], [S-CsO]$_2$, and [VanO], it was observed that after the first cycle these compounds become amorphous, which could represent an advantage in the use of these compounds, since they avoid polymorphic forms and could make the drug more stable.

Another important property to measure with these new compounds was their solubility, since it is a characteristic essential for pharmacological approaches and drug delivery.[225] In this study, the solubility of pure API and organic salts was measured, and double protonation forms presented higher solubility in both solvents tested at 37 °C. The organic salts [INH][Cl], [INH][Cl]$_2$, [INH][S-CsO], [INH][S-CsO]$_2$, [INH][R-CsO] and [INH][R-CsO]$_2$ appeared to present a higher solubility in both solvents tested in comparison with other organic salts, which lead us to evaluate the permeability of these salts in synthetic membranes and determine their permeability over time, to see if a higher solubility could lead to a higher driving force through the membrane. The permeability assays with the Franz cells method in INH and organic salts were performed. The diffusion profiles presented an initial lag phase in all compounds tested, due to the time needed for the solute

to cross the membrane and start to diffuse in the media. In terms of permeability, only $[INH][Cl]_2$ had a permeability that nears the value of INH. The diffusion coefficient, which estimates the mass of a compound that was diffused over time, was higher in the salt $[INH][Cl]_2$ that doubles the diffusion when compared with the monoprotonated form, and presented to be higher than INH itself, which was related to a faster diffusion through the membrane for this compound.[192] However, the other dicationic forms prepared with camphorsulfonates were not able to pass through the membrane, probably due to the higher size of the molecule that makes them unable to cross the synthetic membrane.

The cell viability assays showed that higher concentrations of INH and organic salts (100 mM) were toxic for both cell lines. Despite camphorsulfonates and dicationic chloride salts presented a good solubility of INH, high toxicity at 100 mM and 25 mM was observed. Nevertheless, when used in smaller concentrations these compounds presented to be viable and were considered non-toxic for both cell lines tested.

The toxicity of the different organic salts was further assessed in zebrafish, by evaluating the effects of these compounds as they can cause oxidative stress. After exposure of zebrafish to the different concentrations of INH, $[INH][Cl]_2$ and $[INH][R\text{-}CsO]_2$ mortality after 24 h of exposure was observed, mainly at 15 μM. The oxidative stress is initiated when an imbalance between the production of free reactive oxygen species (ROS, e.g., superoxide anion ($^{\bullet}O_2^-$), hydrogen peroxide (H_2O_2), hydroxyl radical ($OH^{\bullet}$), single oxygen ($^1O_2$)) and antioxidant mechanisms (production of antioxidant enzymes, e.g., CAT, GST, SOD) occurs.[226,227] By observation of the different biomarkers for antioxidant enzymes it can be concluded that these systems somewhat trigger an oxidative stress in cells, since to overcome the excessive production of ROS, the cells activate different enzymatic pathways such as CAT, GST and SOD.

In general, the CAT activity showed to be higher when compared to the respective control. However, with the compound $[INH][R\text{-}CsO]_2$ the values were not considered statistically different when compared to the control, maintaining their normal antioxidant activity when exposed to this compound, and converting the H_2O_2 into H_2O and O_2. Concerning GST activity, no significant statistical differences were observed between the control and the different compounds tested, even varying the concentrations. Overall, concerning antioxidant enzymes production, INH at 15 μM presented reduced antioxidant capacity and, consequently, may suggest higher toxicity when compared to the control. For $[INH][Cl]_2$ and $[INH][R\text{-}CsO]_2$ higher antioxidant capacity was detected at the higher

exposure concentration, despite no statistical differences where observed compared to the control. Regarding the SOD inhibition, INH at 15 μM presented a higher inhibition percentage of SOD, when compared to the control, which can indicate that SOD was downregulated and non-converting the superoxide radical into H_2O_2 and O_2 and, therefore presented some toxicity to the zebrafish, upon exposure. The higher variability observed in the quantification of enzymatic activity could be justified by different factors that were not considered during the assays as individual variability, sex, genetic heritage.[228,229]

The cell injury (e.g., membrane damage) was assessed by lipid peroxidation assay (TBARS) that includes different chain reactions to convert lipid radicals ($LOO^{\bullet}$, lipid peroxyl radicals) into non-radical species (LOOH, lipid hydroperoxide), although these non-radical species could easily decompose into lipid alkoxyl radicals ($LO^{\bullet}$), aldehydes (e.g., MDA, $HOC\text{-}CH_2\text{-}CHO$), alkanes, lipid epoxides and alcohols.[230] The MDA content showed to be in agreement with oxidative stress enzymes results, suggesting higher membrane damage when exposing fish to INH at 15 μM, and it seems to present lower membrane damage when exposing fish to $[INH][Cl]_2$ and $[INH][R\text{-}CsO]_2$ at 15 μM. Regarding the protein homeostasis, measured by total ubiquitins, the same effect was observed being the exposure to INH at the highest concentration of the compound that was found to cause more oxidative stress and, consequently, more damaged proteins in zebrafish.

The following chapter was adapted from the publications:

Santos F., Leitão M.I.P.S., Duarte A.R.C. Properties of therapeutic deep eutectic solvents of L-arginine and ethambutol for tuberculosis treatment. Molecules (2019). 24 (1): 55. DOI: 10.3390/molecules24010055.

Roda A., **Santos F.**, Chua Y.Z., Kumar A., Do H.T., Paiva A., Duarte A.R.C., Held C. Unravelling the nature of citric acid:L-arginine:water mixtures: the bifunctional role of water. Physical Chemistry Chemical Physics (2021). 23: 1706-1717. DOI: 10.1039/D0CP04992A.

Monteiro H., **Santos F**., Paiva A., Duarte A.R.C., Ferreira R.J. Molecular Dynamics studies of therapeutic liquid mixtures and their binding to mycobacteria. Frontiers In Pharmacology (2021). 12 (626735). DOI: 10.3389/fphar.2021.626735.

Santos F., Pires D., Anes E., Duarte A.R.C. Insights into therapeutic liquid mixtures and formulations towards tuberculosis therapy (2022) - **In preparation for submission**.

4

THERAPEUTIC LIQUID MIXTURES

The persistence of TB worldwide and the drawbacks previously described foment the need to find new drugs that present improved properties, namely being targeted to the infection site or testing different drug regimens that can be more patient friendly. Farah et al. enumerate some attractive features that the investigation of new anti-TB drugs should look for, such as: (1) be safe and potent with a bactericidal activity in all stages of TB infection; (2) provide shorter treatments with different combinations that can decrease the amount of drugs taken by patients; (3) find drugs with broad mechanisms of action and low toxicity to treat drug-resistant strains; (4) none or reduced drug-drug interactions; (5) find patient friendly formulations that could be cheaper and available; and also (6) controlled delivery formulations with a higher bioavailability and continuous efficacy for extended periods, allowing to reduce dose frequency.[231]

Recently, therapeutic liquid mixtures have been considered for the development of new drugs or improvement of their properties, while helping in the implementation of more sustainable processes for their production. The preparation of therapeutic liquid mixtures, as THEDES, by incorporating the API in the system or solubilizing the API in a previous prepared eutectic mixture,[185] is a sustainable preparation method that could be used to improve drugs bioavailability.

This chapter focused on the preparation and study of the structure of THEDES prepared by different techniques, to understand their properties and potential in TB therapy. Also, insights on the role of water as a component of the mixtures was studied and molecular dynamic studies were applied to indicate where the interactions by hydrogen bonding could occur. Finally, the activity of the mixtures was tested, assessing their toxicity and antimicrobial activity against *Mtb*.

4.1 Characterization of therapeutic deep eutectic systems (THEDES)

The physicochemical characterization of the different THEDES (based on CA, EMB, L-arg, H_2O and mixtures of CA:EMB:H_2O (1:1:5) with dissolved anti-TB drugs INH, RIF, PZA) was made through different techniques such as POM, NMR and FTIR-ATR to understand the structure of eutectic mixture and also to evaluate the stability of the THEDES, that were maintained at 20-25 °C, during 6 months. Moreover, the liquid mixtures (based on CA, EMB, L-arg, H_2O, Table 2.1 from 2.2.2, Chapter 2) were also characterized concerning their thermal events by DSC and after, bioavailability parameters such as solubility and permeability were evaluated.

4.1.1 Polarized Optical Microscopy

Polarized optical microscopy (POM) was used to observe the different mixtures with a cross polarizer to verify the existence of crystals in the mixtures, detecting if the mixtures were homogeneous or presented in different phases.[232] Uniformly black images in all samples were observed (Figure 4.1a and Figure 4.1b), which means they were amorphous and homogeneous liquids without the formation of crystals.

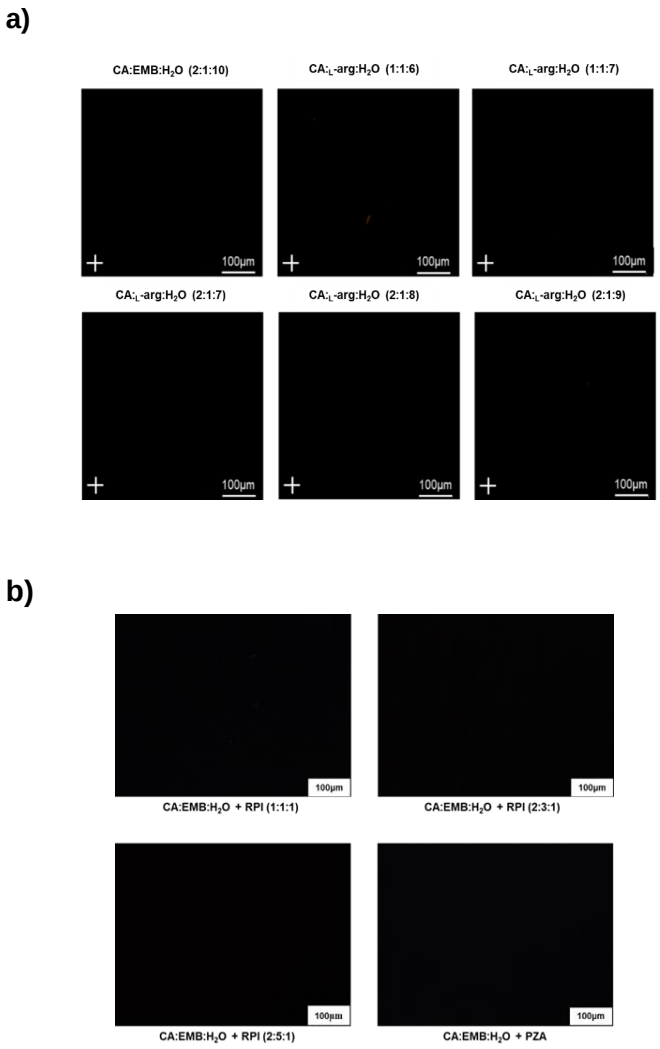

Figure 4.1 - Polarized optical microscopy images of **a)** different THEDES; **b)** THEDES based on CA:EMB:H_2O (1:1:5) and anti-TB drugs, after 6 months of preparation.

4.1.2 Nuclear Magnetic Resonance (NMR) Studies

THEDES were characterized by different NMR techniques to comprehend their structure and possible interactions by hydrogen bonding, that could happen in different chemical groups.[154,161] ^{1}H-NMR, ^{13}C-NMR (Table A.2.2, Appendix A) and ^{1}H-^{1}H NOESY spectra were performed in EMB and THEDES with EMB. From ^{1}H-NMR differences between chemical shifts of the APIs and THEDES were observed, mainly in the groups -NH of EMB that undergoes an upfield shift of 0.1 ppm from the API to THEDES. In this study, ^{1}H-^{1}H nuclear overhauser effect spectroscopy (NOESY) was used to observe direct intermolecular

and intramolecular interactions in THEDES incorporating EMB (Figure 4.2), as this technique identifies spatially close protons. The NOESY spectrum shows interactions between the -OH of the -COOH groups of CA and the -OH and -NH groups of EMB (signal at 12.34 ppm); at 9.14 ppm it can be noticed that the -NH groups of EMB were spatially close to the -OH groups of EMB and -OH groups of CA. At 5.40 ppm the interaction between the -OH groups of EMB -NH group of EMB and the -OH groups of CA were observed. Furthermore, the spectrum showed an interaction between the -C-OH group of CA and the groups -OH and -NH of EMB (signal at 5.15 ppm). Finally, strong interactions between these groups and water were also detected.

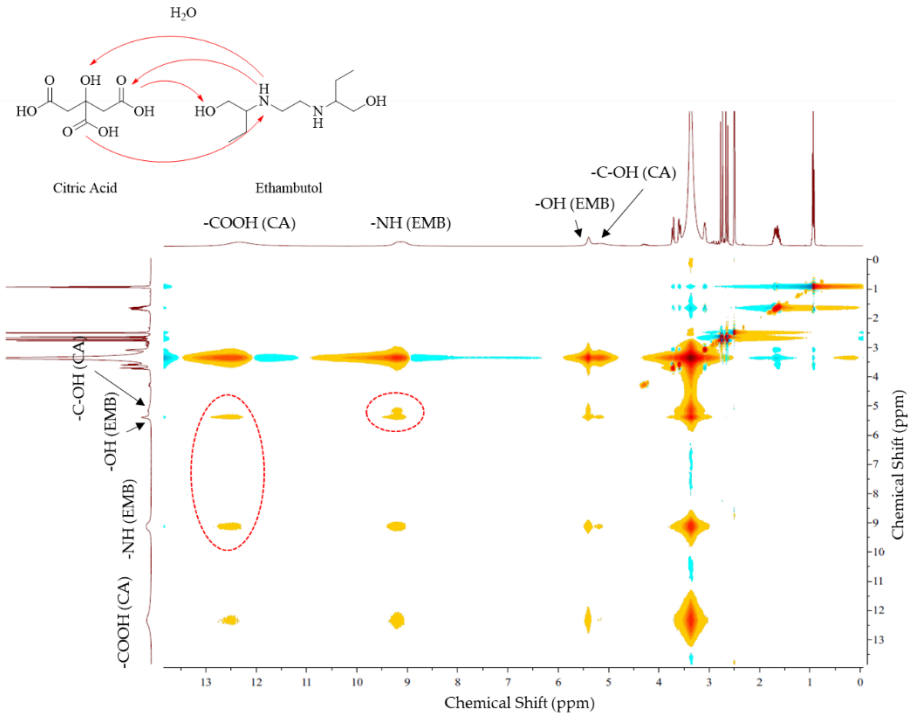

Figure 4.2 - ^{1}H-^{1}H–nuclear overhauser spectroscopy (NOESY) with detected interactions between CA and EMB.

Furthermore, ^{1}H-NMR studies were conducted to observe if significant changes in the structure of THEDES (Table 2.2 from 2.2.2, Chapter 2) 6 months after preparation occurred. As represented in Figure 4.3, the ^{1}H-NMR showed some differences related to the -OH groups, that immediately after preparation presented a sharper peak while after 6 months the peak appeared to be broader. In ^{1}H-NMR, the -OH protons, usually, are quite flexible and their appearance and intensity in the spectra depend on different factors like temperature of analysis, the concentration of the sample, the solvent used to prepare the

samples, among others.[233] The broadness of -OH groups can be explained by some exchange of protons of -OH groups with protons from solvent. Also, slight variations in the concentrations of mixtures when the NMR was performed, could have contributed to the broadening of peaks from -OH groups that appeared near the baseline in all spectra after 6 months. Despite the differences in the broadness of -OH groups, the structure of the liquid formulations appeared to be maintained over time.

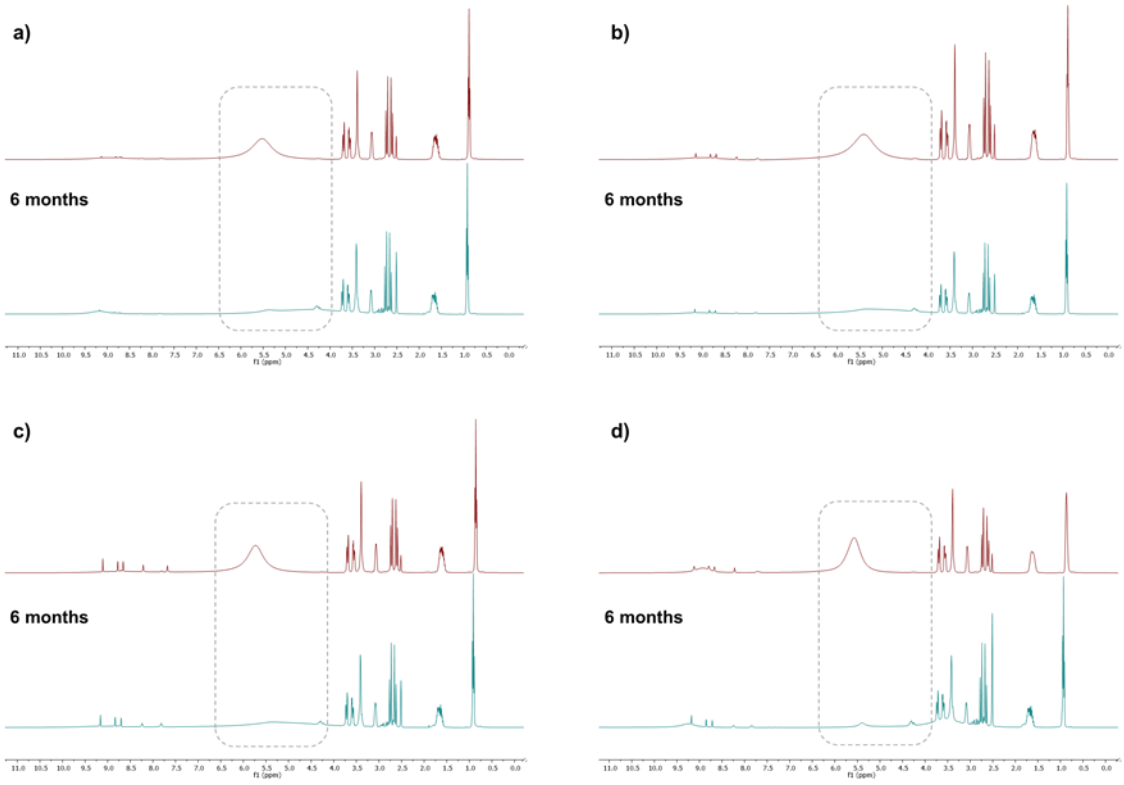

Figure 4.3 - ^{1}H NMR spectra of the therapeutic liquid formulations with superimposition of spectra from 0 and 6 months of formulation. **a)** CA:EMB:H_2O (1:1:5) + RPI (1:1:1), **b)** CA:EMB:H_2O (1:1:5) + RPI (2:3:1), **c)** CA:EMB:H_2O (1:1:5) + RPI (2:5:1), **d)** CA:EMB:H_2O (1:1:5) + PZA.

4.1.3 Fourier-transform infrared spectroscopy (FTIR-ATR)

To further examine the chemical changes that can happen in the structure of liquid formulations and clarify if these formulations could be stable over time, infrared spectroscopy was also performed. This method allowed to detect the presence of different functional groups and bonds and, with attenuated total reflection it was possible to enhance the surface sensitivity and employ liquid samples, like THEDES. The detection of any

changes in the frequency of peaks and their intensity can indicate changes in the chemical structure of the mixtures. In Figure 4.4, an overlap of the spectra of the different periods of time (0 and 6 months) was observed. The first spectrum presents THEDES without adding any anti-TB drugs (INH, RIF, PZA) and comparing this spectrum with the pure components (Figure A.2.1, Appendix A) it was visible that THEDES presented broad peaks, due to presence of water in the mixtures, mainly in the region between 3600-2800 cm^{-1}. However, it was also possible to identify the -OH stretching of EMB, CA (-C-OH) and water in the same region around 3550-3200 cm^{-1}. This confirmed the intermolecular interactions between the different components of THEDES in these groups, and that were previously identified through ^{1}H-^{1}H-NOESY NMR. The presence of -OH groups of CA (-COOH) was identified, approximately, at 3000 cm^{-1} and the -C=O stretch of CA (-COOH) was detected between 1800-1700 cm^{-1}. The peaks between 1500-1400 cm^{-1} appeared to correspond to stretching vibrations of heteroatoms groups. Regarding the solubilization of anti-TB drugs in the system CA:EMB:H_2O (1:1:5), it was observed by FTIR-ATR that the structure of the THEDES was not changed by the presence of these anti-TB drugs. Concerning the stability of these formulations over time, only minor differences were detected in the spectra, which did not affect the chemical structure of the mixtures, thus proving that they were suitable to use for at least 6 months without presenting signals of degradation or losing their functionality by the disruption of the intermolecular bonds.

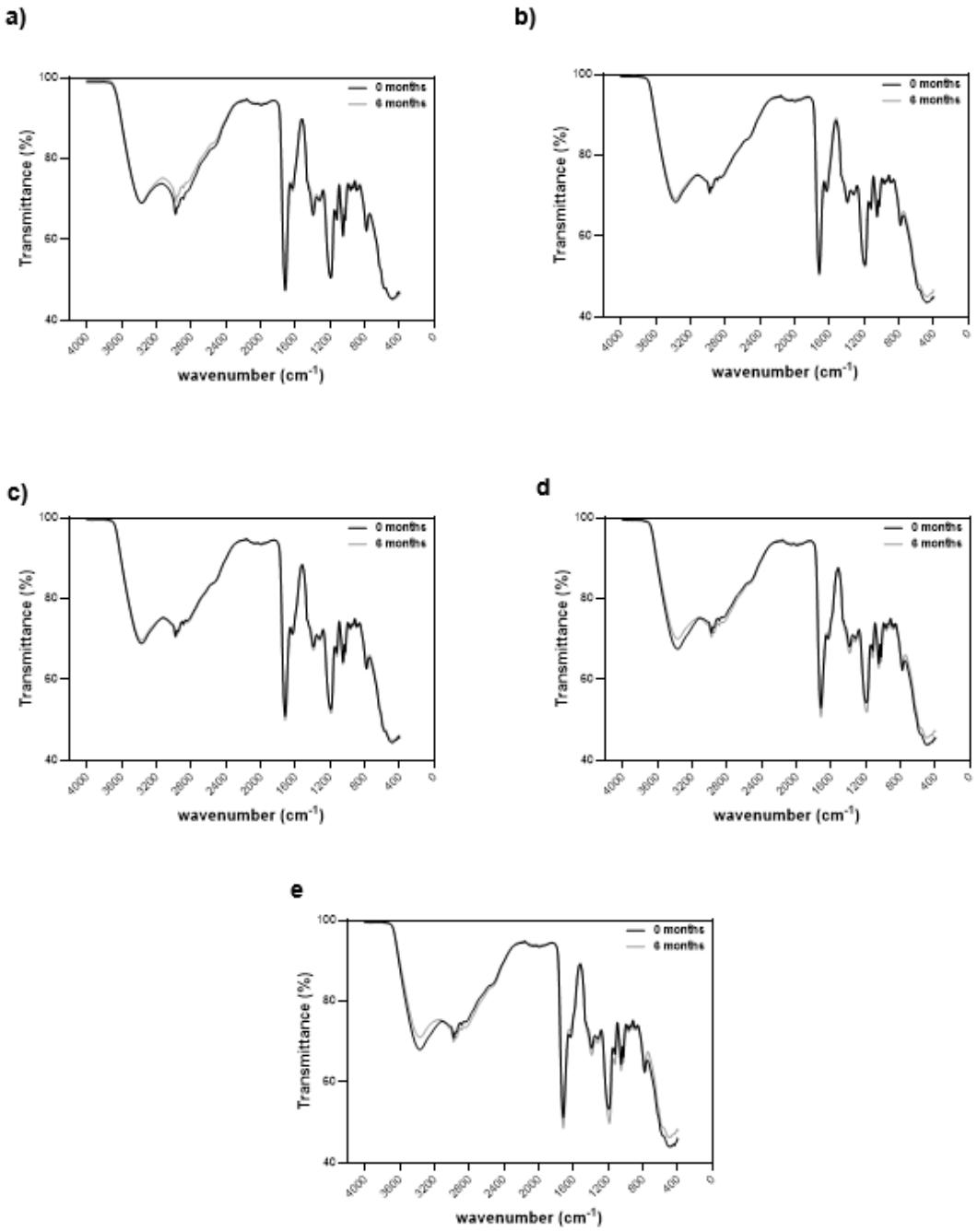

Figure 4.4 - FTIR-ATR spectra of THEDES based on CA:EMB:H_2O (1:1:5) and anti-TB drugs, **a)** CA:EMB:H_2O (1:1:5) + RPI (1:1:1), **b)** CA:EMB:H_2O (1:1:5) + RPI (2:3:1), **c)** CA:EMB:H_2O (1:1:5) + RPI (2:5:1), **d)** CA:EMB:H_2O (1:1:5) + PZA.

4.1.4 Differential Scanning Calorimetry (DSC)

Initially, thermodynamic studies were made through DSC of THEDES prepared with CA, EMB, L-arg and H_2O. As was observed in Figure 4.5, the thermogram of the initial compounds presented peaks of endothermic events. In some of them, two peaks which could indicate different transition stages between the crystalline and amorphous phases was detected.[152,153,234–236] THEDES with EMB in the liquid phase did not present peaks at the endothermic stage. In THEDES with L-arg, a small peak close to 100 °C was observed. This was mostly due to water evaporation at this temperature. The eutectic mixtures were successfully formed, presenting slight thermal transitions below the melting temperature of pure components.

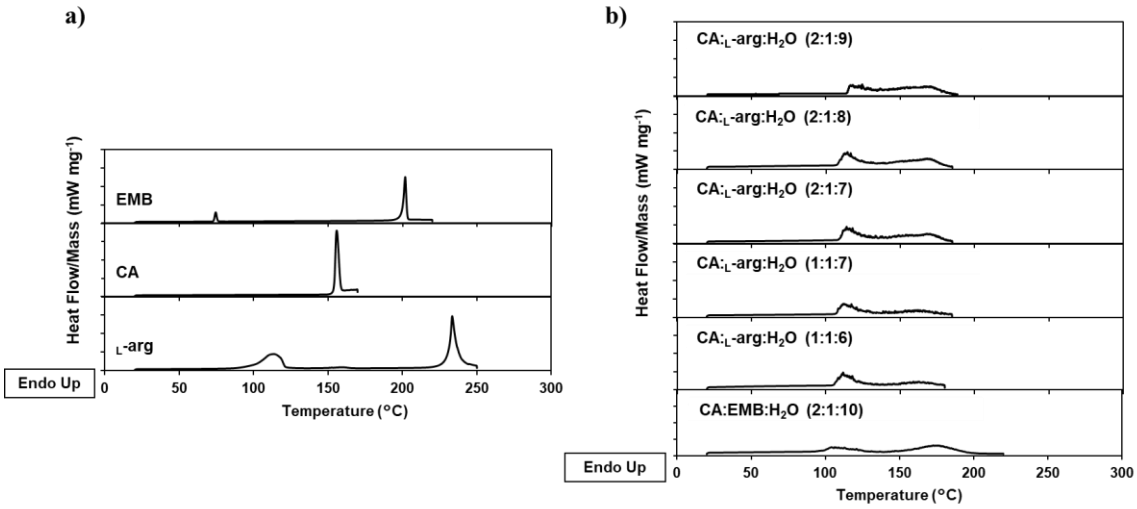

Figure 4.5 - Thermograms obtained in hermetic capsules of (**a**) initial components, and (**b**) THEDES.

4.1.5 Solubility studies of different therapeutic deep eutectic systems and anti-TB drugs

The study of the solubility of the API and THEDES was evaluated in PBS, at 37 °C to simulate physiological conditions. The results obtained were presented in Figure 4.6 and Table 4.1.

Table 4.1 - Solubility of APIs and therapeutic liquid mixtures in PBS (pH 7.4), at 37 ºC.

Compounds	Molar Ratio	Solubility (mg mL^{-1})
EMB	-	4.64 ± 0.07
CA:EMB:H_2O	2:1:10	127.60 ± 0.69
L-arg	-	99.35 ± 0.54
CA:L-arg:H_2O	1:1:6	102.17 ± 0.56
CA:L-arg:H_2O	1:1:7	106.05 ± 0.12
CA:L-arg:H_2O	2:1:7	105.89 ± 0.15
CA:L-arg:H_2O	2:1:8	106.77 ± 0.49
CA:L-arg:H_2O	2:1:9	107.86 ± 0.33

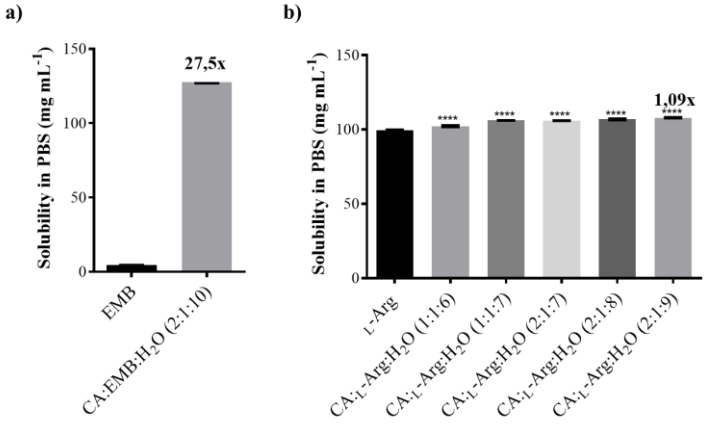

Figure 4.6 - Solubility of THEDES and raw materials with (**a**) EMB, and (**b)** L-arg, in PBS at 37 ºC. Results are presented as mean ± SD and statistically significant differences (****) are shown as $p < 0.05$ in comparison with raw material.

A significant increase in the solubility of EMB in the THEDES form was observed (from 4.64 mg mL^{-1} to 127.60 mg mL^{-1}), compared with EMB. However, in the case of systems with L-arg, only a slight increase in solubility was detected, when compared to the pure API.

Additionally, different anti-TB drugs used in the first-line treatment were dissolved in the liquid mixtures, using them as carriers, and then dissolved in PBS.[234,237–240] Herein, a mixture of the THEDES and PBS (50:50 w/v) was saturated with the compounds INH, PZA and RIF (Figure 4.7).

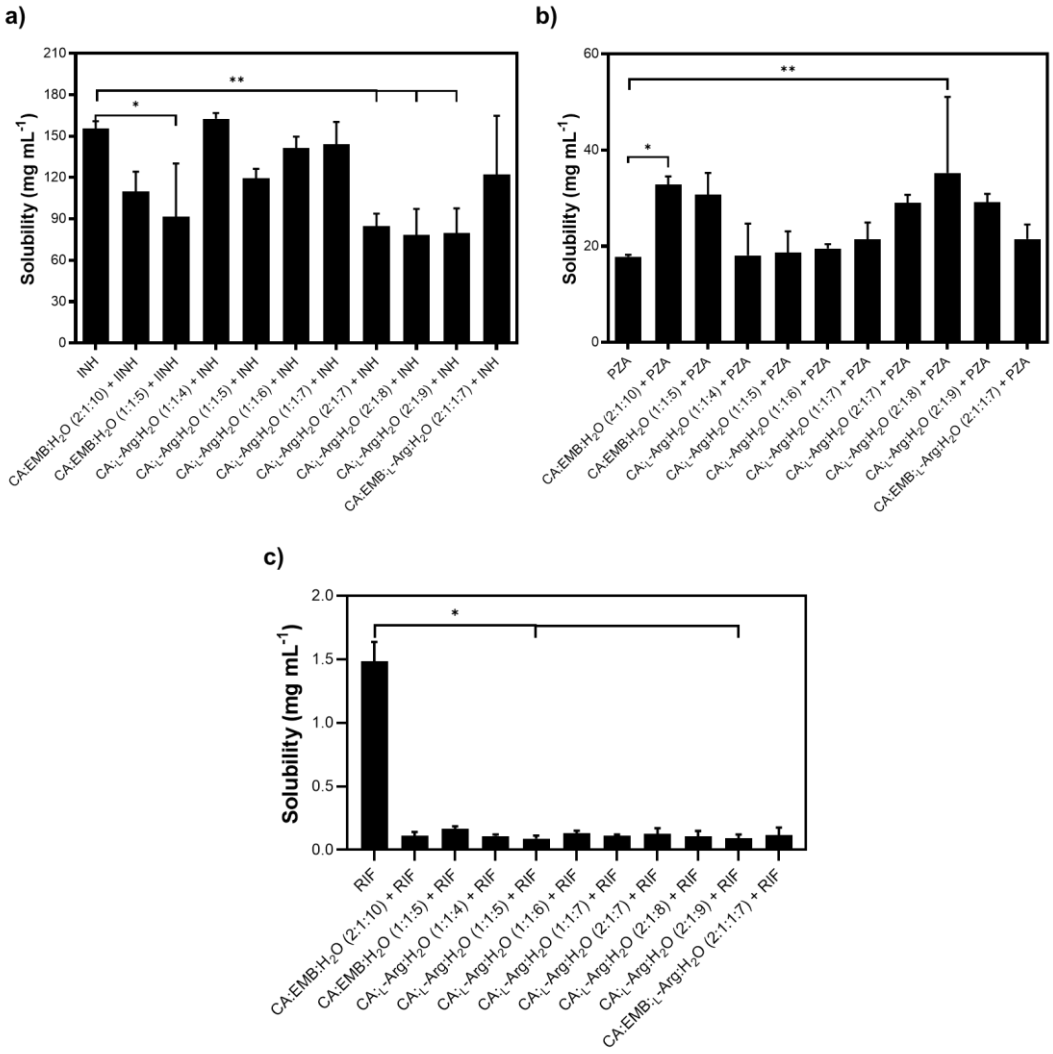

Figure 4.7 - Solubility of different anti-TB drugs (**a)** INH; **b)** PZA and **c)** RIF) in THEDES and PBS. Data are presented as mean ± SD (n = 3), *$p \leq 0.05$, ** ≤ 0.005.

Regarding the solubility assays with anti-TB drugs, mixtures with higher molar ratios of CA and water presented lower solubilization of INH. Probably the higher decrease in the pH of the systems affects the solubilization of INH and possibly its stability. The ones that presented better dissolution of INH were CA:L-arg:H_2O (1:1:4 and 1:1:7), being the formulation 1:1:4 the one that presented a slight increase in solubility compared to INH itself. Contrarily to INH, PZA presented better solubilization in mixtures with higher ratios of CA and water, better than PZA itself. THEDES with EMB incorporated were the ones that presented increased solubility of PZA. In the case of RIF, an improvement on its solubility

was not observed, probably due to the intrinsic characteristics of RIF as it is a large size molecule with a complex structure and a hydrophobic character.[241,242]

4.1.6 Permeability studies on Franz cells with therapeutic deep eutectic systems

The permeability and diffusion coefficients were studied for the EMB and L-arg and THEDES which presented an enhanced performance in the solubility studies and, some variability in molar ratios of CA and water. The assays were carried out using a commercially available polyethersulfone (PES-U) membrane. A rapid diffusion rate was observed in the first minutes and then the diffusion rate stabilizes. The permeability and the diffusion coefficient through the membrane was estimated according to equations 3 and 4 (presented in 2.2.9 of Chapter 2) and presented in Table 4.2.

Table 4.2 - Permeability and diffusion coefficients calculated for the different systems.

Compounds	Permeability (10^{-5} cm s^{-1})	Diffusion Coefficient (10^{-6} cm^2 s^{-1})
EMB	81.9 ± 3.1	13.6 ± 1.0
CA:EMB:H_2O (2:1:10)	128.3 ± 10.4	17.4 ± 1.3
L-arg	36.6 ± 2.4	8.2 ± 0.4
CA:L-arg:H_2O (1:1:7)	21.6 ± 0.2	5.6 ± 0.1
CA:L-arg:H_2O (2:1:9)	23.2 ± 0.3	5.6 ± 0.1

In the case of EMB, the permeability and diffusion coefficient changed, when compared to THEDES, and the systems presented a significant increase in permeability. However, for systems with L-arg, the permeability was lower in THEDES, and the diffusion coefficient did not present significant differences.

4.2 Study of CA:L-arg:H_2O mixtures and possible bifunctional role of water

Water is recognized as a universal solvent due to its ability in establishing hydrogen bonding interactions with the solute. In fact, as stated by Nelson and Cox, "no other molecule has the hydrogen bonding potential of water".[243] Due to this strong capacity in forming hydrogen bonds, either as HBA or HBD, the influence of water on the development of new solvent classes, as the DES, has been explored. Different studies involving the influence of the water in DES conclude that, in general, the addition of water to DES up to 50wt% maintained their original intermolecular network, even after the incorporation of water hydrogen bonds.[244] However, above certain amounts, water can solvate the isolated compounds, disrupting the DES supramolecular complex and forming an aqueous solution.[244–248] More recent studies, also support these findings and further suggest the formation of water-based DES, accompanied by a much deeper melting depression upon water addition compared to the water-free systems.[249,250]

The systems of CA:L-arg:H_2O of mole ratios 1:1:4, 1:1:5, 1:1:6, 1:1:7, 2:1:7, 2:1:8, 2:1:9 prepared were described as DES, given their low water amounts, between 15 to 25 weight percent. However, given the complexity of these systems and the presence of water, other possibilities may be considered. Is the water acting as a solvent, forming a regular aqueous solution? Are the CA and L-arg forming a salt? The nature of these mixtures was explored by parameters commonly used to define thermodynamic properties and the intermolecular interactions of the DES.[251]

In this regard, studies of solid-liquid equilibria (SLE) that could provide information about the composition, temperature range and intermolecular interactions responsible for the solid-liquid phase transitions, through the melting temperatures and the activity coefficients of the mixtures, that allow to evaluate if they present a negative deviation from ideality (Raoult's law) were performed.[252–255] Also, the activity coefficients that translate the cross-interactions affinity between the components of the mixture, evaluating their "predisposition" to cross-interact were determined. Moreover, Perturbed-Chain Statistical Associating Fluid Theory (PC-SAFT), an equation-of-state-based model can be applied in modelling of the SLE of mixtures considering hard-chain fluids as a reference.[252–256] In addition, electrolyte PC-SAFT (ePC-SAFT), is a variant that also accounts for long-range interactions promoted by charged species.[257] Regarding the existence of intermolecular

interactions in the mixtures of CA:L-arg:H_2O, different spectroscopic techniques were applied (FTIR and NMR) to detect intermolecular interactions through shifting of signals that might be involved in the interactions and, also identification of hydrogen bonding interactions.

This work was done in collaboration with Ana Roda and Christoph Held, and only the most relevant findings of this study for the purpose of this thesis are herein reported.

4.2.1 Solid-liquid equilibria

In literature, few attempts have been made to determine the melting properties of L-arg,[258,259] however, due to its early degradation,[260] it was not possible to determine accurate values. Regarding the ternary mixtures of CA:L-arg:H_2O, thermal events were acquired for ratios between 1:1:7 and 1:1:4. The mixtures presented glass transition temperatures (T_g) ranging from 217 to 238 K, respectively. Moreover, the mixtures with higher water content (1:1:7 and 1:1:6) were found to have melting peaks of around 260 K. This phenomenon did not occur for the mixtures with lower water content (1:1:5 and 1:1:4). Since no experimental T_m values for the ternary mixtures could be obtained, it was not possible to apply a thermodynamic correlation model for SLE modelling. Thus, the equation presented below requires a predictive model for the determination of activity coefficients (e.g., PC-SAFT).[261]

$$x_i^L = \frac{1}{\gamma_i^L} \cdot \exp\left\{-\frac{\Delta_m H}{RT}\left(-\frac{T}{T_m}\right)\right\} \quad (7)$$

Equation 7 allowed to calculate the solubility of the component i in the liquid phase $\mathcal{X}_i^L$ at a specified temperature T, considering its activity coefficient Υ_i^L, its melting enthalpy $\Delta_m H$ and its melting temperature T_m and the universal gas constant R (8.314 J mol^{-1} K^{-1}).

Prior to the study of the ternary mixture CA:L-arg:H_2O, the binary combinations of the three components were investigated. In Figure 4.8, it can be observed that the solubility of L-arg in water can be predicted accurately using PC-SAFT parameters. Further, PC-SAFT allowed accurately modelling of literature data for the solubility of CA in water[262,263] (Figure 4.8) using one binary κ_{ij} parameter as listed in Table A.2.3 (Appendix A). The κ_{ij} was adjusted to solubility data above 310 K, as below this temperature CA crystallizes as hydrate.

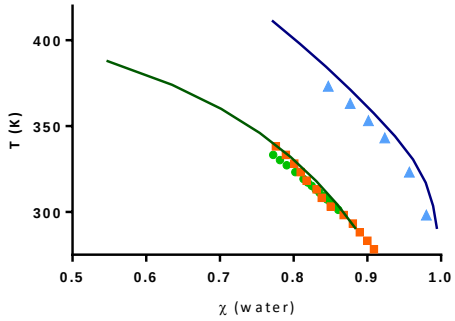

Figure 4.8 - Solubility data of L-arg in water (triangles[264]) and CA in water (squares;[262] circles[263]). Symbols correspond to experimental data while the lines correspond to PC-SAFT modelling results using the melting properties from Table A.2.4 (Appendix A) and the PC-SAFT parameters from Table A.2.5 and Table A.2.6 (Appendix A). χ represents the mole fraction.

The SLE of the binary mixture CA:L-arg was predicted with PC-SAFT using the parameters from Table A.2.6 (Appendix A) and the results were shown in Figure 4.9. A qualitatively similar phase behaviour to the mixture L-arg:H_2O can be observed for CA:L-arg, translating the low solubility of L-arg in both, CA and water. From these, the predicted eutectic point of the mixture CA:L-arg (χ(CA)) ≈ 0.96 with a T_m ≈ 425.4 K) is almost equivalent to T_m of pure CA (426.9 K). Moreover, the values of the activity coefficients of CA and L-arg in this mixture were greater than one (Figure 4.10, χ(water) = 0), indicating rather weak attractive cross-interactions between CA and L-arg. Besides, it presented a positive deviation from the ideal SLE calculations (blue dashed line), strengthening the lack of interactions between CA:L-arg in a binary system.

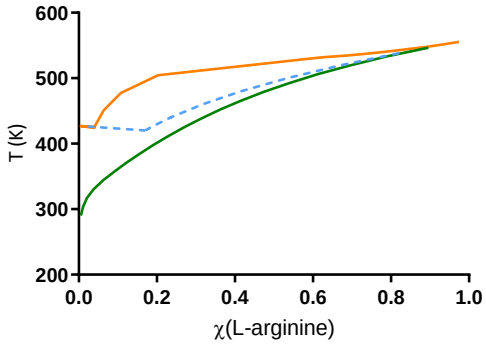

Figure 4.9 - PC-SAFT modelling of the SLE for the binary mixtures L-arg:H_2O (green line) and L-arg:CA (orange line) using the melting properties from Table A.2.1 (Appendix A) and the PC-SAFT parameters from Table A.2.5 and Table A.2.6 (Appendix A). The dashed blue line represents the ideal SLE of L-arg:CA.

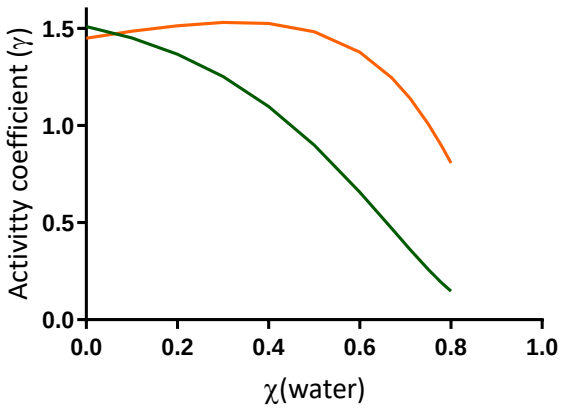

Figure 4.10 - Activity coefficients of CA (green line) and $[L\text{-arg}]^+$ (orange line) when water is added to the mixture CA:L-arg 1:1 (molar), predicted by ePC-SAFT using the parameters from Table A.2.5 and Table A.2.6 (Appendix A). Data from Table A.2.7 (Appendix A).

The PC-SAFT prediction revealed in Figure 4.9, supports the fact that a DES was not formed between CA and L-arg as it could also be confirmed experimentally, and it was found that this mixture appears to be solid at room temperature. This scenario changes, however, upon water addition. As herein reported ternary mixtures of CA:L-arg:H_2O at certain compositions were liquid at room temperature,[183,258] being the SLE of these mixtures studied (Figure 4.11).

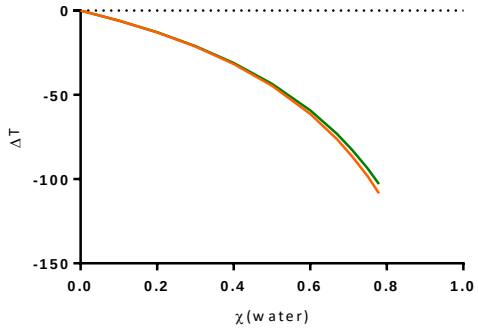

Figure 4.11 - PC-SAFT prediction of the influence of water on T_m (expressed as ΔT) upon water addition to the mixture CA:L-arg 1:1 (molar), using the melting properties from Table A.2.4 (Appendix A) and the PC-SAFT parameters from Table A.2.5 and A.2.6 (Appendix A). Orange line: ΔT for the solubility of CA in the mixture; green line: ΔT for the solubility of L-arg in the mixture. $\Delta T = 0$ corresponds to the binary mixture without water. Data from Table A.2.8 (Appendix A).

PC-SAFT was used to model the ΔT of the system CA:L-arg (at 1:1 molar composition) upon water addition. As observed in Figure 4.11, there was a pronounced

decrease of ΔT with water addition to the system CA:L-arg. In comparison to the binary CA:L-arg, there was a T_m reduction of about 100 K for the ternary mixture of CA:L-arg:H_2O (1:1:7) (molar, χ(water) = 0.78). This deep reduction in T_m could be compliable with the formation of a DES, but it might also be just the formation of a regular solution.

The PC-SAFT predictions showed in Figure 4.8 and Figure 4.11 (binary and ternary mixtures containing water, L-arg, CA) assumed the presence of only neutral species; charges were neglected, as the application of the model requires that the same species were present in the solid or liquid state. However, the pH of the mixture and the pK_a of the molecules define their charge, which can deeply influence interactions and solubility behaviour. When both, L-arg and CA were mixed with water, different pH values and thus, different species will occur. Considering the case of the mixture CA:L-arg:H_2O (1:1:7), the measured pH was about 3.6 (Table A.2.5, Appendix A). As observed in Figure A.2.2 (Appendix A),[265] at this pH, the majority of L-arg molecules will be positively charged, $[\text{L-arg}]^+$; whereas for CA a mixture of the dehydrogenated form, $[\text{citrate}]^-$ and its neutral specie was expected. It is known that the solubility of CA is only slightly affected by pH changes. However, the solubility changes of L-arg species from the isoelectric region (neutral species) to pH values between 2 and 9 ($[\text{L-arg}]^+$) were more significant and must be considered to describe more realistically the interactions between $[\text{L-arg}]^+$,water and CA at these pH values. This was accounted by predicting activity coefficients through ePC-SAFT. The pure-component parameters of the charged species were inherited from the neutral molecules, and a κ_{ij} for the binary $[\text{L-arg}]^+$:H_2O (Table A.2.5, Appendix A) was adjusted according to previous works, by solving dissociation equilibria and solubility.[266–268] For [citrate]:H_2O the κ_{ij} was considered to be the same as the neutral CA:H_2O, given their similar behaviour in terms of solubility. Activity coefficients equal to one correspond to an ideal behaviour while negative (or positive) deviations translate into a higher (or lower) interaction affinity between the constituents of the mixture, respectively.

As observed in Figure 4.10 the activity coefficients of CA (γ_{CA}) in the ternary mixture gradually decrease upon water addition. The decrease from γ_{CA} = 1.51 to values lower than 1, namely for χ(water) = 0.78 with a γ_{CA} = 0.19, highly emphasizes the negative deviation of the mixture from Raoult's law. For $[\text{L-arginine}]^+$, a positive and almost constant deviation from ideality was observed for water molar ratios up to 0.71. Above this water content, the activity coefficient of $[\text{L-arginine}]^+$ ($\gamma_{\text{L-arg}^+}$) decreases pronouncedly, reaching a negative deviation from Raoult's law when χ(water) ≥ 0.78. The lower γ_{CA} in comparison to $\gamma_{\text{L-arg}^+}$ indicated a

higher contribution of CA to the melting depression of the mixture[269] and a higher affinity to establish cross-interactions in the mixture.

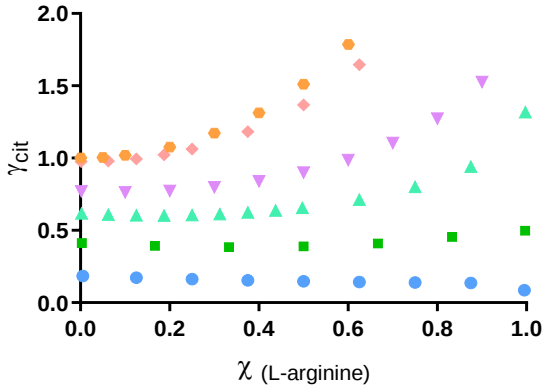

Figure 4.12 - Activity coefficients of CA in the mixture CA:L-arg:H_2O, at different relative mole fraction of L-arg with respect to CA and constant water molar ratios. Circles: χ(water) = 0.8; squares: χ(water) = 0.7; triangles: χ(water) = 0.6; inverted triangles: χ(water) = 0.5; rhombi: χ(water) = 0.2; pentagons: χ(water) = 0.01. PC-SAFT results listed in Tables A.2.9, Appendix A.

Analysing the scenario where water was added to pure CA (χ(L-arg) = 0), there was a decrease of γ_{CA} for increasing water amounts, with negative deviations from ideality ($\gamma_{CA} < 1$) when χ(water) > 0.2. This situation was regularly explained by the water solvation effect. It was also observed that, at low water content, the addition of L-arg increased the activity coefficient of CA in the mixture, probably by inducing competition between species. This behaviour was less noticeable as the χ(water) increased up to 0.6 and changed significantly for χ(water) ≥ 0.7. At this water amount or higher, the γ_{CA} seems to stabilize into an almost constant value for all the L-arg ratios in the mixture. Further, an even more distinct behaviour was observed for χ(water) = 0.8, where the addition of L-arg seems to slightly favour the interactions of CA in the mixture. For that water content, the $\gamma_{L\text{-}arg^+}$ (Figure 4.13) showed a positive deviation from Raoult's law for χ(L-arg) ≤ 0.05, that shifts to a negative deviation from ideality, when χ(L-arg) ≥ 0.1. This emphasizes that the addition of L-arg to the mixture CA:L-arg:H_2O above a certain amount increased cross interactions, but only at high water content. This was a non-regular solution effect.

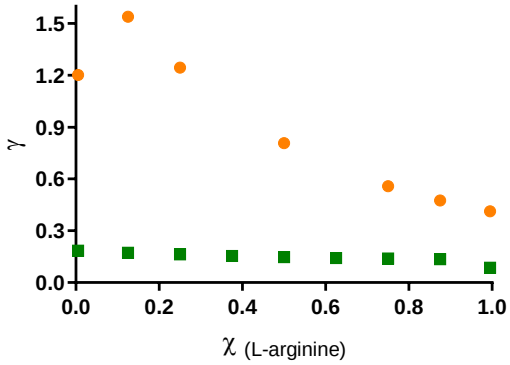

Figure 4.13 - Activity coefficients of [L-arginine]$^+$ (circles) and CA (squares) in the mixture CA:L-arg:H_2O, at a χ(water) = 0.8 and different relative molar ratios of L-arg with respect to CA. PC-SAFT were results listed in Tables A.2.9 and A.2.10, Appendix A.

Interestingly, the mixtures of CA:L-arg:H_2O previously reported to be liquid (1:1:4, 1:1:5, 1:1:6, 1:1:7, 2:1:7, 2:1:8, 2:1:9 mol ratios)[183,258] correspond to water molar contents between 0.7 and 0.8, which coincide within the range where this "non-regular" behaviour was detected. It is certain that the liquid state is stabilized by water mediation, but also preponderantly influenced by the CA and L-arg contents.

4.2.2 Physicochemical analysis

Aiming to complement the investigation on the nature of the mixtures CA:L-arg:H_2O, the mixture CA:L-arg:H_2O (1:1:7) was selected as a model to characterize and compare with aqueous solutions of CA or L-arg, in the same ratio or at the same pH (around 3.5) of the ternary mixture. Furthermore, ternary mixtures with increasing CA molar ratio from 0.1 to 1 were prepared (Table A.2.5, Appendix A) and analysed by FTIR; those that were liquid were also analysed by NMR.

From the ternary mixtures prepared, it was observed that only the ones with citric acid molar ratios ≥ 0.5 formed translucid liquids, with pH < 7. Since the pH alone might be the reason for the solubility increase of L-arg in water, a mixture of the same ratio of L-arg:H_2O (1:7) was prepared and acidified with HCl rather than CA, to identify the role of pH. It was observed that this mixture did not lead to the formation of a liquid at room temperature, neither before nor after acidification. The other way around was also evaluated: changing the pH of the binary mixture CA:H_2O (1:7) (translucid liquid at pH 0.5) to pH = 3.5

using NaOH instead of L-arg causing the formation of a white solid paste at room temperature. These observations support that the liquid formation is not only a function of pH, but it is additionally influenced by the involving species. In this case, the mixture of L-arg and CA in the presence of water seems to have unique properties in addition to pH to promote their liquefaction.

The mixtures and solutions with CA, L-arg and water were also studied by FTIR-ATR, being the functional groups of pure CA and L-arg identified, and the respective stretching and bending vibrations were assigned as summarized in Tables A.2.11 and A.2.13 (Appendix A). The most important changes in the vibrations of the mixtures from Table A.2.11 (Appendix A) in comparison to the pure components are represented in the spectra of Figure 4.14. In the spectra of all mixtures under investigation, the water contribution can be identified by the broadening of the band regions between 3000–3500, 1500–1800 and 500–900cm^{-1}. In the L-arg powder form, two sharp peaks corresponding to the guanidine and primary amine groups can be distinguished at 3302 cm^{-1} and 3357 cm^{-1}, respectively. When water is added (L-arg:H_2O (1:7), Figure 4.14b), a broader peak is observed for the guanidine amines due to their transition to the delocalized charge state. At pH 3.5 (Figure 4.14c), the primary amine is also charged causing the amine peaks to overlap around 3323 cm^{-1}. Additionally, the -OH stretching of L-arg in its pure form (3057 cm^{-1}, Figure 4.14a) shifts to higher frequencies due to the establishment of hydrogen bonding interactions with the surrounding media (Figure 4.14b–d). Regarding CA, the most important vibrations are from the -OH and -C=O stretching of the carboxylic groups, centred at 3297 and 1719 cm^{-1}, respectively. When mixed with water at pH 3.5, the -OH vibrations are broadened and shifted, and the maximum is at 3340 cm^{-1}.

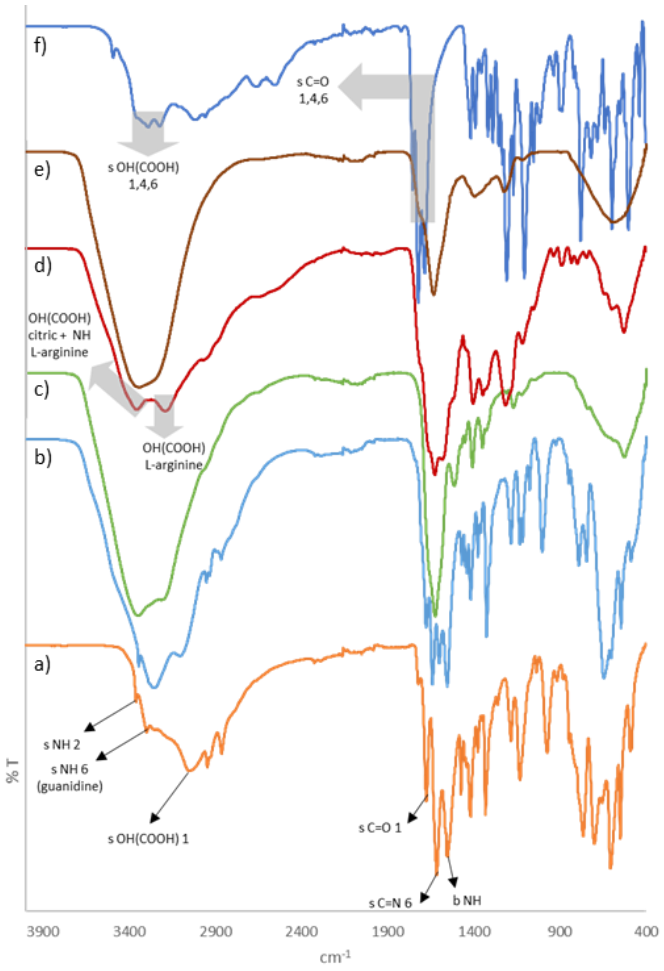

Figure 4.14 - FTIR spectra of **a)** Pure L-arg (orange line); **b)** L-arg:H_2O 1:7 mol (light blue line); **c)** L-arg:H_2O pH=3.5 (green line); **d)** CA:L-arg:H_2O 1:1:7 mol (red line); **e)** CA:H_2O 1:7 mol (brown line); **f)** pure CA (dark blue line). "s" and "b" refer to stretching and bending vibrations, respectively. Numbers attributed according to the chemical structures from Figure A.2.3, Appendix A.

Comparing the CA:H_2O and L-arg:H_2O mixtures at a pH = 3.5 with the ternary system of CA:L- arg:H_2O (1:1:7), it is possible to observe a combined contribution of the same -OH and -NH stretching peaks (Figure 4.14c–e). If the liquids formed by the combination of CA, L-arg and water were promoted by the ionic complexation of $[H_2Cit]^-$ and $[Arg]^+$, the dipole moments of those functional groups would be changed. However, different vibrations in the FTIR spectra were not observed, refuting the salt formation hypothesis.

To sum up, the liquid is neither a case of salt formation nor exclusively induced by the acidic pH value. Thus, other L-arg:CA interactions mediated by water must be the reason for the deep melting point depression of the ternary system, probably H-bonding interactions. Aiming to investigate the formation of hydrogen bonds in the mixtures with

CA:L-arg:H_2O, ^1H and NOESY NMR were performed. ^1H-NMR spectra for the aqueous solutions of the pure components at pH = 3.5 and the CA:H_2O (1:7) mixture were compared with the ternary systems of CA:L-arg:H_2O (1:1:7) and (0.5:1:7) (Figure 4.15).

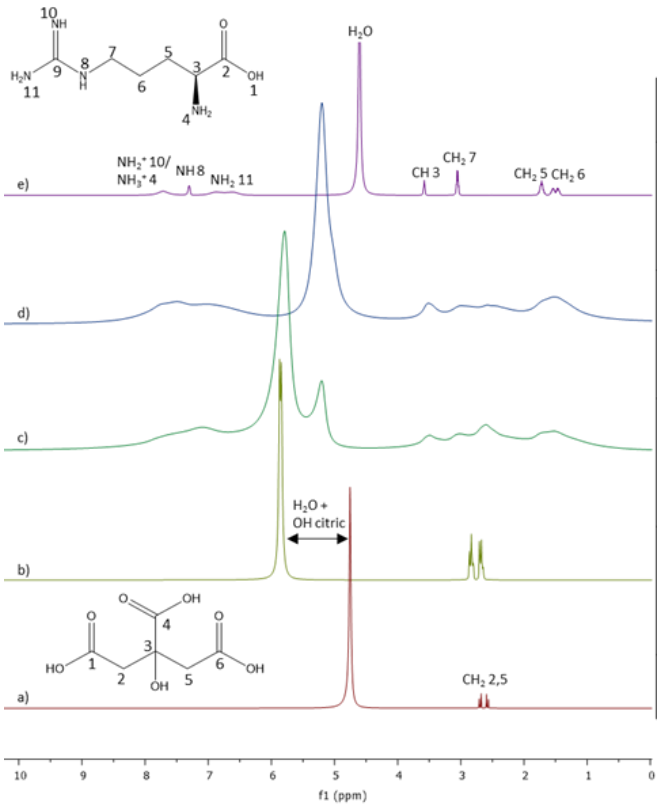

Figure 4.15 - ^1H NMR spectra of **a)** CA:H_2O pH=3.5; **b)** CA:H_2O 1:7; **c)** CA:L-arg:H_2O 1:1:7; **d)** CA:L-arg:H_2O 0.5:1:7; **e)** L-arg:H_2O pH=3.5. The functional groups of the protons detected were identified and numbers were attributed according to the respective chemical structures (see species distribution in Figure A.2.3, Appendix A).

For the system L-arg:H_2O at pH = 3.5, it was possible to identify the protons from water and most of the protons of the L-arg's amine and alkyl groups (Figure 4.15e); whereas for the CA:H_2O at pH = 3.5 or the molar ratio 1:7 it was only possible to detect the alkyl groups and a contribution of the -OH-group protons overlapped with the protons from water. This influence of the -OH group was attributed due to the downfield shift of the concentrated solution of CA (1:7 molar) (5.79 ppm, Figure 4.15b) in comparison to its diluted solution at pH 3.5 (4.79 ppm, Figure 4.15a). Interestingly, the same peak (5.79 ppm) appears in the case of the ternary mixture 1:1:7 (Figure 4.15c), but it is broader. Further, it has a second peak at 5.20 ppm, also appearing in the ternary system 0.5:1:7. Given that the only

difference from the samples of Figure 4.15b to c was the addition of L-arg, the appearance of a new peak is certainly caused by hydrogen bonding interactions with the L-arg molecules, in addition to the ones between CA and water. Regarding the broadening effect observed for the ternary mixtures in comparison to the binary solutions, it might be related to the samples high viscosity. According to Stokes–Einstein–Debye law, high viscosity mixtures lead to slower rotational molecular diffusion[270–273] and longer T2 relaxation times.[274,275] These translate into broader NMR peaks, as previously reported for viscous DES mixtures.[276]

Moreover, in the NOESY spectra of the system CA:L-arg:H_2O (1:1:7) there are cross peaks between the protons from the CA alkyl groups and the protons of L-arg chemical groups (Figure 4.16) that may indicate spatial correlation. In addition to the expected interactions between H_2O–H_2O, CA–H_2O, CA–CA, L-arg–H_2O and L-arg–L-arg, further CA–L-arg and/or mutual interactions between the three components might occur. Combined with the evidence from the ^{1}H-NMR analysis that there is a change in the hydrogen bonding network when CA and L-arg are mixed with water in comparison to their independent water solutions, these findings might be compliable with the formation of a supramolecular network, which is characteristic from DES. To properly address the interactions network between the components that allowed to form the liquid ternary mixtures, dynamic molecular studies would have to be performed. Still, from these results, it is noticeable that the interactions between the water molecules and the functional groups of CA and L-arg, namely, amine, carboxyl and hydroxyl groups may play a major role in establishing those interactions.

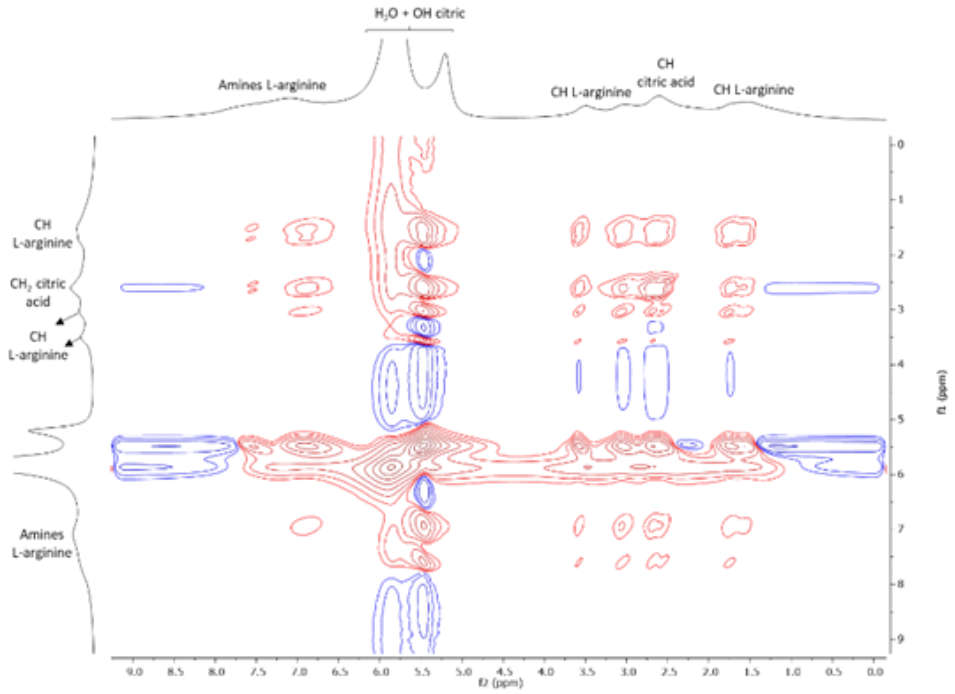

Figure 4.16 - 2D NOESY spectra of the mixture CA:L-arg:H_2O (1:1:7). The functional groups of the protons identified are aligned with the respective peaks.

4.3 Insights into molecular dynamics and docking for therapeutic deep eutectic systems

On the quest to answer some fundamental questions about the type of interactions that can contribute to a stable mixture and how and where they are formed, we have studied our systems using molecular dynamics (MD). MD represents an important tool that could boost the understanding of these mixtures, particularly how the components interact with each other to form a stable mixture,[277,278] by providing insights into the behaviour of atoms and molecules and allowing the prediction of the interactions of a particular system during a pre-determined period of time. In the case of eutectic systems, this type of analysis could give insights about the chemical and physical properties of the systems, such as dynamics of the molecules, radial distribution functions (which describes how density varies as a function of distance from a reference particle), spatial distribution functions of the atoms, self-diffusion coefficients, intermolecular interaction, polar solvation energies, percentage of volume expansion and type of hydrogen bonding interactions. To this matter, MD

simulations had already proven their value by providing valuable knowledge regarding the solubility of APIs[278,279] or through the study of the internal structure of DES at its molecular level.[277,280]

In the following section, MD approach was used to understand how an anti-TB drug, EMB, and a natural compound such as L-arg, which is described as acting as an adjuvant in tuberculosis therapy,[61,258,281] could be stabilized by the presence of CA and/or water in the mixture. This work was done in collaboration with Hugo Monteiro and Ricardo Ferreira and only the most relevant findings of this study for the purpose of this thesis are herein reported.

4.3.1 Molecular dynamics studies

Molecular dynamics is a unique tool that allows probing the internal structure of these therapeutic liquid mixtures and to gain insights on the interactions and configurations of each component at its molecular level.[250,277,278,282] Monteiro and co-workers employed MD simulations to study the molecular structure of the mixtures CA:EMB:H_2O (1:1:5 and 2:1:10), CA:L-arg:H_2O (1:1:7) and CA:EMB:L-arg:H_2O (2:1:1:7).[283]

An initial set of MD simulations were performed comprising each of the liquid mixture component in water (Figure 4.17), namely EMB:H_2O, CA:H_2O, and L-arg:H_2O. While no aggregation could be observed in either CA:H_2O or L-arg:H_2O systems, the system EMB:H_2O remained inhomogeneous, with EMB molecules aggregated mostly due to intermolecular hydrogen bonds (HBs) between the amino (pKa_1 = 6.35 and pKa_2 = 9.35)[284] and hydroxyl groups. Such intermolecular HBs account for nearly 12% of all calculated HBs, with the remaining 88% corresponding to the interactions between the second hydroxyl group and the surrounding H_2O molecules (Figure 4.18). In the L-arg:H_2O systems a similar trend is observed (8% L-arg-L-arg vs. 92% L-arg-H_2O) however, in the CA:H_2O system almost all calculated HBs are between CA and H_2O (99 vs. 1% CA-CA interactions).

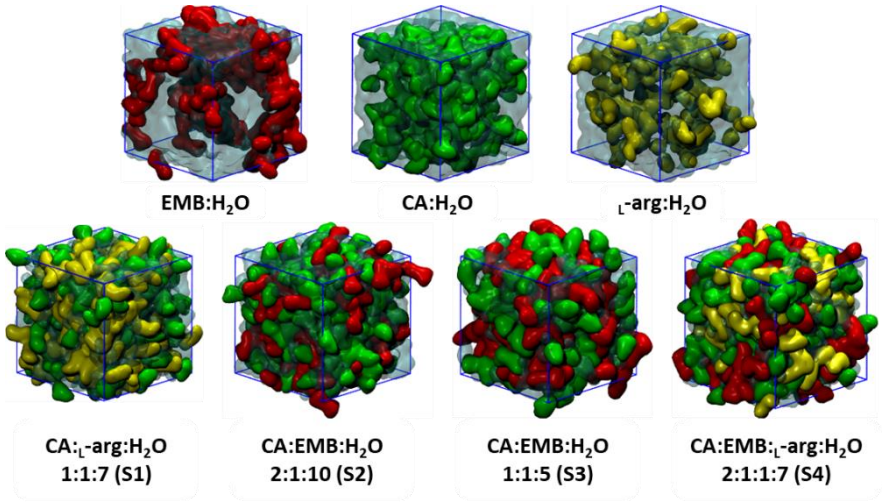

Figure 4.17 - Final configuration (after 1μs MD simulation time) for all studied systems.

When considering a liquid mixture as CA:L-arg:H_2O (S1, Figure 4.18), most of all calculated HBs were observed between L-arg:H_2O and CA:H_2O pairs (46 and 37%, respectively). Quite interestingly, while intermolecular L-arg-L-arg hydrogen-bonding increases (10%), all novel L-arg-CA interactions between both components were accomplished by directly replacing H_2O molecules of the first solvation shell with L-arg. It seems that, even in a low percentage (6%), the newly established HBs are sufficient to improve L-arg solubility and to drive S1 into a more homogeneous state when compared with L-arg:H_2O alone. For EMB-containing systems S2 and S3, again we observe that most of the EMB:H_2O HBs were replaced by the more favourable CA:H_2O interactions (71 and 51% of all calculated HBs for S2 and S3, respectively). In both systems, the number of HBs between EMB:CA was low (2 and 6% for systems S2 and S3, respectively) but sufficient to improve the system's homogeneity, as can be seen by the absence of EMB aggregates in both S2 and S3 when compared with EMB:H_2O mixture (Figure 4.18). Finally, in S4 the introduction of L-arg replaces EMB:H_2O interactions in a larger extent than of CA:H_2O, reaching similar values to those calculated for the S1 system regarding L-arg:L-arg, CA:CA, and L-arg:CA interactions (Figure 4.18). Therefore, the results seem to be in agreement with previous studies in which the increased solvation of CA improves the solubility of both L-arg and EMB.[258] In the following section, we describe which chemical groups are responsible for the intermolecular interactions and which maintain their interactions with the surrounding environment.

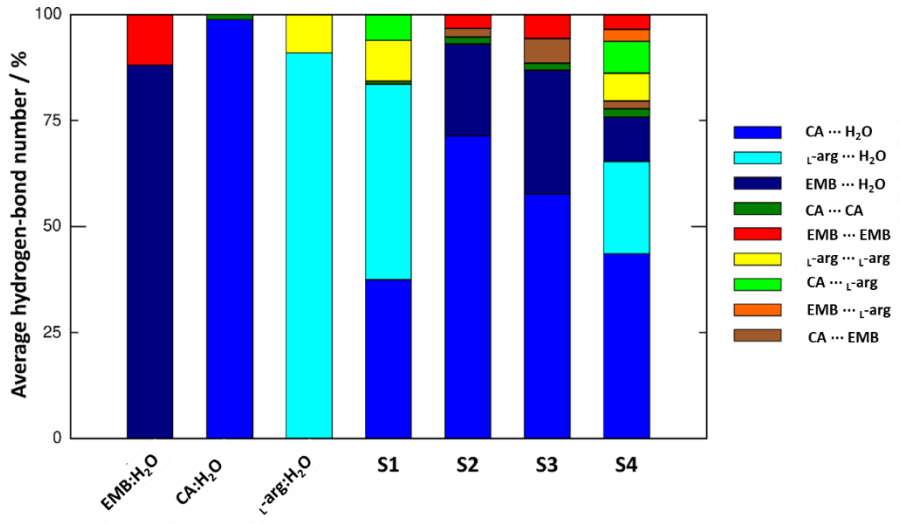

Figure 4.18 - Comparison of the average number of hydrogen bonds between all liquid mixtures components in the studied systems.

To observe the liquid mixtures structure of different systems and the affinity between the molecules that compose the mixture, RDFs for both center-of-mass (c-RDF) and atomic (a-RDF) were calculated. Regarding c-RDF of systems S2 and S3, while changes in the components ratios only had minor alterations, the introduction of L-arg (S4) was revealed by **1**) the appearance of three peaks in the RDF profile at r = 0.38 nm (enabling intermolecular HB with EMB), r = 0.56 nm (HB with CA) and r = 0.82 nm (HB with CA) and **2)** by inducing a slight decrease in the H_2O peak (when compared with S2) while the reinforcing both citrates peaks at r = 0.54 nm and r = 0.85 nm. Therefore, the data suggests that by adding L-arg, the structure of the liquid mixture is reinforced due to its ability to establish intermolecular interactions with both EMB and CA molecules.

Additionally, a-RDF was used to better understand which specific interactions could be responsible for the interactions between the various THEDES components. Concerning direct interactions between CA and EMB, the interactions were established between the hydrogen from CA carboxylic acid group (HBD) and EMB nitrogen atoms (HBA), meaning that $R_2H\text{-}N \cdots H\text{-}O\text{-}CO_{CA}$ in the S2 system (CA:EMB:H_2O, 2:1:10) are two times more frequent than with any of the terminal carboxylic acid groups. However, as titration studies show that EMB has two dissociation constants,[284] we also expected that only one amine group undergoes hydrogen bonding with CA in the former. This does not change in S3 (CA:EMB:H_2O, 1:1:5), nonetheless, the change in the THEDES components ratio promoted

additional interactions, via hydrogen bonding, between the carbonyl moiety of carboxylic acid and the hydrogen atoms bond to the nitrogen atoms (R_2N-H ···O=C-OH), between the amine moiety and H_2O molecules (R_2N-H ··· OH_2) and between the hydroxyl groups of CA and EMB (R_2N-H ··· OH-R). Regarding the hydroxyl groups of EMB, in both systems, only interactions with H_2O molecules were observed, either as hydrogen bond donor or acceptor.

Regarding S4 (CA:EMB:L-arg:H_2O, 2:1:1:7), the addition of L-arg to form a new system fundamentally changed the interaction modes of EMB with the surrounding environment but not with CA. While the interaction of CA and EMB was maintained and even reinforced, additional interactions between the amine group of EMB (HBA) and the carboxylic acid (HBD) moiety of L-arg (R_2H-N ··· H-O-CO L-arg) were observed. The data revealed that only one carboxylic group of CA is essential to promote interactions with the amine groups of EMB and, L-arg although interacting with the same amine groups, prefers to establish intermolecular HBs with EMB hydroxyl groups.

The interaction of the different THEDES components can also be observed from the corresponding SDF. Herein, SDF was used to determine specific interactions between the molecules, using a three-dimensional density distribution of CA, L-arg, and H_2O molecules in a local coordinate system linked with EMB. From Figure 4.19A, it is possible to see that CA mainly occupies a toroidal section around the amine groups of EMB, which is in agreement with the results depicted in the RDF plots. Hence, increased H_2O densities were only found in the vicinity of the hydroxyl groups of EMB, interacting with both hydroxyl groups of EMB and with the terminal carboxylic acid groups of CA, thus assisting in the solubilization of EMB. In Figure 4.19A, B similar density next to the amino groups of EMB could be assigned to CA molecules (green arrow), with L-arg being found in the close vicinity of EMB hydroxyl groups (yellow arrows). Water, although also interacting with the hydroxyl groups of EMB, is more frequently found in the first hydration shell surrounding L-arg or CA. Thus, data suggest that the presence of L-arg confers additional stability to the internal liquid mixture structure by engaging intermolecular interactions with several EMB and CA molecules. However, as CA and L-arg are highly functionalized molecules, the remaining groups are kept immersed in the aqueous environment and assist in the effective solubilization of the THEDES components.

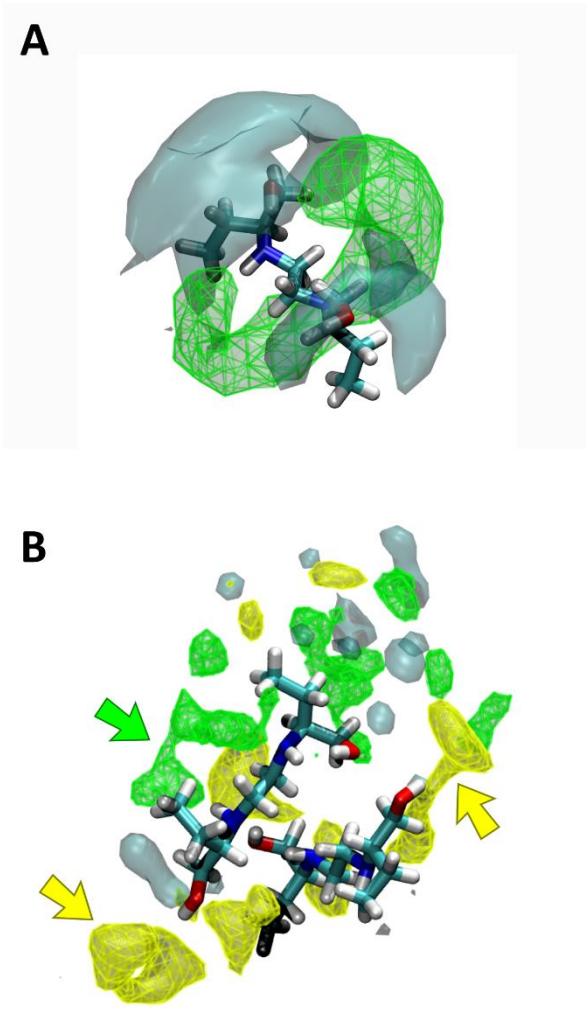

Figure 4.19 - Spatial distribution functions (SDFs) of the components of liquid mixtures around EMB for (**A**) S2 and S3, and (**B**) S4 systems. Specific interactions between CA:EMB and L-arg:EMB are identified in the latter by green and yellow arrows, respectively.

4.3.2 Molecular docking

Following the MD studies on the interactions of the compounds for THEDES, a molecular docking study was also performed to unveil the possibility of CA-promotes an entry pathway for EMB through a mycobacterial ABC transporter, recently published.[285] It is known that the lipidic content in the mycobacterial cell wall, comprising both outer and inner membranes, is highly enriched in diacyl phosphatidylmannosides as Ac_2PIM_2 or Ac_2PIM_6, providing an efficient permeability barrier due to its low fluidity and slowing the passive influx of drugs.[286,287] This was a particular question in which concerns EMB, that was

expected to be positively charged at physiological pH. To that matter a recent publication of a mycobacterial ABC transporter (Rv1819c, PDB ID: 6TQE), described to be involved in the uptake of hydrophilic compounds through the inner mycobacterial membrane,[285] may provide an entry pathway for EMB which was worth to be explored.

In this work, we explored both single and multiple simultaneous ligands docking approaches to understand **1**) if EMB can be internalized via Rv1819c, and **2**) if any of THEDES components may enhance the interaction of EMB with the transporter. When EMB, L-arg, and CA were docked separately (Figure 4.20B), all clusters possess favourable binding energies, but while CA was found to be mostly located in the close vicinity of the R287, both EMB and L-arg largest clusters were found in symmetrical locations, interacting with Q190/G201 in one protomer (EMB) or Q190/D193/N204 in the opposite protomer (L-arg).

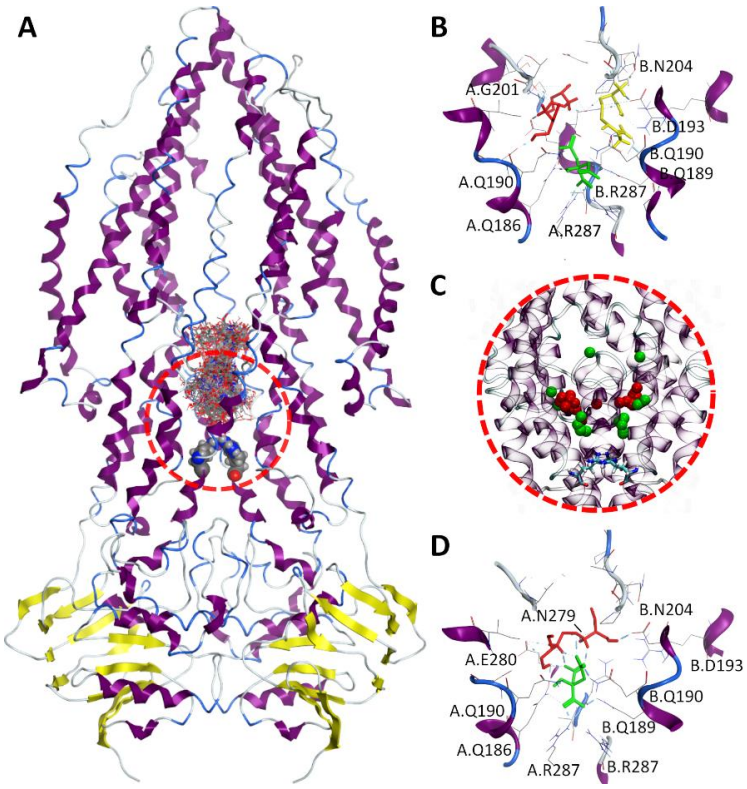

Figure 4.20 - Molecular docking of THEDES components. (**A**) Final configuration for the 100 docking poses from multiple ligand simultaneous docking (MLSD) procedure, with gate residues (Arg287) depicted as volume spheres; (**B**) top-ranked docking poses for CA (green), L-arg (yellow) and EMB (red) obtained with standard molecular docking; (**C**) centers-of-mass for the top 20 poses from MLSD procedure for CA (green) and EMB (red), with gate residues (Arg287) depicted as licorice; and (**D**) top-ranked docking poses for CA (green) and EMB (red) from the MLSD procedure, with hydrogen-bonds depicted in cyan.

Interestingly, this changes when EMB and CA are simultaneously docked. By visualizing the center-of-mass for both EMB and CA (Figure 4.20C), the results seem to suggest that most of the CA molecules were located in the vicinity of the intracellular gate, interacting with R287 or slightly above, but using its negatively charged carboxylate groups to strengthen the interactions between EMB and Rv1819c. When considering the estimated dissociation constants (K_d) this corresponds to a ~150-fold decrease, from 2.26 mM (EMB) to only 14.85 μM (EMB:CA complex), which means that internalization of EMB via Rv1819c would be favoured in the presence of CA. The additional combinations were evaluated through MSLD, for comparison purposes. For instance, replacing CA by L-arg slightly improved its binding affinities, but again no molecules were found in the vicinity of R287. In another combination, including a second CA, the binding affinity sharply decreased and no significant intermolecular HBs were observed. Nonetheless, in the presence of an additional L-arg molecule lower binding energies were restored and even improved. Again, intermolecular HBs between CA:EMB:L-arg, either in the vicinity of R287 (CA:L-arg) or next to the protruding loops (CA:EMB) or, alternatively, with a single CA:EMB pair similar to that was previously observed. Last but more important, K_d further increased to the nanomolar range (884.65 nM). A ≈15-fold increase was observed when compared with the one reported for the CA:EMB complex.

4.4 *In vitro* biological and antibacterial assessment

As mentioned in previous sections, it was possible to formulate THEDES combining EMB and L-arg, in different molar ratios, with CA and H_2O showing an increase on the solubility of the active compounds.[258] In the following section, the assessment of cell viability in different cells lines is presented, as well as the antimicrobial activity against *Mtb* susceptible strain and also the effect of THEDES during macrophages infection with *Mtb*.

4.4.1 Cell viability studies

The assessment of cell viability is essential to understand the behavior of the mixtures formulated *in vitro*. The half-maximal inhibitory concentration (IC_{50}) was assessed, initially, using the Caco-2 cell line, originated from human epithelial colorectal adenocarcinoma

cancer cells and, later in the A549 cell line, human alveolar epithelial cells (Table 4.3). From the results obtained and the calculated IC_{50} through the MTS assay, it was observed that among the pure components used to formulate the mixtures, CA and the anti-TB drug RIF were the ones with lower IC_{50} values. This means that a lower amount of compound is necessary to inhibit by half the cell viability, showing that the pure components presented higher cytotoxicity than when incorporated in the liquid mixtures.

Comparatively, the values obtained for the formulated THEDES largely differ from those obtained for the pure components. From the results obtained and despite L-Arg presented a lower value of IC_{50} than EMB, when mixed with other components of the mixture (CA and water) the mixtures containing EMB presented a slightly lower IC_{50} than mixtures with L-Arg. Different molar ratios of the components, also altered substantially the values of IC_{50}, being the mixtures with higher ratios of CA the ones that presented lower values of IC_{50} and, consequently, higher cytotoxicity, probably due to an increase in the acidity of the mixtures. The increase of water ratio in the mixtures, in general, leads to a slight increase on cell viability. For THEDES, a decrease on cell viability compared to the initial liquid mixture (CA:EMB:H_2O (1:1:5) was observed, due to the addition of small amounts of different anti-TB drugs (INH, PZA, RIF), however, this decrease was not statistically significant.

Table 4.3 - IC_{50} values for pure components and THEDES in Caco-2 cell line and in A549 cell line. Results are expressed as mean ± SD of at least three independent experiments that were performed in triplicate.

	Compounds	IC_{50} (mg mL^{-1}) in Caco-2 cells	IC_{50} (mg mL^{-1}) in A549 cells
Pure Components	CA	0.84 ± 0.58	1.43 ± 0.13
	L-arg	17.72 ± 4.15	12.30 ± 0.56
	EMB	20.57 ± 14.42	21.50 ± 2.94
	INH	-	33.53 ± 1.73
	PZA	-	31.76 ± 5.59
	RIF	-	0.69 ± 0.34
THEDES	CA:EMB:H_2O (2:1:10)	3.99 ± 0.03	2.86 ± 0.60
	CA:EMB:H_2O (1:1:5)	-	3.43 ± 0.55
	CA:EMB:L-arg:H_2O (2:1:1:7)	-	4.10 ± 0.70
	CA:L-arg:H_2O (1:1:4)	-	5.80 ± 1.45
	CA:L-arg:H_2O (1:1:5)	-	5.36 ± 1.33
	CA:L-arg:H_2O (1:1:6)	4.29 ± 0.41	6.62 ± 1.04
	CA:L-arg:H_2O (1:1:7)	6.15 ± 3.46	6.12 ± 0.86
	CA:L-arg:H_2O (2:1:7)	3.43 ± 1.81	3.08 ± 0.99
	CA:L-arg:H_2O (2:1:8)	4.67 ± 0.50	3.24 ± 0.21
	CA:L-arg:H_2O (2:1:9)	4.14 ± 2.90	3.37 ± 0.23
	CA:EMB:H_2O + RPI (1:1:1)	-	2.59 ± 1.28
	CA:EMB:H_2O + RPI (2:3:1)	-	2.51 ± 1.69
	CA:EMB:H_2O + RPI (2:5:1)	-	3.10 ± 1.99
	CA:EMB:H_2O + PZA	-	3.45 ± 0.21

After evaluating the cell viability in Caco-2 and A549 cells, the cell viability in THP-1 macrophages was also evaluated, taking into account the IC_{50} values determined before. Since the lower IC_{50} value was found in RIF (0.69 ± 0.34) it was tested the cell viability for macrophages with concentrations below IC_{50} determined for RIF to guarantee that was found a limit of non-toxic concentration that can be used in further studies with mycobacteria. Figure 4.21 shows the cell viability in macrophages of all the compounds at 0.625 mg mL^{-1} and 0.080 mg mL^{-1}. From the results obtained it was possible to observe that RIF was cytotoxic at 0.625 mg mL^{-1}, yet at 0.080 mg mL^{-1} this was not observed. It can, hence, be assumed that all THEDES and pure compounds (RIF < 0.080 mg mL^{-1}) were non-cytotoxic to macrophages, since they presented a cell viability of nearly 100%.

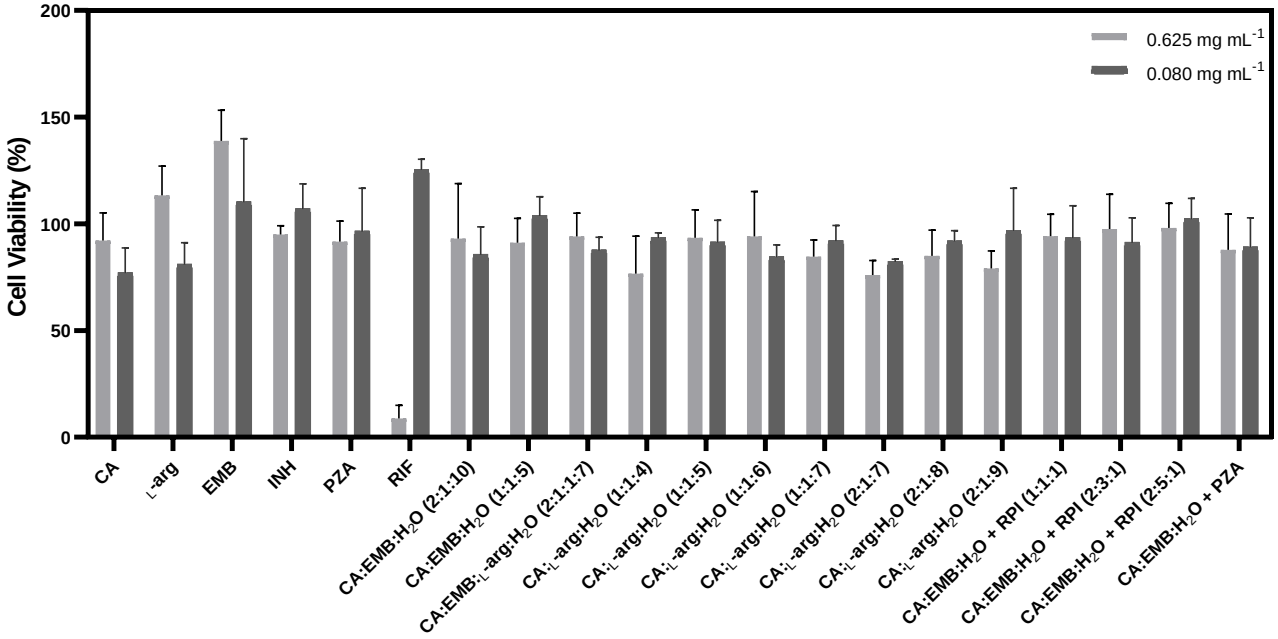

Figure 4.21 - Cell viability evaluated in macrophages at 0.625 mg mL^{-1} and 0.080 mg mL^{-1}. Data are presented as mean ± SD (n = 3).

4.4.2 Permeation studies upon exposure to therapeutic deep eutectic systems

The *in vitro* studies concerning the transport of molecules and/or formulations are important to estimate the ability of the molecules to permeate through different models of

living barriers, such as single monolayers, or co-cultures. In order to mimic a pulmonary barrier, it was used a transwell system that enables the formation of two different microenvironments (apical and basolateral side). On the apical side were cultured alveolar epithelial cells (A549) until they differentiate and establish a cellular monolayer (barrier model), that formed a polarized epithelium and prevented the passage of ion currents along a paracellular pathway. After exposure of THEDES to the pulmonary barrier model, for 6 hours, it was estimated the apparent permeability (Table 4.4) for each compound and observed that anti-TB drugs (EMB, INH, PZA) tested presented higher permeation than the liquid formulations. Between the THEDES, small differences were observed. However, there appears to be a tendency for increased permeability with increasing ratios of drugs present in the formulation. The formulation with PZA presented the lowest permeability, being almost all the compound retained on the apical side.

Table 4.4 - Estimate apparent permeability and cellular uptake from transwell assays, using A549 cellular monolayer as a membrane.

Compound	Papp (10^{-5} cm s^{-1})	Final concentration on apical side (mg mL^{-1})*	Final concentration on basolateral side (mg mL^{-1})	Estimated cellular uptake (mg mL^{-1})
EMB	2.484 ± 1.279	-	-	-
INH	1.663 ± 0.316	-	-	-
PZA	3.007 ± 0.896	-	-	-
RIF	0.339 ± 0.068	-	-	-
CA:EMB:H_2O (1:1:5)	0.714 ± 0.472	-	-	-
CA:EMB:H_2O + RPI (1:1:1)	0.656 ± 0.318	0.016	0.009	1.237
CA:EMB:H_2O + RPI (2:3:1)	0.659 ± 0.484	0.038	0.050	1.223
CA:EMB:H_2O + RPI (2:5:1)	0.715 ± 0.503	0.086	0.049	1.272
CA:EMB:H_2O + PZA	0.292 ± 0.113	1.085	0.003	0.220

*Indicative value, estimated from one replica.

Regarding the cellular uptake estimated for each formulation in the A549 cellular monolayer, it was possible to infer that a large amount of the compounds studied were internalized by the cells instead of passing through the apical to basolateral side, which justifies the lower permeation of the formulations through the barrier model of A549 cells.

4.4.3 Antimicrobial activity in H37Rv

The antimicrobial activity was evaluated in the drug-susceptible *Mtb* strain H37Rv with concentrations that proved to be non-toxic for cell lines (16 – 0.125 μg mL^{-1}), and the values of minimal inhibitory concentration (MIC) and minimal bactericidal concentration (MBC) were calculated and are presented in Table 4.5.

Table 4.5 - MICs and MBCs determined *in vitro* in *Mycobacterium tuberculosis* (H37Rv), after 7 days of treatment.

Compound	MIC (μg mL^{-1})	MBC (μg mL^{-1})	Compound	MIC (μg mL^{-1})	MBC (μg mL^{-1})
CA	> 16	> 16	CA:L-arg:H_2O (1:1:5)	> 16	n.d.
L-arg	> 16	> 16	CA:L-arg:H_2O (1:1:6)	> 16	n.d.
EMB	1	2	CA:L-arg:H_2O (1:1:7)	> 16	> 16
INH	< 0.125	< 0.125	CA:L-arg:H_2O (2:1:7)	> 16	n.d.
PZA	> 16	> 16	CA:L-arg:H_2O (2:1:8)	> 16	n.d.
RIF	< 0.125	0.25	CA:L-arg:H_2O (2:1:9)	> 16	> 16
CA:EMB:H_2O (2:1:10)	4	8	CA:EMB:H_2O + RPI (1:1:1)	2	4
CA:EMB:H_2O (1:1:5)	2	4	CA:EMB:H_2O + RPI (2:3:1)	2	4
CA:EMB:L-arg:H_2O (2:1:1:7)	4	8	CA:EMB:H_2O + RPI (2:5:1)	2	4
CA:L-arg:H_2O (1:1:4)	> 16	n.d.	CA:EMB:H_2O + PZA	2	8

*n.d. non-determined

From the determination of MIC and MBC values, it was observed some variability in the pure components, being as expected anti-TB drugs more effective and with lower MICs and MBCs than CA and L-Arg, except for PZA which is known to only be active at low pH values.[288] Regarding THEDES the ones that have EMB in their composition were the ones that presented better activity against H37Rv, being the one with a lower ratio of CA and water (CA:EMB:H_2O (1:1:5)) the one that presented a better performance against H37Rv. Considering THEDES prepared based on CA:EMB:H_2O (1:1:5) and different amounts of anti-TB drugs, a similar activity was observed in comparison to the THEDES alone, except for the formulation in which only PZA was added, which require higher concentrations to inhibit viability of the bacteria.

4.4.4 Effects on *Mtb* (H37Rv) during macrophages infection

The infection of THP-1 macrophages with H37Rv and posterior treatment with the THEDES was performed to evaluate the effect of the THEDES in a model of infection, in which the macrophages phagocytose the bacteria. The selected concentrations tested did not affect the viability of macrophages, as expected from the viability studies shown previously and were in the range of MICs tested. Two approaches were followed. A single dose of 16 μg mL^{-1} was given to the macrophages infected as well as two doses of 8 μg mL^{-1}, one at day 0 plus a new dose of 8 μg mL^{-1} on day 3 post-infection. It was observed that compared to the control, the mixture and the formulations presented antibacterial activity against H37Rv decreasing the CFU over the entire time-course of experiment, inhibiting the growth of the bacteria until at least 9 days of culture (Figure 4.22). It was also interesting to observe that although the pattern of antibacterial activity presented is similar, the treatment with an initial dose of 8 μg mL^{-1} and reinforcement after 3 days with an additional 8 μg mL^{-1} presented to be less effective than the administration of a single higher dose at the beginning of infection (16 μg mL^{-1}). As expected, with the increase of the ratio of anti-TB drugs dissolved in the THEDES it was observed an increase in the antibacterial activity against H37Rv.

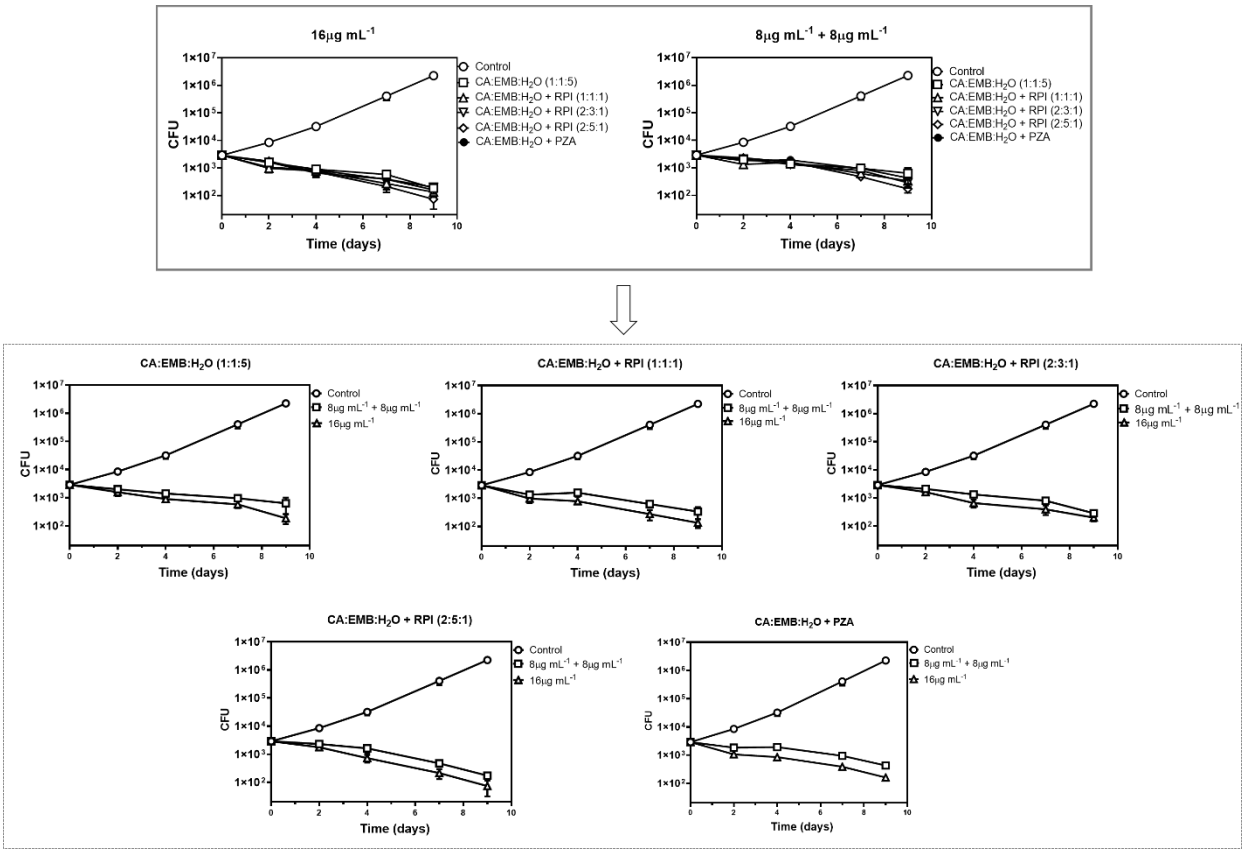

Figure 4.22 - Intracellular activity of THEDES in macrophages infected with H37Rv. The activity was evaluated at different time points, for 9 days, using different concentrations: 16 μg mL^{-1} and 8 μg mL^{-1} plus another dose of 8μg mL^{-1} on day 3. Colony-forming units (CFU) were determined by counting the colonies originated from surviving bacteria at each time point. Data are presented as mean ± SD (n = 3), ****$p \leq 0.001$, when compared to the control.

4.5 Discussion

The preparation of novel eutectic systems continues to be a challenge because the mechanisms that trigger the hydrogen bonding formation in the systems are not yet completely understood.[153] During this work, the aim was to produce therapeutic liquid mixtures, as THEDES, with anti-TB drugs incorporated and understand how the different components interact with each other. After optimization, ten different eutectic systems

(Table 2.1 (Chapter 2, 2.2.2)) were successfully produced, rendering a clear and transparent liquid at room temperature.

The eutectic systems were characterized by POM, where the images appeared as black images, indicating amorphous and homogeneous liquids, without the formation of any solid crystals. NMR (^{1}H, ^{13}C, HMBC and NOESY) was used to study the structure of mixtures and confirmed the presence of different chemical groups of CA, EMB and L-arg in THEDES, as well as to evaluate the stability of the systems over time. The interactions between the compounds, particularly in the amine groups of EMB, were detected, and the mixtures presented a delocalization of the chemical shift (9.24 ppm to 9.14 ppm), which we hypothesized that was due to interactions by hydrogen bonding formed with -OH of CA and H_2O. In which concerns the hydrogen-bonded protons, changes in the chemical shift could be observed when eutectic mixtures form a liquid structure, as we observed the upfield shift in the amine groups of EMB.[185] Regarding the thermodynamic characterization, the mixtures were firstly studied by DSC to observe phase transitions of individual components and therapeutic liquid mixtures. Around 100-120 °C, within THEDES components phase transitions appear in the thermogram indicating that these systems could start to be unstable at these temperatures; also water evaporation could justify the destabilization of the mixtures. According to literature, the systems must have melting temperatures below the melting peaks of the individual components.[153,235] Dai and co-workers have found that small amounts of water resulted in systems that are liquid at room temperature, besides that, the presence of water also resulted in a reduced time of preparation and a decrease in the viscosity of the systems.[154,245] The stability of the DES with small amounts of water, generally is increased and the solubilizing capacity could also be tuned. However, adding superior amounts of water (up to 50% of water content) could lead to dilution of DES and results in a loss of the existing hydrogen bonding, characteristic of these solvents.[154,235,245] In the case of the THEDES herein reported, the presence of water is fundamental to the preparation of the systems.

The solubility of the compounds is, also, an important parameter for evaluating the features of THEDES prepared and observe if they are promising for future incorporation into medicines. A significant increase in the solubility of EMB in the THEDES was observed, however for the systems containing L-arg the difference was not so noticeable. In the case of the permeability studies on a synthetic membrane of the different compounds, a similar behaviour was observed. While the permeability of EMB was increased in THEDES form, in

the case of L-arg the THEDES presented a lower permeability compared to the pure API. The diffusion coefficient of the systems presented the same characteristic behaviour of permeability, as higher diffusion coefficients mean faster diffusion of the compound through the membrane. Duarte et al. described that a higher solubility leads to higher driving force through the membrane in permeability studies,[185] and our results also confirm this. As expected, the permeability and diffusion coefficient of EMB in THEDES was higher, as its solubility was highly increased. This was not the case in the systems with L-arg. The parameters of the biopharmaceutics classification system are described in the literature, and classify the APIs in four different classes, class I high soluble and high permeable; class II low soluble and high permeable; class III high soluble and low permeable, and class IV low soluble and low permeable.[185] An API is considered highly soluble when the volume to dissolve 1 mg is lower than 250 mL, which was verified in the THEDES with EMB that present a solubility of 127.6 mg mL^{-1}. A compound is considered highly permeable if presents permeability higher than $6x10^{-6}$ cm s^{-1} and the THEDES with EMB presented a permeability of $128.3x10^{-5}$ cm s^{-1} which was, hence, higher than the reference value. According to literature and the Biopharmaceutical Classification System (BCS), EMB is classified as a class III compound, i.e., a compound with high solubility but low permeability. The results obtained in this work (Table 4.2) showed that THEDES can tailor the bioavailability of APIs and it can be postulated that EMB can change its classification from class III to class I, being in the THEDES form, highly soluble and highly permeable.[185,289]

One of the questions raised when preparing these liquid mixtures was if they were regular solutions or eutectic mixtures, as they present water in their composition. Taking that into consideration, SLE modelling through PC-SAFT and ePC-SAFT was applied to mixtures with CA, L-arg and H_2O, which show that these mixtures are prone to strong non-ideal behaviour induced by water addition. Water has a bifunctional role as it causes not only an acidic environment (formation of charged species) but it also acts as a hydrogen bonding mediator for L-arg and CA. As the phase behaviour depends on the ratio of mixtures components, the thermodynamic model ePC-SAFT was used as a qualitative predictive model to evaluate the influence of H_2O on the SLE. This prediction tool was particularly useful as it was not possible to obtain experimental SLE data for the system, due to decomposition, low melting or ultra-low melting points. Within this context, the influence of H_2O on CA:L-arg mixtures was studied in terms of SLE and activity coefficients. Novel melting properties of L-arg were by the first time determined through FSC, as this was

required for SLE modelling. ePC-SAFT predicted a transition from positive to negative deviation from Raoult's law upon the addition of H_2O to CA:L-arg at certain molar ratios. This rendered an estimated deep decrease in the T_m of these mixtures upon H_2O addition as well as increased intermolecular interactions. Furthermore, the hypothesis of salt formation and pH influence to explain the deep decrease of T_m were explored. However, both could be contradicted (by pH control measurements without either CA or L-arg and by the FTIR analysis). Finally, the formation of an altered hydrogen bonding network was confirmed by NMR spectroscopy. The observed non-ideal behaviour of the mixture and the hydrogen bonding formation in the mixture are consistent with the hypothesis of DES formation and the occurrence of strong non-ideal solvation of the CA and L-arg species in H_2O. In this scenario, considering the high potential of H_2O to establish hydrogen bonding interactions, it is challenging to distinguish between non-ideal solvation and eutectic systems formation. Both phenomena are mainly promoted by hydrogen bonding interactions between the constituents, causing depression on the melting temperatures. To the best of our knowledge, the only difference reported in the literature that differentiates a eutectic system from a regular solution is the structural network organization. Whereas eutectic systems are recognized by the supramolecular complexes formed between their components, aqueous solutions are considered when the solvation of isolated components occurs.[244–250] Still, it was confirmed the crucial bifunctional role of H_2O (formation of charged species and mediated hydrogen-bonded interactions between CA and L-arg). Therefore, either being a eutectic system or a non-ideal aqueous solution, these ternary mixtures have new properties and might be considered independent systems from conventional solvents.

To gain insights into the interactions and configurations of different components in the THEDES and how they can influence the activity of drugs we also perform molecular dynamics studies and molecular docking. From the initial set of MD simulations, it was observed that EMB:H_2O forms aggregates and non-homogenous mixtures, while when combined in a THEDES with CA and H_2O the aggregates disappear, and the system's homogeneity is improved. By calculating RDFs and SDFs of THEDES components it was possible to have insights about which groups were involved in intermolecular interactions. The RDF and SDF data showed that only one carboxylic group of CA was essential to promote interactions with the amine groups of EMB, and that L-arg, although also interacting with the same amine groups, prefers to establish intermolecular HBs with EMB hydroxyl groups. Therefore, it was conceivable that both CA and L-arg provide a greater

balance between hydrophobicity and hydrophilicity when interacting with EMB, while the remaining functional groups continue immersed in the aqueous environment structuring the THEDES. Molecular docking was also performed, and data suggests that the presence of CA and/or L-arg may also have an important role for EMB uptake by mycobacteria, apart from the prevention of EMB aggregation when present in the liquid mixture. Herein, the exploitation of a possible entry pathway through the ABC transporter Rv1819c using single and multiple simultaneous ligand docking suggests that CA may have a critical role in increasing the binding affinity of EMB towards Rv1819c by mediating specific interactions with its intracellular gate, formed by an L-arg pair from both protomers (R287). Although we present a valid route for the uptake of EMB by mycobacteria, other entry routes, e.g., via direct interaction with the lipidic membrane or by means of other undisclosed transporters, cannot be discarded.

After exploring the possibility of formulating THEDES with anti-TB drugs of first-line treatment, we obtained stable THEDES that were combined with other anti-TB drugs to obtain formulations that can be useful in TB therapy. Our data indicated that in terms of solubility the chosen mixtures can increase the solubility of PZA, using mixtures with EMB and higher ratios of CA and water. In the case of INH, it was noted that mixtures with higher ratios of CA decrease its the solubility in physiological media and, also for RIF, it was detected a decrease of its solubility in all hydrophilic mixtures, due to its large size and hydrophobic character.

The formulations made combining THEDES and anti-TB drugs, were based on the system CA:EMB:H_2O (1:1:5), owing to previous studies that made possible to achieve mixtures with at least one of anti-TB drug incorporated[258] and, also the molecular dynamics studies that enabled to observe the strengthening of molecular interactions between the components for this system.[283] From the present study, it was possible to observe that this system can increase the solubility of PZA, which can be important for a possible readjustment of the dose of PZA used in TB therapy, as this is one of the drugs that requires a higher dose to be effective against *Mtb*.[290,291] Additionally, the system CA:EMB:H_2O (1:1:5) was capable to solubilize INH and RIF, which is essential to formulate therapeutic liquid mixtures with the four anti-TB drugs, as proposed in this study. Herein, it was possible to demonstrate the physicochemical stability of the formulations, during 6 months storage, using different and complementary techniques. The POM indicates that all the drugs present in the THEDES were completely dissolved, since any crystal formation or precipitate

appeared in the formulations. Regarding NMR and FTIR-ATR studies, the data suggests that despite the signal corresponding to -OH groups presented itself broader after 6 months, comparing to the initial formulation, it is not a significant alteration in the chemical structure of the formulations, as we could confirm by FTIR-ATR.

Cell viability studies of these mixtures were performed in different cell lines (Caco-2, A549 and THP-1 macrophages) and demonstrated that CA and RIF are the major contributors to the cytotoxicity of the systems, although in macrophages, for the two concentrations tested, these mixtures did not reveal to be cytotoxic. Furthermore, the estimated cellular uptake in A549 cells indicates that, in the case of the liquid formulations, a higher concentration of the formulation was accumulated inside the cells in a non-toxic concentration instead of permeating from apical to basolateral side, except for formulations with PZA that remain in the apical side. The permeability of the THEDES through this pulmonary barrier model was lower compared to the pure drugs, being hypothesized that the THEDES stays in the epithelium and was not absorbed to the systemic circulation, remaining at the site of infection. The antimicrobial activities reported here for the first-line anti-TB drugs are in accordance to previous studies.[292–295] RIF and INH were the ones that presented a more pronounced effect against *Mtb* (H37Rv). Concerning THEDES prepared, the ones with EMB presented higher activity against *Mtb* (H37Rv) with MIC values of 2 μg mL^{-1} (CA:EMB:H_2O (1:1:5)) and 4 μg mL^{-1} (CA:EMB:H_2O (2:1:10) and CA:EMB:L-arg:H_2O (2:1:1:7)), also the liquid formulations presented a similar value to the mixture CA:EMB:H_2O (1:1:5), which confirms our second proposition. Regarding the intracellular activity of the THEDES after macrophage infection, it was possible to confirm their antibacterial activity. The treatment of macrophages was conducted following two different approaches: one in which 16 μg mL^{-1} were administered at the beginning of infection and evaluated for 9 days; and the other where 8 μg mL^{-1} were administered at the beginning of infection and then reinforced at day 3 of infection with additional 8 μg mL^{-1}. A more pronounced effect against the growth of *Mtb* was observed with an administration of a single higher dose at the beginning.

In general, it was possible to prepare stable THEDES and dissolve different anti-TB drugs in this system CA:EMB:H_2O (1:1:5). The water presented in these systems is essential for their formation and to form hydrogen bonds between the components of each mixture. Regarding their antimicrobial activity it was maintained, being effective against *Mtb* (H37Rv). Due to its promising results, more studies should be performed in resistant

bacterial strains to assess the effectiveness of THEDES against resistant *Mtb*, and explore different combinations should also be a possibility to have in consideration.

5

COMBINATORIAL APPROACH OF THEDES WITH ORGANIC SALTS

Different sustainable approaches have been reported in the literature to address the problems of bioavailability of numerous APIs and the waste generated by the synthesis and manufacturing of drug delivery formulations by the pharmaceutical industries. In this thesis, we focus mostly on answering the problems of bioavailability of APIs for TB therapy through the synthesis of organic salts and preparation of THEDES. In previous chapters, it was described the development of organic salts using INH as cation, since it is one of the anti-TB drugs used as first-line treatment of TB, during all treatment and in preventive treatments. In this context, we synthesized several organic salts using INH as cation in combination with suitable anions and studied their properties, observing that dicationic forms, as $[INH][Cl]_2$, improved the solubility and permeability of INH in simulated physiological media.

The preparation of THEDES using INH was also explored (Table A.2.1, Appendix A), however it was not possible to reach a stable liquid mixture with INH incorporated. Hereupon, to prepare stable liquid mixtures with an anti-TB of first-line treatment incorporated we used EMB, which present a less complex chemical structure than INH and presents more hydrogen bonding groups than INH, which can facilitate the formation of stable eutectic mixtures. It was possible to achieve stable liquid mixtures with EMB incorporated (Table 2.1 from 2.2.2, Chapter 2).

As we could not design a system with the same API incorporated, either in the form of an organic salt or a THEDES, we followed a combinatorial strategy. In this sense, it was

prepared a THEDES dissolving the organic salt [INH][Cl]$_2$ together with PZA and RIF in the system CA:EMB:H_2O (1:1:5). Herein, the dissolution of [INH][Cl]$_2$ in the THEDES was investigated, compared with pure INH, and evaluated in terms of its ability to change the stability of the formulation and regarding its *in vitro* biological viability and activity against *Mtb* (H37Rv).

5.1 Stability studies

The stability studies, as mentioned before, were followed through POM, NMR and FTIR-ATR, after 6 months of preparation and storing at room temperature (20-25 °C). From the POM images captured with a cross polarizer, black images were observed, indicating homogeneity and absence of crystals in the systems of CA:EMB:H_2O + RPI and CA:EMB:H_2O + RP[INH][Cl]$_2$, after 6 months of preparation (Figure 5.1).

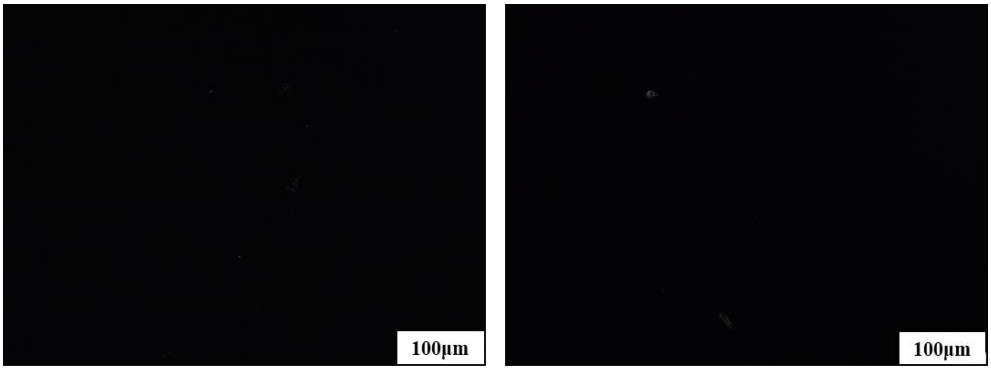

Figure 5.1 - POM images obtained from THEDES solubilized with INH and [INH][Cl]$_2$.

The ^{1}H-NMR studies, as showed in Figure 5.2, revealed some differences from 0 to 6 months related to -OH groups. As previously observed for the other THEDES, after preparation the signal corresponding to -OH groups presented to be sharper than after 6 months, which can be explained by the flexibility of these protons regarding the appearance and intensity in the spectra.[233] Due to this characteristic of -OH protons, it was considered that the structure of the THEDES was maintained and they did not affect the stability of the formulations. However, in the case of mixture CA:EMB:H_2O + RP[INH][Cl]$_2$ differences in the spectra were also observed, corresponding to aromatic protons of INH, that after 6

months appeared with a slight deviation and as doublet, which is characteristic of $[INH][Cl]_2$.[296] Taking that into consideration, the mixture CA:EMB:H_2O + RP$[INH][Cl]_2$ was considered stable after 6 months. These variations occurring in the spectra can also be explained by slight differences in the concentration of mixtures during preparation of samples and the presence of small concentrations of water in deuterated solvent.

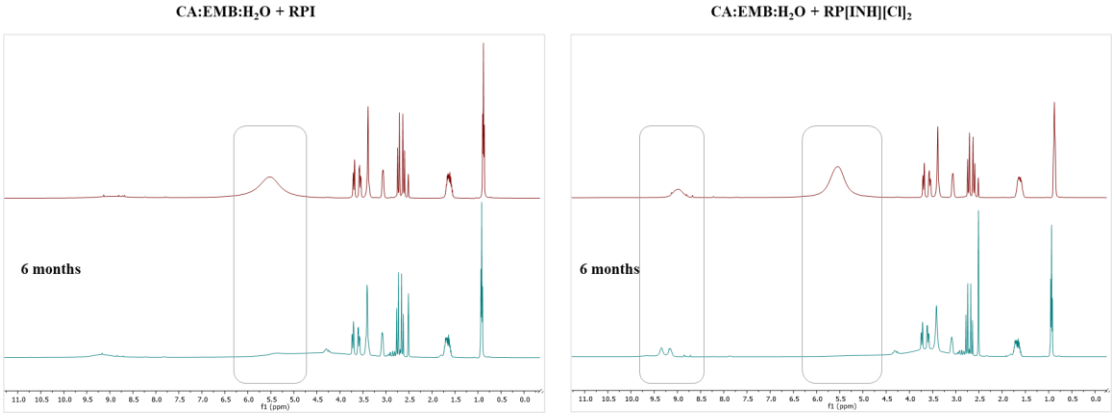

Figure 5.2 - ^1H NMR superimpose of systems CA:EMB:H_2O + RPI and CA:EMB:H_2O + RP$[INH][Cl]_2$, between 0 and 6 months of preparation.

Additionally, infrared spectroscopy was performed in order to understand if the variations observed in the NMR spectra were relevant to change the chemical structure of the formulations. From Figure 5.3, it was possible to observe an overlap of the spectra at 0 and 6 months, which indicated that the THEDES present minor differences regarding the intensity of the peaks that did not affect their stability and chemical structure. Being observed characteristic signals in the region of -OH stretching (3550-3200 cm^{-1}) and also broad peaks due to presence of water in the mixtures, which corroborates the NMR studies.

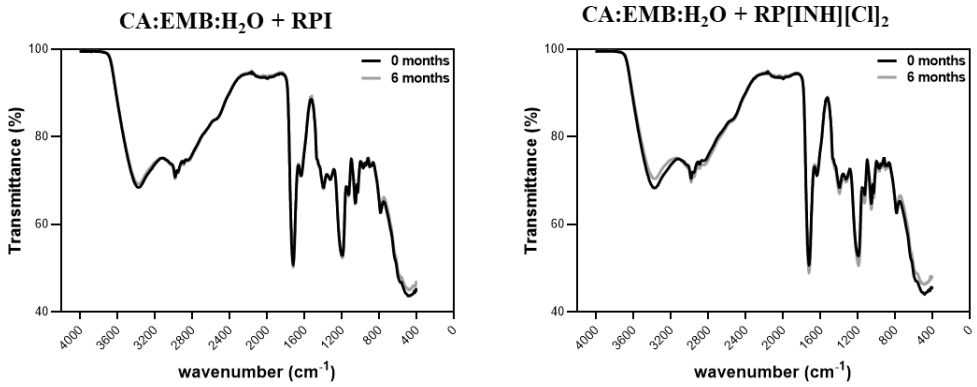

Figure 5.3 - FTIR-ATR spectra of systems CA:EMB:H_2O + RPI and CA:EMB:H_2O + RP[INH][Cl]$_2$, between 0 and 6 months of preparation.

5.2 Biological evaluation and antimicrobial activity

The biological and antimicrobial assessment was carried out through different approaches, being cell viability evaluated in A549 cells and THP-1 macrophages, and the cellular permeability assessed by the transwell assay with A549 cells. Then, the antimicrobial activity was evaluated against *Mtb* (H37Rv).

From cell viability in A549 cells (Table 5.1) it was observed that the dicationic form [INH][Cl]$_2$ presented much higher cytotoxicity to epithelial alveolar cells than INH, however when small amounts of INH salt (0.4 mg mL^{-1}) dissolved in liquid system with other anti-TB drugs (0.4 mg mL^{-1} PZA and RIF) the cell viability increases, since the amounts added were in the range of non-toxic concentrations.

Table 5.1 - IC_{50} values for pure components and systems CA:EMB:H_2O + RPI and CA:EMB:H_2O + RP[INH][Cl]$_2$ in A549. Results were expressed as mean ± SD of at least three independent experiments that were performed in triplicate.

	Compounds	IC_{50} (mg mL^{-1}) in A549 cells
Pure components	INH	33.53 ± 1.73
	[INH][Cl]$_2$	1.52 ± 0.77
THEDES	CA:EMB:H_2O + RPI	2.59 ± 1.28
	CA:EMB:H_2O + RP[INH][Cl]$_2$	3.12 ± 0.15

Regarding cell viability studies with macrophages the dissolution of organic salt $[INH][Cl]_2$ did not affect the viability of macrophages at the concentrations tested (0.625 mg mL^{-1} and 0.08 mg mL^{-1}), being the cell viability > 80% in all compounds and systems tested (Figure 5.4).

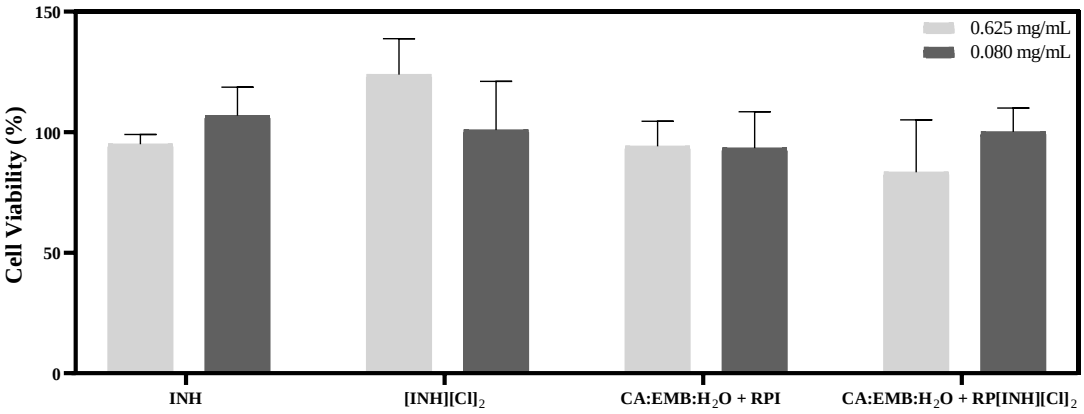

.

Figure 5.4 - Cell viability evaluated in macrophages at 0.625 mg mL^{-1} and 0.080 mg mL^{-1}. Data are presented as mean ± SD (n = 3).

Another study performed, was the apparent permeability assessment using an A549 cell monolayer as membrane. Comparing INH with the organic salt, it was observed a lower permeability of the organic salt comparing to pure INH. On the other hand, in the case of THEDES, and despite the values of the lower apparent permeability determined for the formulation with the organic salt, the differences were not statistically significant, when compared to the formulation with INH (Table 5.2). In which concerns the concentration values obtained in apical and basolateral side, it was noted that the permeation through the cell membrane was overly low in both formulations. However, in the case of formulation with organic salt dissolved the low permeation is derived from a higher concentration in the apical side and cellular uptake by A549 cells. In the case of the formulation with pure INH, almost all the compound is internalized by A549 cells, not passing through the apical side to basolateral side.

Table 5.2 - Estimated apparent permeability and cellular uptake from transwell assays, using A549 cellular monolayer as membrane.

Compound	Papp (10^{-5} cm s^{-1})	Final concentration on apical side (mg mL^{-1})*	Final concentration on basolateral side (mg mL^{-1})	Estimated cellular uptake (mg mL^{-1})
INH	1.663 ± 0.316	-	-	-
$[INH][Cl]_2$	0.718 ± 0.155	-	-	-
CA:EMB:H_2O + RPI	0.656 ± 0.318	0.016	0.009	1.237
CA:EMB:H_2O + RP$[INH][Cl]_2$	0.536 ± 0.452	0.815	0.012	0.494

*Indicative value, estimated from one replica.

The antimicrobial activity, against *Mtb*, of these THEDES was also evaluated and no significant differences were observed concerning the concentrations needed to inhibit the growth or be bactericidal to *Mtb* susceptible strain (H37Rv) (Table 5.3).

Table 5.3 - MICs and MBCs determined *in vitro* in *mycobacterium tuberculosis* (H37Rv), after 7 days of treatment.

Compound	MIC (μg mL^{-1})	MBC (μg mL^{-1})
INH	< 0.125	< 0.125
[INH][Cl]2	0.125	n.d.
CA:EMB:H_2O + RPI	2	4
CA:EMB:H_2O + RP$[INH][Cl]_2$	2	4

*n.d. non determined

Finally, the effect on macrophages that were infected with H37Rv and then treated with these formulations was evaluated. From Figure 5.5, it was noticeable that the administration of a single dose of 16 μg mL^{-1} of each formulation was more effective against the bacteria than the multiple dose administration of minor doses (8 μg mL^{-1}). Concerning the effect of formulations with INH or organic salt dissolved, the effect was quite similar and were not considered statistically different.

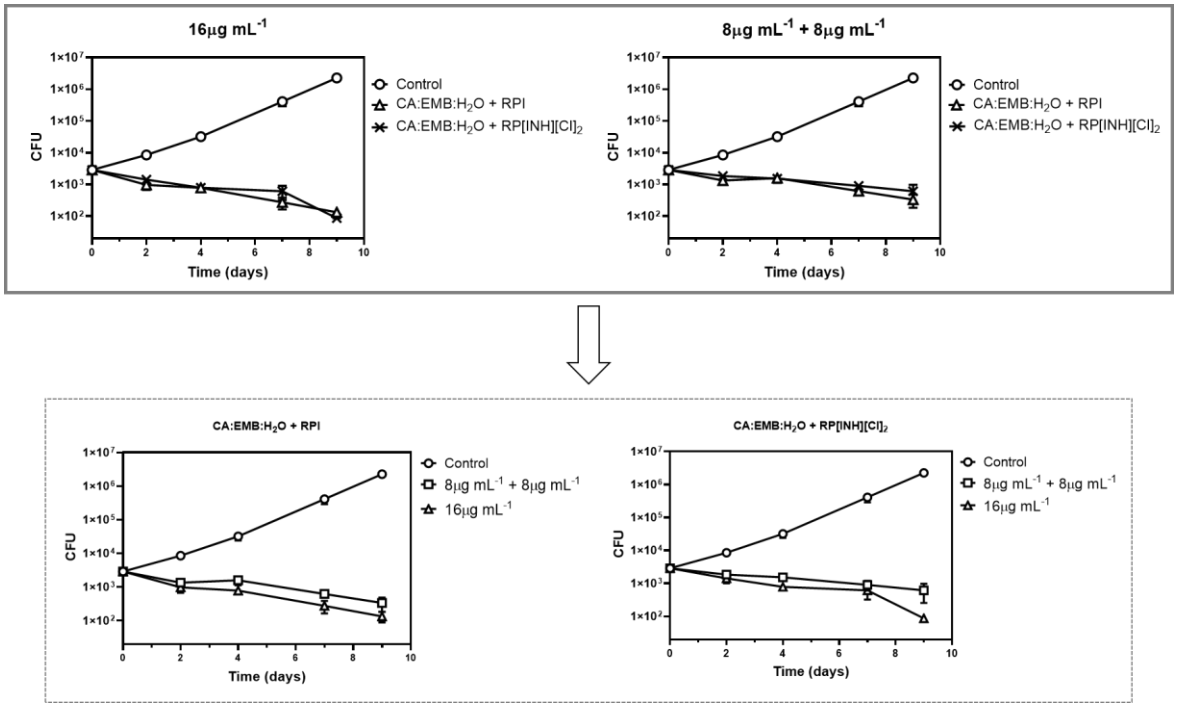

Figure 5.5 - Intracellular activity of therapeutic liquid formulations with INH and $[INH][Cl]_2$ in macrophages infected with H37Rv. The activity was evaluated at different time points, for 9 days, using different concentrations: 16 μg mL^{-1} and 8 μg mL^{-1} plus another dose of 8 μg mL^{-1} at day 3. Colony-forming units (CFU) were determined by counting the colonies originated from surviving bacteria at each time point. Data are presented as mean ± SD (n = 3), ****$p \leq 0.001$, when compared to the control.

5.3 Discussion

One of the goals of this thesis was to explore the use of organic salts and therapeutic liquid mixtures, as eutectic systems, for TB therapy. While the first idea would be to compare both approaches, this turned out not be viable as the first molecule chosen to synthetize organic salts, INH, did not render a eutectic formulation itself. Therefore, we compared the performance of the pure active pharmaceutical ingredient, INH, with the organic salt synthetized, when they were dissolved in a liquid formulation, as THEDES, which was used as a carrier. The dissolution of the organic salt $[INH][Cl]_2$ in the system CA:EMB:H2O (1:1:5) together with PZA and RIF was successfully accomplished, resulting in a stable mixture, similarly to the ones with INH dissolved.

Regarding the biological activity of these formulations, higher cytotoxicity of dicationic organic salt $[INH][Cl]_2$ was detected. However, for liquid formulations the cell viability was again increased. In the studies with macrophages all the compounds and systems were considered non-toxic, presenting a cell viability higher than 80%. When evaluating the permeation through a cellular membrane, the INH presented better permeation compared to organic salt and formulations. The formulation with organic salt was mainly retained in apical side, contrarily to formulation with INH that was internalized by A549 cells. The antimicrobial activity evaluated against *Mtb* was similar for both formulations with INH and organic salt, and when macrophages were infected with *Mtb* and treated with different scheme doses of formulations, the single and higher dose of administration of formulations revealed to be the more effective.

Overall, the dissolution of an organic salt in a THEDES was achieved producing a mixture with demonstrated stability until 6 months. Despite the relatively higher toxicity of the organic salt, when dissolved in THEDES the cell viability increases and regarding the antimicrobial activity it is maintained with organic salt in the mixture. The major difference occurs in permeability of the mixture with organic salt. Despite the previous studies with synthetic membranes revealed an increase of permeability with the organic salt comparing to INH, this was not observed for the experimental determinations of permeability using transwell and a cell monolayer. Using a biological membrane, either $[INH][Cl]_2$ or INH dissolved in the liquid mixture were not permeable, since almost all the concentration of organic salt remains in apical side, while with INH in the mixture it is internalized by A549 cells.

To the best of our knowledge, we herein report for the first time the possibility to combine organic salts and THEDES, taking advantage of both approaches towards the development of alternative therapies. From the experiments carried out it can be concluded that it is possible to use a THEDES as a carrier for an organic salt and, despite the fact that for this particular API did not render major differences in comparison with the pure API, it may open exciting possibilities for future developments of combinatorial formulations.

The following chapter was adapted from the publication:

Roda A., **Santos F.**, Matias A.A., Paiva A. and Duarte A.R.C. Design and processing of drug delivery formulations of therapeutic deep eutectic systems for tuberculosis. Journal of Supercritical Fluids (2020). 161 (104826). DOI: 10.1016/j.supflu.2020.104826.

6

DEVELOPMENT OF MATRICES FOR TB THERAPY

In previous chapters, we describe the development and characterization of THEDES based on CA, L-arg, EMB and H_2O, focusing tuberculosis therapy.[184,258,283] The systems produced showed an improvement of the solubility and permeability of the pharmaceutical components in comparison to its isolated solid forms. These characteristics can be promising to adjust the dose needed for effective TB treatment. Since TB affects mainly the pulmonary system, we believe that a local administration would be more efficient. For that reason, we tested the encapsulation of the developed THEDES to design a delivery system suitable for local administration, for example by spray inhalation. The formulation of delivery systems incorporating LTTMs is quite recent[163,297–300] and the use of supercritical fluid technology for this purpose is not extensively explored.[163,301] $scCO_2$ technology is a very attractive platform, widely used for the formulation of pharmaceutical products since $scCO_2$ is a green, cheap, abundant and recyclable solvent. Most importantly, it allows to produce solvent-free final products, avoiding further purification steps.[178]

Different supercritical atomization techniques have been explored for the design of distinct drug delivery systems. Herein, we investigate different SCF technologies that could be used for atomization and encapsulation of THEDES and their formulations. Firstly, Roda and co-workers performed studies of phase liquid equilibria with THEDES and CO_2, using the mixture CA-L-arg:H_2O (1:1:7) as model. After observing the phase behaviour of the combination THEDES-CO_2, the particles from gas saturated solution (PGSS) method was chosen as a suitable supercritical technology for particle atomization of THEDES. PGSS is a $scCO_2$ technology that uses CO_2 as a solute, being solubilized in the carrier while decreasing its melting temperature. In this technique, the CO_2 can also be dissolved into the bioactive component or may act as dispersive agent of the bioactive in the melted carrier. When

depressurizing the mixture, the expansion and cooling of CO_2 by the Joule-Thomson effect causes the precipitation of the carrier, which solidifies and forms the particles.[302,303]

Pursuing the optimization of morphology and particle size distribution to properly match a pulmonary administration, the atomization through supercritical anti-solvent (SAS) and supercritical assisted atomization (SAA) was also explored, in collaboration with the Salerno University (Italy). SAS technology is described as a process that uses $scCO_2$ as an anti-solvent, causing the precipitation of the solute (THEDES + carrier), that was initially dissolved in an organic solvent.[302] In turn, SAA is described as a process that uses $scCO_2$ as a co-solute for the solution containing the compound (THEDES + carrier).[304]

The main findings of these studies are presented in the next subsections.

6.1 Encapsulation and atomization of therapeutic liquid mixtures and formulations through $scCO_2$ technology

6.1.1 Particles from gas saturated solutions

6.1.1.1 Phase equilibria of therapeutic liquid mixtures and CO_2

The phase equilibria of the THEDES + CO_2 mixture was performed visually, for the mixture CA:L-arg:H_2O (1:1:7), which was used as model, by observing the physical state of the isothermal mixture at certain composition when varying the pressure by compression of the mixture. The transition of the two-to-one phase, would correspond to the solubility measurement, expressed as the dew or bubble point of the system. However, within the range of conditions studied and in respect to the solubility of THEDES in CO_2 (Table 6.1), it was not possible to observe single-phase transitions.

Table 6.1 - Phase equilibria of THEDES in CO_2, at different mole fractions (χ), 40 °C and pressures up to 30 MPa.

χ CO_2	χ THEDES	Observation
0.638	0.362	2 phases (liquid + gas)
0.785	0.215	2 phases (liquid + gas)
0.886	0.114	2 phases (liquid + gas)

The existence of two phases within the experimental conditions of pressure and temperature, indicated that the solubility of THEDES in CO_2 was not significant, at least in the ratios herein described. In fact, above certain pressures (> 10 MPa), water separation from the THEDES was observed, forming a triphasic system (THEDES + H_2O + CO_2). This phenomenon was already reported for other liquid-liquid mixtures.[305] It should be considered for processing as it may change the THEDES composition under this pressure and temperature conditions. Interestingly, during depressurization of the high-pressure device with the THEDES + CO_2 mixtures, foaming phenomenon was observed, indicating that CO_2 can be dissolved in the THEDES liquid phase. Upon depressurization, there was a decrease in the CO_2 solubility which caused its release, expansion and consequent foaming of the sample.

From the phase equilibria studies of mixture of THEDES + CO_2, it was observed the possibility of water separation from THEDES during processing, mainly, at higher pressures and CO_2 contents. Hereupon, for PGSS processing the lowest conditions of pressure and temperature necessary to melt the carrier were chosen and, the apparatus used was described by Lack and co-workers.[186] The carrier selected was glycerol monostearate (GMS), that is considered biocompatible and safe by FDA[183] and, also has been previously reported to be processable by PGSS at working pressures between 6 and 23 MPa and temperatures from 57 to 80 °C.[306–308] Within the supercritical region, full lipid melting was observed at 8.5MPa and 65 °C, which were set as the processing conditions for PGSS in this work. Additionally, the THEDES of CA:L-arg:H_2O with decrescent amounts of water, from 1:1:7 up to 1:1:4 molar ratio were prepared and their encapsulation through PGSS was compared to evaluate the water influence in the process.

6.1.1.2 Morphological characterization

The morphology of the particles produced through PGSS was analysed by SEM, from which was possible to observe a spongy-spherical structure (Figure 6.1). This kind of structures are normally porous, which is a characteristic of particles processed by PGSS, due to the rapid and cooling expansion of CO_2, which can form surface holes, foams or sponge-like structures.[309,310]

THEDES are viscous liquids, which, if present at the particles surface would cause them to be sticky and agglomerated. The particles herein obtained had a free-flowing powder consistency, suggesting that the liquid THEDES was successfully incorporated

within the core of the lipidic particles. Moreover, as observed, the particles containing THEDES (Figure 6.1a-d) and the empty lipidic particles (Figure 6.1e) presented a similar morphology. The similarity between their surface supports our assumption that the external part was only composed by the GMS while THEDES may be entrapped internally in the particles. This hypothesis was corroborated by EDS analysis (Table 6.2). The nitrogen element, characteristic from the arginine compound of THEDES, was not identified in the particles surface. The only chemical elements detected were carbon and oxygen, the main components of GMS.

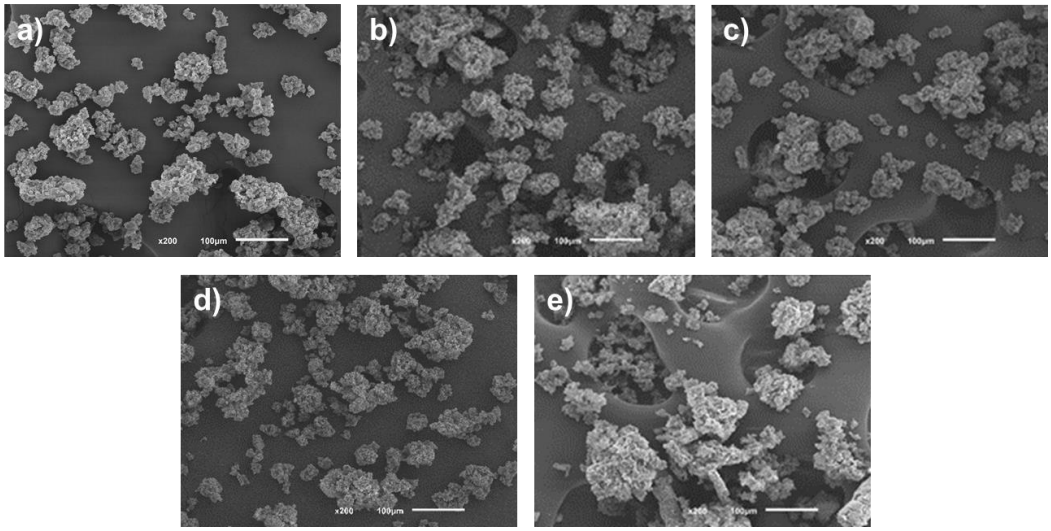

Figure 6.1 - SEM micrographs of GMS particles obtained through PGSS containing THEDES of CA:L-arg:H_2O at a molar ratio of **a)** 1:1:7; **b)** 1:1:6; **c)** 1:1:5; **d)** 1:1:4 and **e)** empty GMS particles.

In terms of particle size, all the produced particles presented similar mean sizes, between 14 and 23 μm (Table 6.2). Regarding the particle size distribution, all the particulate systems were slightly polydisperse (PDI > 0.2, Table 6.2), presenting a gaussian distribution within the same size range (Figure 6.2). The encapsulation of THEDES showed no significative influence in the particles size, when compared to GMS particles precipitated alone.

Table 6.2 - Chemical weight composition, mean geometrical particle size and, polydispersity index (PDI) of the GMS particles with no THEDES (empty) and with THEDES of CA:L-arg:H_2O at the molar ratios of 1:1:7, 1:1:6, 1:1:5 and 1:1:4.

GMS particles	Surface weight composition (%)		Mean particle size (μm)	PDI
	Carbon	Oxygen		
Empty	82.7	17.3	17 ± 8	0.251
CA:L-arg:H_2O (1:1:7)	82.2	17.8	14 ± 7	0.288
CA:L-arg:H_2O (1:1:6)	82.9	17.1	23 ± 13	0.337
CA:L-arg:H_2O (1:1:5)	78.9	21.1	19 ± 11	0.342
CA:L-arg:H_2O (1:1:4)	81.7	18.3	20 ± 11	0.291

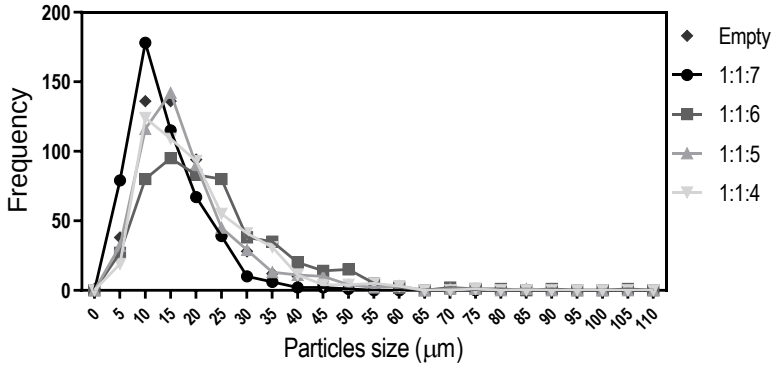

Figure 6.2 - Geometrical particle size distribution of the GMS particles with no therapeutic liquid mixtures and with therapeutic liquid mixtures of CA:L-arg:H_2O at the molar ratios 1:1:7, 1:1:6, 1:1:5 and 1:1:4.

6.1.1.3 Encapsulation efficiency (EE)

The encapsulation efficiency was determined after simple disruption of the lipidic matrix without the need for a rising step. As observed in Figure 6.3, the mean encapsulation efficiency of THEDES in the GMS particles varied from 60 to 92%.

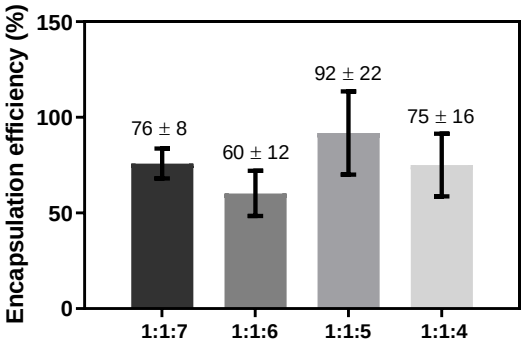

Figure 6.3 - Encapsulation efficiencies determined for the different THEDES processed through PGSS.

Although this difference was quite large, no statistically significant differences were observed due to the intrinsic heterogeneity within each particulate system. From the results obtained, there was no evident pattern related to the water content in THEDES, so it may be concluded that the water content did not influence the encapsulation process. The observed differences and intrinsic variability might be due to the manual depressurization of the system during processing. Slight changes during depressurization may cause high sample heterogeneity. However, in a scale up perspective this could be easily overcome by incorporating an automatic depressurization control or by continuous PGSS processing.[186]

6.1.1.4 Drug release profile

One of the goals of the work was to explore the possibility of formulating a suitable drug-delivery system with THEDES, as eutectic systems for administration as inhalable particles, expecting to have a fast and local release of the drug. These systems are expected to be more efficient reaching bacteria, while avoiding systemic toxicity.[311] From the 24 h release profile (Figure 6.4) it was observed a burst release at the time point of 5 minutes, followed by a successive increase of therapeutic liquid mixtures in solution, up to 5h, after which a plateau is reached.

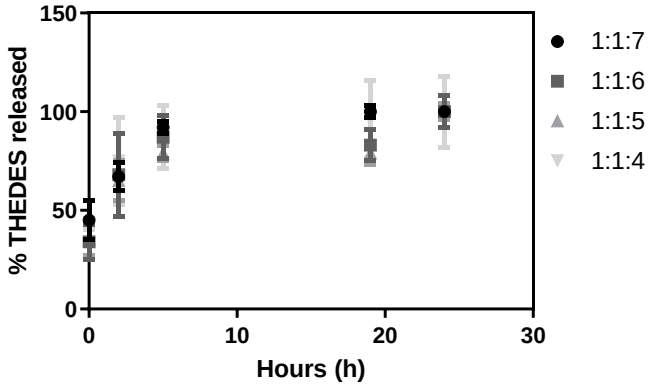

Figure 6.4 - Release profile of THEDES from PGSS particles, namely THEDES of CA:L-arg:H_2O at molar ratios of 1:1:7, 1:1:6, 1:1:5 and 1:1:4.

This fast release might be explained by the porosity of the particles prepared. This behaviour is compliant with the nasal administration as it is a non-invasive therapy. It further allows to control the dose administrated and the direct absorption of therapeutic agents without passing through the acidic environment of stomach and hepatic first-pass metabolism.[312]

6.1.2 Supercritical anti-solvent (SAS)

The supercritical anti-solvent technology, reported several times for micronization of drugs by Reverchon and co-workers,[181,187,188,313,314] was used to test the atomization of THEDES, containing anti-TB drugs incorporated. The solute was composed by different THEDES as presented in Table 2.2 (Chapter 2, 2.2.2) and the carrier chosen was polyvinylpyrrolidone (PVP). PVP is a polymer that is considered an amorphous, biodegradable, biocompatible, and is FDA-approved.[304,315] Several studies of supercritical atomization, report the used of PVP due to its high solubility in different organic solvents and its stabilizer ability of active principles, protecting them from oxidation.[316]

The studies were carried out using the proportion 4:1 PVP:THEDES (w/w), being two different concentrations tested in the liquid solution. Also, different solvents were tested for encapsulation process as DMSO and mixtures of ethanol/acetone (50:50), with a constant pressure of 12 MPa and temperature in the precipitator of 40 °C (Table 6.3).[181] The established conditions of pressure and temperature were based on different experiments conducted by Reverchon and co-workers to produce rifampicin particles, being concluded

that using DMSO as a solvent at 40 °C and at 12 MPa or more, particles with diameters lower than 1 µm were obtained.[181]

Table 6.3 - Conditions tested for formation of particles with THEDES and PVP, through SAS technology.

Solute	Solvent	Concentration (mg mL^{-1})	Observations
PVP + Therapeutic liquid mixture (4:1)	DMSO	10	Coalescent and aggregate particles
		50	
	EtOH/Acetone (50:50)	10	Gel, no particles formed

In general, after the experiments, small amounts of coalescent particles or viscous agglomerates of particles were obtained. This effect could be explained by different composition of THEDES (CA:EMB:H_2O + anti-TB drugs), that despite being soluble in organic solvents could react differently with $scCO_2$, which did not allowed the formation of stable particles at the conditions tested. In future studies, other conditions of optimization process could be tested, varying parameters like pressure, temperature, flow rate of liquid solution and the ratio between THEDES and PVP, during SAS processing.

6.1.3 Supercritical assisted atomization (SAA)

Having in consideration that $scCO_2$ could possible solubilize in some extend the THEDES we tried to produce particles through supercritical assisted atomization (SAA) that is also a technology reported by Reverchon and co-workers for the production of micro and nanoparticles for pharmaceutical applications.[182,189,190] The SAA apparatus includes three main vessels: the saturator, precipitator and condenser. The SAA process involves the solubilization of the liquid solution by $scCO_2$ or near to critical CO_2 close to saturation (in the saturator), then the solution is atomized through a nozzle in a near-atmospheric-pressure vessel (in the precipitator) where heated nitrogen will cause solvent evaporation and the particles are formed.[190] In the end of process the gaseous flow of CO_2, nitrogen and solvent is sent to a condenser.[315]

In SAA process we use the same polymer as a carrier (PVP) as tested in the SAS, and the same proportion of PVP/THEDES (4:1 w/w) with a final concentration of liquid solution of 10 mg mL^{-1}. The solvent used was ethanol and the pressure used was ≈ 7 MPa at 40 °C in

the saturator, and 70 °C in the precipitator and condenser. Using this supercritical technology, it was then possible to obtain homogenous particles.

The particles produced by SAA were characterized by SEM as represented in Figure 6.5, and it is possible to observe the heterogeneity among the size of the particles and also some particle aggregation, mainly, in samples of CA:EMB:H_2O + RPI, CA:EMB:H_2O + RPI (2:3:1) and CA:EMB:H_2O + PZA. This aggregation could be explained by water absorption that made them, in these cases, slightly sticky. To overcome this problem some changes in the storage conditions could be done as protecting the particles from humidity.[96] Further, stability studies should be done to avoid fast degradation, comprising for example, evaluation of chemical and physical stability of the particles in different time periods.

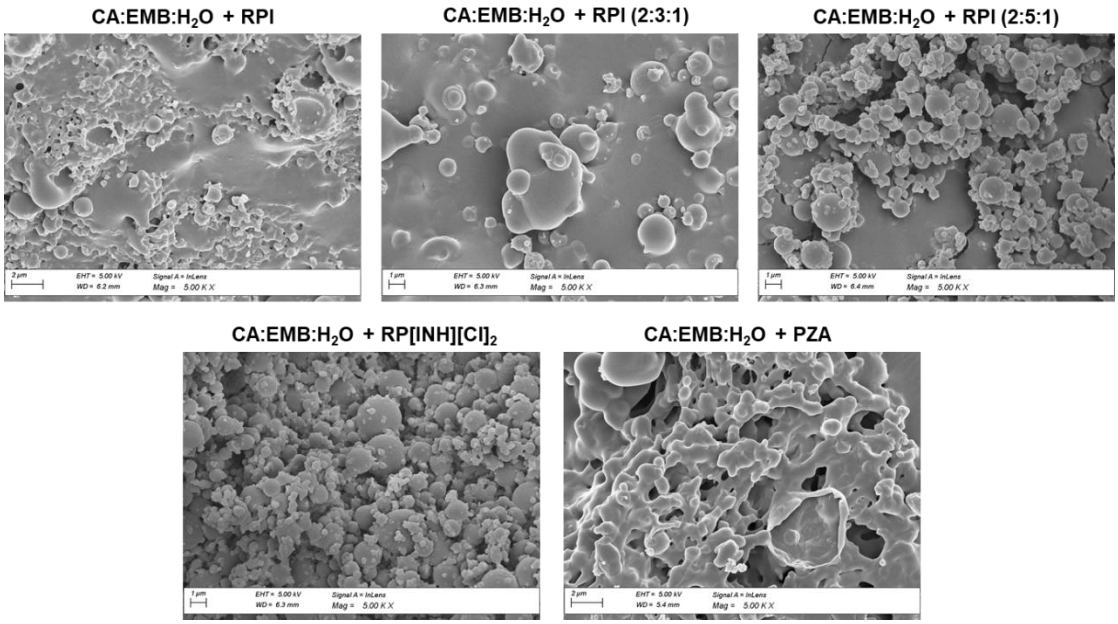

Figure 6.5 - SEM images of PVP particles obtained through SAA with THEDES.

Regarding the particle size measurements, SEM images provide some clues about the size of the particles observing that their size is lower than 2 μm. To determine the accurate particle size and evaluate their suitability to be applied in TB therapy, as inhalable particles, dynamic light scattering (DLS) was employed (Table 6.4). All particles presented a size below 500 nm with slight polydispersity associated, corroborating the SEM images.

Table 6.4 - Particle size and polydispersity index of particles formed with PVP and THEDES measured by dynamic light scattering. Data are presented as mean ± SD of triplicates.

PVP particles	Particle size (Ø nm)	PDI
CA:EMB:H_2O + RPI	394 ± 42	0.245 ± 0.020
CA:EMB:H_2O + RPI (2:3:1)	239 ± 51	0.215 ± 0.026
CA:EMB:H_2O + RPI (2:5:1)	166 ± 24	0.327 ± 0.132
CA:EMB:H_2O + RP[INH][Cl]$_2$	322 ± 77	0.327 ± 0.060
CA:EMB:H_2O + PZA	300 ± 71	0.428 ± 0.121

6.2 Cell viability studies

Cell viability studies were performed, firstly, with PGSS particles in L929 cell line and it was observed that the cell viability was not compromised by any of the THEDES, GMS and formulated particles, since it presented a mean value above 80% in all cases (Figure 6.6). Although, it presents some variability between the systems and the particles, this might be due to the heterogeneity of the particles tested, as previously explained. The THEDES 1:1:4 and its respective particle formulation presented the lowest viability and the highest variability. This might be due to its higher viscosity (lower water content). In literature, it is reported that the higher viscosity of eutectic systems can decrease the cell viability and influence intracellular activities.[238,317] However, no statistical significant differences were encountered between the systems tested.

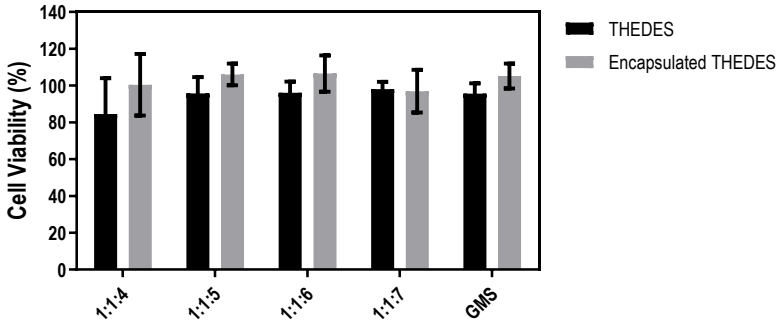

Figure 6.6 - Cell viability assay for THEDES and encapsulated THEDES in L929 cell line. Unprocessed GMS and GMS empty particles were used as control.

Particles formulated with PVP was also evaluated regarding cell viability in A549 cells. From Figure 6.7, it can be affirmed that PVP particles do not present cytotoxicity in the concentration tested (2 mg mL^{-1}), presenting a viability above 80%, which turn them suitable for further studies in mycobacteria.

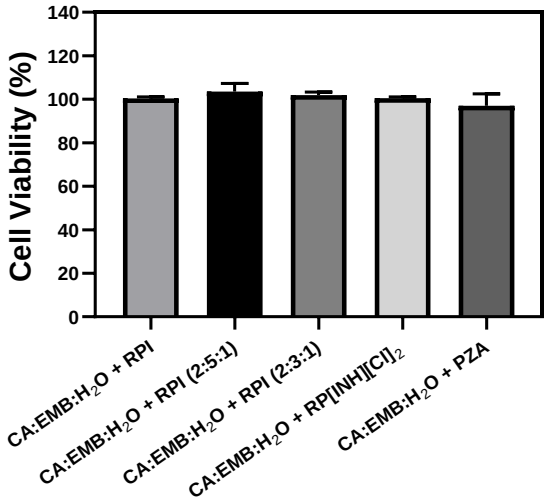

Figure 6.7 - Cell viability assessment in A549 cells for particles formulated with PVP and THEDES. Data are presented as mean ± SD of at least three independent replicas, made in triplicates.

6.3 Discussion

The development of drug delivery matrices, that could be suitable for TB therapy, using supercritical fluid technology (PGSS, SAS, SAA) was explored. From different technologies tested to formulate inhalable particles, it was concluded that PGSS and SAA are appropriate to process these THEDES, contrarily to SAS that did not allow the formation of particles, in conditions tested.

Considering the eventual application of the produced particles as inhalable formulations for TB therapy, it is important to analyse the influence of their particle size for that purpose. Despite the micronization of THEDES by PGSS (14–23 μm), the size achieved was larger than the one that could reach the alveolus (≈ 0.5-1 μm). However, their aerodynamic size might be lower due to their porosity. Porous particles may present lower densities than non-porous particles, which confer them an adequate aerodynamic diameter for deposition in alveolus. Thus, to produce an inhalation device targeting the alveolus,

optimization processes and/or use of different supercritical fluid technology, for example SAA, should be performed. SAA technology was applied to achieve lower particle size that could reach to nano scale, being all particles formulated with a diameter lower than 500 nm (150-400 nm), despite some heterogeneity and polydispersity detected.

Regarding encapsulation efficiency after PGSS processing, it varies between 60-92% and drug release profile indicates a fast initial release followed by a crescent increase of THEDES release in solution and, after 5 h, the plateau was reached. Also, cell viability assays with particles encapsulated through PGSS and SAA were performed, and particles were considered non-toxic and suitable for further studies in *Mtb*.

7

CONCLUSIONS AND FUTURE PERSPECTIVES

The work developed during this thesis was centered on exploring alternative approaches for TB therapy, mainly, through the study of green and sustainable solvents. The use of green solvents by pharmaceutical industries have been explored to reduce the costs of drug production as well as the generated waste, showing additionally a great potential for application in drug development, in order to improve pharmacokinetics and pharmacodynamics of the drugs. TB therapy is still a challenge, due to prolonged treatment, several adverse effects that compromise the patient compliance and, the multidrug resistance to anti-TB drugs. Therefore, our purpose with this work was to address the challenge of TB therapy with alternative solvents, namely, finding alternative treatments or improving the existing ones.

Throughout this work, different achievements were accomplished. In particular, the synthesis of organic salts based on INH as a cation showed to be a promising strategy for the enhancement of some of physical, thermal and biological properties of original INH, mainly in cases of di-protonation. Furthermore, the dicationic forms can contribute to enhance the characteristics of the drugs, such as solubility and stability as well as to eliminate the polymorphic forms.

Also, the development of THEDES was possible by the incorporation of EMB and L-arg in different stable liquid systems. The evaluation of the THEDES properties was essential to understand their suitability for pharmaceutical applications and hypothesize which mechanisms are involved in their formation. Moreover, the NMR studies indicated possible hydrogen bond formation in amine groups of EMB, carboxyl groups of CA and water. The systems incorporating EMB were capable to increase its solubility and permeability in

synthetic membranes, when compared to pure API, being then considered as class I, i.e., highly soluble and highly permeable. Also, THEDES prepared were able to solubilize INH, PZA and RIF and, the mixture CA:EMB:H_2O (1:1:5) increased the solubility of PZA.

Despite the questions raised about the water presence in the THEDES, from different studies presented throughout this work it was possible to conclude that water was essential to stabilize therapeutic liquid mixtures and facilitate their formation, decreasing their viscosity and contributing to hydrogen bond formation, acting as a hydrogen bond mediator between different components of the mixture. Molecular dynamic studies were also explored, in this work, to understand the internal structure of THEDES and confirm the molecular interactions observed by the different spectroscopic characterization. From these analyses it was confirmed that the water content in the mixtures acts as a stabilizing agent and the different ratios of CA could promote additional interactions by hydrogen bonding in the system CA:EMB:H_2O (1:1:5). According to the data obtained, the formation of a quaternary system as CA:EMB:L-arg:H_2O (2:1:1:7), suggested a more stable mixture since stronger intermolecular interactions could be formed, due to the ability of arginine to disrupt the water-mediated hydrogen bond network, while promoting hydrogen bonding with the other components of the mixture. The MD data of these THEDES corroborates that. The carboxyl groups of CA establish intermolecular interactions with the amine groups of EMB; when L-arg is present in the liquid mixtures it prefers to interact with the hydroxyl groups of EMB, contributing to the solubility of EMB and L-arg in water. Furthermore, from molecular docking studies, different approaches were used to observe if the internalization of EMB via the mycobacterial ABC transporter (Rv1819c) was propitious by the liquid mixtures, and if the presence of CA and L-arg in the systems increases the affinity to the transporter. According to our findings, the different ratios of CA in the mixtures did not have a direct impact in the EMB affinity to the binding site of the transporter. Nonetheless, an important role for CA as a mediator for EMB interaction with Rv1819c could also be hypothesized. This computational approach applied to these THEDES represents an important step to understand the molecular interactions established between the different components of these low melting transition liquid mixtures, as well as the effect of some modifications in properties of active compounds facilitating the entry of the anti-TB drug, EMB, in the mycobacterial cell.

The formulation of therapeutic liquid mixtures with the four anti-TB drugs was successfully accomplished by dissolving the different anti-TB drugs of first-line treatment in

the same THEDES. The permeability of these mixtures in a A549 monolayer showed that they were not absorbed to the systemic circulation, remaining at the site of infection. These mixtures had proven antibacterial activity against *Mtb* (H37Rv) with more pronounced effect when a single higher dose of THEDES (16 µg mL^{-1}) was administrated at the beginning of infection. In order to meet the needs of the TB patients and inhalable formulation was envisaged. For this purpose, THEDES were encapsulated through different supercritical technology processes, being here for the first time reported the encapsulation of THEDES by PGSS processing. Additionally, SAS and SAA processing of THEDES were tested, however, only SAA demonstrated to be suitable to form particles with an adequate size for pulmonary delivery.

Overall, the main goals of this work were achieved allowing a new approach using different alternative solvents and combine them to address tuberculosis therapy. The strategies explored demonstrated potential to be applied in new pharmaceutical approaches to target TB more effectively. However, more studies should be carried out pursuing complex models for the *in vitro* evaluation of mechanisms involved in their activity, and the evaluation of their potential in resistant strains of *Mtb* will be essential for major advances into applications in TB therapy. Also, the study of more promising systems in clinical practice should be pursued, through clinical isolates from TB patients, which could enable to precision medicine and modulate the therapy to each patient.

REFERENCES

1. Geneva: World Health Organization. Global Tuberculosis Report 2021. in Licence: CC BY-NC-SA 3.0 IGO (2021).
2. Dooley, K. E., Phillips, P. P. J., Nahid, P. & Hoelscher, M. Challenges in the clinical assessment of novel tuberculosis drugs. *Adv. Drug Deliv. Rev.* 102, 116–122 (2016).
3. Kümmerer, K. Sustainable from the very beginning: rational design of molecules by life cycle engineering as an important approach for green pharmacy and green chemistry. *Green Chem.* 9, 899–907 (2007).
4. Kümmerer, K. Pharmaceuticals in the environment. *Annu. Rev. Environ. Resour.* 35, 57–75 (2010).
5. Cizmas, L., Sharma, V. K., Gray, C. M. & McDonald, T. J. Pharmaceuticals and personal care products in waters: occurrence, toxicity, and risk. *Environ. Chem. Lett.* 13, 381–394 (2015).
6. Ali, H. & Khan, E. Environmental chemistry in the twenty-first century. *Environ. Chem. Lett.* 15, 329–346 (2017).
7. Blasco, J. & DelValls, A. Impact of emergent contaminants in the environment: environmental risk assessment. *Handb. Environ. Chem.* 5, 169–188 (2008).
8. Anastas, P. & Eghbali, N. Green chemistry: principles and practice. *Chem. Soc. Rev.* 39, 301–312 (2010).
9. Welton, T. Solvents and sustainable chemistry. *Proc. R. Soc. Chem. A* 471, 1–26 (2015).
10. Daniel, T. M. The history of tuberculosis. *Respir. Med.* 100, 1862–1870 (2006).
11. Floyd, K., Glaziou, P., Zumla, A. & Raviglione, M. The global tuberculosis epidemic and progress in care, prevention, and research: an overview in year 3 of the End TB era. *Lancet Respir. Med.* 6, 299–314 (2018).
12. Reid, M. J. A. *et al.* Building a tuberculosis-free world: The Lancet Commission on

tuberculosis. *Lancet* 393, 1331–1384 (2019).

13. Shampo, M. A. & Rosenow, E. C. A history of tuberculosis on stamps. *Chest* 136, 578–582 (2009).
14. Müller, R., Roberts, C. A. & Brown, T. A. Genotyping of ancient Mycobacterium tuberculosis strains reveals historic genetic diversity. *Proc. R. Soc. B* 281, 1–8 (2014).
15. Pezzella, A. T. History of pulmonary tuberculosis. *Thorac. Surg. Clin.* 29, 1–17 (2019).
16. Dulberger, C. L., Rubin, E. J. & Boutte, C. C. The mycobacterial cell envelope — a moving target. *Nat. Rev. Microbiol.* 18, 47–59 (2020).
17. Eddy, J. J. The ancient city of Rome, its empire, and the spread of tuberculosis in Europe. *Tuberculosis* 95, S23–S28 (2015).
18. Fogel, N. Tuberculosis: A disease without boundaries. *Tuberculosis* 95, 527–531 (2015).
19. Murray, J. F., Schraufnagel, D. E. & Hopewell, P. C. Treatment of tuberculosis: A historical perspective. *Ann. Am. Thorac. Soc.* 12, 1749–1759 (2015).
20. Salvatore, P. P. & Zhang, Y. Tuberculosis: molecular basis of pathogenesis from *Reference Module in Biomedical Sciences* 1–15 (Elsevier Inc., 2017). doi:10.1016/b978-0-12-801238-3.95697-6.
21. Al-Humadi, H. W., Al-Saigh, R. J. & Al-Humadi, A. W. Addressing the challenges of tuberculosis: A brief historical account. *Front. Pharmacol.* 8, 1–10 (2017).
22. Wong, E. B., Cohen, K. A. & Bishai, W. R. Rising to the challenge: new therapies for tuberculosis. *Trends Microbiol.* 21, 493–501 (2013).
23. Pontali, E. *et al.* Regimens to treat multidrug-resistant tuberculosis: Past, present and future perspectives. *Eur. Respir. Rev.* 28, 1–7 (2019).
24. Tiberi, S. *et al.* The challenge of the new tuberculosis drugs. *Presse Med.* 46, e41–e51 (2017).
25. Bahuguna, A. & Rawat, D. S. An overview of new antitubercular drugs, drug candidates, and their targets. *Med. Res. Rev.* 40, 263–292 (2020).
26. Fitzgerald, D. W., Sterling, T. R. & Haas, D. W. 251 - Mycobacterium tuberculosis. *Mand. Douglas, Bennett's Princ. Pract. Infect. Dis.* 2, 2787–2818 (2015).
27. Uplekar, M. & Raviglione, M. WHO's End TB Strategy: From stopping to ending the global TB epidemic. *Indian J. Tuberc.* 62, 196–199 (2015).
28. Geneva: World Health Organization. *The End TB Strategy*. *World Health Organization* (2015).
29. Patel, S., Maheshwari, A. & Chandra, A. Biomarkers for wound healing and their

evaluation. *J. Wound Care* 25, 46–55 (2016).

30. Kaur, M., Garg, T., Rath, G. & Goyal, A. K. Current nanotechnological approaches for an effective delivery of bioactive drug molecules in the treatment of tuberculosis. *Crit. Rev. Ther. Drug Carr. Syst.* 31, 49–88 (2014).
31. Pai, M. *et al.* Tuberculosis. *Nat. Rev. Dis. Prim.* 2, 1–23 (2016).
32. Kaur, I. P. & Singh, H. Nanostructured drug delivery for better management of tuberculosis. *J. Control. Release* 184, 36–50 (2014).
33. Adami, A. J. & Cervantes, J. L. The microbiome at the pulmonary alveolar niche and its role in Mycobacterium tuberculosis infection. *Tuberculosis* 95, 651–658 (2015).
34. Wallis, R. S. & Hafner, R. Advancing host-directed therapy for tuberculosis. *Nat. Rev. Immunol.* 15, 255–263 (2015).
35. Magalhães, J., Vieira, A., Santos, S. & Pinheiro, M. *Oral Administration of Nanoparticles-Based TB Drugs* from *Multifunctional Systems for Combined Delivery, Biosensing and Diagnostics* , (eds. Grumezescu A.M.) (Elsevier Inc., 2017). doi:10.1016/B978-0-323-52725-5/00016-2.
36. Brennan, P. J. Structure , function , and biogenesis of the cell wall of Mycobacterium tuberculosis. *Tuberculosis* 83, 91–97 (2003).
37. Geneva: World Health Organization. WHO Operational handbook on tuberculosis. Module 1: prevention - tuberculosis preventive treatment. in Licence: CC BY-NC-SA 3.0 IGO (2020).
38. McLean, M. R., Lu, L. L., Kent, S. J. & Chung, A. W. An Inflammatory Story: Antibodies in Tuberculosis Comorbidities. *Front. Immunol.* 10, 1–20 (2019).
39. Pandey, R. & Ahmad, Z. Nanomedicine and experimental tuberculosis : facts , flaws , and future. *Nanomedicine Nanotechnology, Biol. Med.* 7, 259–272 (2011).
40. Torfs, E., Piller, T., Cos, P. & Cappoen, D. Opportunities for overcoming mycobacterium tuberculosis drug resistance: Emerging mycobacterial targets and host-directed therapy. *Int. J. Mol. Sci.* 20, (2019).
41. Zumla, A., Nahid, P. & Cole, S. T. Advances in the development of new tuberculosis drugs and treatment regimens. *Nat. Publ. Gr.* 12, 388–404 (2013).
42. Brennan, P. & Nikaido, H. The envelope of mycobacteria. *Annu. Rev. Biochem.* 64, 29–63 (1995).
43. Viveiros, M., Leandro, C. & Amaral, L. Mycobacterial efflux pumps and chemotherapeutic implications. *Int. J. Antimicrob. Agents* 22, 274–278 (2003).

44. Marrakchi, H., Lanéelle, M. A. & Daffé, M. Mycolic acids: Structures, biosynthesis, and beyond. *Chem. Biol.* 21, 67–85 (2014).
45. Toole, R. F. O. & Gautam, S. S. The host microbiome and impact of tuberculosis chemotherapy. *Tuberculosis* 113, 26–29 (2018).
46. Silva, C. *et al.* Exploring the contribution of mycobacteria characteristics in their interaction with human macrophages. *Microsc. Microanal.* 19, 1159–1169 (2013).
47. Napier, R. J. *et al.* Imatinib-Sensitive tyrosine kinases regulate mycobacterial pathogenesis and represent therapeutic targets against tuberculosis. *Cell Host Microbe* 10, 475–485 (2011).
48. Kroesen, V. M. *et al.* Non-steroidal anti-inflammatory drugs as host-directed therapy for tuberculosis: A systematic review. *Front. Immunol.* 8, 1–9 (2017).
49. Vilaplana, C. *et al.* Ibuprofen therapy resulted in significantly decreased tissue bacillary loads and increased survival in a new murine experimental model of active tuberculosis. *J. Infect. Dis.* 208, 199–202 (2013).
50. Ivanyi, J. & Zumla, A. Non-steroidal anti-inflammatory drugs for adjunctive tuberculosis treatment. *J. Infect. Dis.* 208, 185–188 (2013).
51. Amaral, L., Martins, M. & Viveiros, M. Enhanced killing of intracellular multidrug-resistant Mycobacterium tuberculosis by compounds that affect the activity of efflux pumps. *J. Antimicrob. Chemother.* 59, 1237–1246 (2007).
52. Adams, K. N. *et al.* Drug tolerance in replicating mycobacteria mediated by a macrophage-induced efflux mechanism. *Cell* 145, 39–53 (2011).
53. Lim, L. E. *et al.* Anthelmintic avermectins kill mycobacterium tuberculosis, including multidrug-resistant clinical strains. *Antimicrob. Agents Chemother.* 57, 1040–1046 (2013).
54. Maiga, M. *et al.* Successful shortening of tuberculosis treatment using adjuvant host-directed therapy with FDA-approved phosphodiesterase inhibitors in the mouse model. *PLoS One* 7, 1–8 (2012).
55. Rybniker, J. *et al.* Lansoprazole is an antituberculous prodrug targeting cytochrome bc 1. *Nat. Commun.* 6, 1–8 (2015).
56. Vashisht, R. & Brahmachari, S. K. Metformin as a potential combination therapy with existing front-line antibiotics for Tuberculosis. *J. Transl. Med.* 13, 1–3 (2015).
57. Farazi, A., Didgar, F. & Sarafraz, A. The effect of vitamin D on clinical outcomes in tuberculosis. *Egypt. J. Chest Dis. Tuberc.* 66, 419–423 (2017).
58. Eklund, D. *et al.* Vitamin D enhances IL-1β secretion and restricts growth of

Mycobacterium tuberculosis in macrophages from TB patients. *Int. J. Mycobacteriology* 2, 18–25 (2013).

59. Harishankar, M., Anbalagan, S. & Selvaraj, P. Effect of Vitamin D3on chemokine levels and regulatory T-cells in pulmonary tuberculosis. *Int. Immunopharmacol.* 34, 86–91 (2016).
60. Schön, T. *et al.* Arginine as an adjuvant to chemotherapy improves clinical outcome in active tuberculosis. *Eur. Respir. J.* 21, 483–488 (2003).
61. Farazi, A., Shafaat, O., Sofian, M. & Kahbazi, M. Arginine Adjunctive Therapy in Active Tuberculosis. *Tuberc. Res. Treat.* 2015, 1–5 (2015).
62. Costa, A. *et al.* The formulation of nanomedicines for treating tuberculosis. *Adv. Drug Deliv. Rev.* 102, 102–115 (2016).
63. Sosnik, A., Carcaboso, Á. M., Glisoni, R. J., Moretton, M. A. & Chiappetta, D. A. New old challenges in tuberculosis : Potentially effective nanotechnologies in drug delivery ☆. *Adv. Drug Deliv. Rev.* 62, 547–559 (2010).
64. Lennernäs, H. & Abrahamsson, B. The use of biopharmaceutic classification of drugs in drug discovery and development: current status and future extension. *J. Pharm. Pharmacol.* 57, 273–285 (2005).
65. Pham, D. D., Fattal, E. & Tsapis, N. Pulmonary drug delivery systems for tuberculosis treatment. *Int. J. Pharm.* 478, 517–529 (2015).
66. Harrison, A. P., Erlwanger, K. H., Elbrønd, V. S., Andersen, N. K. & Unmack, M. A. Gastrointestinal-tract models and techniques for use in safety pharmacology. *J. Pharmacol. Toxicol. Methods* 49, 187–199 (2004).
67. Bernkop-Schnürch, A. Nanocarrier systems for oral drug delivery: Do we really need them? *Eur. J. Pharm. Sci.* 49, 272–277 (2013).
68. Renukuntla, J., Vadlapudi, A. D., Patel, A., Boddu, S. H. S. & Mitra, A. K. Approaches for enhancing oral bioavailability of peptides and proteins. *Int. J. Pharm.* 447, 75–93 (2013).
69. Luciani-Giacobbe, L. C., Lorenzutti, A. M., Litterio, N. J., Ramírez-Rigo, M. V. & Olivera, M. E. Anti-tuberculosis site-specific oral delivery system that enhances rifampicin bioavailability in a fixed-dose combination with isoniazid. *Drug Deliv. Transl. Res.* 11, 894–908 (2021).
70. Avachat, A. M. & Bhise, S. B. Tailored release drug delivery system for Rifampicin and Isoniazid for enhanced bioavailability of Rifampicin. *Pharm. Dev. Technol.* 16, 127–136

(2011).

71. Genina, N., Boetker, J. P., Colombo, S., Harmankaya, N. & Rantanen, J. Anti-tuberculosis drug combination for controlled oral delivery using 3D printed compartmental dosage forms : From drug product design to in vivo testing. *J. Control. Release* 268, 40–48 (2017).
72. Silva, A. Segregated Delivery of Rifampicin and Isoniazid from Fixed Dose Combination Bilayer Tablets for the Treatment of Tuberculosis. *Br. J. Pharm. Res.* 4, 1781–1801 (2014).
73. Jahagirdar, P. S., Gupta, P. K., Kulkarni, S. P. & Devarajan, P. V. Intramacrophage Delivery of Dual Drug Loaded Nanoparticles for Effective Clearance of Mycobacterium tuberculosis. *J. Pharm. Sci.* 109, 2262–2270 (2020).
74. Öblom, H. *et al.* 3D-Printed Isoniazid Tablets for the Treatment and Prevention of Tuberculosis—Personalized Dosing and Drug Release. *AAPS PharmSciTech* 20, 1–13 (2019).
75. Pandit, S., Roy, S., Pillai, J. & Banerjee, S. Formulation and intracellular trafficking of lipid-drug conjugate nanoparticles containing a hydrophilic antitubercular drug for improved intracellular delivery to human macrophages. *ACS Omega* 5, 4433–4448 (2020).
76. Bhandari, R. & Kaur, I. P. Pharmacokinetics, tissue distribution and relative bioavailability of isoniazid-solid lipid nanoparticles. *Int. J. Pharm.* 441, 202–212 (2013).
77. Pandey, R., Zahoor, A., Sharma, S. & Khuller, G. K. Nanoparticle encapsulated antitubercular drugs as a potential oral drug delivery system against murine tuberculosis. *Tuberculosis* 83, 373–378 (2003).
78. Kajjari, P. B., Manjeshwar, L. S. & Aminabhavi, T. M. Novel pH- and temperature-responsive blend hydrogel microspheres of sodium alginate and PNIPAAm-g-GG for controlled release of isoniazid. *AAPS PharmSciTech* 13, 1147–1157 (2012).
79. Chen, T. *et al.* Lower cytotoxicity, high stability, and long-term antibacterial activity of a poly(methacrylic acid)/isoniazid/rifampin nanogel against multidrug-resistant intestinal Mycobacterium tuberculosis. *Mater. Sci. Eng. C* 58, 659–665 (2016).
80. Shetab Boushehri, M. A., Dietrich, D. & Lamprecht, A. Nanotechnology as a platform for the development of injectable parenteral formulations: A comprehensive review of the know-hows and state of the art. *Pharmaceutics* 12, 1–53 (2020).
81. Giri, T. K. *Solid lipid nanoparticles for the delivery of drug molecules* from *Materials for*

Biomedical Engineering (eds. Grumezescu, A. and Holban A.M.) (Elsevier Inc., 2019). doi:10.1016/b978-0-12-818433-2.00016-9.

82. Wissing, S. A., Kayser, O. & Müller, R. H. Solid lipid nanoparticles for parenteral drug delivery. *Adv. Drug Deliv. Rev.* 56, 1257–1272 (2004).
83. Joshi, M. D. & Müller, R. H. Lipid nanoparticles for parenteral delivery of actives. *Eur. J. Pharm. Biopharm.* 71, 161–172 (2009).
84. Tyagi, P. & Subramony, J. A. Nanotherapeutics in oral and parenteral drug delivery: Key learnings and future outlooks as we think small. *J. Control. Release* 272, 159–168 (2018).
85. Chachlioutaki, K. *et al.* Electrospun orodispersible films of isoniazid for pediatric tuberculosis treatment. *Pharmaceutics* 12, 1–14 (2020).
86. El-Ridy, M. S. *et al.* Niosomal encapsulation of ethambutol hydrochloride for increasing its efficacy and safety. *Drug Deliv.* 22, 21–36 (2015).
87. El-Ridy, M. S., Mostafa, D. M., Shehab, A., Nasr, E. A. & Abd El-Alim, S. Biological evaluation of pyrazinamide liposomes for treatment of Mycobacterium tuberculosis. *Int. J. Pharm.* 330, 82–88 (2007).
88. Zhu, B. & Xu, Y. Chitosan microspheres enhance the immunogenicity of an Ag85B-based fusion protein containing multiple T-cell epitopes of Mycobacterium tuberculosis. *Eur. J. Pharm. Biopharm.* 66, 318–326 (2007).
89. Trousil, J. *et al.* Antitubercular nanocarrier monotherapy: Study of In Vivo efficacy and pharmacokinetics for rifampicin. *J. Control. Release* 321, 312–323 (2020).
90. Adeleke, O. A., Tsai, P. C., Karry, K. M., Monama, N. O. & Michniak-Kohn, B. B. Isoniazid-loaded orodispersible strips: Methodical design, optimization and in vitro-in silico characterization. *Int. J. Pharm.* 547, 347–359 (2018).
91. Anjani, Q. K. *et al.* Versatility of hydrogel-forming microneedles in in vitro transdermal delivery of tuberculosis drugs. *Eur. J. Pharm. Biopharm.* 158, 294–312 (2021).
92. Rossi, I. *et al.* Sodium hyaluronate nanocomposite respirable microparticles to tackle antibiotic resistance with potential application in treatment of mycobacterial pulmonary infections. *Pharmaceutics* 11, 1–23 (2019).
93. Mitchison, D. A. & Fourie, P. B. The near future : Improving the activity of rifamycins and pyrazinamide. *Tuberculosis* 90, 177–181 (2010).
94. Yıldız-Peköz, A. & Ehrhardt, C. Advances in pulmonary drug delivery. *Pharmaceutics*

12, 1–7 (2020).

95. de Castro, A. M. *et al.* Role of water on deep eutectic solvents (DES) properties and gas transport performance in biocatalytic supported DES membranes. *Sep. Purif. Technol.* 255, (2021).

96. Gaspar, D. P. *et al.* Rifabutin-loaded solid lipid nanoparticles for inhaled antitubercular therapy : Physicochemical and in vitro studies. *Int. J. Pharm.* 497, 199–209 (2016).

97. Eedara, B. B. *et al.* Development and characterization of high payload combination dry powders of anti-tubercular drugs for treating pulmonary tuberculosis. *Eur. J. Pharm. Sci.* 118, 216–226 (2018).

98. Pinheiro, M., Ribeiro, R., Vieira, A., Andrade, F. & Reis, S. Design of a nanostructured lipid carrier intended to improve the treatment of tuberculosis. *Drug Des. Devel. Ther.* 10, 2467–2475 (2016).

99. Vieira, A. C. C. *et al.* Mannosylated solid lipid nanoparticles for the selective delivery of rifampicin to macrophages. *Artif. Cells, Nanomedicine Biotechnol.* 46, 653–663 (2018).

100. Vieira, A. C. C. *et al.* Mucoadhesive chitosan-coated solid lipid nanoparticles for better management of tuberculosis. *Int. J. Pharm.* 536, 478–485 (2018).

101. Grenha, A. *et al.* Inhalable locust bean gum microparticles co-associating isoniazid and rifabutin : therapeutic assessment in a murine model of tuberculosis. *Eur. J. Pharm. Biopharm.* 147, 38-44 (2019).

102. Connor, G. O. *et al.* Inhalable poly (lactic- co -glycolic acid) (PLGA) microparticles encapsulating all-trans-Retinoic acid (ATRA) as a host-directed , adjunctive treatment for Mycobacterium tuberculosis infection. *Eur. J. Pharm. Biopharm.* 134, 153–165 (2019).

103. Ahmad, M. I., Nakpheng, T. & Srichana, T. The safety of ethambutol dihydrochloride dry powder formulations containing chitosan for the possibility of treating lung tuberculosis. *Inhal. Toxicol.* 26, 908–917 (2014).

104. Sharma, A. *et al.* Targeted pulmonary delivery of Epigallocatechin gallate (EGCG), a green tea polyphenol controls the growth of Mycobacterium tuberculosis by enhancing the autophagy and suppressing bacterial burden. *ACS Biomater. Sci. Eng.* 6, 4126–4140 (2020).

105. Truzzi, E. *et al.* In vivo biodistribution of respirable solid lipid nanoparticles surface-decorated with a mannose-based surfactant: A promising tool for pulmonary

tuberculosis treatment? *Nanomaterials* 10, 1–15 (2020).

106. Rodrigues, S. *et al.* Carrageenan from red algae: an application in the development of inhalable tuberculosis therapy targeting the macrophages. *Drug Deliv. Transl. Res.* 10, 1675–1687 (2020).
107. Nabi, B., Rehman, S., Aggarwal, S., Baboota, S. & Ali, J. Nano-based anti-tubercular drug delivery: an emerging paradigm for improved therapeutic intervention. *Drug Deliv. Transl. Res.* 10, 1111–1121 (2020).
108. Gaspar, M. *et al.* Developments on Drug Delivery Systems for the Treatment of Mycobacterial Infections. *Curr. Top. Med. Chem.* 8, 579–591 (2008).
109. Bento, C. M., Gomes, M. S. & Silva, T. Looking beyond typical treatments for atypical mycobacteria. *Antibiotics* 9, 1–25 (2020).
110. Warner, J. C., Cannon, A. S. & Dye, K. M. Green chemistry. *Environ. Impact Assess. Rev.* 24, 775–799 (2004).
111. Anastas, P. T. & Warner, J. C. *Green Chemistry Everyone's Doing It ! A New Kind of Chemistry*. *Green Chemistry: Theory and Practice* (1998).
112. Dunn, P. J. The importance of Green Chemistry in Process Research and Development. *Chem. Soc. Rev.* 41, 1452–1461 (2012).
113. Jessop, P. G. Green / Alternative Solvents. *Encyclopedia of Sustainable Technologies*. 3, 611–619 (2017).
114. Martín-Aranda, R. M. & López-Sanz, J. Green solvents for pharmaceutical industry from *Green Solvents I: Properties and Applications in Chemistry* (eds. Mohammad, A. & Inamuddin) 147–173 (Springer Science & Business Media Dordrecht, 2012). doi:10.1007/978-94-007-1712-1.
115. Byrne, F. P. *et al.* Tools and techniques for solvent selection: green solvent selection guides. *Sustain. Chem. Process.* 4, 1–24 (2016).
116. Zhou, F., Hearne, Z. & Li, C. J. Water—the greenest solvent overall. *Curr. Opin. Green Sustain. Chem.* 18, 118–123 (2019).
117. Bubalo, M. C., Vidovi, S., Redovnikovic, I. R. & Jokic, S. Green solvents for green technologies. *J. Chem. Technol. Biotechnol.* 90, 1631–1639 (2015).
118. Santos, F. & Duarte, A. R. C. Therapeutic Deep Eutectic Systems for the Enhancement of Drug Bioavailability from *Deep eutectic solvents for medicine, gas solubilization and extraction of natural substances* (eds. S., F., Costa Gomes, M. & Lichtfouse, E.) 103–129 (Springer, 2021). doi:10.1007/978-3-030-53069-3_3.

119. Frizzo, C. P. *et al.* Pharmaceutical Salts : Solids to Liquids by Using Ionic Liquid Design from *Ionic Liquids - New Aspects for the Future* (eds. Kadokawa J.) 557–578 (2013). doi: 10.5772/51655.
120. Brennecke, J. F. & Maginn, E. J. Ionic liquids: innovative fluids for chemical processing. *AIChE J.* 47, 2384–2389 (2001).
121. Wilkes, J. S. A short history of ionic liquids - from molten salts to neoteric solvents. *Green Chem.* 4, 73–80 (2002).
122. Ruß, C. & König, B. Low melting mixtures in organic synthesis - An alternative to ionic liquids? *Green Chem.* 14, 2969–2982 (2012).
123. Vanda, H., Dai, Y., Wilson, E. G., Verpoorte, R. & Choi, Y. H. Green solvents from ionic liquids and deep eutectic solvents to natural deep eutectic solvents. *Comptes Rendus Chim.* 21, 628–638 (2018).
124. Wilkes, J. S., Levisky, J. A., Wilson, R. A. & Hussey, C. L. Dialkylimidazolium chloroaluminate melts: a new class of room-temperature ionic liquids for electrochemistry, spectroscopy and synthesis. *Inorg. Chem.* 21, 1263–1264 (1982).
125. Frade, R. F. M. Ionic Liquids in Green Chemistry-Prediction of Ionic Liquids Toxicity Using Different Models from *Green Chemistry for Environmental Remediation* (eds. R., S. & V., S.) 343–355 (Scrivener Publishing LLC, 2011). doi:10.1002/9781118287705.ch11.
126. Kohno, Y. & Ohno, H. Ionic liquid/water mixtures: From hostility to conciliation. *Chem. Commun.* 48, 7119–7130 (2012).
127. Pena-Pereira, F. & Namieśnik, J. Ionic liquids and deep eutectic mixtures: sustainable solvents for extraction processes. *ChemSusChem* 7, 1784–1800 (2014).
128. Domínguez de María, P. & Maugeri, Z. Ionic liquids in biotransformations : from proof-of-concept to emerging deep-eutectic-solvents. *Curr. Opin. Chem. Biol.* 15, 220–225 (2011).
129. Hough, W. L. *et al.* The third evolution of ionic liquids: Active pharmaceutical ingredients. *New J. Chem.* 31, 1429–1436 (2007).
130. Ferraz, R., Branco, L. C., Prudêncio, C., Noronha, J. P. & Petrovski, Ž. Ionic Liquids as Active Pharmaceutical Ingredients. *ChemM* 6, 975–985 (2011).
131. Kudlak, B., Owczarek, K. & Namiesnik, J. Selected issues related to the toxicity of ionic liquids and deep eutectic solvents — a review. *Environ. Sci. Pollut. Res.* 22, 11975–11992 (2015).
132. Dias, A. R., Costa-Rodrigues, J., Fernandes, M. H., Ferraz, R. & Prudêncio, C. The

anticancer potential of ionic liquids. *ChemMedChem* 12, 11–18 (2017).

133. Philippi, F., Pugh, D., Rauber, D., Welton, T. & Hunt, P. A. Conformational design concepts for anions in ionic liquids. *Chem. Sci.* 11, 6405–6422 (2020).
134. Welton, T. Ionic liquids: a brief history. *Biophys. Rev.* 10, 691–706 (2018).
135. Fumino, K. & Ludwig, R. Analyzing the interaction energies between cation and anion in ionic liquids: The subtle balance between Coulomb forces and hydrogen bonding. *J. Mol. Liq.* 192, 94–102 (2014).
136. Matthews, R. P. *et al.* A structural investigation of ionic liquid mixtures. *Phys. Chem. Chem. Phys.* 18, 8608–8624 (2016).
137. Clark, K. D., Emaus, M. N., Varona, M., Bowers, A. N. & Anderson, J. L. Ionic liquids: solvents and sorbents in sample preparation. *J. Sep. Sci.* 41, 209–235 (2018).
138. Balk, A., Holzgrabe, U. & Meinel, L. Pro et contra' ionic liquid drugs - Challenges and opportunities for pharmaceutical translation. *Eur. J. Pharm. Biopharm.* 94, 291–304 (2015).
139. Cherukuvada, S., Kaur, R. & Row, T. N. G. Co-crystallization and small molecule crystal form diversity: from pharmaceutical to materials applications. *Cryst. Eng. Comm.* 19, 8528–8555 (2016).
140. Bhatt, J. D., Patel, T. S., Chudasama, C. J. & Patel, K. D. Microwave-Assisted Synthesis of Novel Pyrazole Clubbed Polyhydroquinolines in an Ionic-Liquid and their Biological Perspective. *Chemistry Select* 3, 3632–3640 (2018).
141. Bhat, M. A., Al-Omar, M. A., Naglah, A. M. & Ali Khan, A. [Et3NH][HSO4]-mediated efficient synthesis of novel xanthene derivatives and their biological evaluation. *J. Saudi Chem. Soc.* 24, 425–433 (2020).
142. Faria, R. A. & Bogel-Łukasik, E. Solubilities of pharmaceutical and bioactive compounds in trihexyl (tetradecyl) phosphonium chloride ionic liquid. *Fluid Phase Equilib.* 397, 18–25 (2015).
143. Cherukuvada, S. & Nangia, A. Polymorphism in an API ionic liquid : ethambutol dibenzoate trimorphs. *Cryst. Eng. Comm.* 10–13 (2012).
144. Cherukuvada, S. & Nangia, A. Salts and ionic liquid of the antituberculosis drug S,S-ethambutol. *Cryst. Growth Des.* 13, 1752–1760 (2013).
145. Diniz, L. F., Carvalho, P. S., Melo, C. C. De, Ellena, J. & Sa, U. De. Reducing the Hygroscopicity of the Anti-Tuberculosis Drug (S, S) - Ethambutol Using Multicomponent Crystal Forms. *Cryst. Growth Des*. 17, 2622-2630 (2017).

146. Divya, M. B. & Guruprasad, L. Activity and thermal stability of Mycobacterium tuberculosis PE1 and PE2 proteins esterase domain in the presence of aprotic ionic liquids. *Spectrochim. Acta - Part A Mol. Biomol. Spectrosc.* 225, 117477 (2020).
147. Guthrie, F. On Eutexia. *Proc. Phys. Scoiety London* 6, 462–482 (1884).
148. Francisco, M., Van Den Bruinhorst, A. & Kroon, M. C. Low-transition-temperature mixtures (LTTMs): A new generation of designer solvents. *Angew. Chemie - Int. Ed.* 52, 3074–3085 (2013).
149. Abbott, A. P., Capper, G., Davies, D. L., Rasheed, R. K. & Tambyrajah, V. Novel solvent properties of choline chloride/urea mixtures. *Chem. Commun.* 70–71 (2003).
150. Abbott, A. P., Boothby, D., Capper, G., Davies, D. L. & Rasheed, R. Deep Eutectic Solvents Formed Between Choline Chloride and Carboxylic Acids. *J. Am. Chem. Soc* 126, 9142 (2004).
151. Abbott, A. P., Capper, G. & Gray, S. Design of improved deep eutectic solvents using hole theory. *ChemPhysChem* 7, 803–806 (2006).
152. Abbott, A. P., Ahmed, E. I., Prasad, K., Qader, I. B. & Ryder, K. S. Liquid pharmaceuticals formulation by eutectic formation. *Fluid Phase Equilib.* 448, 2–8 (2017).
153. Aroso, I. M. *et al.* Dissolution enhancement of active pharmaceutical ingredients by therapeutic deep eutectic systems. *Eur. J. Pharm. Biopharm.* 98, 57–66 (2016).
154. Dai, Y., van Spronsen, J., Witkamp, G., Verpoorte, R. & Choi, Y. H. Natural deep eutectic solvents as new potential media for green technology. *Anal. Chim. Acta* 766, 61–68 (2013).
155. Pedro, S. N., Freire, M. G., Freire, C. S. R. & Silvestre, A. J. D. Deep eutectic solvents comprising active pharmaceutical ingredients in the development of drug delivery systems. *Expert Opinion on Drug Delivery* 16, 497–506 (2019).
156. Santana, A. P. R. *et al.* Sustainable synthesis of natural deep eutectic solvents (NADES) by different methods. *J. Mol. Liq.* 293, 111452 (2019).
157. Barros, A. A. *et al.* Green solvents for enhanced impregnation processes in biomedicine. *Curr. Opin. Green Sustain. Chem.* 5, 82–87 (2017).
158. Hansen, B. B. *et al.* Deep Eutectic Solvents: A Review of Fundamentals and Applications. *Chem. Rev.* (2021).
159. Álvarez, M. S. & Zhang, Y. Sketching neoteric solvents for boosting drugs bioavailability. *J. Control. Release* 311–312, 225–232 (2019).
160. Choi, Y. H. *et al.* Are natural deep eutectic solvents the missing link in understanding

cellular metabolism and physiology? *Plant Physiol.* 156, 1701–1705 (2011).

161. Liu, Y. *et al.* Natural deep eutectic solvents: Properties, applications, and perspectives. *J. Nat. Prod.* 81, 679–690 (2018).
162. Stott, P. W., Williams, A. C. & Barry, B. W. Transdermal delivery from eutectic systems: enhanced permeation of a model drug, ibuprofen. *J. Control. Release* 50, 297–308 (1998).
163. Aroso, I. M. *et al.* Design of controlled release systems for THEDES — Therapeutic deep eutectic solvents , using supercritical fl uid technology. *Int. J. Pharm.* 492, 73–79 (2015).
164. Zakrewsky, M. *et al.* Choline and Geranate Deep Eutectic Solvent as a Broad-Spectrum Antiseptic Agent for Preventive and Therapeutic Applications. *Adv. Healthc. Mater.* 5, 1282–1289 (2016).
165. Zainal-Abidin, M. H., Hayyan, M., Ngoh, G. C., Wong, W. F. & Looi, C. Y. Emerging frontiers of deep eutectic solvents in drug discovery and drug delivery systems. *J. Control. Release* 316, 168–195 (2019).
166. Cherukuvada, S. & Nangia, A. Eutectics as improved pharmaceutical materials : design , properties and characterization. *Chem. Commun.* 50, 906–923 (2014).
167. Rajbongshi, T. *et al.* Preparation of pyrazinamide eutectics vs. cocrystals based on supramolecular synthon variations. *Cryst. Growth Des.* 18, 6640–6651 (2018).
168. Yiin, C. L. *et al.* Characterization of natural low transition temperature mixtures (LTTMs): Green solvents for biomass delignification. *Bioresour. Technol.* 199, 258–264 (2016).
169. Perna, F. M., Vitale, P. & Capriati, V. Deep eutectic solvents and their applications as green solvents. *Curr. Opin. Green Sustain. Chem.* 21, 27–33 (2020).
170. Durand, E., Lecomte, J. & Villeneuve, P. From green chemistry to nature: The versatile role of low transition temperature mixtures. *Biochimie* 120, 119–123 (2016).
171. Pasquali, I. & Bettini, R. Are pharmaceutics really going supercritical? *Int. J. Pharm.* 364, 176–187 (2008).
172. Knez, Ž., Hrnčič, M. K. & Skerget, M. Particle Formation and Product Formulation Using Supercritical Fluids. *Annu. Rev. Chem. Biomol. Eng.* 6, 379–407 (2015).
173. Badens, E., Masmoudi, Y., Mouahid, A. & Crampon, C. The Journal of Supercritical Fluids Current situation and perspectives in drug formulation by using supercritical fl uid technology. *J. Supercrit. Fluids* 134, 274–283 (2018).

174. Fages, J., Lochard, H., Letourneau, J. J., Sauceau, M. & Rodier, E. Particle generation for pharmaceutical applications using supercritical fluid technology. *Powder Technol.* 141, 219–226 (2004).
175. Kankala, R. K., Zhang, Y. S., Wang, S. Bin, Lee, C. H. & Chen, A. Z. Supercritical Fluid Technology: An Emphasis on Drug Delivery and Related Biomedical Applications. *Adv. Healthc. Mater.* 6, (2017).
176. Chakravarty, P., Famili, A., Nagapudi, K. & Al-Sayah, M. A. *Using supercritical fluid technology as a green alternative during the preparation of drug delivery systems*. *Pharmaceutics* 11, (2019).
177. Reverchon, E., Adami, R., Cardea, S. & Porta, G. Della. Supercritical fluids processing of polymers for pharmaceutical and medical applications. *J. Supercrit. Fluids* 47, 484–492 (2009).
178. Duarte, A. R. C., Mano, J. F. & Reis, R. L. Supercritical fluids in biomedical and tissue engineering applications : a review. *Int. Mater. Rev.* 54, 214–222 (2009).
179. Lovskaya, D. D., Lebedev, A. E. & Menshutina, N. V. Aerogels as drug delivery systems : In vitro and in vivo evaluations. *J. Supercrit. Fluids* 106, 115–121 (2015).
180. Patomchaiviwat, V., Paeratakul, O. & Kulvanich, P. Formation of inhalable rifampicin-poly(l-lactide) microparticles by supercritical anti-solvent process. *AAPS PharmSciTech* 9, 1119–1129 (2008).
181. Reverchon, E., De Marco, I. & Porta, G. D. Rifampicin microparticles production by supercritical antisolvent precipitation antisolvent precipitation. *Int. J. Pharm.* 243, 83–91 (2002).
182. Reverchon, E. & Della Porta, G. Micronization of antibiotics by supercritical assisted atomization. *J. Supercrit. Fluids* 26, 243–252 (2003).
183. Roda, A., Santos, F., Matias, A. A., Paiva, A. & Duarte, A. R. C. Design and processing of drug delivery formulations of therapeutic deep eutectic systems for tuberculosis. *J. Supercrit. Fluids* 161, 104826 (2020).
184. Roda, A. *et al.* Unravelling the nature of citric acid : L -arginine : water mixtures : the bifunctional role of water. *Phys. Chem. Chem. Phys.* 23, 1706–1717 (2021).
185. Duarte, A. R. C. *et al.* A comparison between pure active pharmaceutical ingredients and therapeutic deep eutectic solvents: Solubility and permeability studies. *Eur. J. Pharm. Biopharm.* 114, 296–304 (2017).
186. Lack, E. *et al.* Particle generation with supercritical CO2. in (Natex, 2005).

187. Reverchon, E. Supercritical antisolvent precipitation of micro- and nano-particles. *J. Supercrit. Fluids* 15, 1–21 (1999).
188. Reverchon, E., Marco, I. De & Torino, E. Nanoparticles production by supercritical antisolvent precipitation : A general interpretation. *J. Supercrit. Fluids* 43, 126–138 (2007).
189. Reverchon, E. Supercritical-Assisted Atomization To Produce Micro- and / or Nanoparticles of Controlled Size and Distribution. 2405–2411 (2002).
190. Marco, I. De & Franco, P. Effect of the Carrier on the Coprecipitation of Curcumin through Supercritical-Assisted Atomization. *Chem. Engineering* 5,59 (2021).
191. Krstić, M., Popović, M., Dobričić, V. & Ibrić, S. Influence of Solid Drug Delivery System Formulation on Poorly Water-Soluble Drug Dissolution and Permeability. *Molecules* 20, 14684–14698 (2015).
192. Silva, J. M. *et al.* Tailored freestanding multilayered membranes based on chitosan and alginate. *Biomacromolecules* 15, 3817–3826 (2014).
193. ISO/EN10993-11. Biological evaluation of medical devices - Part 11: Tests for systemic toxicity. *International Organization for Standardization* 1–26 (2009).
194. Bradford, M. M. A rapid and sensitive method for the quantitation of microgram quantities of protein utilizing the principle of protein-dye binding. *Anal. Biochem.* 72, 248–254 (1976).
195. Keen, J. H., Habig, W. H. & Jakoby, W. B. Mechanism for the several activities of the glutathione S-transferases. *J. Biol. Chem.* 251, 6183–6188 (1976).
196. Johansson, L. H. & Håkan Borg, L. A. A spectrophotometric method for determination of catalase activity in small tissue samples. *Anal. Biochem.* 174, 331–336 (1988).
197. Sun, Y., Oberley, L. W. & Li, Y. A simple method for clinical assay of superoxide dismutase. *Clin. Chem.* 34, 497–500 (1988).
198. Uchiyama, M. & Mihara, M. Determination of malonaldehyde precursor in tissues by thiobarbituric acid test. *Anal. Biochem.* 86, 271–278 (1978).
199. Madeira, D., Costa, P. M., Vinagre, C. & Diniz, M. S. When warming hits harder: survival, cellular stress and thermal limits of Sparus aurata larvae under global change. *Mar. Biol.* 163, 1–14 (2016).
200. Sekhon, B. S. Ionic liquids : Pharmaceutical and Biotechnological Applications. *Asian J. Pharm. Biol. Res.* 395–411 (2011).
201. Hough, W. L. & Rogers, R. D. Ionic liquids then and now: From solvents to materials

to active pharmaceutical ingredients. *Bull Chem Soc Jpn* 80, 2262–2269 (2007).

202. Marrucho, I. M., Branco, L. C. & Rebelo, L. P. N. Ionic Liquids in Pharmaceutical Applications. *Annu. Rev. Chem. Biomol. Eng.* 5, 527–546 (2014).
203. Berton, P. *et al.* Transdermal Bioavailability in Rats of Lidocaine in the Forms of Ionic Liquids, Salts, and Deep Eutectic. *ACS Medicnal Chemistry Letters* 6–11 (2017).
204. Florindo, C. *et al.* Evaluation of solubility and partition properties of ampicillin-based ionic liquids. *Int. J. Pharm.* 456, 553–559 (2013).
205. Ferraz, R. *et al.* Antitumor Activity of Ionic Liquids Based on Ampicillin. *ChemMedChem* 10, 1480–1483 (2015).
206. Ferraz, R. *et al.* Development of novel ionic liquids based on ampicillin. *Medchemcomm* 3, 494–497 (2012).
207. Teixeira, S. *et al.* A Novel Approach for Bisphosphonates: Ionic Liquids and Organic Salts from Zoledronic Acid. *ChemMedChem* 14, 1767–1770 (2019).
208. Santos, M. M. *et al.* Ionic Liquids and Salts from Ibuprofen as Promising Innovative Formulations of an Old Drug. *ChemMedChem* 14, 907–911 (2019).
209. Teixeira, S., Santos, M. M., Fernandes, M. H., Costa-Rodrigues, J. & Branco, L. C. Alendronic Acid as Ionic Liquid: New Perspective on Osteosarcoma. *Pharmaceutics* 12, 293 (2020).
210. Wallis, R. S. *et al.* Tuberculosis-advances in development of new drugs, treatment regimens, host-directed therapies, and biomarkers. *Lancet Infect. Dis.* 16, e34–e46 (2016).
211. Machado, D., Lecorche, E., Mougari, F. & Cambau, E. Efflux Pumps and Their Implications in Drug Resistance and Virulence. *Frontiers in Microbiology* 9, 1–10 (2018).
212. Machado, D. *et al.* Contribution of efflux to the emergence of isoniazid and multidrug resistance in Mycobacterium tuberculosis. *PLoS One* 7, (2012).
213. Martins, F. *et al.* Design, synthesis and biological evaluation of novel isoniazid derivatives with potent antitubercular activity. *Eur. J. Med. Chem.* 81, 119–138 (2014).
214. Martins, F., Ventura, C., Santos, S. & Viveiros, M. QSAR Based Design of New Antitubercular Compounds: Improved Isoniazid Derivatives Against Multidrug-Resistant TB. *Curr. Pharm. Des.* 20, 4427–4454 (2013).
215. Sousa, E. H. S. *et al.* Isoniazid metal complex reactivity and insights for a novel anti-tuberculosis drug design. *J. Biol. Inorg. Chem.* 17, 275–283 (2012).
216. Battini, S., Mannava, M. K. C. & Nangia, A. Improved Stability of Tuberculosis Drug

Fixed-Dose Combination Using Isoniazid-Caffeic Acid and Vanillic Acid Cocrystal. *J. Pharm. Sci.* 107, 1667–1679 (2018).

217. Swapna, B., Maddileti, D. & Nangia, A. Cocrystals of the tuberculosis drug isoniazid: Polymorphism, isostructurality, and stability. *Cryst. Growth Des.* 14, 5991–6005 (2014).
218. Diniz, L. F. *et al.* Novel Isoniazid cocrystals with aromatic carboxylic acids: Crystal engineering, spectroscopy and thermochemical investigations. *J. Mol. Struct.* 1153, 58–68 (2018).
219. Forte, A., Melo, C. I., Bogel-łukasik, R. & Bogel-łukasik, E. A favourable solubility of isoniazid, an antitubercular antibiotic drug, in alternative solvents. *Fluid Phase Equilib.* 318, 89–95 (2012).
220. Aitipamula, S., Wong, A. B. H., Chow, P. S. & Tan, R. B. H. Novel solid forms of the anti-tuberculosis drug, Isoniazid: Ternary and polymorphic cocrystals. *CrystEngComm* 15, 5877–5887 (2013).
221. Frade, R. F. M. *et al.* Toxicological Evaluation of Ionic Liquids Effect of Ionic Liquids on Human Colon Carcinoma HT-29 and CaCo-2 Cell Lines from *Ionic Liquid Applications: Pharmaceuticals, Therapeutics, and Biotechnology* (eds. Malhotra S.) (2010). doi: 10.1021/bk-2010-1038.ch011.
222. Frade, R. F. M., Matias, A., Branco, L. C., Afonso, A. M. & Duarte, C. M. M. Effect of ionic liquids on human colon carcinoma HT-29 and CaCo-2 cell lines. *Green Chem.* 9, 873-877 (2007).
223. Sarcevica, I., Orola, L., Veidis, M. V., Podjava, A. & Belyakov, S. Crystal and Molecular Structure and Stability of Isoniazid Cocrystals with Selected Carboxylic Acids. *Cryst. Growth Des.* 13, 1082–1090 (2013).
224. Zhang, K. *et al.* Discovery of new polymorphs of the tuberculosis drug isoniazid. *CrystEngComm* 22, 2705–2708 (2020).
225. Savjani, K. T., Gajjar, A. K. & Savjani, J. K. Drug Solubility: Importance and Enhancement Techniques. *ISRN Pharm.* 2012, 1–10 (2012).
226. Shastri, M. D. *et al.* Role of Oxidative Stress in the Pathology and Management of Human Tuberculosis. *Oxid. Med. Cell. Longev.* 2018, 1–10 (2018).
227. Manke, A., Wang, L. & Rojanasakul, Y. Mechanisms of Nanoparticle-Induced Oxidative Stress and Toxicity. *Biomed Res. Int.* 2013, 1–15 (2013).
228. Matos, B. *et al.* Toxicity Evaluation of Quantum Dots (ZnS and CdS) Singly and Combined in Zebrafish (Danio rerio). *Int. J. Environ. Res. Public Health* 17, 232 (2019).

229. Gagnon, M. M. & Hodson, P. V. Field studies using fish biomarkers – How many fish are enough? *Mar. Pollut. Bull.* 64, 2871–2876 (2012).
230. Valavanidis, A., Vlahogianni, T., Dassenakis, M. & Scoullos, M. Molecular biomarkers of oxidative stress in aquatic organisms in relation to toxic environmental pollutants. *Ecotoxicol. Environ. Saf.* 64, 178–189 (2006).
231. Farah, S. I., Abdelrahman, A. A., North, E. J. & Chauhan, H. Opportunities and challenges for natural products as novel antituberculosis agents. *Assay Drug Dev. Technol.* 14, 29–38 (2016).
232. Xiang, C. & Barron, A. R. The Analysis of Liquid Crystal Phases using Polarized Optical Microscopy. *Phys. Methods Chem. Nanosci.* 2–10 (2011).
233. Charisiadis, P. *et al.* 1H-NMR as a structural and analytical tool of intra- and intermolecular hydrogen bonds of phenol-containing natural products and model compounds. *Molecules* 19, 13643–13682 (2014).
234. Morrison, H. G., Sun, C. C. & Neervannan, S. Characterization of thermal behavior of deep eutectic solvents and their potential as drug solubilization vehicles. *Int. J. Pharm.* 378, 136–139 (2009).
235. Craveiro, R. *et al.* Properties and thermal behavior of natural deep eutectic solvents. *J. Mol. Liq.* 215, 534–540 (2016).
236. Lavor, E. P., Freire, F. D., Aragão, C. F. S., Raffin, F. N. & Moura, T. F. A. L. Application of thermal analysis to the study of anti-tuberculosis drug compatibility . Part 1. *Jounal Therm. Anal. Calorim.* 108, 207–212 (2012).
237. Roda, A., Paiva, A. & Duarte, A. R. C. Therapeutic liquid formulations based on low transition temperature mixtures for the incorporation of anti-inflammatory drugs. *Pharmaceutics* 13, 1–16 (2021).
238. Silva, J. M. M., Reis, R. L., Paiva, A. & Duarte, A. R. C. Design of functional therapeutic deep eutectic solvents based on Choline Chloride and Ascorbic Acid. *ACS Sustain. Chem. Eng.* 6, 10355–10363 (2018).
239. Tajmir, F. & Roosta, A. Solubility of cefixime in aqueous mixtures of deep eutectic solvents from experimental study and modeling. *J. Mol. Liq.* 303, 112636 (2020).
240. Li, Z. & Lee, P. I. Investigation on drug solubility enhancement using deep eutectic solvents and their derivatives. *Int. J. Pharm.* 505, 283–288 (2016).
241. Motiei, M., Gouveia, L. P. De, Khalili, R. & Fei, H. Nanoparticle-Based Rifampicin Delivery System Development. 1–19 (2021).

242. Ermondi, G. *et al.* Rifampicin as an example of beyond-rule-of-5 compound : ionization beyond water and lipophilicity beyond octanol/water. *Eur. J. Pharm. Sci.* 161, 105802 (2021).
243. Nelson, D. L. & Cox, M. M. *Lehninger Principles of Biochemistry*. (2017).
244. El Achkar, T., Fourmentin, S. & Greige-Gerges, H. Deep eutectic solvents: An overview on their interactions with water and biochemical compounds. *J. Mol. Liq.* 288, (2019).
245. Dai, Y., Witkamp, G. J., Verpoorte, R. & Choi, Y. H. Tailoring properties of natural deep eutectic solvents with water to facilitate their applications. *Food Chem.* 187, 14–19 (2015).
246. Hammond, O. S., Bowron, D. T. & Edler, K. J. The Effect of Water upon Deep Eutectic Solvent Nanostructure: An Unusual Transition from Ionic Mixture to Aqueous Solution. *Angew. Chemie - Int. Ed.* 56, 9782–9785 (2017).
247. Passos, H., Tavares, D. J. P., Ferreira, A. M., Freire, M. G. & Coutinho, J. A. P. Are Aqueous Biphasic Systems Composed of Deep Eutectic Solvents Ternary or Quaternary Systems? *ACS Sustain. Chem. Eng.* 4, 2881–2886 (2016).
248. Baz, J., Held, C., Pleiss, J. & Hansen, N. Thermophysical properties of glyceline – water mixtures investigated by molecular modelling. *Phys. Chem. Chem. Phys.* 21, 6467-6476 (2019).
249. López-Salas, N. *et al.* Looking at the 'water-in-Deep-Eutectic-Solvent' System: A Dilution Range for High Performance Eutectics. *ACS Sustain. Chem. Eng.* 7, 17565–17573 (2019).
250. Sapir, L. & Harries, D. Restructuring a Deep Eutectic Solvent by Water: The Nanostructure of Hydrated Choline Chloride/Urea. *J. Chem. Theory Comput.* 16, 3335–3342 (2020).
251. Degam, G. Deep Eutectic Solvents Synthesis, Characterization and Applications in Pretreatment of Lignocellulosic Biomass. Doctoral thesis from South Dakota State University (2017).
252. Pontes, P. V. A. *et al.* Measurement and PC-SAFT modeling of solid-liquid equilibrium of deep eutectic solvents of quaternary ammonium chlorides and carboxylic acids. *Fluid Phase Equilib.* 448, 69-80 (2017).
253. Crespo, E. A. *et al.* Characterization and Modeling of the Liquid Phase of Deep Eutectic Solvents Based on Fatty Acids/Alcohols and Choline Chloride. *Ind. Eng. Chem.*

Res. 56, 12192–12202 (2017).

254. Crespo, E. A. *et al.* The Role of Polyfunctionality in the Formation of [Ch]Cl-Carboxylic Acid-Based Deep Eutectic Solvents. *Ind. Eng. Chem. Res.* 57, 11195–11209 (2018).
255. Martins, M. A. . *et al.* Tunable hydrophobic eutectic solvents based on terpenes and monocarboxylic acids. *ACS Sustain. Chem. Eng.* 6, 8836–8846 (2018).
256. Alkhatib, I. I. I., Bahamon, D., Llovell, F., Abu-Zahra, M. R. M. & Vega, L. F. Perspectives and guidelines on thermodynamic modelling of deep eutectic solvents. *J. Mol. Liq.* 298, 112183 (2020).
257. Held, C., Reschke, T., Mohammad, S., Luza, A. & Sadowski, G. ePC-SAFT revised. *Chem. Eng. Res. Des.* 92, 2884–2897 (2014).
258. Santos, F., Leitão, M. I. P. S. & Duarte, A. R. C. Properties of therapeutic deep eutectic solvents of L-arginine and ethambutol for tuberculosis treatment. *Molecules* 24, (2019).
259. *CRC Handbook of Chemistry and Physics*. Eds. Lide D.R. (CRC Press LLC, 2005).
260. Weiss, I. M., Muth, C., Drumm, R. & Kirchner, H. O. K. Thermal decomposition of the amino acids glycine, cysteine, aspartic acid, asparagine, glutamic acid, glutamine, arginine and histidine. *BMC Biophysics* 1–15 (2018).
261. Meng, X., Ballerat-Busserolles, K., Husson, P. & Andanson, J. M. Impact of water on the melting temperature of urea+choline chloride deep eutectic solvent. *New J. Chem.* 40, 4492–4499 (2016).
262. Apelblat, A. & Manzurola, E. Solubility of oxalic, malonic, succinic, adipic, maleic, malic, citric, and tartaric acids in water from 278.15 to 338.15 K. *J. Chem. Thermodyn.* 19, 317–320 (1987).
263. Yang, H. & Wang, J. Solubilities of 3-Carboxy-3-hydroxypentanedioic Acid in Ethanol, Butan-1-ol, Water, Acetone, and Methylbenzene. *J. Chem. Eng. Data* 1449–1451 (2011).
264. Amenda, J. P. & Helgesonb, H. C. Solubilities of the common L-a-amino acids as a function of temperature and solution pH. *Pure & Appl. Chem.* 69, 935–942 (1997).
265. Gutz, I. G. R. CurTiPot - pH and Acid-Base Titration Curves: analysis and simulation freeware.
266. Lange, L., Lehmkemper, K. & Sadowski, G. Predicting the aqueous solubility of pharmaceutical cocrystals as a function of pH and temperature. *Cryst. Growth Des.* 16, 2726–2740 (2016).
267. Lange, L., Schleinitz, M. & Sadowski, G. Predicting the Effect of pH on Stability and

Solubility of Polymorphs, Hydrates, and Cocrystals. *Cryst. Growth Des.* 16, 4136–4147 (2016).

268. Wysoczanska, K., MacEdo, E. A., Sadowski, G. & Held, C. Solubility Enhancement of Vitamins in Water in the Presence of Covitamins: Measurements and ePC-SAFT Predictions. *Ind. Eng. Chem. Res.* 58, 21761–21771 (2019).
269. Alhadid, A., Mokrushina, L. & Minceva, M. Modeling of solid–liquid equilibria in deep eutectic solvents: A parameter study. *Molecules* 24, 1–19 (2019).
270. Stokes, G. G. Volume the Ninth. *Trans. Cambridge Philos. Soc.* 9, 5 (1856).
271. Einstein, A. Zur Theorie der Brownschen Bewegung. *Ann. Phys.* 324, 371–381 (1906).
272. Debye, P. Polar Molecules. (The Chemical Catalog Company, Inc., 1929).
273. Koenderink, G. H. *et al.* On the validity of Stokes–Einstein–Debye relations for rotational diffusion in colloidal suspensions. *Faraday Discuss.* 123, 335–354 (2003).
274. Dote, J. L., Kivelson, D. & Schwartz, R. N. A molecular quasi-hydrodynamic free-space model for molecular rotational relaxation in liquids. *J. Phys. Chem.* 85, 2169–2180 (1981).
275. Zhang, L. & Greenfield, M. L. Rotational relaxation times of individual compounds within simulations of molecular asphalt models. *J. Chem. Phys.* 132, 184502 (2010).
276. Mann, S. K., Pham, T. N., McQueen, L. L., Lewandowski, J. R. & Brown, S. P. Revealing Intermolecular Hydrogen Bonding Structure and Dynamics in a Deep Eutectic Pharmaceutical by Magic-Angle Spinning NMR Spectroscopy. *Mol. Pharm.* 17, 622–631 (2020).
277. Kumari, P., Shobhna, Kaur, S. & Kashyap, H. K. Influence of Hydration on the Structure of Reline Deep Eutectic Solvent: A Molecular Dynamics Study. *ACS Omega* 3, 15246–15255 (2018).
278. Gutiérrez, A., Aparicio, S. & Atilhan, M. Design of arginine-based therapeutic deep eutectic solvents as drug solubilization vehicles for active pharmaceutical ingredients. *Phys. Chem. Chem. Phys.* 21, 10621–10634 (2019).
279. Gutiérrez, A., Atilhan, M. & Aparicio, S. A theoretical study on lidocaine solubility in deep eutectic solvents. *Phys. Chem. Chem. Phys.* 20, 27464–27473 (2018).
280. Fetisov, E. O. *et al.* First-Principles Molecular Dynamics Study of a Deep Eutectic Solvent: Choline Chloride/Urea and Its Mixture with Water. *J. Phys. Chem. B* 122, 1245–1254 (2018).
281. Schön, T. *et al.* Effects of a food supplement rich in arginine in patients with smear

positive pulmonary tuberculosis - A randomised trial. *Tuberculosis* 91, 370–377 (2011).

282. Cao, C., Nian, B., Li, Y., Wu, S. & Liu, Y. Multiple hydrogen-bonding interactions enhance the solubility of starch in natural deep eutectic solvents: molecule and macroscopic scale insights. *J. Agric. Food Chem.* 67, 12366–12373 (2019).
283. Monteiro, H., Santos, F., Paiva, A., Duarte, A. R. C. & Ferreira, R. J. Molecular dynamics studies of therapeutic liquid mixtures and their binding to mycobacteria. *Front. Pharmacol.* 12, 1–11 (2021).
284. Beggs, W. H. & Andrews, F. A. Chemical characterization of ethambutol binding to Mycobacterium smegmatis. *Antimicrob. Agents Chemother.* 5, 234–239 (1974).
285. Rempel, S. *et al.* A mycobacterial ABC transporter mediates the uptake of hydrophilic compounds. *Nature* 580, 409–412 (2020).
286. Sartain, M. J., Dick, D. L., Rithner, C. D., Crick, D. C. & Belisle, J. T. Lipidomic analyses of Mycobacterium tuberculosis based on accurate mass measurements and the novel 'Mtb LipidDB'. *J. Lipid Res.* 52, 861–872 (2011).
287. Bansal-Mutalik, R. & Nikaido, H. Mycobacterial outer membrane is a lipid bilayer and the inner membrane is unusually rich in diacyl phosphatidylinositol dimannosides. *Proc. Natl. Acad. Sci.* 111, 4958–4963 (2014).
288. Salfinger, M. & Heifets, L. B. Determination of pyrazinamide MICs for Mycobacterium tuberculosis at different pHs by the radiometric method. *Antimicrob. Agents Chemother.* 32, 1002–1004 (1988).
289. Lindenberg, M., Kopp, S. & Dressman, J. B. Classification of orally administered drugs on the World Health Organization Model list of Essential Medicines according to the biopharmaceutics classification system. *Eur. J. Pharm. Biopharm.* 58, 265–278 (2004).
290. Nahid, P. *et al.* Official American Thoracic Society/ Centers for Disease Control and Prevention/ Infectious Diseases Society of America Clinical Practice Guidelines : Treatment of Drug-Susceptible Tuberculosis. *Clin. Infect. Dis. IDSA Guidel.* 63, 147–195 (2016).
291. Claire du Toit, L., Pillay, V. & Danckwerts, M. P. Tuberculosis chemotherapy: current drug delivery approaches. *Respir. Res.* 7, 1–18 (2006).
292. TB Alliance. Rifampin. *Tuberculosis* 88, 151–154 (2008).
293. TB Alliance. Pyrazinamide. *Tuberculosis* 88, 141–144 (2008).
294. TB Alliance. Isoniazid. *Tuberculosis* 88, 112–116 (2008).
295. TB Alliance. Ethambutol. *Tuberculosis* 88, 102–105 (2008).

296. Santos, F., Branco, L. C. & Duarte, A. R. C. Organic salts based on isoniazid drug: synthesis, bioavailability and cytotoxicity studies. *Pharmaceutics* 12, 952 (2020).
297. Roda, A., Matias, A. A., Paiva, A. & Duarte, A. R. C. Polymer science and engineering using deep eutectic solvents. *Polymers (Basel).* 11, 1–22 (2019).
298. Mano, F. *et al.* Production of poly(vinyl alcohol) (PVA) fibers with encapsulated natural deep eutectic solvent (NADES) using electrospinning. *ACS Sustain. Chem. Eng.* 3, 2504–2509 (2015).
299. Mano, F. *et al.* Production of electrospun fast-dissolving drug delivery systems with therapeutic eutectic systems encapsulated in Gelatin. *AAPS PharmSciTech* 18, 2579–2585 (2017).
300. Silva, J. M. *et al.* Development of innovative medical devices by dispersing fatty acid eutectic blend on gauzes using supercritical particle generation processes. *Mater. Sci. Eng. C* 99, 599–610 (2019).
301. Abranches, D. O. *et al.* Can cholinium chloride form eutectic solvents with organic chloride-based salts? *Fluid Phase Equilib.* 493, 120–126 (2019).
302. Martín, A. & Cocero, M. J. Micronization processes with supercritical fluids : Fundamentals and mechanisms. *Advanced Drug Delivery Reviews* 60, 339–350 (2008).
303. Nuchuchua, O. *et al.* Characterization of drug delivery particles produced by supercritical carbon dioxide technologies. *J. Supercrit. Fluids* 128, 244–262 (2017).
304. Liparoti, S., Adami, R. & Reverchon, E. Supercritical Assisted Atomization: effect of operative conditions on PVP microparticle size and morphology. *J. Supercrit. Fluids* 97, 31–35 (2015).
305. Scurto, A. M., Aki, S. N. V. K. & Brennecke, J. F. CO2 as a Separation Switch for Ionic Liquid/Organic Mixtures. *J. Am. Chem. Soc.* 124, 10276–10277 (2002).
306. Carmo, C. S. *et al.* A way to prepare a liposoluble natural pink colourant. *Green Chem.* 17, 1510–1518 (2015).
307. Sousa, A. R. S., Simplício, A. L., Sousa, H. C. & Duarte, C. M. M. Preparation of glyceryl monostearate-based particles by PGSS®—Application to caffeine. *J. Supercrit. Fluids* 43, 120–125 (2007).
308. Mandžuka, Z. & Knez, Ž. Influence of temperature and pressure during PGSS™ micronization and storage time on degree of crystallinity and crystal forms of monostearate and tristearate. *J. Supercrit. Fluids* 45, 102–111 (2008).
309. Knez, Ž. & Weidner, E. Precipitation of solids with dense gases from *Industrial*

Chemistry Library 9, 587–611 (2001).

310. Hanu, L. G., Alessi, P., Kilzer, A. & Kareth, S. Manufacturing and characterization of water filled micro-composites. *J. Supercrit. Fluids* 66, 274–281 (2012).
311. Hickey, A. J., Durham, P. G., Dharmadhikari, A. & Nardell, E. A. Inhaled drug treatment for tuberculosis: Past progress and future prospects. *J. Control. Release* 240, 127–134 (2016).
312. Parumasivam, T. *et al.* Dry powder inhalable formulations for anti-tubercular therapy. *Adv. Drug Deliv. Rev.* 102, 83–101 (2016).
313. Franco, P., Reverchon, E. & De Marco, I. PVP/ketoprofen coprecipitation using supercritical antisolvent process. *Powder Technol.* 340, 1–7 (2018).
314. Prosapio, V., De Marco, I., Scognamiglio, M. & Reverchon, E. Folic acid–PVP nanostructured composite microparticles by supercritical antisolvent precipitation. *Chem. Eng. J.* 277, 286–294 (2015).
315. Di Capua, A. *et al.* β -Carotene / PVP microspheres produced by Supercritical Assisted Atomization. *Powder Technol.* 346, 228–236 (2019).
316. Wu, J. C. C., Ray, S., Gizdavic-nikolaidis, M., Jin, J. & Cooney, R. P. Effect of polyvinylpyrrolidone on storage stability , anti oxidative and anti-bacterial properties of colloidal polyaniline. *Synth. Met.* 217, 202–209 (2016).
317. Hayyan, M. *et al.* Natural deep eutectic solvents: cytotoxic profile. *Springerplus* 5, 913 (2016).
318. Held, C., Cameretti, L. F. & Sadowski, G. Measuring and modeling activity coefficients in aqueous amino-acid solutions. *Ind. Eng. Chem. Res.* 50, 131–141 (2011).
319. Meltzer, V. & Pincu, E. Thermodynamic study of binary mixture of citric acid and tartaric acid. *Cent. Eur. J. Chem.* 10, 1584-1589 (2012).
320. Cameretti, L. F. & Sadowski, G. Modeling of aqueous amino acid and polypeptide solutions with PC-SAFT. *Chem. Eng. Process. Process Intensif.* 47, 1018–1025 (2008).
321. Merck. IR Spectrum Table & Chart. *Merck* Available at: https://www.sigmaaldrich.com/DE/de/technical-documents/technical-article/analytical-chemistry/photometry-and-reflectometry/ir-spectrum-table%0Ahttps://www.sigmaaldrich.com/NZ/en/technical-documents/technical-article/analytical-chemistry/photometry-and-ref. (Accessed: 23rd July 2020)
322. Mallik, T. & Kar, T. Growth and characterization of nonlinear optical L-arginine dihydrate single crystals. *J. Cryst. Growth* 285, 178–182 (2005).

323. Gowri, S., Sathiyabama, J. & Rajendran, S. Corrosion Inhibition Effect of Carbon Steel in Sea Water by L-Arginine-Zn 2+ System. *Int. J. Chem. Eng.* 2014, 1–9 (2014).
324. Petrosyan, A. M. & Sukiasyan, R. P. Vibrational spectra of L-arginine nitrates. *J. Mol. Struct.* 874, 51–56 (2008).
325. Mikeš, P., Brož, A., Sinica, A., Asatiani, N. & Bačáková, L. In vitro and in vivo testing of nanofibrous membranes doped with alaptide and L-arginine for wound treatment. *Biomed. Mater.* 15, 065023 (2020).
326. Pimpang, P., Sumang, R. & Choopun, S. Effect of concentration of citric acid on size and optical properties of fluorescence graphene quantum dots prepared by tuning carbonization degree. *Chiang Mai J. Sci.* 45, 2005–2014 (2018).
327. Bichara, L. C., Lanús, H. E., Ferrer, E. G., Gramajo, M. B. & Brandán, S. A. Vibrational Study and Force Field of the Citric Acid Dimer Based on the SQM Methodology. *Adv. Phys. Chem.* 2011, 1–10 (2011).

APPENDIX A

A.1 Organic Salts based on Isoniazid

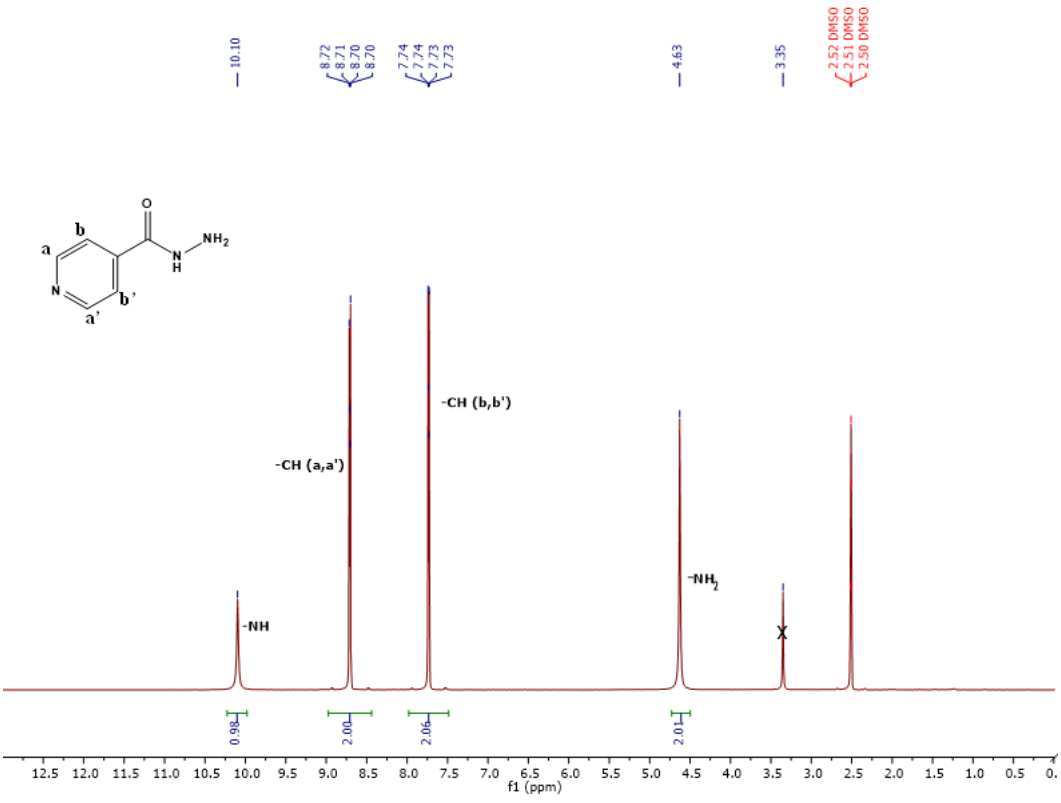

Figure A.1.1 - ^{1}H NMR spectra of INH.

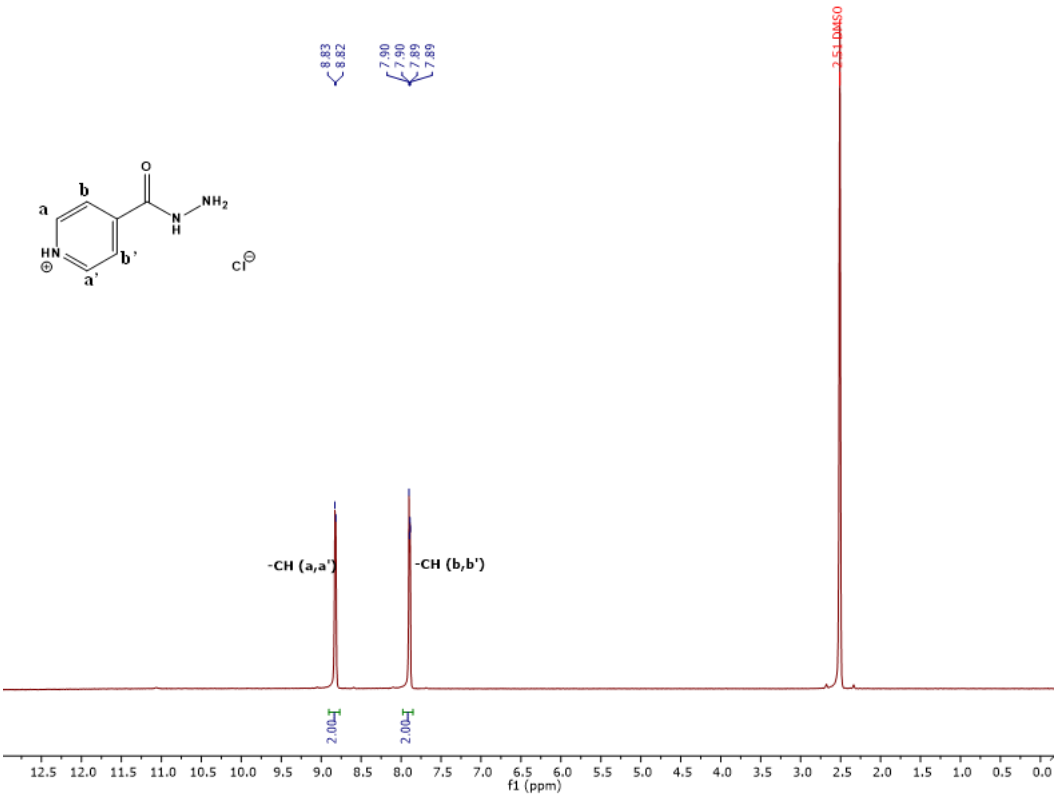

Figure A.1.2 - ^{1}H NMR spectra of [INH][Cl].

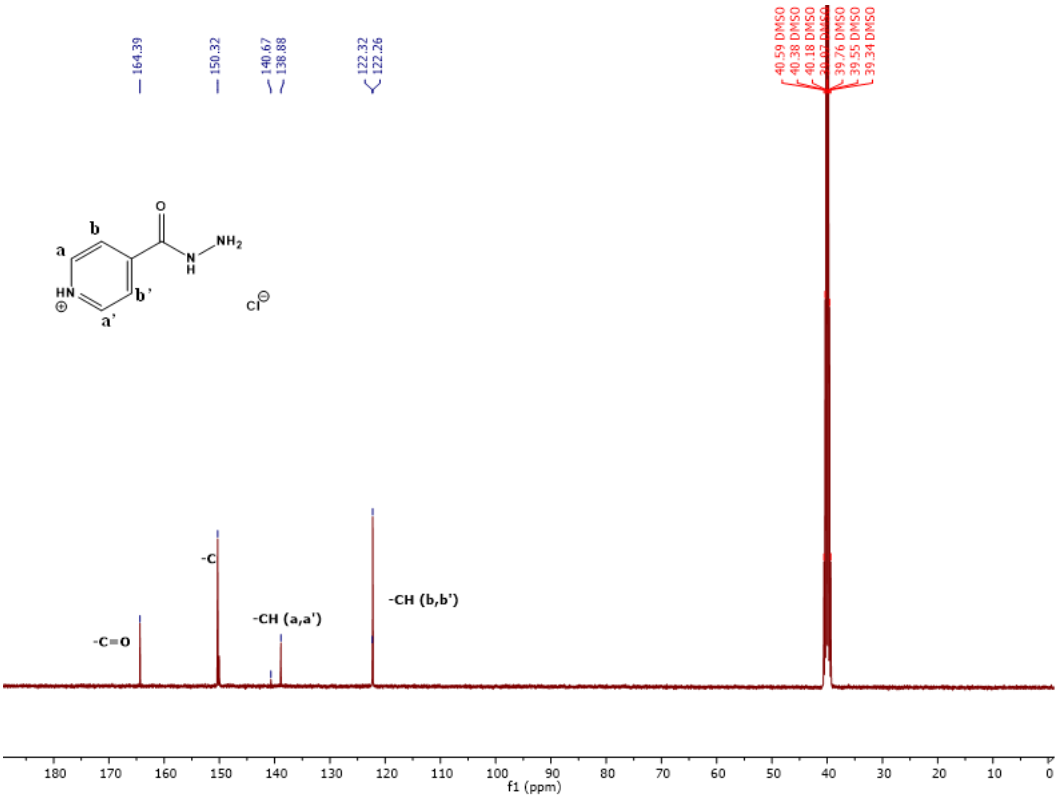

Figure A.1.3 - ^{13}C NMR spectra of [INH][Cl].

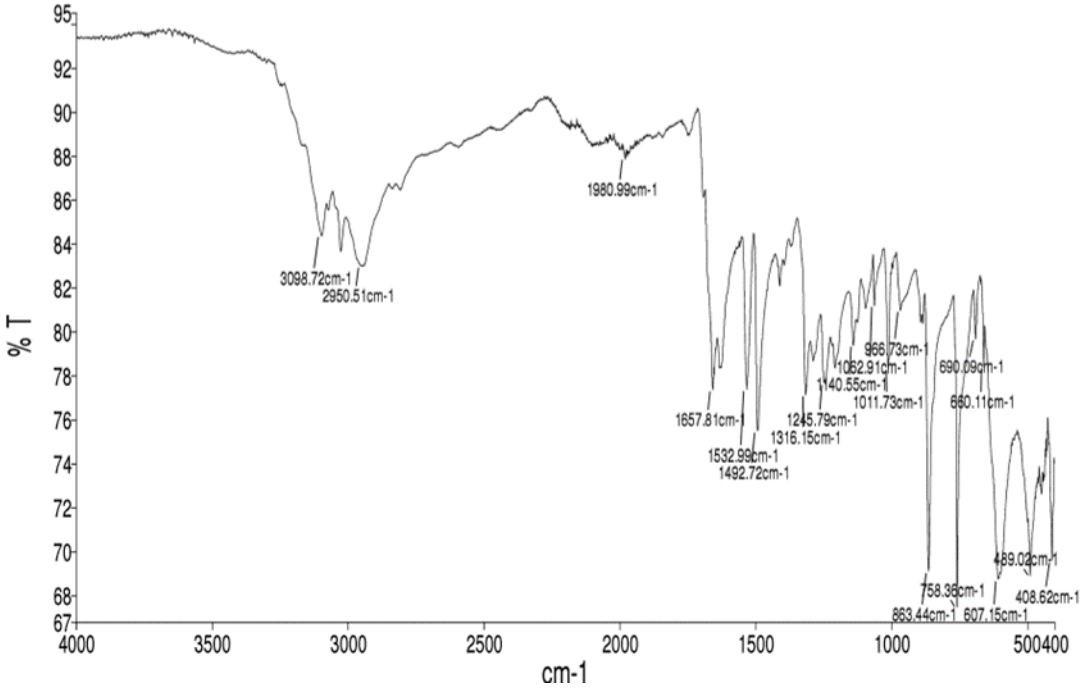

Figure A.1.4 - FTIR-ATR spectra of [INH][Cl].

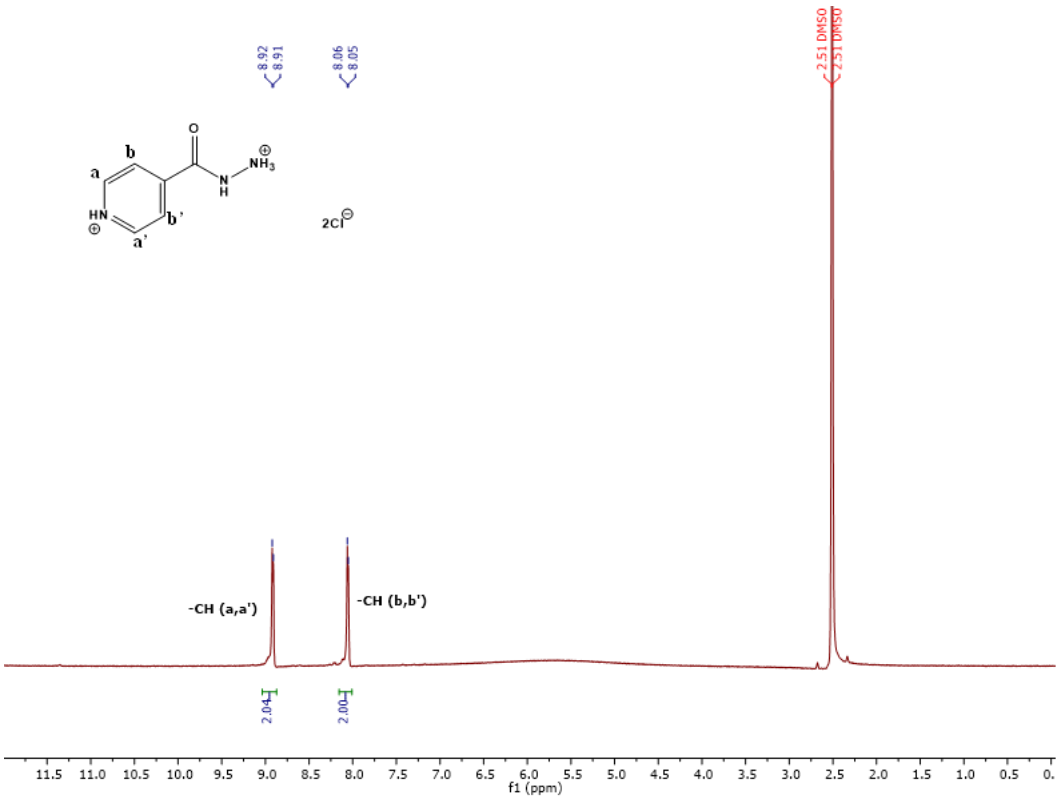

Figure A.1.5 - ^{1}H NMR spectra of $[INH][Cl]_2$.

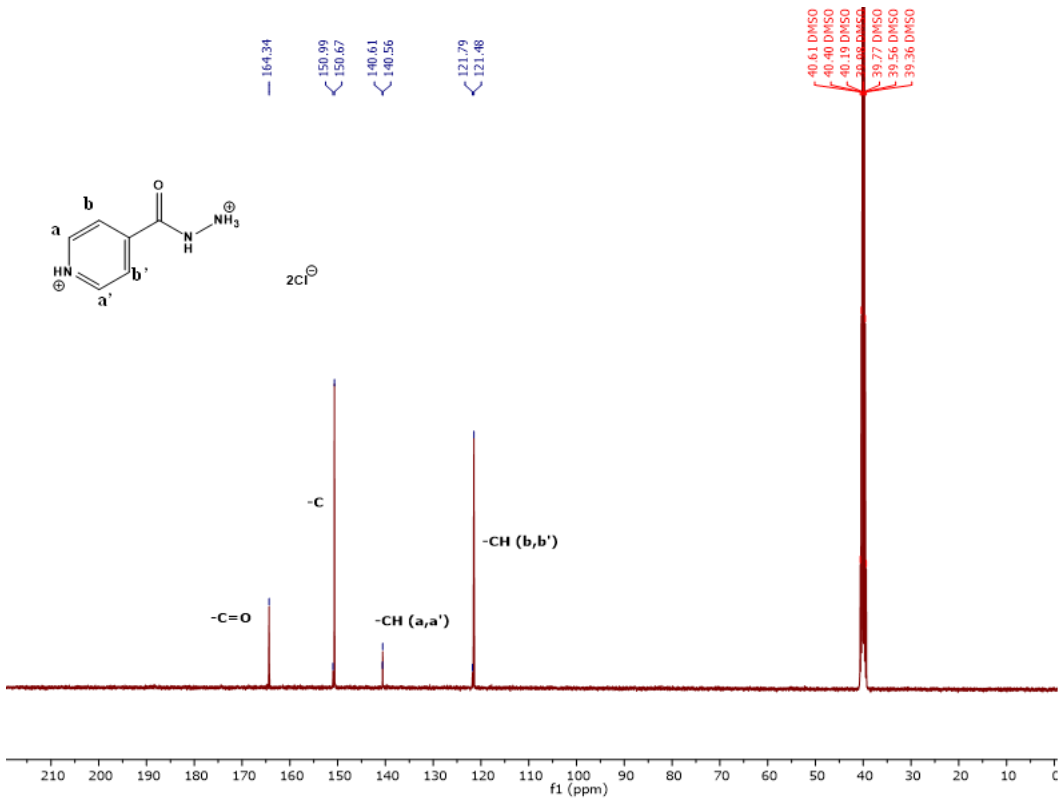

Figure A.1.6 - ^{13}C NMR spectra of $[INH][Cl]_2$.

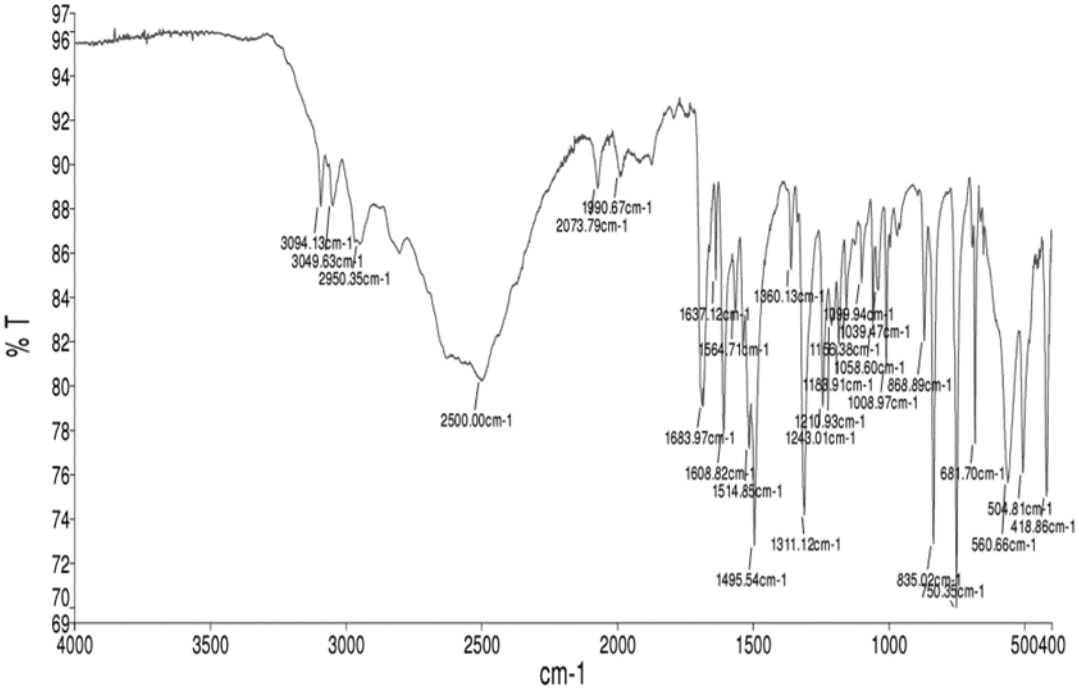

Figure A.1.7 - FTIR-ATR spectra of $[INH][Cl]_2$.

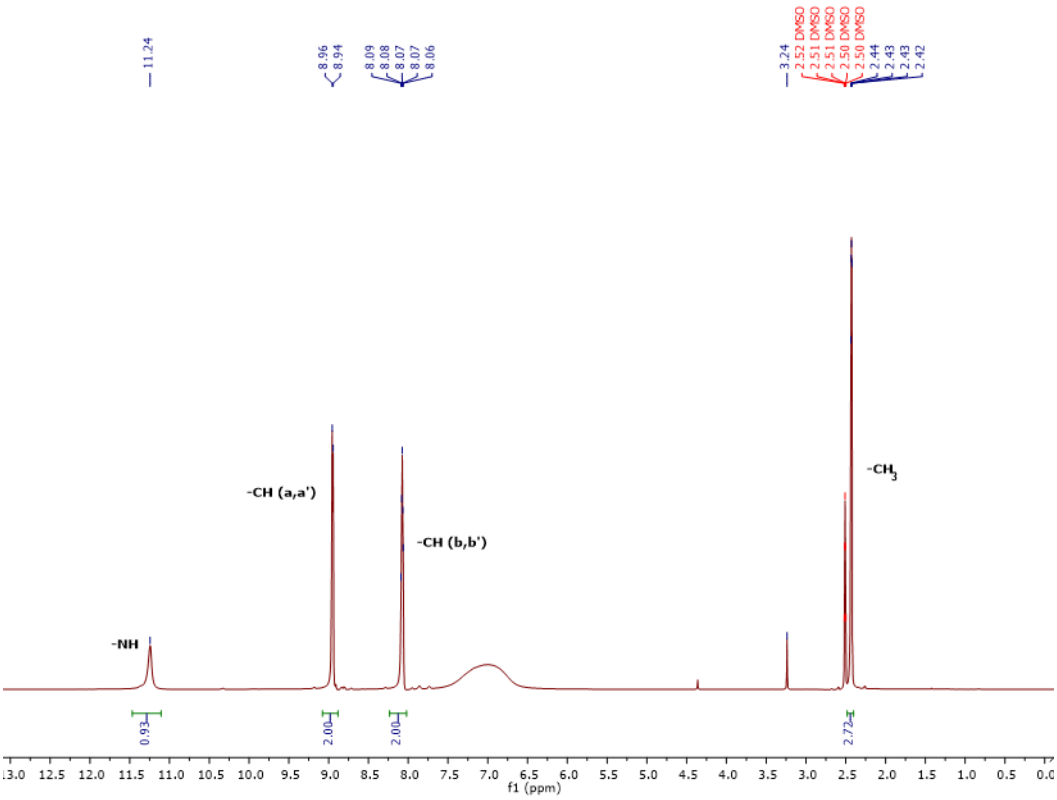

Figure A.1.8 - ^{1}H NMR spectra of [INH][MsO].

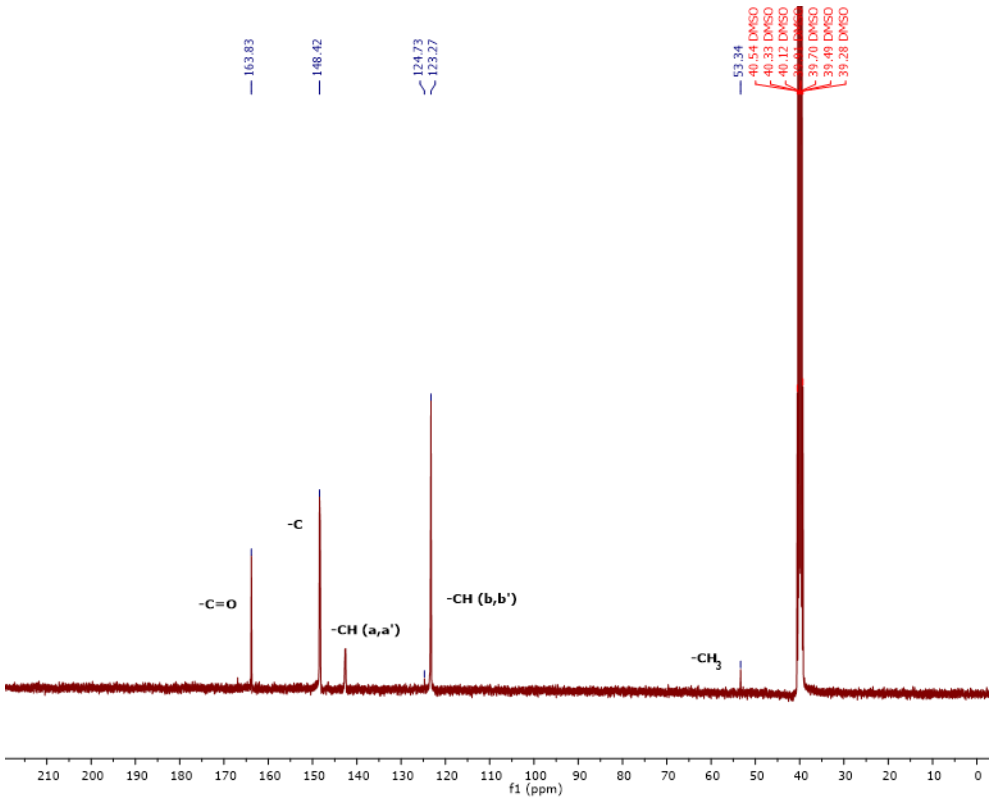

Figure A.1.9 - ^{13}C NMR spectra of [INH][MsO].

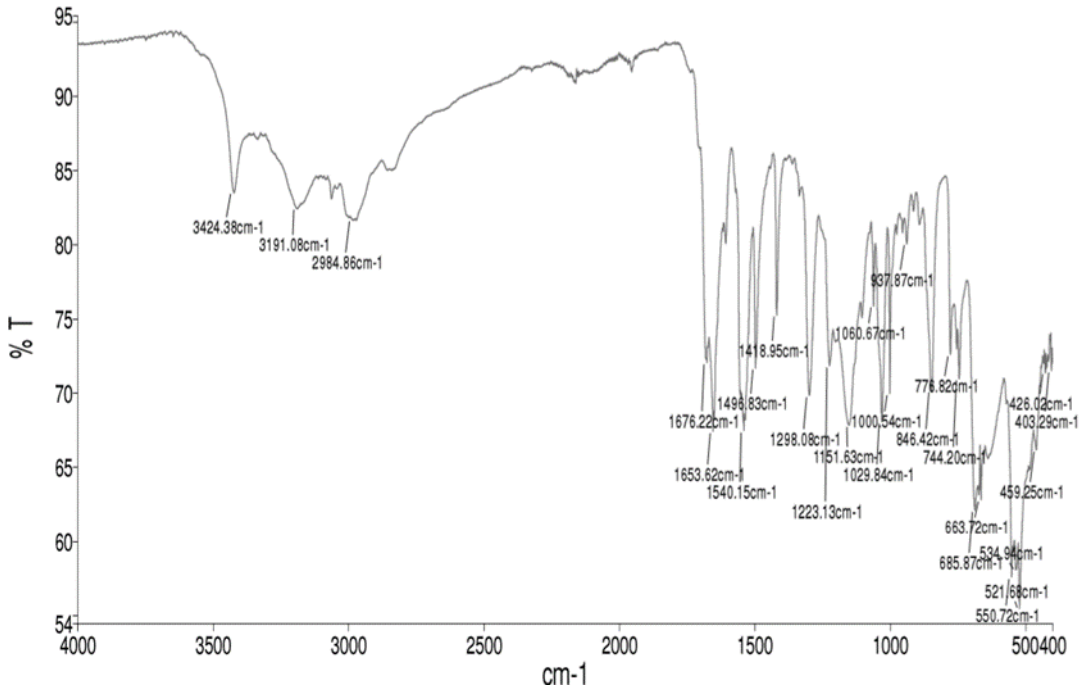

Figure A.1.10 - FTIR-ATR spectra of [INH][MsO].

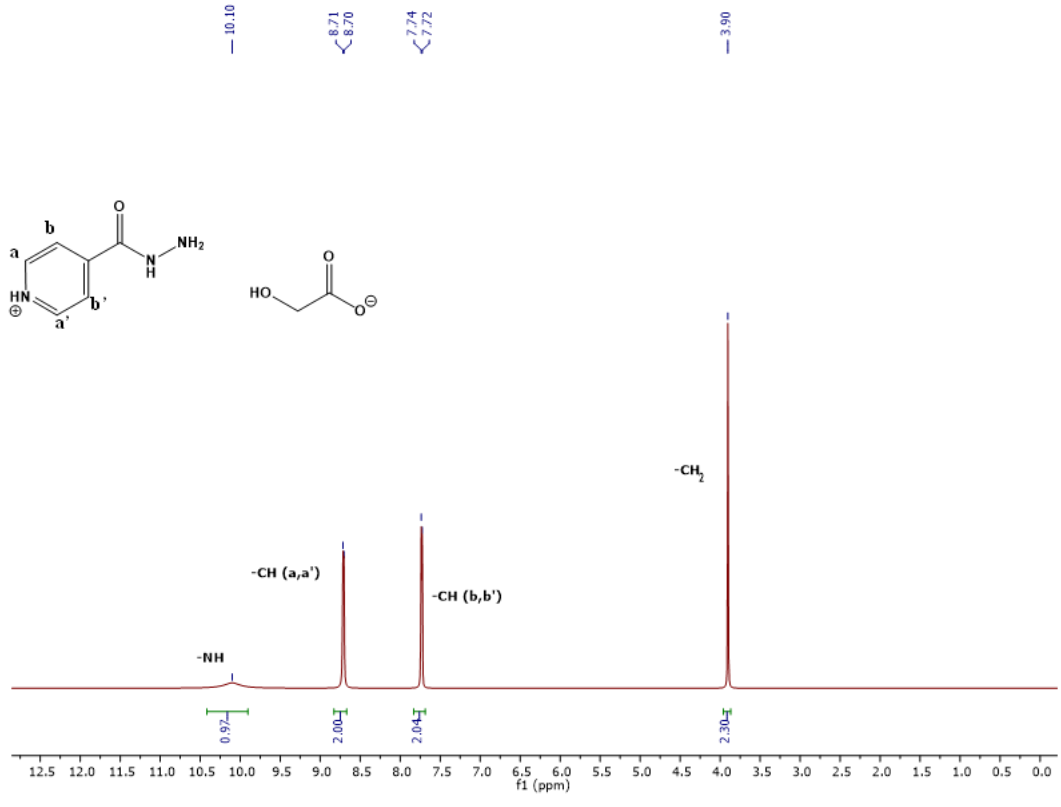

Figure A.1.11 - ^{1}H NMR spectra of [INH][GcO].

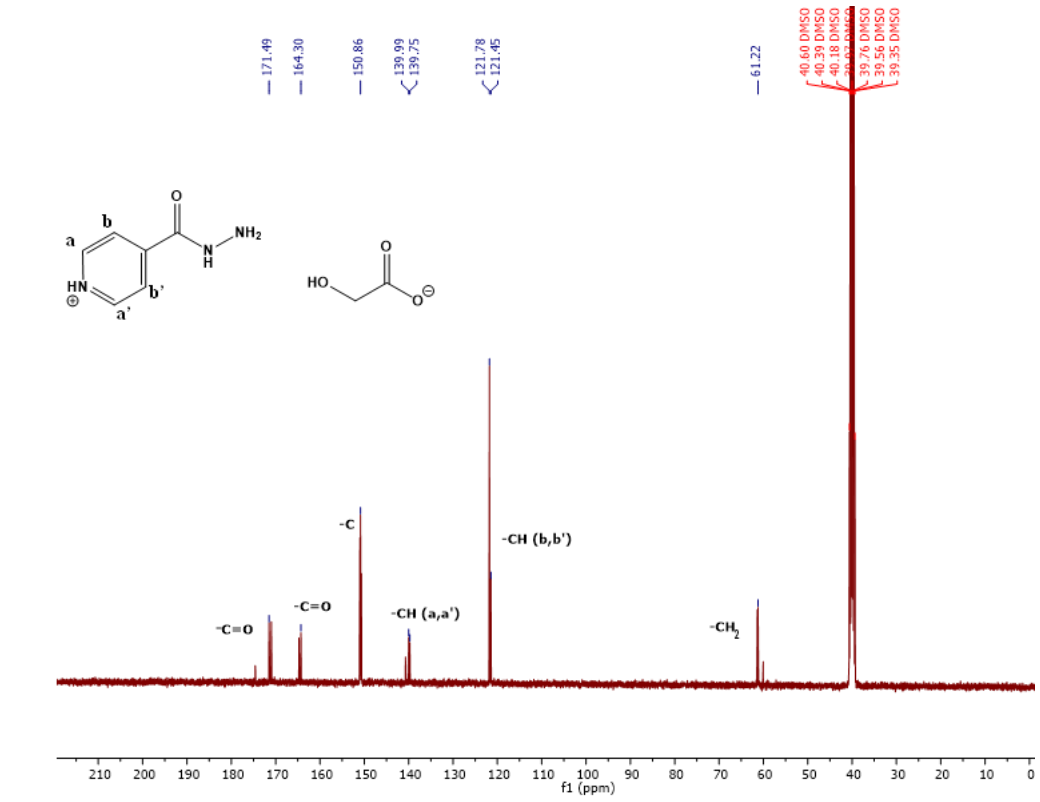

Figure A.1.12 - ^{13}C NMR spectra of [INH][GcO].

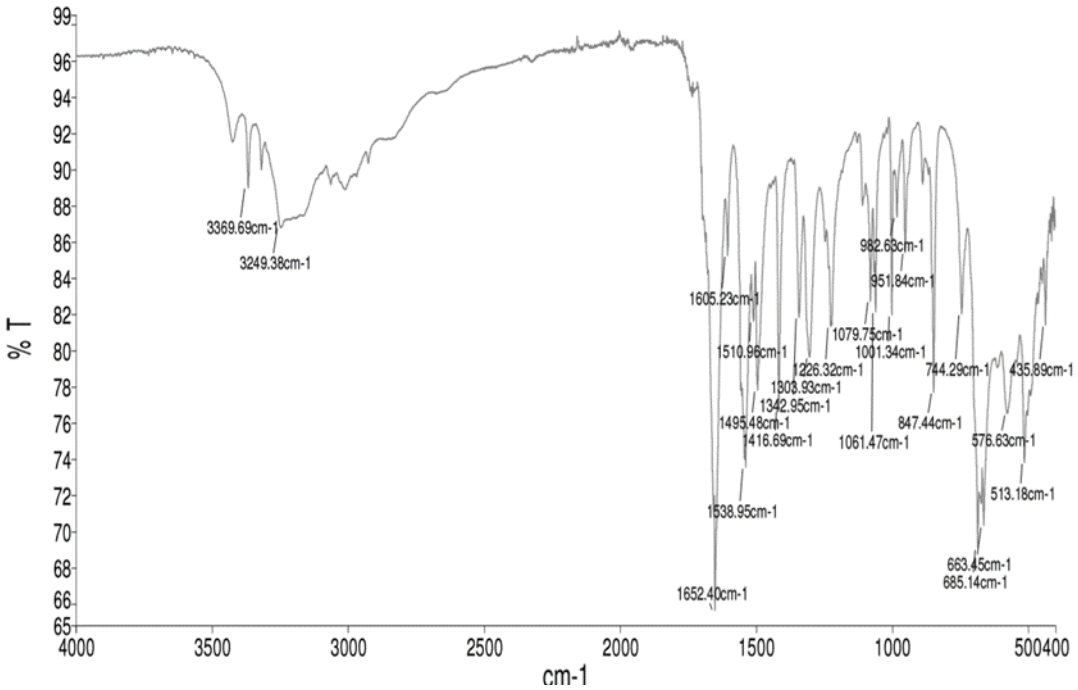

Figure A.1.13 - FTIR-ATR spectra of [INH][GcO].

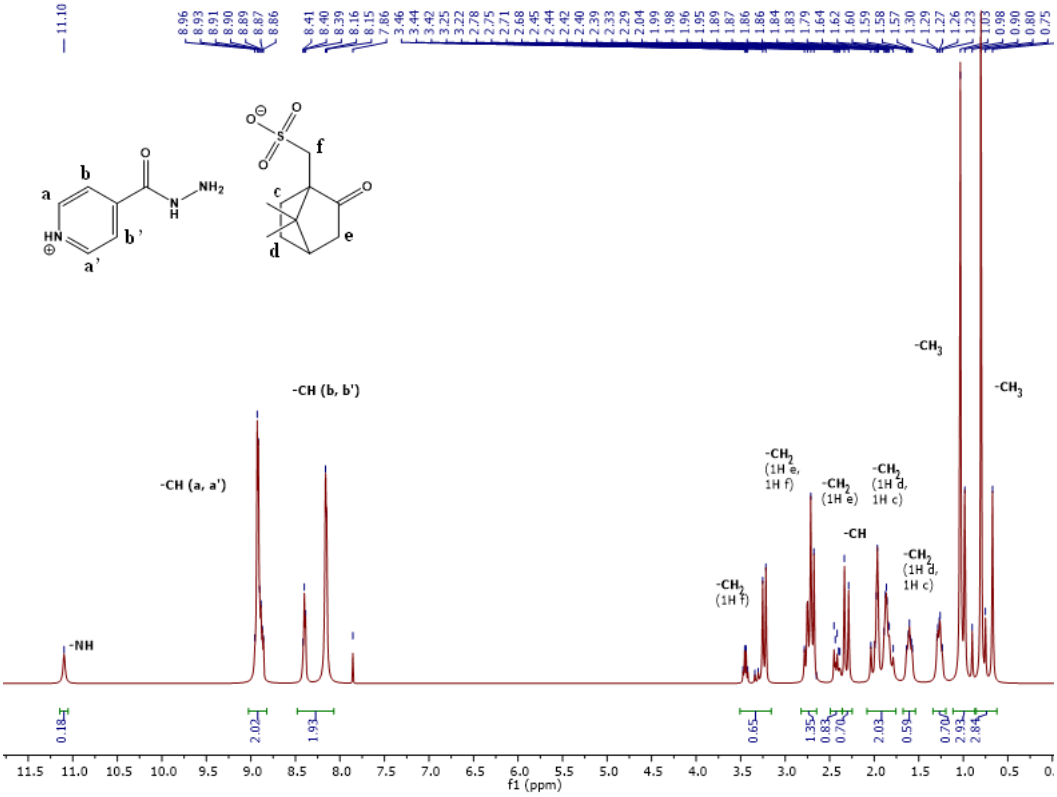

Figure A.1.14 - ^{1}H NMR spectra of [INH][S-CsO].

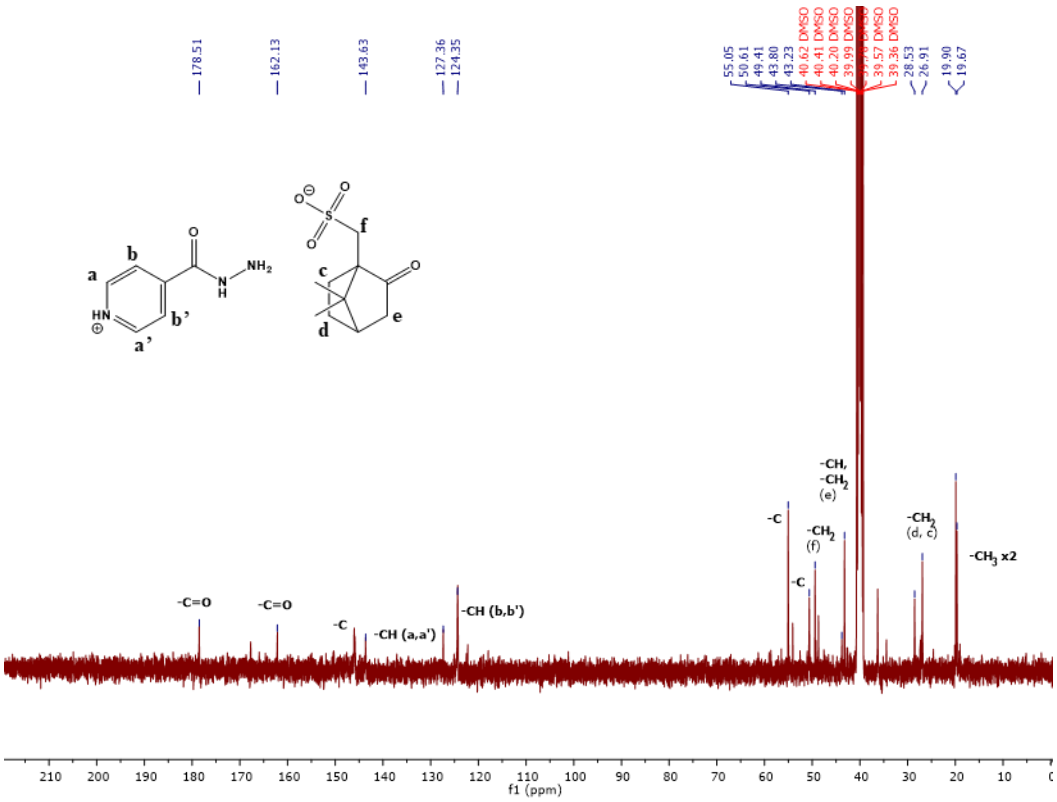

Figure A.1.15 - ^{13}C NMR spectra of [INH][S-CsO].

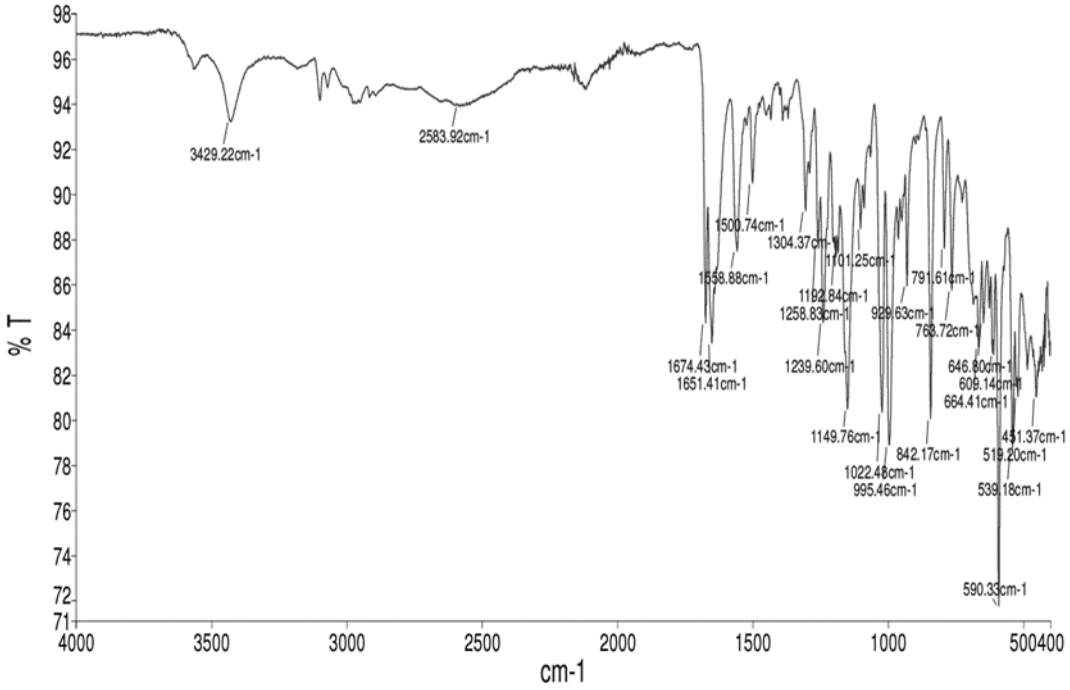

Figure A.1.16 - FTIR-ATR spectra of [INH][S-CsO].

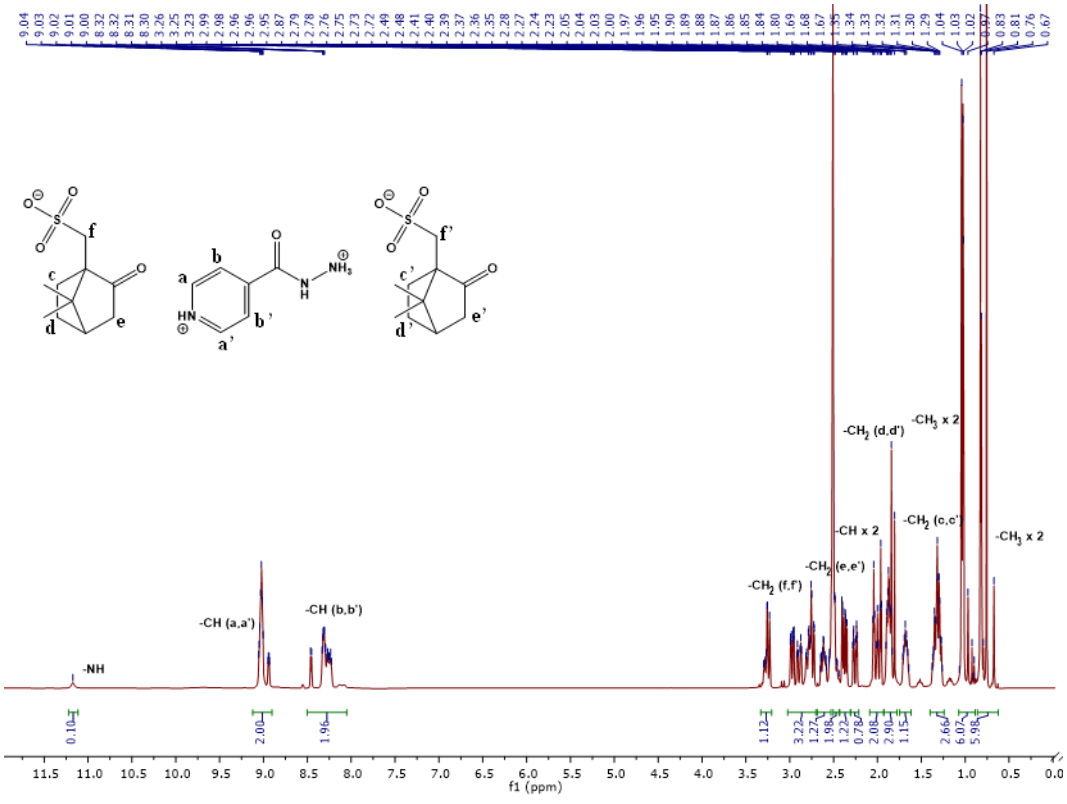

Figure A.1.17 - ^{1}H NMR spectra of [INH][S-CsO]$_2$.

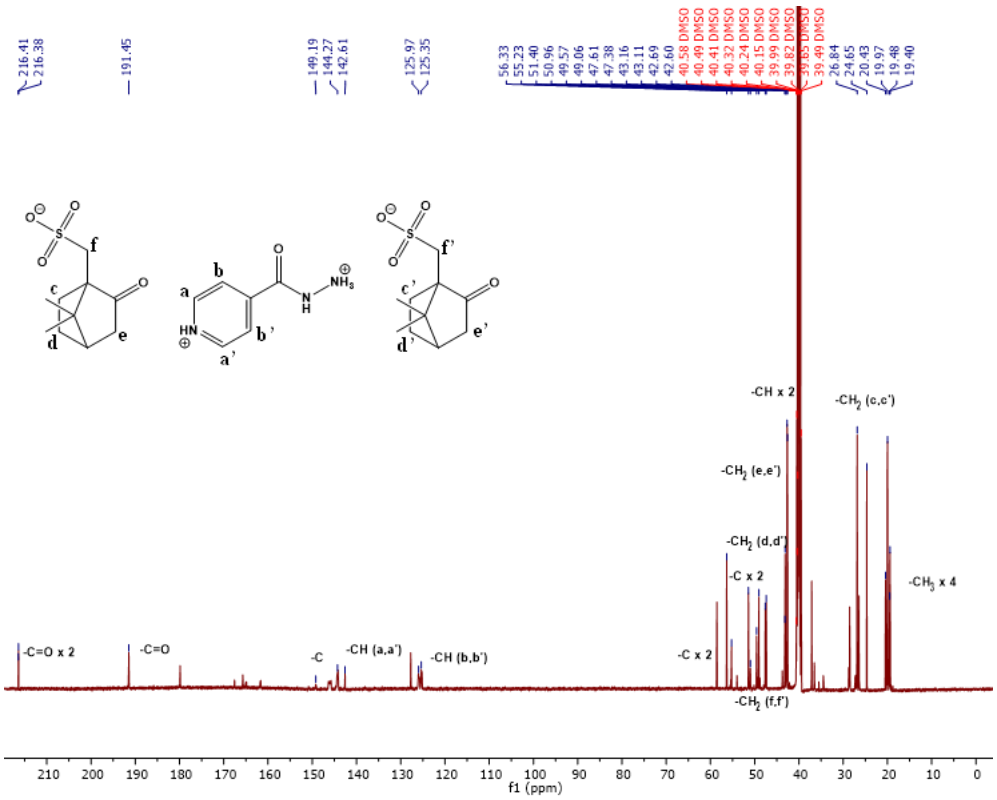

Figure A.1.18 - ^{13}C NMR spectra of [INH][S-CsO]$_2$.

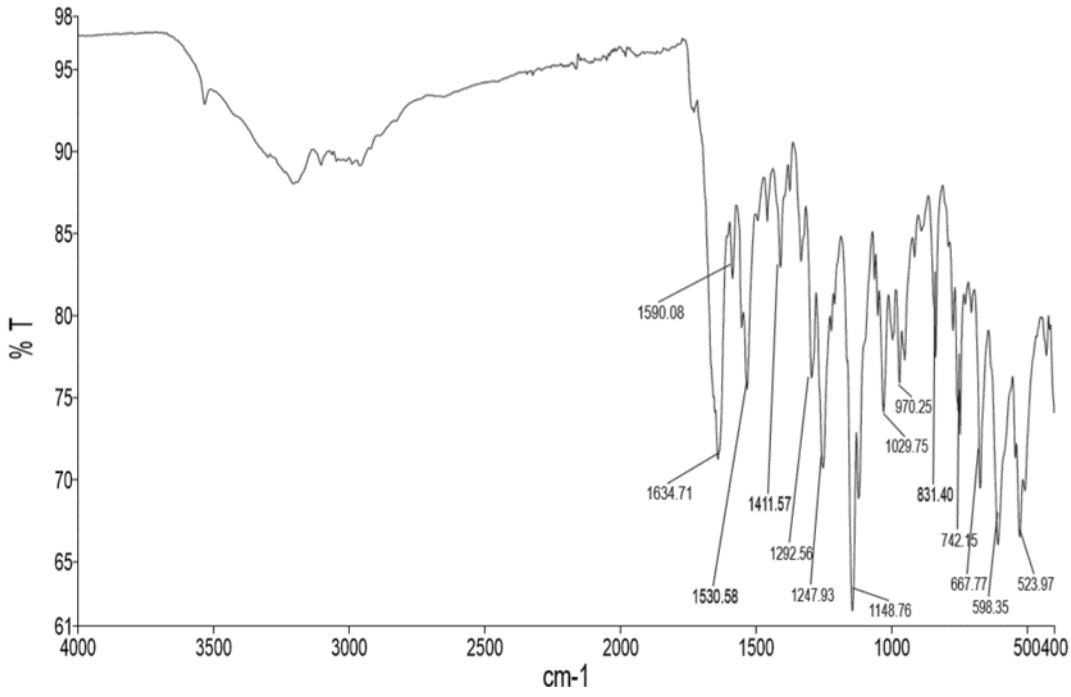

Figure A.1.19 - FTIR-ATR spectra of [INH][S-CsO]$_2$.

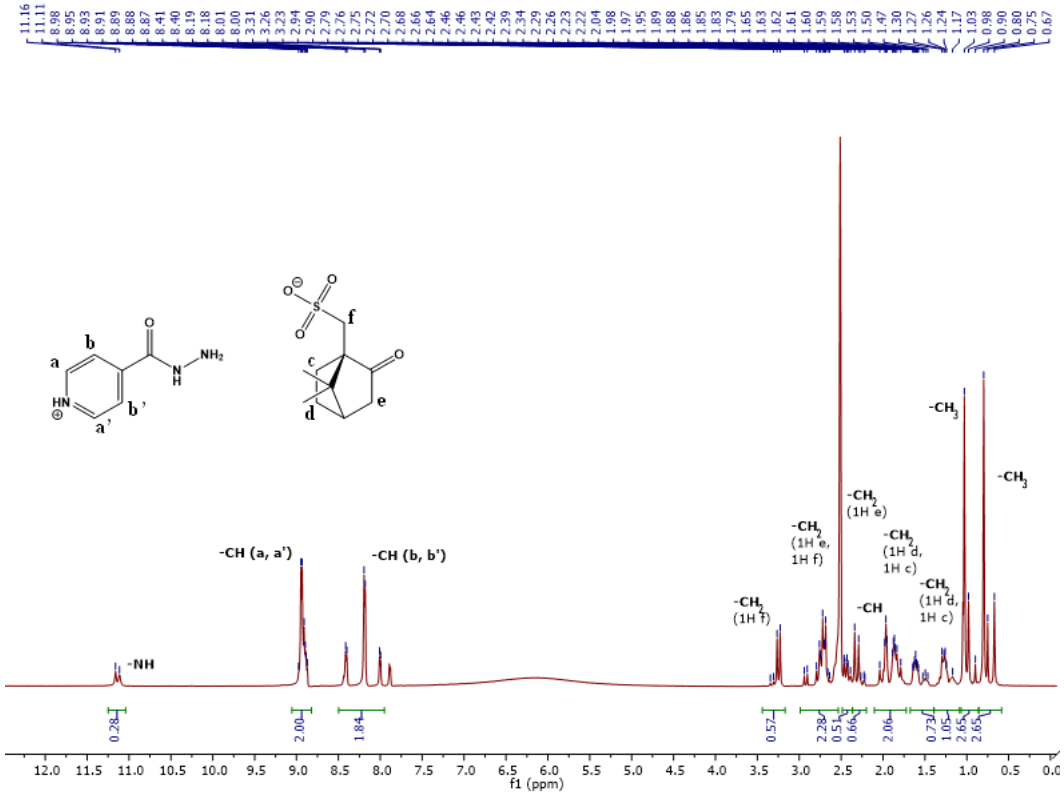

Figure A.1.20 - [1]H NMR spectra of [INH][R-CsO].

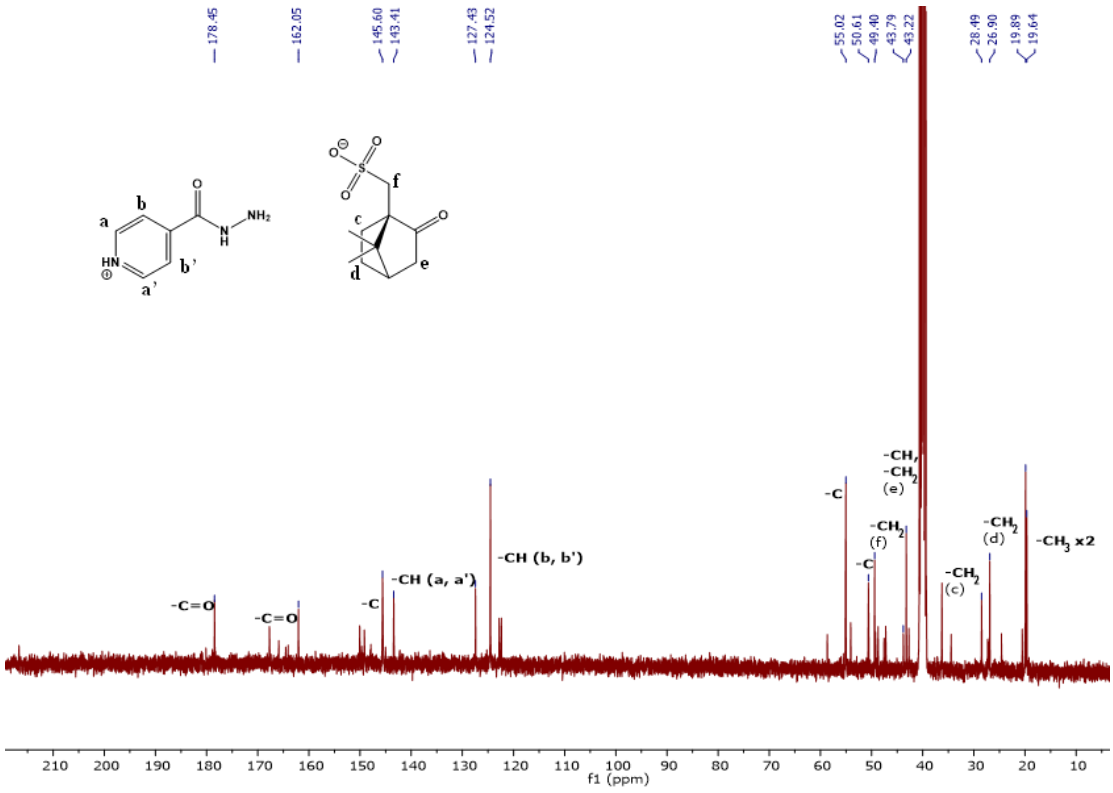

Figure A.1.21 - [13]C NMR spectra of [INH][R-CsO].

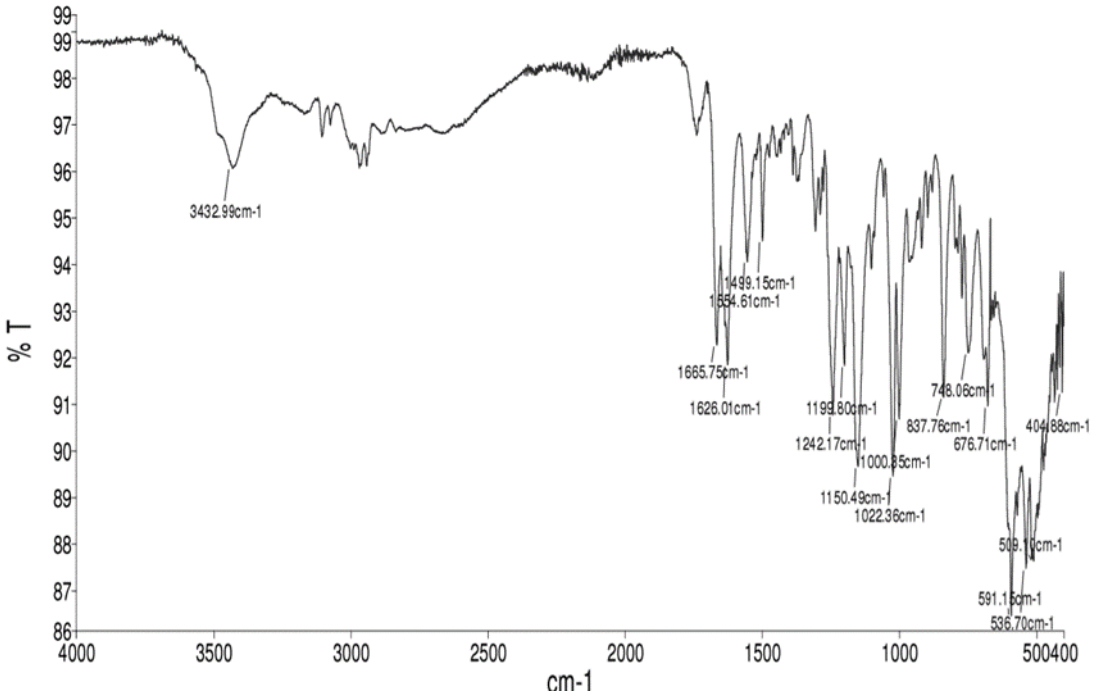

Figure A.1.22 - FTIR-ATR spectra of [INH][R-CsO].

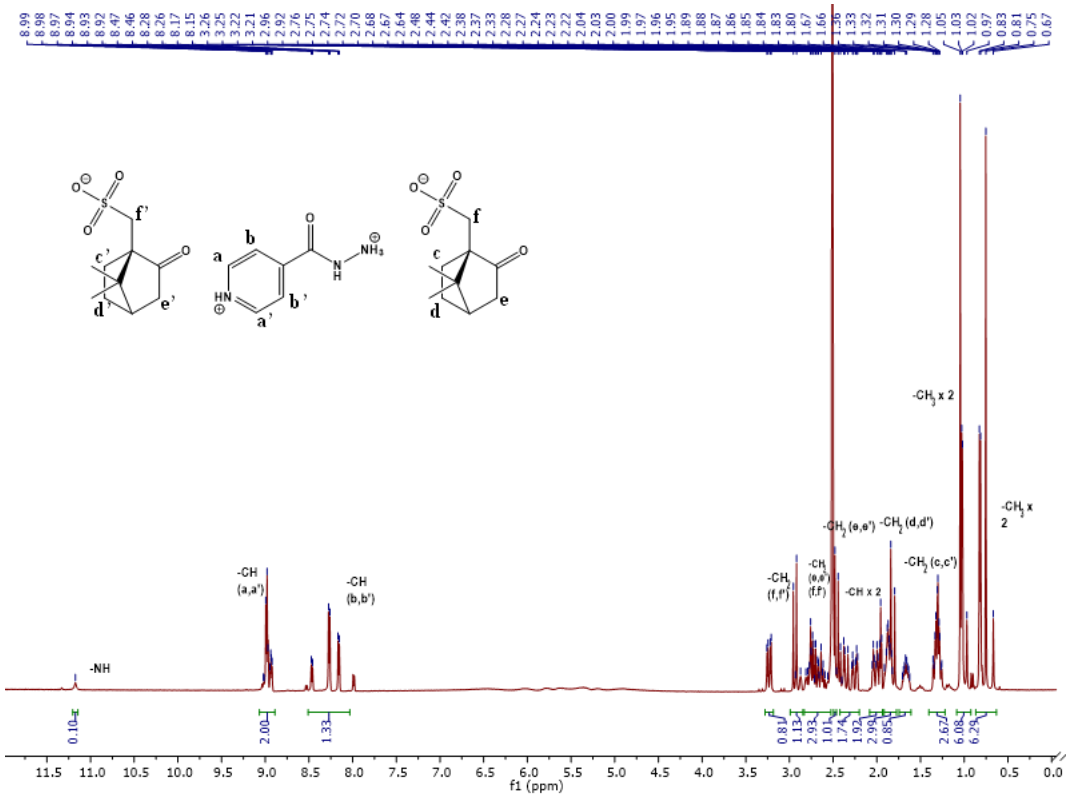

Figure A.1.23 - ^{1}H NMR spectra of $[INH][R\text{-}CsO]_2$.

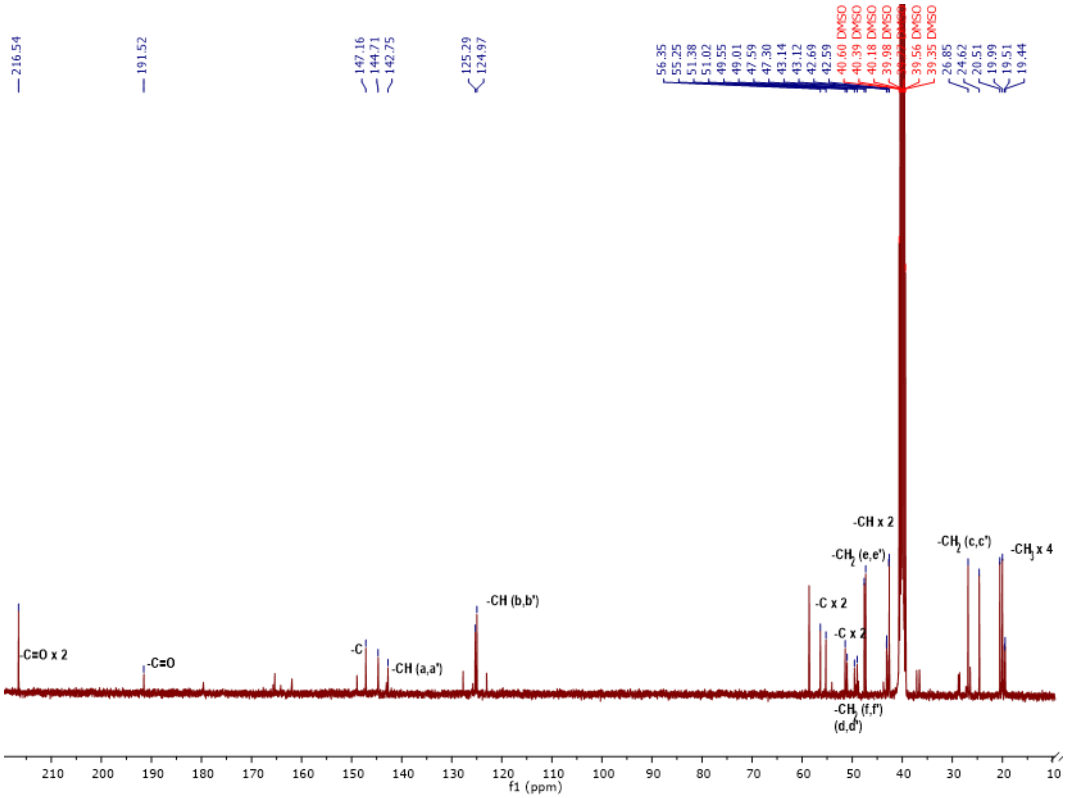

Figure A.1.24 - ^{13}C NMR spectra of [INH][R-CsO]$_2$.

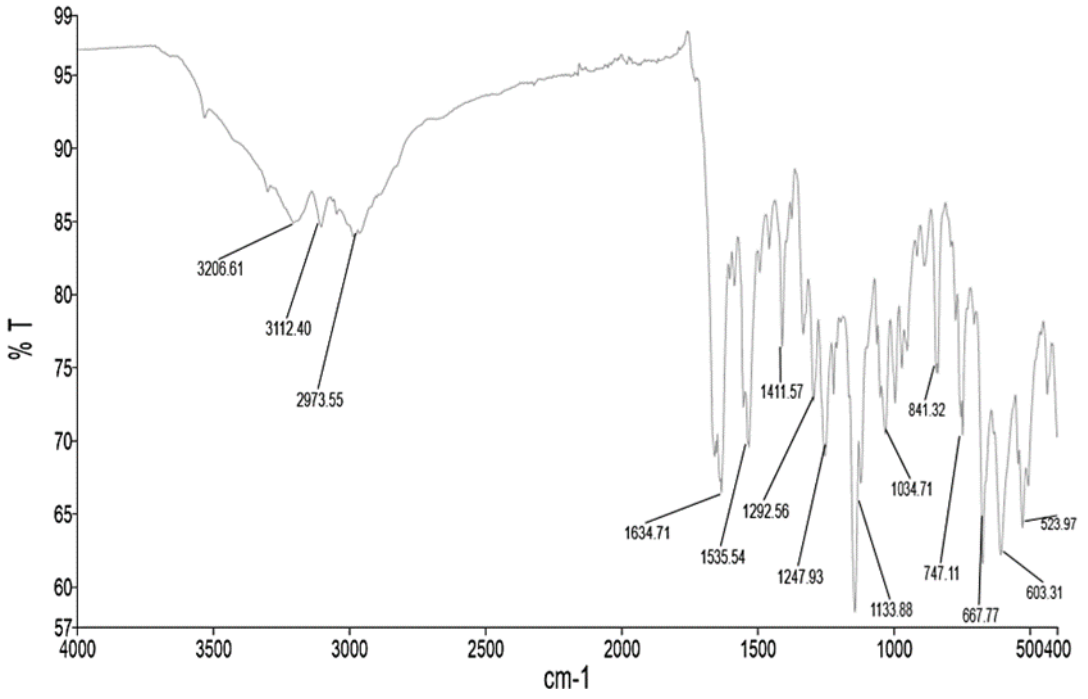

Figure A.1.25 - FTIR-ATR spectra of [INH][R-CsO]$_2$.

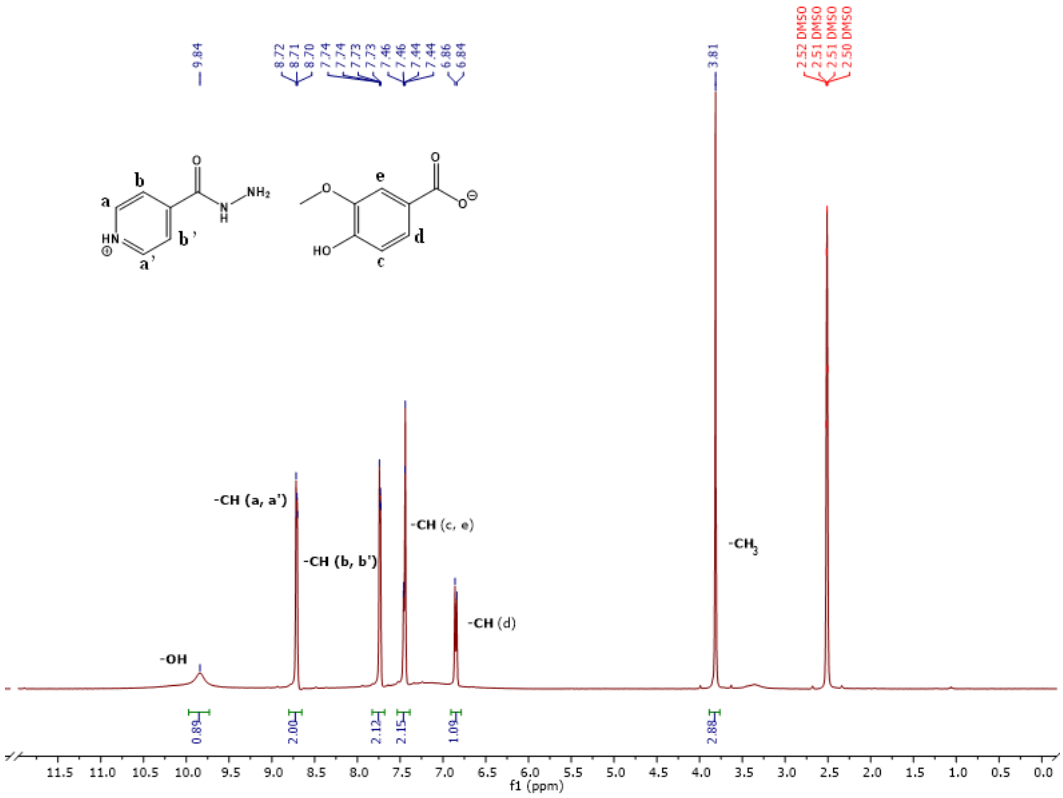

Figure A.1.26 - [1]H NMR spectra of [INH][VanO].

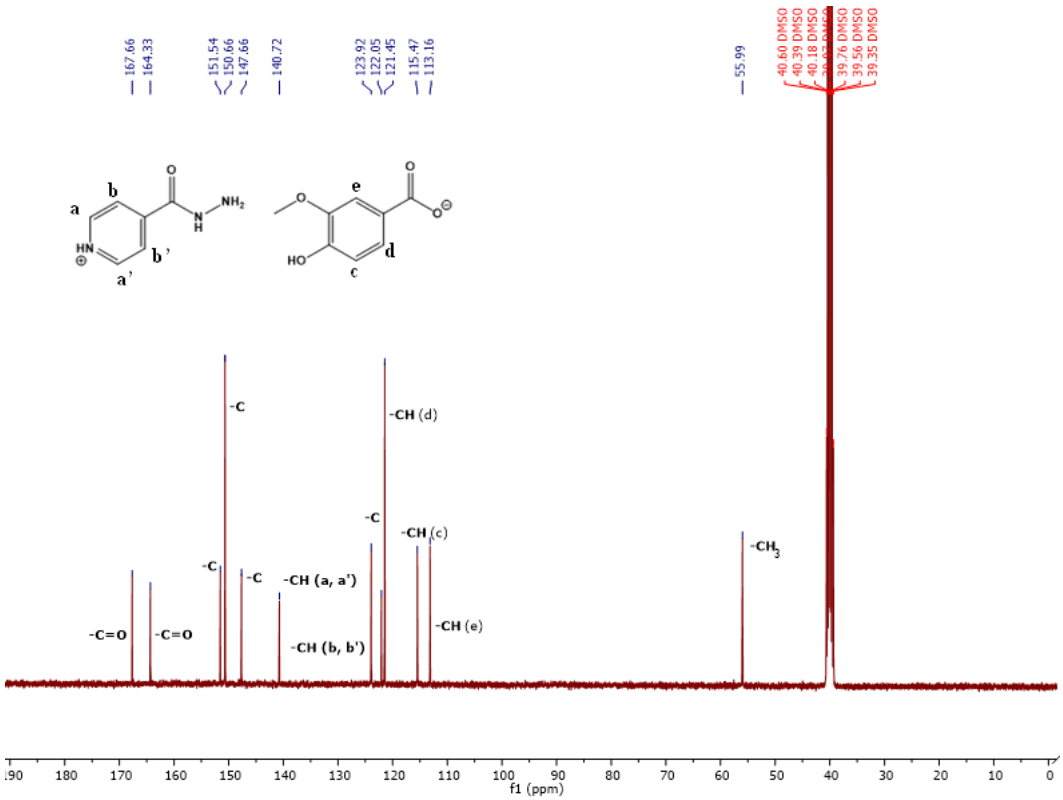

Figure A.1.27 - [13]C NMR spectra of [INH][VanO].

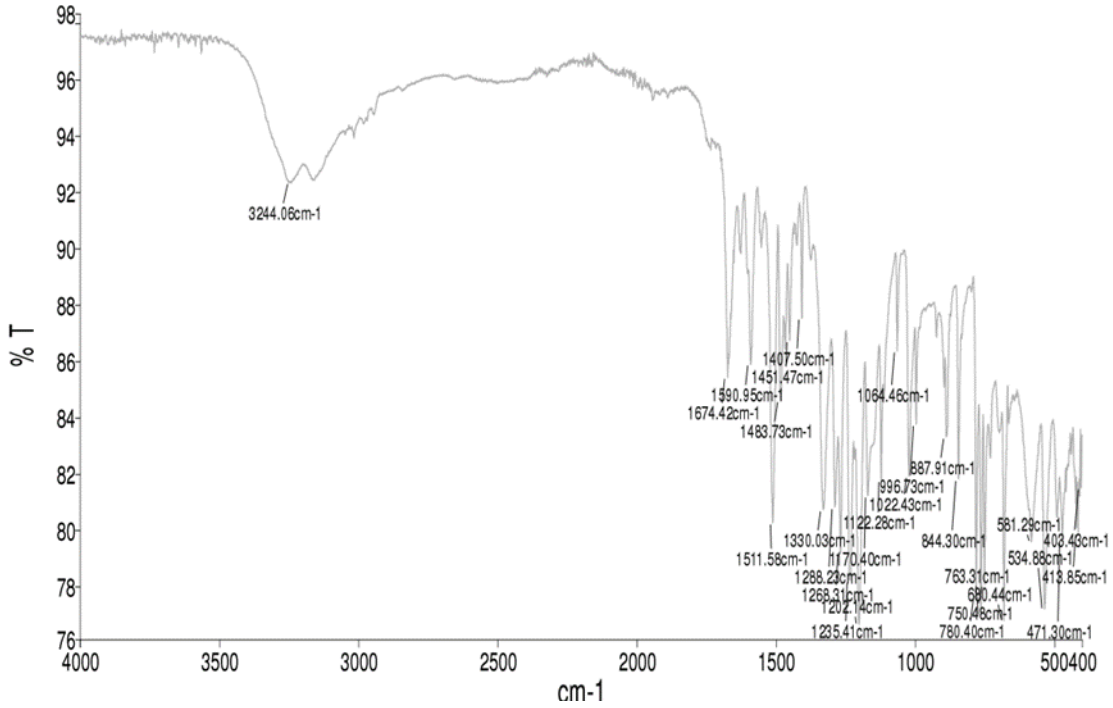

Figure A.1.28 - FTIR-ATR spectra of [INH][VanO].

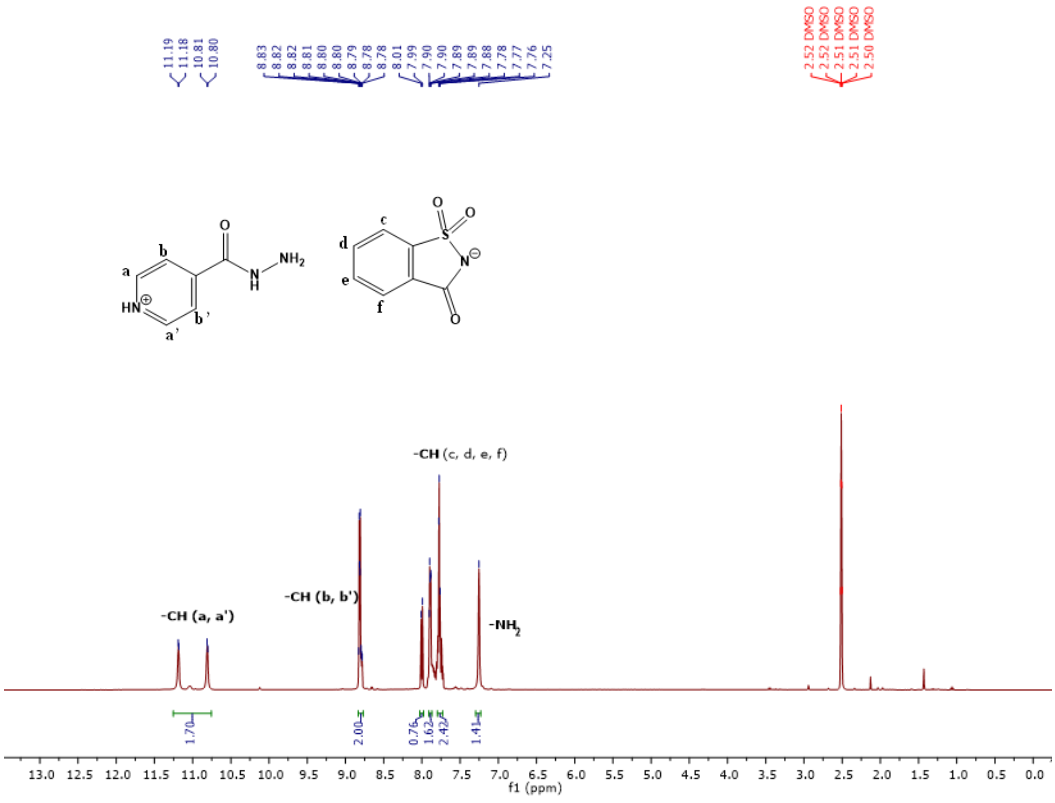

Figure A.1.29 - ^{1}H NMR spectra of [INH][Sac].

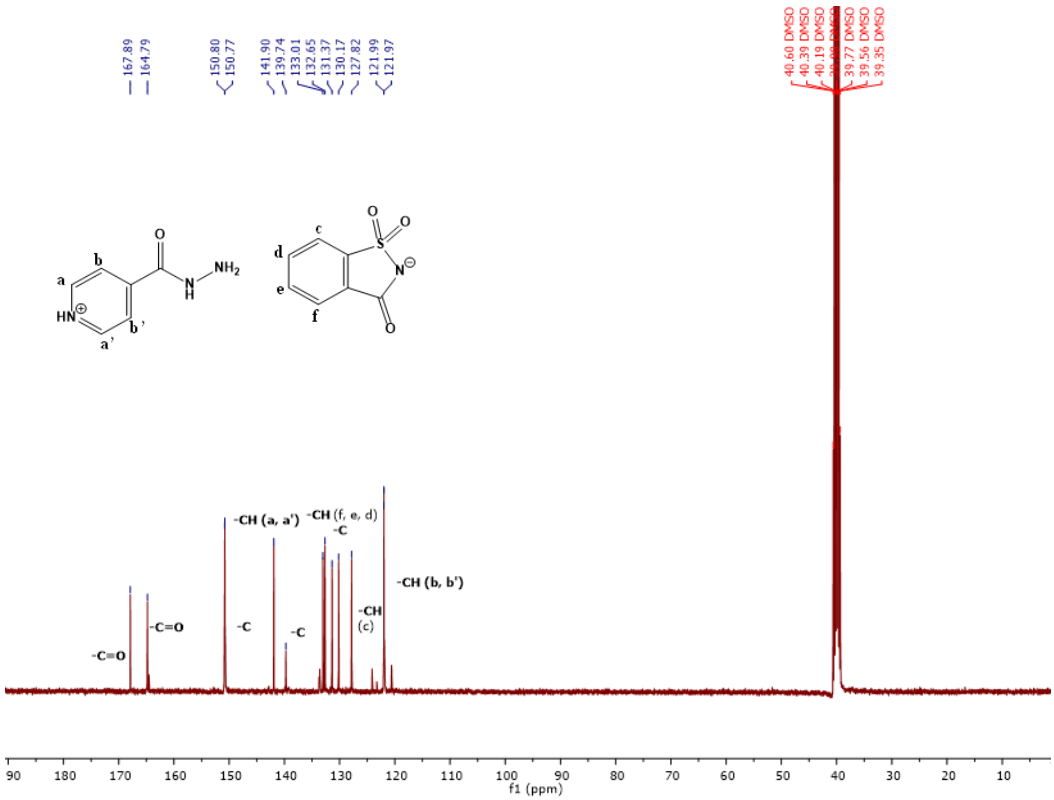

Figure A.1.30 - ^{13}C NMR spectra of [INH][Sac].

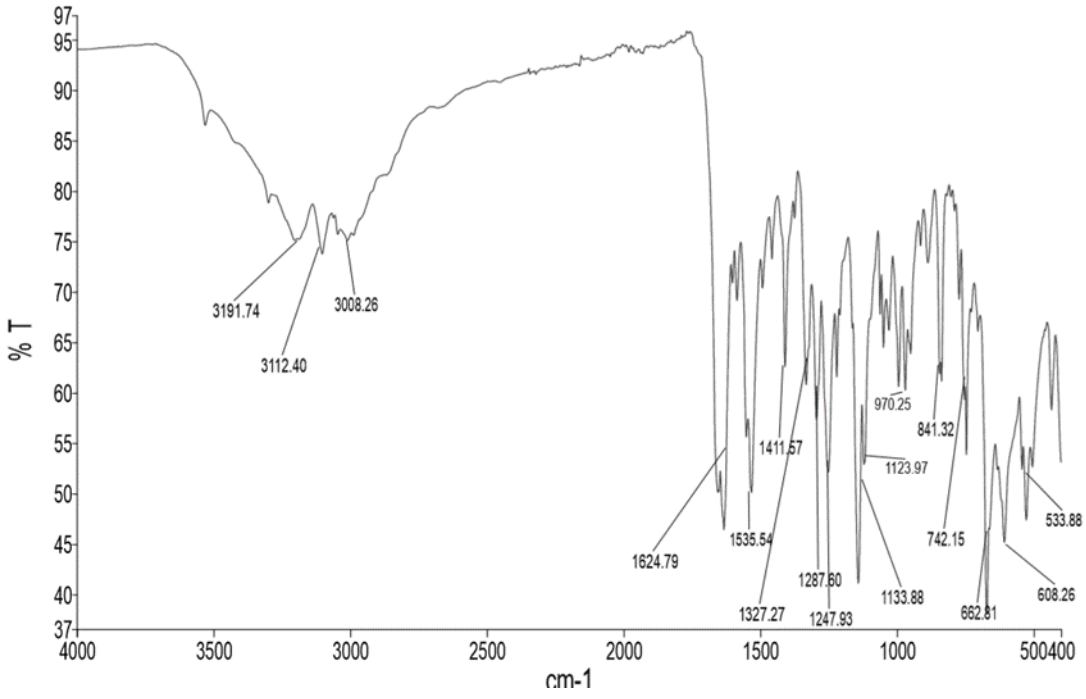

Figure A.1.31 - FTIR-ATR spectra of [INH][Sac].

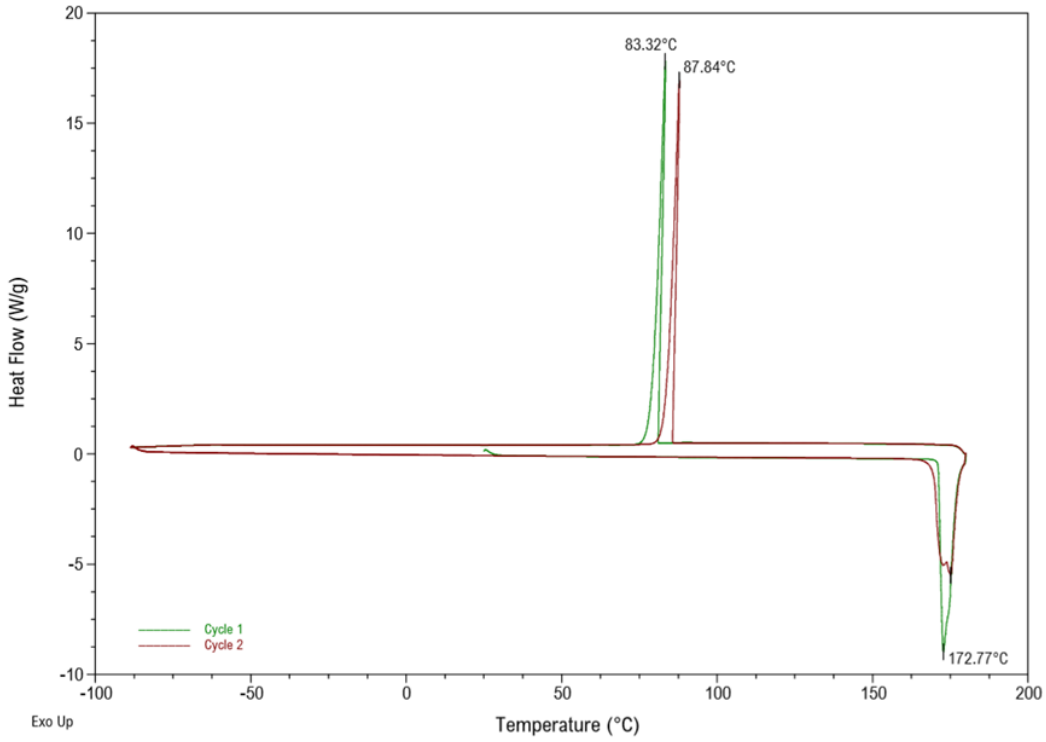

Figure A.1.32 – Thermogram of INH (DSC).

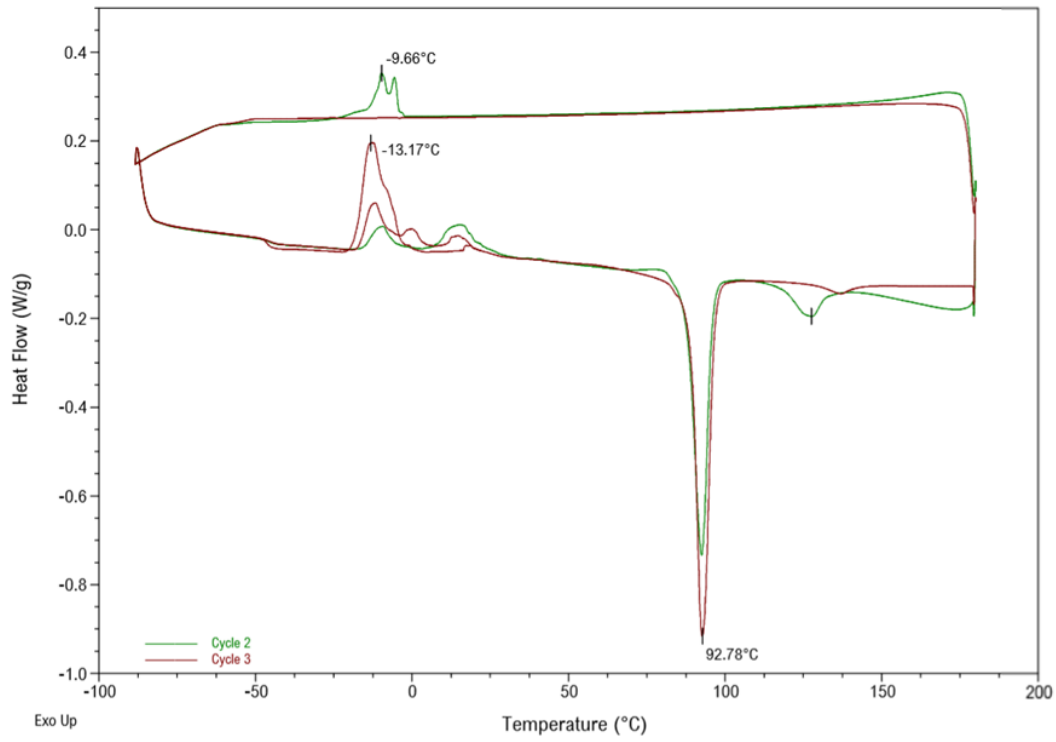

Figure A.1.33 – Thermogram of [INH][Cl] (DSC).

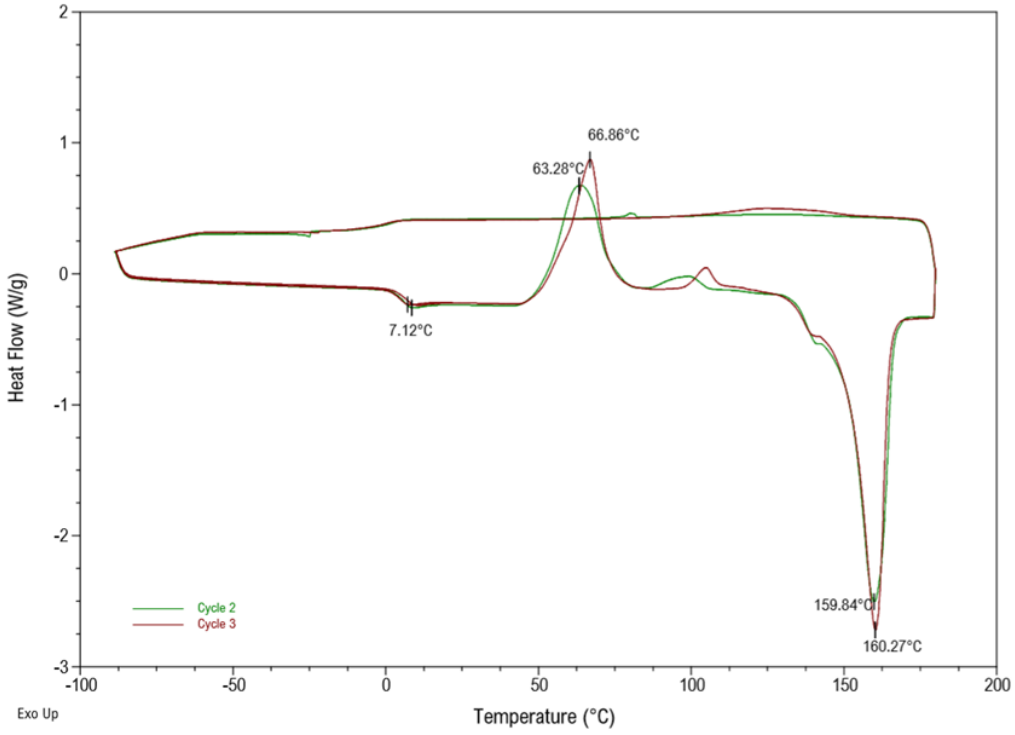

Figure A.1.34 – Thermogram of $[INH][Cl]_2$ (DSC).

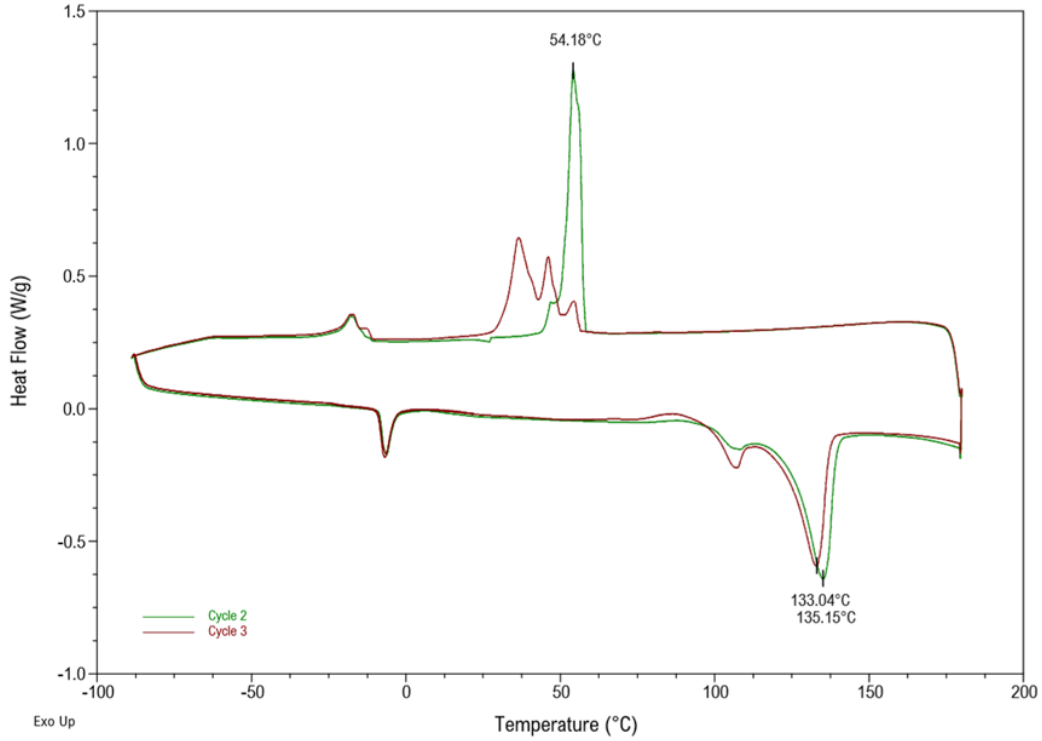

Figure A.1.35 – Thermogram of [INH][MsO] (DSC).

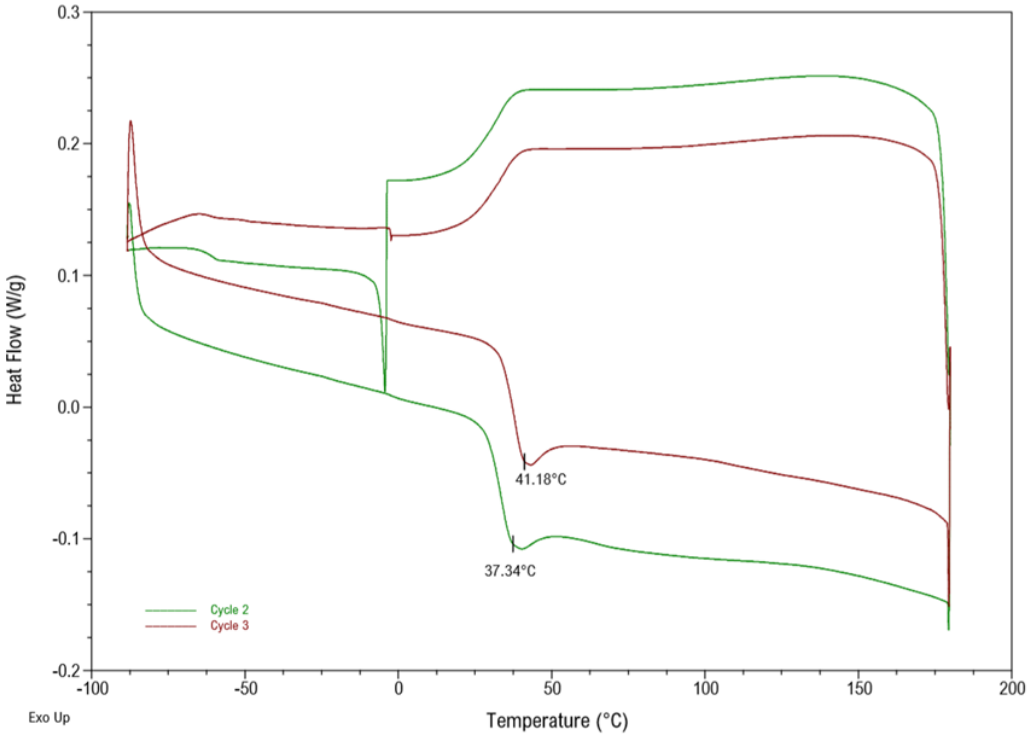

Figure A.1.36 – Thermogram of [INH][GcO] (DSC).

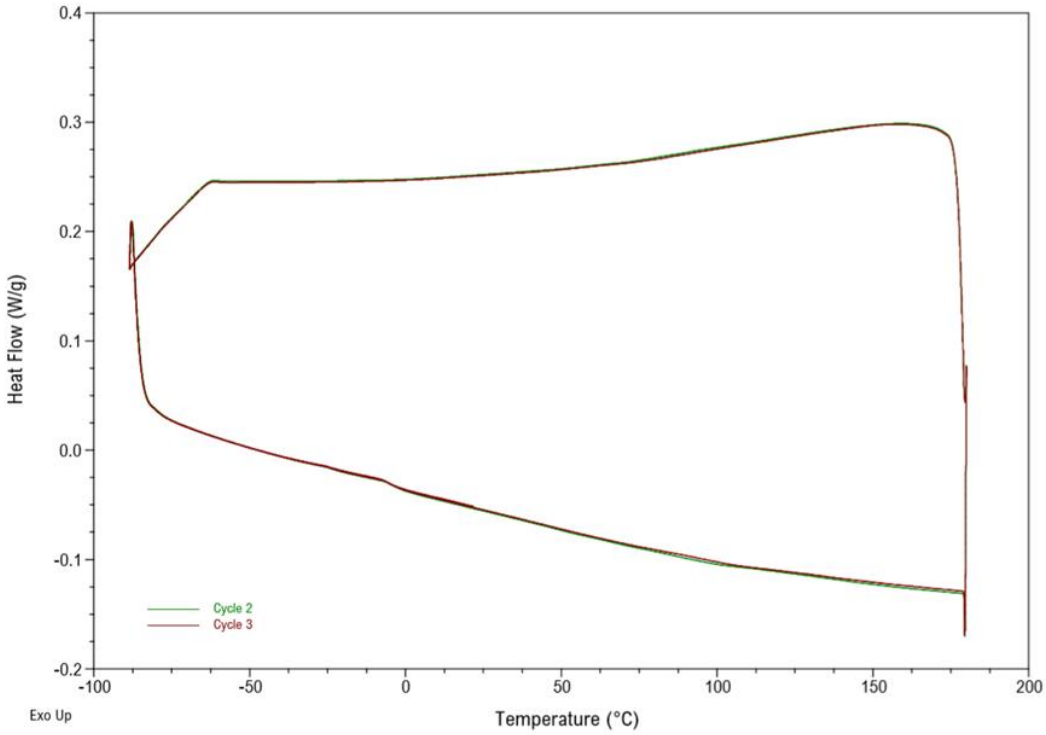

Figure A.1.37 – Thermogram of [INH][S-CsO] (DSC).

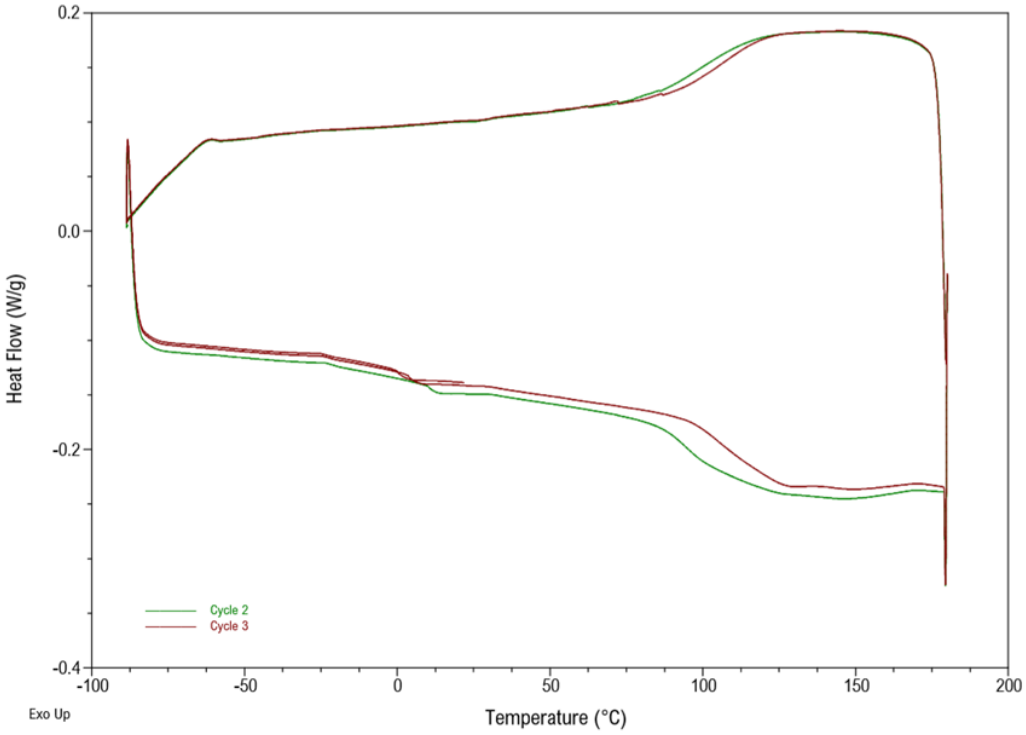

Figure A.1.38 – Thermogram of [INH][S-CsO]$_2$ (DSC).

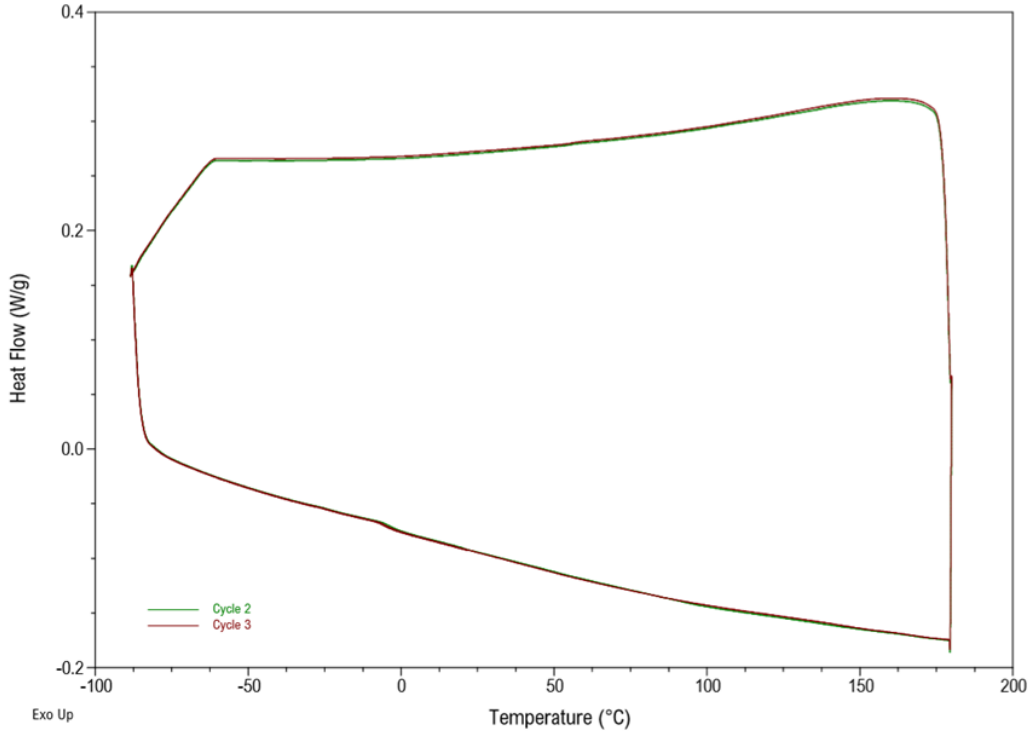

Figure A.1.39 – Thermogram of [INH][R-CsO] (DSC).

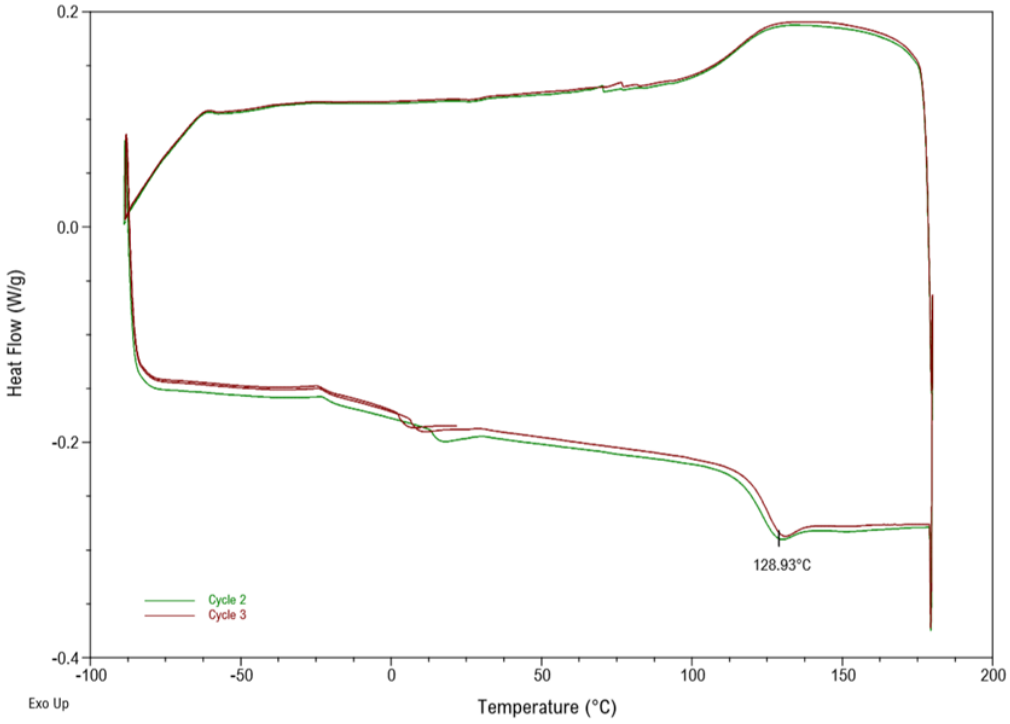

Figure A.1.40 – Thermogram of [INH][R-CsO]$_2$ (DSC).

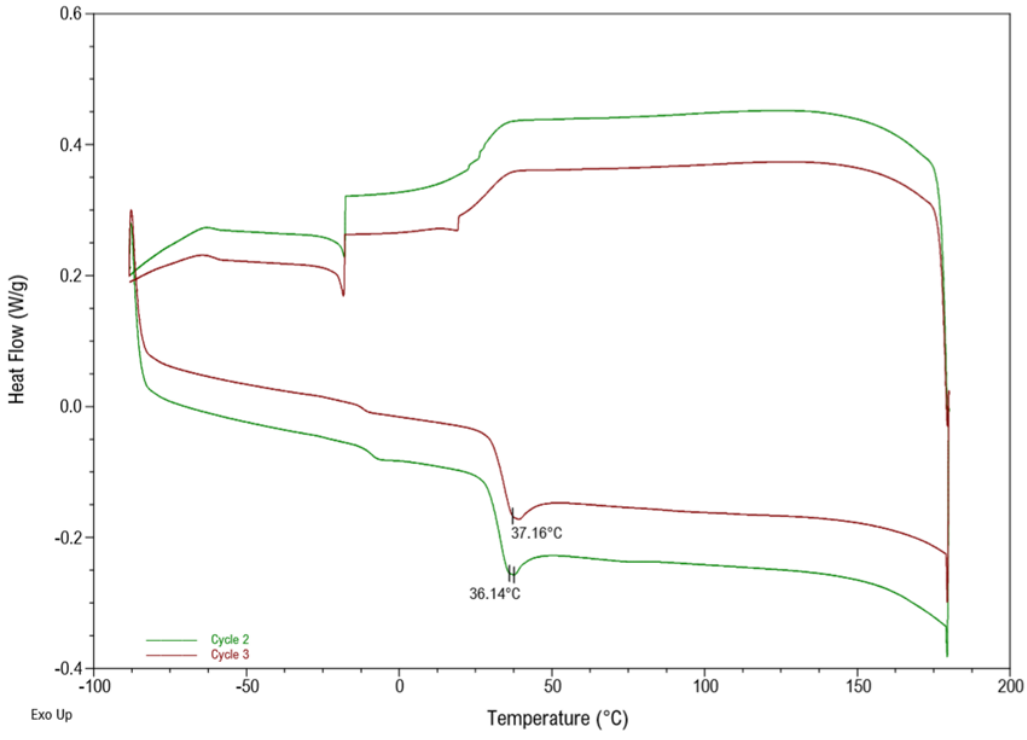

Figure A.1.41 – Thermogram of [INH][VanO] (DSC).

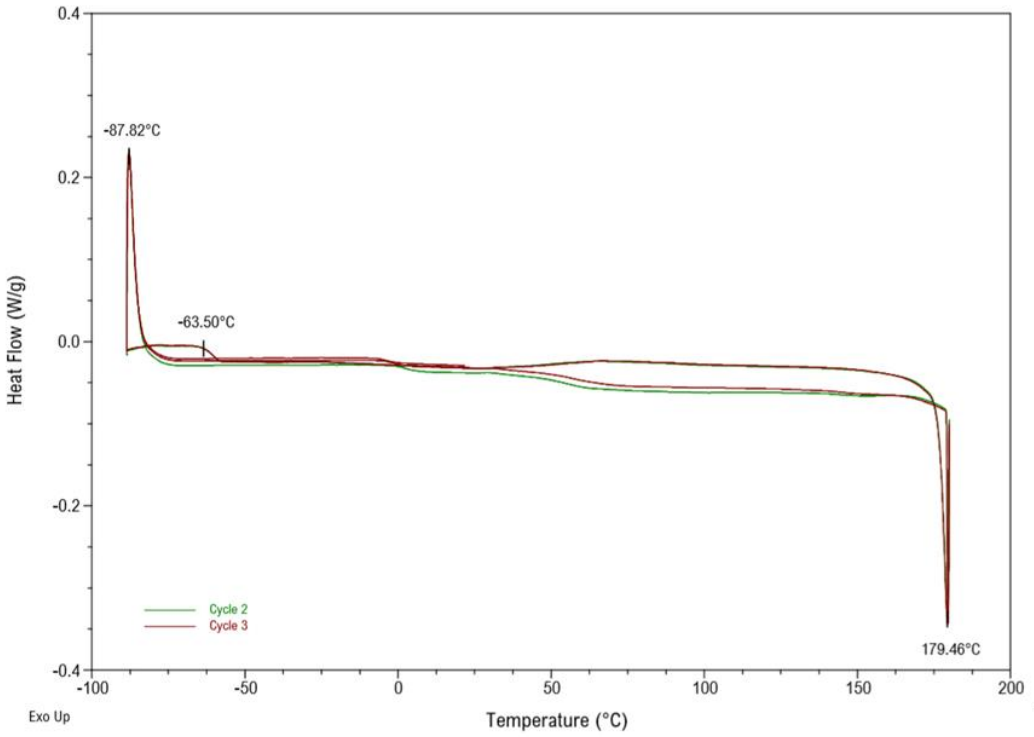

Figure A.1.42 – Thermogram of [INH][Sac] (DSC).

A.2 Therapeutic Liquid Mixtures

Table A.2.1 - Different attempts to prepare therapeutic liquid mixtures and/or eutectic systems, that do not form stable liquid mixtures.

Compounds	Molar Ratio
Citric Acid:L-arginine	1:1 ; 1:2 ; 2:1
Citric Acid:L-arginine:H_2O	1:1:3 ; 1:2:3 ; 2:1:3 ; 1:2:5
Glycerol:L-arginine	1:1 ; 1:2 ; 2:1 ; 3:1 ; 4:1
Glycerol:L-arginine:Ethambutol:H_2O	4:1:1:3 ; 4:1:2:3
L-arginine:Glutamic Acid	1:1
L-arginine:Glutamic Acid:H_2O	1:1:1 ; 1:1:2 ; 1:1:4 ; 1:1:6
L-arginine:Oxalic Acid	1:1
L-arginine:Oxalic Acid:H_2O	1:1:1 ; 1:1:2 ; 1:1:3
L-arginine:Tartaric Acid	1:1

L-arginine:Tartaric Acid:H_2O	1:1:1 ; 1:1:2 ; 1:1:3
L-arginine:Malic Acid	1:1
L-arginine:Malic Acid:H_2O	1:1:1 ; 1:1:3
L-arginine:Ascorbic Acid	1:1
Citric Acid:Ethambutol:L-arginine:H_2O	2:1:1:5
L-arginine:Ethambutol	1:1:2
Lactic Acid:Ethambutol	1:1 ; 1:2 ; 2:1 ; 4:1
Geraniol:Ethambutol	1:1 ; 1:2 ; 2:1
Urea:Ethambutol	1:1 ; 1:2 ; 2:1
Urea:Ethambutol:H_2O	1:1:1 ; 1:2:2 ; 2:1:2 ; 1:1:3 ; 1:2:5 ; 2:1:3
Oxalic Acid:Ethambutol	1:1 ; 1:2 ; 2:1
Oxalic Acid:Ethambutol:H_2O	1:1:1 ; 1:2:2 ; 2:1:2 ; 1:1:3 ; 1:2:4 ; 2:1:3
Menthol:Ethambutol	1:1 ; 1:2 ; 2:1 ; 5:2 ; 7:3
Malonic Acid:Ethambutol	1:1 ; 1:2 ; 2:1
Malonic Acid:Ethambutol:H_2O	1:2:2 ; 2:1:2 ; 1:1:2 ; 1:2:6 ; 2:1:1 ; 1:1:4 ; 1:1:5 ; 1:1:6 ; 7:3:2 ; 5:2:2
Glycerol:Ethambutol	1:1 ; 1:2 ; 2:1 ; 4:1 ; 6:1 ; 8:1
Citric Acid:Ethambutol	1:1 ; 1:2 ; 2:1
Citric Acid:Ethambutol:H_2O	5:2:3 ; 7:3:3 ; 1:1:10 ; 1:2:4 ; 2:1:6 ; 4:1:4 ; 5:1:2 ; 4:1:5 ; 5:1:4 4:1:7 ; 4:1:9 ; 1:2:5 ; 2:1:5 ; 1:1:3 ; 2:1:7
Ethambutol:Choline Chloride	1:2 ; 2:1 ; 1:4 ; 4:1
Ethambutol:Isoniazid:Choline Chloride	1:1:4
Ethambutol:Isoniazid:Choline Chloride:H_2O	1:1:4:2 ; 1:1:4:4 ; 1:1:4:7 ; 1:1:4:10 ; 1:1:4:12
Citric Acid:Isoniazid	1:1 ; 1:2 ; 2:1 ; 4:1 ; 5:3
Citric Acid:Isoniazid:H_2O	1:1:8 ; 1:2:8 ; 2:1:8 ; 1:1:15 ; 1:2:15 ; 2:1:15 ; 4:1:2 ; 4:1:4 4:1:5 ; 4:1:6
Glycerol:Isoniazid	1:1 ; 2:1 ; 1:2 ; 3:1 ; 4:1 ; 3:2 ; 2:3
Geraniol:Isoniazid	1:1 ; 1:2 ; 2:1
Lactic Acid:Isoniazid	1:1 ; 1:2 ; 2:1
Isoniazid:Betaine	1:1 ; 1:2 ; 2:1 ; 1:4
Isoniazid:Betaine:H_2O	1:1:1 ; 2:1:1 ; 1:2:1 ; 1:4:1 ; 1:1:3 ; 2:1:2 ; 1:2:3 ; 1:4:3 ; 1:1:5 2:1:5 ; 1:2:6 ; 1:4:5
Isoniazid:Vanillic Acid	2:1
Isoniazid:Vanillic Acid:H_2O	2:1:1 ; 2:1:3 ; 2:1:7 ; 2:1:10
Isoniazid:Choline Chloride	1:1 ; 1:2 ; 1:3 ; 2:1
Isoniazid:Hydroquinone	1:1 ; 1:2 ; 3:2

Isoniazid:L-arginine	1:1 ; 1:2
Isoniazid:Vanillin	1:1
Isoniazid:Vanillin:H_2O	1:1:3 ; 1:1:5
Isoniazid:Ascorbic Acid	3:1 ; 3:4
Isoniazid:Ascorbic Acid:H_2O	3:1:3 ; 3:4:3
Isoniazid:Lactic Acid	2:3 ; 3:2
Isoniazid:L-serine	2:1 ; 1:1
Isoniazid:L-serine:H_2O	2:1:2 ; 1:1:2 ; 2:1:4 ; 1:1:3 ; 2:1:6 ; 1:1:4 ; 1:1:10 ; 2:1:10
Isoniazid:D-Glucose	2:1 ; 3:1 ; 4:1
Isoniazid:D-Glucose:H_2O	2:1:3 ; 3:1:3 ; 4:1:3 ; 2:1:5 ; 3:1:5 ; 4:1:5 ; 2:1:7 ; 3:1:7 ; 4:1:7 2:1:10 ; 3:1:10 ; 4:1:10
Isoniazid:Urea	1:2 ; 3:2
Isoniazid:Urea:H_2O	1:2:2 ; 3:2:2 ; 1:2:3 ; 3:2:4 ; 1:2:4 ; 3:2:6 ; 1:2:5 ; 3:2:10
Isoniazid:Ethambutol:Betaine	1:1:1 ; 1:2:1 ; 4:3:1
Isoniazid:Ethambutol:Betaine:H_2O	1:1:1:2 ; 1:2:1:2 ; 4:3:1:6 ; 1:1:1:4 ; 1:2:1:4 ; 4:3:1:10 ; 1:1:1:6 1:2:1:6 ; 4:3:1:12 ; 1:2:1:5 ; 1:1:1:5 ; 4:3:1:5
Isoniazid:Myo-Inositol	3:1 ; 1:3 ;2:1
Isoniazid:Myo-Inositol:H_2O	3:1:3 ; 1:3:3 ; 2:1:3
Isoniazid:Malonic Acid	2:1 ; 3:2
Isoniazid:Malonic Acid:H_2O	2:1:2 ; 3:2:2
Glycerol:Pyrazinamide	2:1
Isoniazid:Pyrazinamide	1:1
Isoniazid:Pyrazinamide:H_2O	1:1:3 ; 1:1:5
Ethambutol:Isoniazid:Pyrazinamide	1:1:1
Ethambutol:Isoniazid:Pyrazinamide:H_2O	1:1:1:3 ; 1:1:1:6 ; 1:1:1:8
Ethambutol:Isoniazid:Pyrazinamide:Vanillin	1:1:1:1
Ethambutol:Isoniazid:Pyrazinamide:Vanillin:H_2O	1:1:1:1:3 ; 1:1:1:1:5 ; 1:1:1:1:8
Citric Acid:Ethambutol:Pyrazinamide:H_2O	1:1:1:5
Citric Acid:Isoniazid:Rifampicin:H_2O	1:1:0.25:5
Citric Acid:Ethambutol:Isoniazid:Rifampicin:H_2O	1:1:1:0.25:10
Citric Acid:Ethambutol:Isoniazid:Pyrazinamide:Rifampicin:H_2O	1:1:0.4:2.5:0.15:3 ; 1:1:0.4:2.5:0.15:5 ; 1:1:0.4:2.5:0.15:7 1:1:0.4:2.5:0.15:10 ; 1:1:0.4:2.5:0.15:15 ; 1:1:1:1:0.25:3 1:1:1:1:0.25:5 ; 1:1:1:1:0.25:7 ; 1:1:1:1:0.25:10 1:1:1:1:0.25:15

Table A.2.2 - Chemical shifts of ^{1}H and ^{13}C NMR of pure components and different therapeutic liquid mixtures prepared.

Compounds	Chemical shifts ^{1}H (ppm)				Chemical shifts ^{13}C (ppm)			
	$-CH_2$	-COH	-OH	-NH	-C=O	2x -C=O	-COH	$-CH_2$
Citric Acid	2.65; 2.75	5.15; 12.37	-	-	174.83	171.58	72.74	43.01
Ethambutol	-	-	9.24	5.40	-	-	-	-
CA:EMB:H_2O (2:1:10)	2.65; 2.75	5.15; 12.34	9.14	5.40	174.67	171.67	72.59	42.82
CA:L-arginine:H_2O (1:1:6)	2.50; 2.57	-	-	-	177.34	172.09	71.87	44.50
CA:L-arginine:H_2O (1:1:7)	2.51; 2.58	-	-	-	176.97	171.70	71.67	44.29
CA:L-arginine:H_2O (2:1:7)	2.56; 2.64	-	-	-	176.12	171.52	71.99	43.72
CA:L-arginine:H_2O (2:1:8)	2.57; 2.66	-	-	-	176.02	171.65	72.14	43.66
CA:L-arginine:H_2O (2:1:9)	2.56; 2.65	-	-	-	176.28	171.82	72.22	43.82

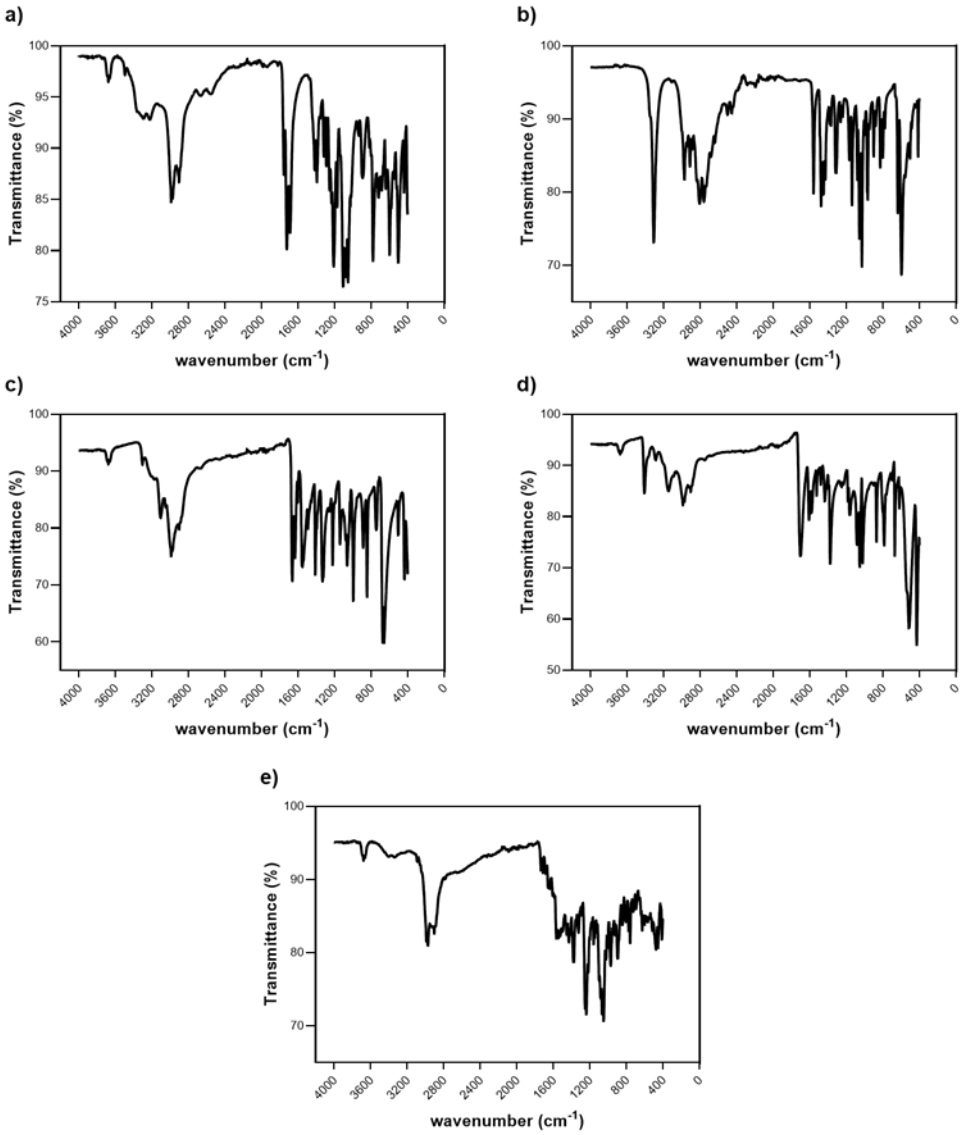

Figure A.2.1 – FTIR-ATR of pure components: **a)** CA; **b)** EMB; **c)** INH; **d)** PZA; **e)** RIF.

Table A.2.3 - Binary parameters applied in PC-SAFT modelling.

Binary pair	κ_{ij}^{a}	κ_{ij}^{T}	Reference
L-arg:H_2O	-0.0145	-	[318]
$[L\text{-}arg]^+$:H_2O	-0.045	-	This work
CA:H_2O	-0.11	-	This work
L-arg:CA	-	-	-

Table A.2.4 - Melting temperature and enthalpy of the pure components used in this work.

Compounds	T_m (K)	$\Delta_m H$ (KJ mol^{-1})	Reference
L-arg	558 ± 7	25 ± 3	This work
CA	426.9	40.32[a]	This work[a319]

[a]The T_m was obtained experimentally while $\Delta_m H$ was used from data presented by Meltzer and Pincu. [319]

Table A.2.5 - Summary of the mixtures prepared with CA, L-arg and H_2O, their ratio, physical state and pH.

Mixture	Molar ratio	Physical state	pH
CA:L-arg:H_2O	0.1:1:7	White solid paste	-
CA:L-arg:H_2O	0.2:1:7	White solid paste	-
CA:L-arg:H_2O	0.5:1:7	Translucid liquid	4.76
CA:L-arg:H_2O	1:1:7	Translucid liquid	3.58 ± 0.15
CA:H_2O	1:7	Translucid liquid	0.46
CA:H_2O pH 3.5	1:7	White solid paste	-
CA:H_2O pH 3.5	-[a]	Translucid liquid	3.62
L-arg:H_2O	1:7	White solid paste	-
L-arg:H_2O pH 3.5	-[b]	Translucid liquid	3.43

[a]Diluted with H_2O until a translucid liquid was obtained.

[b]Diluted with water and HCl until a translucid liquid at pH around 3.5 was obtained.

Table A.2.6 - Pure-component parameters used for PC-SAFT modelling. The pure-component parameters of ChCl, urea, and L-arg were fitted to experimental data of their aqueous solutions in the mentioned references by using the pure-component parameters of H_2O as listed here. Thus, such parameters are not independent of each other; this explains the use of these parameters without further considering changes or improvements within this manuscript.

Compound	σ_i (Å)	u_i/κ_B	m_i^{seg}	$\varepsilon^{AiBi}/\kappa_B$	κ^{AiBi}	N_{HBD}/N_{HBA}	Reference
H_2O	2.7927[a]	353.9449	1.204659	2425.67	0.04509	1/1	[320]
L-arg[b]	2.6572	349.7065	9.90818	2555.45	0.03926	3/1	[318]
CA[b]	2.7230	227.1800	8.54600	2488.00	0.04400	4/4	[254]

[a]Temperature-dependent segment diameter used according to data presented by Cameretti and Sadowski.[320]

[b]Pure-component parameters of their charged species set equal to the neutral molecules.

Table A.2.7 - Activity coefficients predicted by ePC-SAFT for CA (γ_{CIT}) and [L-arg]$^+$ (γ_{arg^+}) in the mixture CA:L-arg:H_2O.

χ (H_2O)	χ (CA)	χ (L-arg)	γ_{CIT}	γ_{arg^+}
0	0.50	0.50	1.51	1.45
0.10	0.45	0.45	1.45	1.49
0.20	0.40	0.40	1.37	1.52
0.30	0.35	0.35	1.25	1.53
0.40	0.30	0.30	1.10	1.53
0.50	0.25	0.25	0.90	1.48
0.60	0.20	0.20	0.66	1.38
0.67	0.165	0.165	0.47	1.25
0.71	0.145	0.145	0.36	1.14
0.75	0.125	0.125	0.26	1.01
0.78	0.11	0.11	0.19	0.89
0.80	0.10	0.10	0.15	0.81

Table A.2.8 - T_m variation (ΔT) predicted by PC-SAFT for CA and L-arg in the mixture CA:L-arg:H_2O. ΔT = 0 correspond to the binary mixture without water.

χ (H_2O)	χ (CA)	χ (L-arg)	ΔT (CA)	ΔT (L-arg)
0	0.50	0.50	0	0
0.10	0.45	0.45	-5	-7
0.20	0.40	0.40	-11	-16
0.30	0.35	0.35	-19	-26
0.40	0.30	0.30	-28	-39
0.50	0.25	0.25	-39	-55
0.60	0.20	0.20	-54	-76
0.67	0.165	0.165	-68	-95
0.71	0.145	0.145	-78	-108
0.75	0.125	0.125	-89	-123
0.78	0.11	0.11	-98	-137
0.80	0.10	0.10	-105	-146

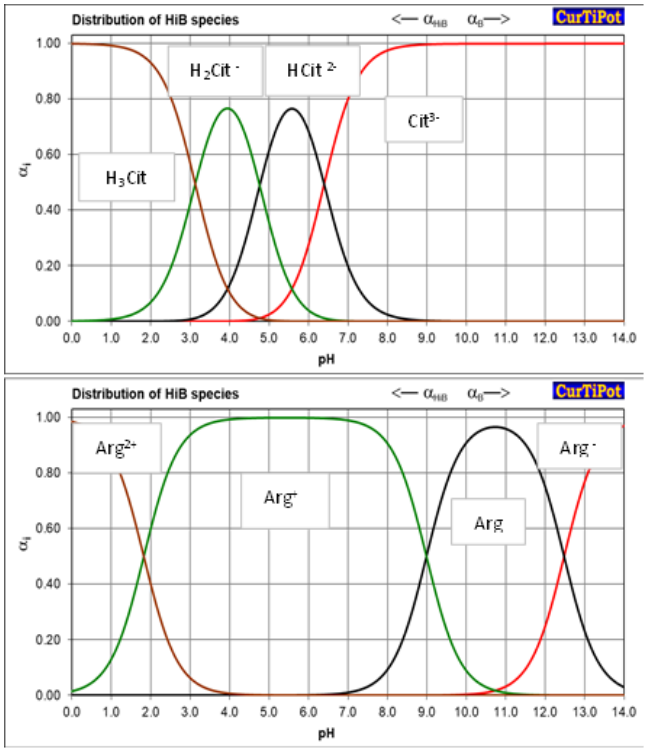

Figure A.2.2 – Diagram of the relative distribution of species (α_i) depending on pH, for CA (up) and L-arg (down). Calculated by CurTiPot[265] using pka's from Table A.2.8.

Table A.2.9 - Activity coefficients predicted by ePC-SAFT for CA (γ_{CIT}) in the mixture CA:L-arg:H_2O, at a water molar ratio of 0.8 and different mole fractions of L-arg and CA.

χ (H_2O)	χ (L-arg)	χ (CA)	χ (L-arg) in respect to CA	γ_{CIT}
0.8	0.199	0.001	0.995	0.09
0.8	0.175	0.025	0.875	0.14
0.8	0.15	0.05	0.75	0.14
0.8	0.125	0.075	0.625	0.14
0.8	0.1	0.1	0.5	0.15
0.8	0.075	0.125	0.375	0.15
0.8	0.05	0.15	0.25	0.16
0.8	0.025	0.175	0.125	0.17
0.8	0.001	0.199	0.005	0.18

Table A.2.10 - Activity coefficients predicted by ePC-SAFT for $[L\text{-arg}]^+$ (γ_{arg^+}) in the mixture CA:L-arg:H_2O, at a water molar ratio of 0.8 and different mole fractions of L-arg and CA.

χ (H_2O)	χ (CA)	χ (L-arg)	χ (L-arg) in respect to CA	γ_{arg^+}
0.8	0.001	0.199	0.995	0.41
0.8	0.025	0.175	0.875	0.48
0.8	0.05	0.15	0.75	0.56
0.8	0.1	0.1	0.5	0.81
0.8	0.15	0.05	0.25	1.24
0.8	0.175	0.025	0.125	1.54
0.8	0.199	0.001	0.005	1.20

Table A.2.11 - Assignment of L-arg functional groups to the respective FTIR wavenumber. Functional group number's according to Figure A.2.3.

Wavenumber (cm^{-1})	Assignment	Reference
3358	s N-H 4	[269,321–323]
3302	s N-H 6 (guanidine)	[269,321–323]
3057	s OH (COOH) 1	[269]
2946	s CH 5,6,7	[269,321–323]
2863		
1722	-	-
1676	s C=O (COOH) 1	[269,322–324]
1612	s C=N 9	[269,321]
1553	b NH	[269,321,323]
1472		
1422	b CH+ / b OH	[269,323,324]
1374		
1330	-	-
1279	-	-
1180	s C-N 3	[269,321–323]
1137	s C-N 9 (guanidine) +/ b NH	
979	b OH	[323]
766	b NH	[321]
701	-	-
607		
551	b COO- 1	[269,323]
495		

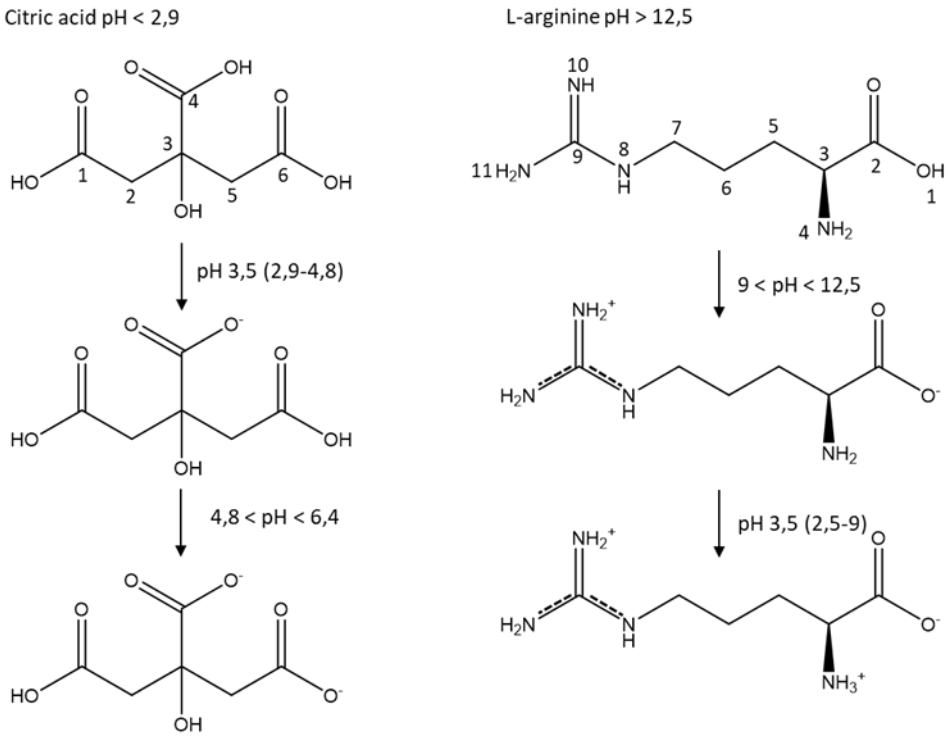

Figure A.2.3 – Chemical structure of CA (left) and L-arg (right) at different pH's according to pka's from Table A.2.8.

Table A.2.12 - pka's of CA and L-arg. Functional group number's according to Figure A.2.3.

	CA	**L-arg**
pKa	2.9 (COOH 4)	2.5 (OH 1)
	4.8 (COOH 6)	9 (NH_2 4)
	6.4 (COOH 1)	12.5 (guanidine 8, 10, 11)

Table A.2.13 - Assignment of CA functional groups to the respective FTIR wavenumber. Functional group number's according to Figure A.2.3.

Wavenumber (cm^{-1})	Assignment	Reference
3499	s OH 4	-
3370		
3290	s OH(COOH) 1, 4, 6	[269,325–327]
3242		
3000	s CH 2, 5	[325,326]
2993		
2640	OH(COOH) 4	-
2531		
1750		
1719	s C=O 1, 4, 6	[269,325,326]
1681		
1421	b CH	[326]
1394	b OH	[269,326]
1351	b CH	[326]
1314	b COH + b CH	[326]
1292	b CH	[326]
1207	b CH + s COH	[326]
1171	b C-OH	[326]
1103	s CC	[326]
1055	s CC(COOH)	[326]
1025	-	-
944	s C-O	[326]
904	c CC	[326]
775	b CH/ s CC	[269,325,326]
725	-	-
687	-	-
635	-	-
599	b OH	[326]
505	b COOH	[326]
441	-	-
404	-	-

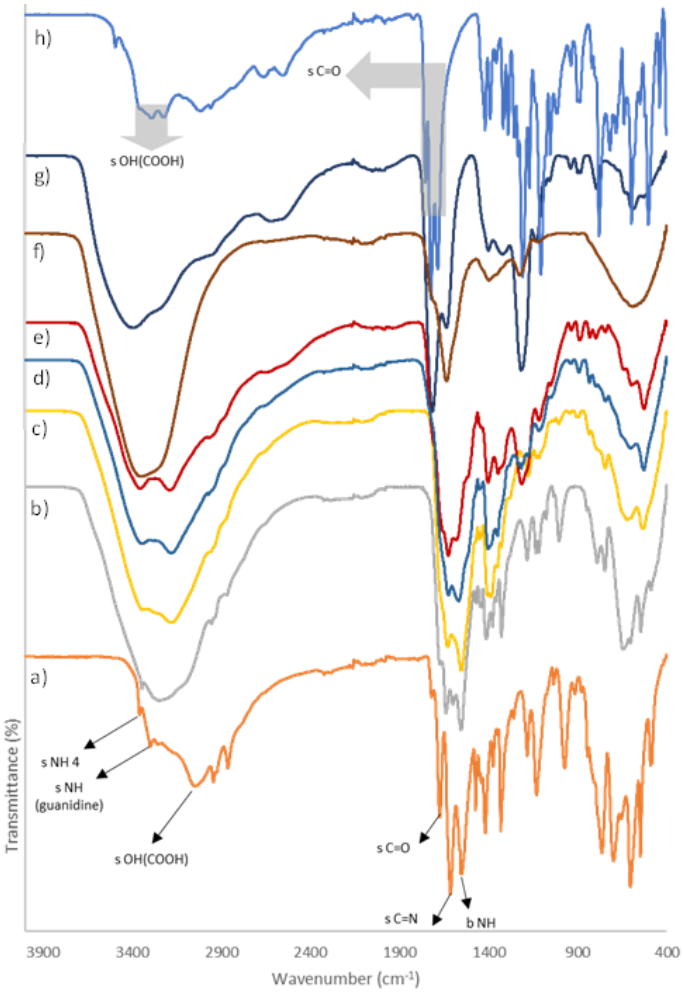

Figure A.2.4 – FTIR spectra of **a)** pure L-arg (orange line); **b)** CA:L-arg:H_2O 0.1:1:7 mol (grey line); **c)** CA:L-arg:H_2O 0.2:1:7 mol (yellow line); **d)** CA:L-arg:H_2O 0.5:1:7 mol (blue line); **e)** CA:L-arg:H_2O 1:1:7 mol (red line); **f)** CA:H_2O pH 3.5 (brown line); **g)** CA:H_2O 1:7 mol (dark blue line); **h)** pure CA (light blue line). s and b refer to stretching and bending vibrations, respectively. Numbers attributed according to the chemical structures from Figure A.2.3.

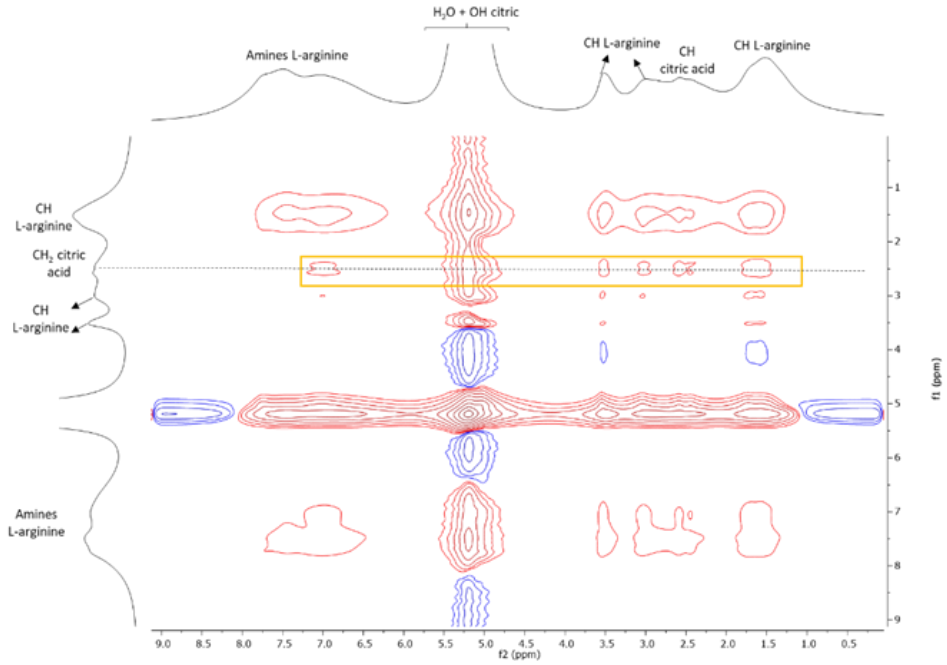

Figure A.2.5 – 2D NOESY spectra of the mixture CA:L-arg:H_2O 0.5:1:7 mol. The functional groups of the protons identified are aligned with the respective peaks.

⟨2022⟩

Márcia Filipa Carvalho dos Santos

EXPLORING ANT-TUBERCULOSIS DRUGS THROUGH GREEN SOLVENTS FOR EFFECTIVE TREATMENT OF TUBERCULOSIS